

**CFD MODELING AND EXPERIMENTAL STUDY OF VACUUM  
MEMBRANE DISTILLATION FOR REMOVAL OF DYES FROM  
AQUEOUS SOLUTIONS**

**Ph.D. Thesis**

**Rakesh Baghel  
(2014RCH9050)**



**DEPARTMENT OF CHEMICAL ENGINEERING  
MALAVIYA NATIONAL INSTITUTE OF TECHNOLOGY JAIPUR  
April-2019**

CFD MODELING AND EXPERIMENTAL STUDY OF VACUUM  
MEMBRANE DISTILLATION FOR REMOVAL OF DYES FROM  
AQUEOUS SOLUTIONS

*Submitted in*

*fulfillment of the requirements for the degree of*

**Doctor of Philosophy**

by

**RAKESH BAGHEL  
(2014RCH9050)**

Under the Supervision of

**Dr. Sushant Upadhyaya**

**Prof. S.P. Chaurasia**



**DEPARTMENT OF CHEMICAL ENGINEERING  
MALAVIYA NATIONAL INSTITUTE OF TECHNOLOGY JAIPUR**

**April-2019**

**©Malaviya National Institute of Technology Jaipur - 2019**  
**All Rights Reserved**

***THIS THESIS IS DEDICATED IN THE LOVING MEMORY OF MY MOTHER***

***“Late Mrs. SHEELA DEVI”***

## DECLARATION

I, **Rakesh Baghel**, declare that this thesis titled, “**CFD Modeling and Experimental Study of Vacuum Membrane Distillation for Removal of Dyes from Aqueous Solutions**” and the work presented in it, are my own. I confirm that:

- This work was done wholly or mainly while in candidature for a research degree at this university.
- Where any part of this thesis has previously been submitted for a degree or any other qualification at this university or any other institution, this has been clearly stated.
- Where I have consulted the published work of others, this is always clearly attributed.
- Where I have quoted from the work of others, the source is always given. With the exception of such quotations, this thesis is entirely my own work.
- I have acknowledged all main sources of help.
- Where the thesis is based on work done by myself, jointly with others, I have made clear exactly what was done by others and what I have contributed myself.

Date:

Rakesh Baghel  
(2014RCH9050)

## CERTIFICATE

This is to certify that the thesis entitled “**CFD Modeling and Experimental Study of Vacuum Membrane Distillation for Removal of Dyes from Aqueous Solutions**” being submitted by **Rakesh Baghel (2014RCH9050)** is a bonafide research work carried out under my supervision and guidance in fulfillment of the requirement for the award of the degree of Doctor of Philosophy in the Department of Chemical Engineering, Malaviya National Institute of Technology Jaipur, India. The matter embodied in this thesis is original and has not been submitted to any other University or Institute for the award of any other degree.

Place: Jaipur

Date:

**Dr. Sushant Upadhyaya**  
**Associate Professor**  
**Dept. Of Chemical Engineering**  
**MNIT Jaipur**

Place: Jaipur

Date:

**Dr. S. P. Chauraisa**  
**Professor**  
**Dept. Of Chemical Engineering**  
**MNIT Jaipur**

## ACKNOWLEDGEMENT

*To create something in words is quite a difficult task without God's inspiration, elder's blessing, younger's love and cooperation of friends. The completion of any interdisciplinary project depends upon the cooperation coordination and the combined effort of several resources of knowledge skill, labour and time. The precious guidance and spiritual help of guide's cannot be fulfilled by thanks.*

*First of all, I take this auspicious opportunity to express my deep sense of gratitude to my supervisor **Dr. Sushant Upadhyaya**, (Associate Professor), Department of Chemical Engineering, MNIT Jaipur for giving me this opportunity to work under his guidance. His helpful advice, continuous inspiration, support and understanding are exceptional. Without their constructive guidance, enthusing, decisive approach and persistent help, this thesis would not have been possible. They have been constant encouragement and support throughout my course, especially for the useful suggestions given during the course of my thesis period. I am extremely fortunate to have **Dr. Sushant Upadhyaya** as my guide.. I am equally grateful to co-supervisor **Dr. S. P. Chaurasia**, Professor, Chemical Engineering Department, MNIT Jaipur for his generous help during each and every step during the course of the investigation as well as overall professional development. I have no words to express my feeling towards my co-guide's extremely kind and tolerant attitude all the time.*

*I express my sincere gratitude to **Prof. Kailash Singh**, Head of Department, and all the faculty members of the department for their invaluable guidance and encouraging me during my research work. I am especially desirous of acknowledging the entire D.R.E.C. members, **Dr. Kailash Singh, Dr. Prabhat Pandit and Prof. A. B. Gupta**; for their inspiring advice, immense help, whole hearted support and constant encouragement throughout the tenure of the research work. I would like to pay my lot of respect and thanks to very dynamic Institute **Director, Prof. Udaykumar R. Yaragatti**, to provide all supports of fund from Institute for the installation of my research work without any delay.*

*I would like to thank **Mr. Ramesh Sharma**, senior technician, Chemical Engineering Department, Malaviya National Institute of Technology Jaipur for his efforts in the modification and fabrication of the experimental setup. I am very thankful to **Dr. Jitendra Kumar Singh**, Assistant Professor, JK Lakshmi Pat University Jaipur, for their valuable support during my research work. I am also very thankful to my labmate **Ms. Sarita Kalla**, Research Scholar for her valuable suggestions and inputs. I would like to take this opportunity to thank my friends and colleagues whose immense help me during my research tenure are **Mr. Ajay Sujan, Ms. Priya***

*Pal, Ms. Komal Sharma, Mr. Shivendu, Ms. Renu, Mr. Gaurav Kataria, Mr. Leelesh, Mr. Shivraj Chandel, Ms. Ekta Chaturvedi, Ms. Tanuja Joshi, Mr. Gaurav Gopal.*

*No major project can be completed without cooperation and encouragement of one's family. The words are not worthy to mention love and continuous support of my grandparents **Mr. Raghunath Singh Baghel** and **Mrs. Srimati Devi** and my father **Mr. Gya Prasad Baghel** who remained the pillar of inspiration for me since the beginning of my life and whose everlasting encouragement, blessing, love, affection and sacrifices brought me here up to. I am also thankful to my Siblings, **Ms. Bhavana, Ms. Arti Baghel, Ms. Archna Baghel, Mr. Amit Baghel and Ms. Keerti Baghel** for their moral support.*

*I also express my gratitude to all other people who knowingly, unknowingly helped me in this tenure.*

*Ultimately I am very grateful to my almighty GOD, "God is indefinable something which we all feel but which we don't know". Who gave me opportunity to get in research area and for his blessing.*

**RAKESH BAGHEL**



## ABSTRACT

In the present work, experimental and numerical modeling is carried out for removal of dyes from aqueous solutions using vacuum membrane distillation. The experimental lab setup is fabricated for conducting the various experiments at different operating conditions at different concentrations of dyes for two types of membranes (PTFE and PVDF) of same pore size of 0.22  $\mu\text{m}$ . The central composite design (CCD) and ANOVA have been used for optimizing the process parameters such as feed temperature, vacuum degree, flow rate, and initial dye concentration. A CFD model is also developed for determining the membrane interfacial temperatures and permeate flux which comprising heat and mass transfer effects using COMSOL multi-physics commercial software. From the central composite design of optimization, it was found that 85  $^{\circ}\text{C}$  of feed temperature, 750 mmHg of vacuum degree, 5 lpm of flow rate and 30ppm of initial dye concentration for the maximization of permeate flux, percentage removal and minimization of specific energy consumption for both PTFE and PVDF membranes. At the optimum conditions of operating parameters, the permeate flux was found to be 53.89 and 54.51  $\text{kg}/\text{m}^2\cdot\text{h}$ , specific energy consumption was found to be 2.98, and 2.23 kWh/kg and percentage removal were found to be 99.69% and 99.85% in case of PTFE and PVDF membrane respectively.

The exponential increment in permeate flux from 1.95 to 53.51  $\text{kg}/\text{m}^2\cdot\text{h}$  and 2.85 to 55.12  $\text{kg}/\text{m}^2\cdot\text{h}$  was observed on increasing feed temperature from 25 to 85  $^{\circ}\text{C}$  at the flow rate of 5 lpm and vacuum degree of 750 mmHg and initial dye concentration of 30 ppm for PTFE and PVDF membrane respectively. This is due to exponential increment in trans-membrane vapor pressure difference (driving force) on increasing the feed temperature. The comparison of CCD and CFD model was carried out with experimental flux and it was found that CFD model was best fitted with  $R^2$  and MAPE as 0.995 and 7.63 in case of PTFE membrane and 0.991 and 5.81 in case of PVDF membrane. The specific energy consumption was also reduced from 7.12 to 0.95 kWh/kg and 6.89 to 0.72 kWh/kg on increasing feed temperature from 25 to 85  $^{\circ}\text{C}$  because the amount of permeate volume is increased effectively. The linear increment in permeate flux was observed on increasing the vacuum degree from 670 to 750 mmHg and flow rate from 2 to 10 lpm for both membranes.

The effect of operating time on permeate flux was also analyzed and it was found that the permeate flux is reduced up to 4.5% and 8.08% in 60 hrs at the feed temperature of 85  $^{\circ}\text{C}$ , vacuum degree of 750 mmHg, flow rate of 5 lpm and initial dye concentration of 30ppm in case

of PTFE and PVDF membrane respectively. This reduction in permeate flux was due to deposition of dye molecules at the surface of the membrane which blocked the pores of the membrane. SEM images with EDS have confirmed the deposition of dye molecules at the membrane surface and the pore size distribution graph confirms the reduction in pore size after the 60 hours of operating time.

The heat and mass transfer correlations was developed at the varying feed temperature from 25 to 85 °C, flow rate of 2 to 10 lpm at vacuum degree of 730 and 750mmHg and initial dye concentration of 30ppm. The heat transfer correlation was obtained as  $Nu = 1.25 Re^{0.87} Pr^{0.33}$ . The heat transfer coefficient is significantly increased with increasing feed temperature which confirmed that heat is transferring with vapor molecules. The mass transfer correlation was obtained as  $Sh = 45.58 Re^{0.13} Sc^{0.33}$ . The heat and mass transfer coefficient of dye-water system is compared with available NaCl-water mixture to understand the system behaviour.

The experimental recovery was also calculated through the VMD process and it was found to be 70% in 60 hours for lab scale setup with membrane area of 0.00212 m<sup>2</sup>. The sensitivity analysis of feed temperature and vacuum degree is also checked with permeate flux. The ANN model is also developed for predicting the permeate flux using 4 input and 1 output conditions. The developed ANN model was found to be best fitted with experimental conditions as compared to central composite design model.

## Table of Content

Declaration-----	i
Certificate-----	ii
Acknowledgement-----	iii
Abstract-----	v
Table of Content-----	vii
List of Figures-----	xii
List of Tables-----	xiv
Nomenclature-----	xvi
List of Publications-----	xviii
CHAPTER 1. INTRODUCTION-----	1
1.1. Organization of Thesis -----	4
CHAPTER 2. LITERATURE REVIEW-----	5
2.1. Membrane Distillation Configurations-----	6
2.1.1. Direct Contact Membrane Distillation-----	6
2.1.2. Air Gap Membrane Distillation-----	6
2.1.3. Sweeping Gas Membrane Distillation -----	7
2.1.4. Vacuum Membrane Distillation -----	7
2.2. Characterization of membrane for VMD -----	11
2.2.1. Membrane Thickness-----	11
2.2.2. Membrane Porosity-----	12
2.2.3. Membrane Tortuosity -----	12
2.2.4. Liquid Entry Pressure and Wettability-----	13
2.2.5. Thermal Conductivity-----	13
2.2.6. Membrane pore size and pore size distribution -----	14
2.2.6.1. Scanning Electron (SE) & Atomic Force (AF) Microscopy -----	14
2.2.6.2. Gas permeation method (Permeability test) -----	15
2.3. Membrane Modules-----	18
2.3.1. Plate and frame module-----	18

2.3.2. Tubular module -----	19
2.3.3. Hollow fibre membrane-----	19
2.3.4. Capillary module-----	19
2.3.5. Spiral wound module-----	20
2.4. Transport mechanism in VMD-----	22
2.4.1. Heat Transfer -----	22
2.4.1.1. Heat transfer through feed bulk side boundary layers-----	22
2.4.1.2. Heat transfer by conduction through the membrane -----	25
2.5. Mass Transfer-----	27
2.5.1. Mass transfer through feed side boundary layer -----	27
2.5.2. Mass transport through the membrane pores -----	28
2.6. Temperature and concentration polarization -----	31
2.6.1. Temperature polarization coefficient -----	31
2.7. Membrane Fouling-----	32
2.7.1. Types of Fouling -----	32
2.7.1.1. Inorganic fouling -----	33
2.7.1.2. Organic fouling -----	33
2.7.1.3. Biological fouling -----	33
2.7.2. Different factors affecting the membrane fouling-----	34
2.7.2.1. Temperature -----	34
2.7.2.2. Water sources and dissolved gases -----	34
2.7.3. Effects of fouling -----	34
2.7.3.1. Membrane pore wetting -----	35
2.7.3.2. Chemical and physical degradation of membrane -----	35
2.7.3.3. Polarization Enhancement-----	35
2.7.3.4. Reduction in permeate amount -----	36
2.8. Operating parameters affecting VMD process-----	36

2.8.1. Feed Temperature-----	36
2.8.2. Feed Concentration-----	38
2.8.3. Vacuum Degree-----	39
2.8.4. Operating Time-----	40
<b>CHAPTER 3. THEORETICAL AND MATHEMATICAL ASPECTS-----</b>	<b>42</b>
3.1. Computational fluid dynamic (CFD) simulation for permeate flux-----	42
3.1.1. Geometry development and meshing-----	42
3.1.2. Equations involved in CFD study in COMSOL Multiphysics-----	45
3.1.3. Solution of governing equations-----	47
3.2. Recovery-----	48
3.3. Sensitivity analysis-----	50
3.4. Artificial Neural Network (ANN)-----	52
3.4.1. Back-propagation Algorithm-----	52
3.4.2. Models-----	52
3.4.3. Neural Network toolbox (NNtool)-----	55
<b>CHAPTER 4. EXPERIMENTAL MATERIALS AND METHODS-----</b>	<b>57</b>
4.1. Materials used:-----	57
4.1.1. Distilled water-----	57
4.1.2. Methylene Blue-----	57
4.1.3. Naphthol Blue Black Dye-----	58
4.1.4. Sudan III Dye-----	59
4.1.5. Basic Red 9 dye-----	59
4.2. Experimental Setup-----	61
4.3. Experimental Procedure-----	64
4.4. UV-Vis spectrophotometer-----	64
4.5. Microscopic methods for characterization-----	65
4.6. Permeate flux, Specific energy consumption and percentage removal calculation-----	67

CHAPTER 5. RESULTS AND DISCUSSIONS -----	68
5.1. Statistical analysis of Experiments -----	68
5.2. Central Composite Design for PTFE and PVDF membranes -----	68
5.2.1. CCD model analysis for PTFE and PVDF membrane -----	70
5.2.2. Second-Order Model and Analysis of Variance-----	76
5.2.3. Optimization and percentage contribution of process variables -----	82
5.2.3.1. Percentage contribution of process variables-----	82
5.2.3.2. Optimization for PTFE and PVDF membrane -----	82
5.3. Estimation of Permeate flux and membrane surface temperatures using CFD -----	84
5.4. Effect of process variables on various responses in PTFE and PVDF membrane-----	88
5.4.1. Effect of feed temperature-----	88
5.4.2. Effect of vacuum degree-----	96
5.4.3. Effect of flow rate -----	96
5.5. Interaction effects of process variables -----	97
5.5.1. Interaction effects for permeate flux -----	97
5.5.2. Interaction effects for specific energy consumption-----	100
5.5.3. Interaction effects for percentage removal-----	101
5.6. Development of Heat and Mass Transfer Correlation -----	104
5.6.1. Heat Transfer Correlation -----	104
5.6.2. Mass Transfer Correlation-----	109
5.7. Membrane Characterization and fouling study -----	113
5.8. Recovery Model-----	119
5.8.1. Effect of operating parameters on recovery-----	120
5.9. Sensitivity analysis-----	124
5.9.1. Sensitivity of permeate flux to feed temperature-----	124
5.9.2. Sensitivity of permeate flux to vacuum degree-----	125
5.9.3. Sensitivity of permeate flux to flow rate -----	125

5.9.4. Sensitivity of permeate flux to membrane characteristics -----	126
5.10. ANN modeling for permeate flux -----	127
CHAPTER 6. CONCLUSIONS & FUTURE RECOMMENDATIONS -----	131
References-----	134
Appendix-----	148

## List of Figures

Figure 2.1 various membrane distillation techniques .....	8
Figure 2.2: Gas permeation setup .....	16
Figure 2.3: Schematic diagram of different laboratory-scale membrane modules.....	21
Figure 3.1 Overview of Computational fluid dynamics simulation .....	42
Figure 3.2: Membrane module with membrane test cell .....	44
Figure 3.3: Meshing of the test cell .....	44
Figure 3.4: Flow chart for the numerical simulation of VMD process.....	48
Figure 3.5 Block diagram for recovery analysis through VMD .....	49
Figure 3.6: Non-linear Transfer Functions used for Synaptic Inhibition.....	54
Figure 3.7: Structure of neural network with single hidden layer .....	55
Figure 3.8: Data manager graphical user interface .....	56
Figure 4.1: Schematic Diagram of Vacuum membrane Distillation unit .....	62
Figure 4.2: Pictorial diagram of lab scale vacuum membrane distillation unit .....	63
Figure 4.3: Scanning Electron Microscope.....	66
Figure 4.4: SEM Opened Sample Chamber.....	66
Figure 5.1: Residual Plots for PTFE Membrane.....	73
Figure 5.2: Residual Plots for PVDF Membrane.....	74
Figure 5.3: Pareto graphic analysis of Percentage contributions of each factor for PTFE membrane.....	80
Figure 5.4: Pareto graphic analysis of Percentage contributions of each factor for PVDF membrane.....	81
Figure 5.5: Optimization of process variables for PTFE and PVDF membrane .....	83
Figure 5.6: Temperature contour at 328 °K/55 °C feed temperature .....	86
Figure 5.7: Temperature contour inside membrane module at 358 °K/85 °C feed temperature...	87
Figure 5.8: Contour for convective heat flux.....	88
Figure 5.9: Effect of feed temperature on fractional contribution of Poiseuille flow.....	90
Figure 5.10: Effect of feed temperature of permeate flux and specific energy consumption (a) PTFE and (b) PVDF membrane.....	91
Figure 5.11: Effect of feed temperature on temperature polarization coefficient (a) PTFE membrane, (b) PVDF membrane .....	92
Figure 5.12 Effect of vacuum degree on permeate flux for different membranes.....	93
Figure 5.13: Effect of vacuum degree on temperature polarization coefficient .....	94
Figure 5.14: Effect of flow rate on permeate flux and specific energy consumption.....	95



Figure 5.15: Interaction plots of permeate flux for PTFE membrane.....	99
Figure 5.16: Interaction plots of permeate flux for PVDF membrane.....	99
Figure 5.17 Interaction plots of specific energy consumption for PTFE membrane.....	102
Figure 5.18: Interaction plots of specific energy consumption for PVDF membrane.....	102
Figure 5.19: Interaction plots of percentage removal for PTFE membrane .....	103
Figure 5.20: Interaction plots of percentage removal for PVDF membrane .....	103
Figure 5.21: Fitting of heat transfer correlation at 30 ppm initial dye concentration .....	106
Figure 5.22: Effect of feed temperature on heat transfer coefficient.....	107
Figure 5.23: Comparison of heat transfer coefficient of Dye-water and NaCl-water mixture ...	108
Figure 5.24: Fitting of mass transfer correlation at 30 ppm initial dye concentration.....	110
Figure 5.25: Effect of Feed Temperature on mass transfer coefficient .....	112
Figure 5.26: Comparison of mass transfer coefficient of Dye-water and NaCl-water mixture..	113
Figure 5.27: Effect of operating time on permeate flux.....	114
Figure 5.28: Surface morphology analysis of PTFE membrane (a) fresh, and (b) used membrane after 60hrs using SEM and EDS analysis .....	116
Figure 5.29: Surface morphology analysis of PVDF membrane (a) fresh, and (b) used membrane after 60hrs using SEM and EDS analysis .....	117
Figure 5.30: Pore size distribution of Fresh and used membranes for PTFE and PVDF membrane .....	118
Figure 5.31: SEM images of PTFE and PVDF membrane after washing .....	118
Figure 5.32: Variation of Dye concentration and volume of feed in tank with operating time..	119
Figure 5.33: Comparison of experimental and model recovery .....	120
Figure 5.34: Effect of (a) feed temperature and (b) vacuum degree on percentage recovery with time .....	122
Figure 5.35: Effect of (a) Feed flow rate and (b) Feed concentration on percentage recovery with time .....	123
Figure 5.36: Sensitivity of permeate flux to feed temperature .....	124
Figure 5.37: Sensitivity of permeate flux to vacuum degree .....	125
Figure 5.38: Sensitivity of permeate flux to flow rate .....	126
Figure 5.39: Sensitivity of permeate flux to membrane characteristics.....	126
Figure 5.40: Create network for Training and Adapting learning function.....	128
Figure 5.41: Fitting of artificial neural network with experimental data.....	129

## List of Tables

Table 1.1: Comparison of different dye removal techniques.....	2
Table 2.1: Advantages and disadvantages of different MD configurations.....	8
Table 2.2: Commercially available membranes used by some researchers.....	16
Table 2.3: Various Heat Transfer Correlations.....	24
Table 2.4: Different aspects of heat and mass transfer in VMD.....	26
Table 2.5 Various mass transfer correlations.....	28
Table 2.6: Collision diameter of various species .....	29
Table 2.7 Effect of feed temperature on permeate flux .....	37
Table 2.8: Effect of feed concentration on permeate flux .....	38
Table 2.9: Effect of vacuum pressure on permeate flux .....	39
Table 3.1: Cell dimensions of the membrane and its module.....	43
Table 3.2: Boundary Conditions .....	46
Table 4.1: Properties of distilled water .....	57
Table 4.2: Properties of methylene blue .....	57
Table 4.3: Properties of Naphthol Blue Black Dye .....	58
Table 4.4: Properties of Sudan III Dye .....	59
Table 4.5: Properties of Basic Red 9 Dye.....	60
Table 4.6: Properties of the used membranes .....	61
Table 4.7: Specifications of different instruments attached in experimental setup .....	62
Table 4.8: Properties of UV-vis spectrophotometer .....	64
Table 5.1: Statistical analysis of experimental runs.....	68
Table 5.2: Relationship between coded and actual values.....	70
Table 5.3: Experimental levels of independent variables for PTFE and PVDF membrane .....	70
Table 5.4: Four-factorial central composite design regarding coded and actual values .....	70
Table 5.5. Observed and predicted outputs of various experimental runs.....	75
Table 5.6: Analysis of Variance for PTFE Membrane .....	78
Table 5.7: Analysis of Variance for PVDF Membrane .....	79
Table 5.8: Confirmation test for PTFE and PVDF membrane .....	83
Table 5.9: Grid Independence test .....	84
Table 5.10: Comparative analysis of feed temperature on permeate flux for PTFE and PVDF membrane.....	92
Table 5.11: Comparative analysis of vacuum degree on permeate flux for PTFE and PVDF membrane.....	93

Table 5.12: Comparative analysis of flow rate on permeate flux for PTFE and PVDF membrane .....	95
Table 5.13: Experimental and model data for heat transfer correlation at 30 ppm initial dye concentration.....	104
Table 5.14: Experimental and model data for mass transfer correlation at 30 ppm initial dye concentration.....	110
Table 5.15: Weights for Artificial Neural Network.....	128
Table 5.16: Comparison of ANN and CCD model with Experimental Flux.....	130

## Nomenclature

$A$	Antoine Coefficient for water (Pa)
$a$	Membrane factor
$B$	Antoine Coefficient for water (Pa.K)
$B_m$	Pore geometric coefficient of membrane
$C$	Antoine Coefficient for water (K)
$C_F$	Concentration of solute in feed ( $\text{kg/m}^3$ )
$C_P$	Concentration of solute in permeate ( $\text{kg/m}^3$ )
$C_R$	Concentration of solute in retentate ( $\text{kg/m}^3$ )
$D_{eff}$	Effective diffusivity (m/s)
$d_h$	Hydraulic diameter (m)
$D_k$	Diffusivity due to Knudsen flow (m/s)
$D_p$	Diffusivity due to Poiseuille flow (m/s)
$H$	Overall heat transfer coefficient ( $\text{W/m}^2.\text{K}$ )
$h_f$	Feed side heat transfer coefficient ( $\text{W/m}^2.\text{K}$ )
$h_m$	Membrane heat transfer coefficient ( $\text{W/m}^2.\text{K}$ )
$h_p$	Permeate side heat transfer coefficient ( $\text{W/m}^2.\text{K}$ )
$\Delta H$	Latent heat of vaporization of water, J/mol
$k$	Overall mass transfer coefficient (m/s)
$k_f$	Feed side mass transfer coefficient (m/s)
$k_m$	Membrane side mass transfer coefficient (m/s)
$k_p$	Permeate side mass transfer coefficient (m/s)
$N$	Total Permeate flux ( $\text{kg/m}^2.\text{h}$ )
$N_{K-P}$	Flux due to Knudsen-Poiseuille diffusion ( $\text{kmol/m}^2.\text{s}$ )
$M$	Molar mass of gas passing through membrane (g/mol)
$\Delta P$	Hydraulic pressure difference (Pa)
$P_{fm}$	Pressure on feed side membrane surface (Pa)
$P_{pm}$	Pressure on permeate side membrane surface (Pa)
$Q_F$	Flow rate of feed ( $\text{m}^3/\text{s}$ )
$Q_P$	Flow rate of Permeate ( $\text{m}^3/\text{s}$ )
$Q_R$	Flow rate of Retentate ( $\text{m}^3/\text{s}$ )
$R$	Universal Gas constant (J/mol.K)
$r$	Mean pore size of the membrane ( $\mu\text{m}$ )

$r_{max}$	Maximum pore size of the membrane ( $\mu\text{m}$ )
$T$	Temperature of the gas ( $^{\circ}\text{C}$ )
$T_f$	Bulk feed side temperature ( $^{\circ}\text{C}$ )
$T_{fm}$	Feed side membrane surface temperature ( $^{\circ}\text{C}$ )
$T_p$	Permeate side temperature ( $^{\circ}\text{C}$ )
$T_{pm}$	Permeate side membrane surface temperature ( $^{\circ}\text{C}$ )
$V_m$	Minimum specified feed volume in tank ( $\text{m}^3$ )

### ***Greek Symbols***

$\varepsilon$	Membrane porosity
$\delta_m$	Thickness of the membrane ( $\mu\text{m}$ )
$\tau$	Membrane tortuosity
$\rho_m$	Density of the membrane ( $\text{kg}/\text{m}^3$ )
$\rho_{pol}$	Density of polymeric material ( $\text{kg}/\text{m}^3$ )
$\gamma_i$	Surface coefficient of the liquid
$\theta$	Contact angle between water molecules and membrane surface
$\eta$	Viscosity of water-vapor ( $\text{kg}/\text{m}\cdot\text{s}$ )
$\lambda_m$	Thermal conductivity of the membrane ( $\text{W}/\text{m}\cdot\text{K}$ )
$\lambda_{max}$	Maximum absorbance wavelength of dye
$\lambda_p$	Thermal conductivity of polymeric material ( $\text{W}/\text{m}\cdot\text{K}$ )
$\lambda_a$	Thermal conductivity of air ( $\text{W}/\text{m}\cdot\text{K}$ )

## List of Publications

### List of Research Papers Published in Refereed Journals

1. **Rakesh Baghel**, Sushant Upadhyaya, S.P. Chaurasia, Kailash Singh, Sarita Kalla, “Optimization of process variables by the application of response surface methodology for naphthol blue black dye removal in vacuum membrane distillation” Journal of Cleaner Production, 199, pp.900–915 (2018).
2. **Rakesh Baghel**, Sarita Kalla, Sushant Upadhyaya, S.P. Chaurasia, “Treatment of Sudan III dye from wastewater using vacuum membrane distillation” Journal of Basic and Applied Engineering Research, 4(3), pp.237–241 (2017).
3. **Rakesh Baghel**, Sushant Upadhyaya, Kailash Singh, S.P. Chaurasia, A.B. Gupta, Rajeev Kumar Dohare, “A review on membrane applications and transport mechanisms in vacuum membrane distillation” Reviews in Chemical Engineering, 34(1), pp.73–106 (2017).

### List of Papers Presented/Published in International Conferences Proceedings

1. **Rakesh Baghel**, Sarita Kalla, S.P. Chaurasia, Sushant Upadhyaya, “Removal of basic red 9 azo dye by using flat sheet PVDF membrane in vacuum membrane distillation” accepted for oral presentation in CHEMCON 2018.
2. **Rakesh Baghel**, Sarita Kalla, Sushant Upadhyaya, S.P. Chaurasia, “Treatment of Sudan III Dye from waste water using using Vacuum Membrane Distillation” published in International conference on Recent Trends in “Chemical, Environmental, Bioprocess, Textile, Mining, Material and Metallurgical Engineering” in 2017.
3. **Rakesh Baghel**, Sushant Upadhyaya, Kailash Singh, S.P. Chaurasia and A.B. Gupta “Central Composite Design for Parametric Study in Vacuum Membrane Distillation for Naphthol Blue Black Dye Removal” presented in CHEMCON 2016.

### List of Allied Papers

#### International Journal Publications

1. Sushant Upadhyaya, Kailash Singh, S.P. Chaurasia, **Rakesh Baghel**, Jitendra Kumar Singh, Rajeev Kumar Dohare, “Sensitivity analysis and Taguchi application in vacuum membrane distillation” Published in Membrane and Water Treatment (2018).

2. Sarita Kalla, **Rakesh Baghel**, Sushant Upadhyaya, Kailash Singh “Experimental and Mathematical Study of Air Gap Membrane Distillation for Aqueous HCl Azeotropic Separation” Published in Journal of Chemical Technology & Biotechnology (2018),
3. Jitendra Kumar Singh, Sushant Upadhyaya, S.P. Chaurasia, **Rakesh Baghel** “Study on Membrane fouling in Vacuum Membrane Distillation for Desalination” Published in International Journal of Basic and Applied Engineering Research (2017) vol.4(3).

### **International Conference Publications**

1. Sarita Kalla, Sushant Upadhyaya, Kailash Singh, Rakesh Baghel, “Taguchi optimization approach for azeotropic mixture separation using air gap membrane distillation” accepted for oral presentation in CHEMCON-2018.
2. Tanuja joshi, Rakesh Baghel, Sushant Upadhyaya “Taguchi Design Optimization for Dilute Ethanol Removal by Air Gap Membrane Distillation” accepted in InDACON held on April 20-21, 2018.
3. Swati Dubey, Rakesh Baghel, Sushant Upadhyaya, S. P. Chaurasia (2015) "Effects of Operating Parameters on Permeate Flux in Vacuum Membrane Distillation", 2<sup>nd</sup> International Conference on Desalination using Membrane Technology, Singapore, 26 - 29 July 2015.
4. Jitendra Kumar Singh, Sushant Upadhyaya ,S. P. Chaurasia & Rakesh Baghel, (2016)" Energy Consumption Study on Vacuum Membrane distillation for Desalination, International Conference on Clean India Technology Role of Desalination and Water Purification (InDA-APDA 2016) organized by Indian Desalination association at Chennai Feb., 11-13,2016.
5. Sushant Upadhyaya, Kailash Singh, Jitendra Singh, Rakesh Baghel, & S.P. Chaurasia,“ Artificial Neural Network Modeling of Vacuum Membrane Distillation for Desalination” International Conference on Desalination for the Environment: Clean Water and Energy, Organized by Elsevier at Marriott Park Hotel, Rome, Italy, 22–26 May 2016.

## **CHAPTER 1. INTRODUCTION**

---

The accessibility of safe drinking water is diminishing hugely while its demand is improving under social and monetary parts. It is a major problem in our nation to meet out safe savoring water in urban and country territories. The groundwater accessible in over 90% of the territories is containing multi-particles over as far as possible and making the risk for a prudent treatment system to make it ok to drink water. It is notable that 97% of the aggregate water store on earth is salty water and around 3% is fresh water. 2% water is in the form of icecaps, icy masses on north and south post, whose usage is an intense activity. Just 0.5% of aggregate water accessible on the earth could be used as new water by humanity, while its vast majority fall in the classification of utilized groundwater which is non-sustainable(Li & Tian 2009).

Colors are a natural substance which includes fragrant aryl rings that contain delocalized electron frameworks. Colors are widely utilized in material, calfskin tanning, paper generation, sustenance, hair colorings businesses, and so forth. Another utilization of these engineered hues colors is in groundwater following to decide particular surface territory of enacted slime, wastewater treatment, and sewage and so on. Compound goes into normal sea-going frameworks by a few means, viz. coordinate dumping of squanders originating from enterprises and so forth and effluents from wastewater treatment plants with ill-advised treatment. Also, tremendous amounts of these solutes are being found even in the wake of voyaging long separations from their cause. Deficient treatment of dyestuff containing effluents prompts shading pollution of the earth, for example, soil and characteristic water bodies. Shortage of consumable water is one of the real dangers for living creatures because of compound contamination of water which is caused by synthetic contaminants from overwhelming metals, colors, solvents, pesticides, and so forth. Indeed, low thought discharges prompt a significant number of unending impacts that typically distinguished after an extended period (Criscuoli et al. 2013).

It has been anticipated that the worldwide material market was worth 1557.1 billion USD with the creation of more than 88.5 million tons every year until the finish of 2015. The commitment of creating nations in the worldwide material market has come to 58.6 % as far as expense inside a decade ago. The vast majority of the colors utilized in material handling are inadequate in the total obsession of colors to textures, and in this way, 20% of colors enter the earth which produces color containing hues effluents. The worldwide generation of dyestuffs is around 10 million kg for every year, roughly 2 million kg of dynamic color every year enter the biosphere, either in broke down or suspended shape in the water.



A small amount of dye in water is not acceptable for drinking and other work from the safety point of view. Even little amount of dye is visible in water due to the presence of chromophores which are responsible for the color of the dye. Due to the presence of dye, the BOD and COD level of the water body is increased, and also it disturbs the photosynthesis of the aquatic plants by reducing the penetration of the sunlight into the water and thus the DO level in water is decreased which is very harmful to aquatic animals. Moreover, dyes are carcinogenic and toxic which damage the living organism. So, the treatment of dyes before discharge is essential.

**Table 1.1: Comparison of different dye removal techniques**

Process	Technology	Advantages	Disadvantages	References
Conventional process	Adsorption	High removal, low-cost adsorbents	The insignificant effect for removal of disperse dyes, regeneration of adsorbent is difficult	(Hameed et al. 2007; Tan et al. 2008)
	Biodegradation Coagulation/ Flocculation	Simple and economic	Produced high sludge and disposal problems	(Xuezhi Zhang et al. 2016; Kiran et al. 2006)
Recovery based processes	Membrane technique	Very high removal, can remove all types of dyes	Expensive and treatment of large volume is difficult	(Mericq et al. 2010; Baghel, Upadhyaya, et al. 2017)
	Oxidation	Efficient and Rapid removal	High energy consumption, chemicals are required	(Zhong et al. 2010)
	Ion-Exchange	Sorbent loss is negligible, high removal	Can't be used for disperse dyes, high cost	(Thomas 1944)
Advanced removal processes	Advanced Oxidation	No Sludge, higher removal	Costly, by-products formation, constraint to technical knowledge	(Dao et al. 2016; Ahmadi et al. 2005)
	Biomass	Operating cost is lower; toxic effect is negligible	Process is slow which depends on various parameters such as salts concentration and pH	(Chu & Chen 2002; Hameed & Ahmad 2009)
	Selective Bioadsorbents	Highly selective, no regeneration is required	Chemical modification is required	(Khattri & Singh 2000)

Various treatment technologies have been developed for the removal of dyes from wastewater. The most common adsorption process is used for the removal of dyes. However, other conventional techniques such as photochemical, chemical techniques are used for removal of dyes from wastewater (Crini 2006; Zhong et al. 2010; Navarro et al. 2009; Singh et al. 2011). The comparative analysis of different dye removal techniques is given in Table 1.1. Nowadays, membrane-based processes are also extensively used for the treatment of wastewater containing non-volatile solutes.

Membrane-based separation processes can be majorly classified according to their working principles, which are mainly the following: pressure-driven membrane processes, concentration driven membrane processes, electrical driven membrane processes, and thermal driven membrane processes. Membrane distillation is considered as a new and prominent technique for the removal of dyes from wastewater. Membrane distillation (MD) process is the hybrid system of thermal distillation and the membrane technology known for about 50 years. In this process, the vapor molecules are transported through the non-wetted porous hydrophobic membrane, the driving force being the vapor pressure difference across both sides of the membrane. The membrane in MD acts as a physical barrier which does not allow the passing of liquid molecules through the membrane and forms liquid/vapor interface at the entrance on the pores of the membrane. The first patent was made in 1963 on MD and the first paper published after four years later. The MD processes became more attractive and interesting in the early 1980s when the novel membranes with better membrane characteristics became available. MD became more promising separation technique due to the capability to utilize waste and alternative energy sources for different purposes. Simultaneous heat and mass transfer occur in all the MD configurations such as (i) direct contact membrane distillation (DCMD), (ii) air gap membrane distillation (AGMD), (iii) sweeping gas membrane distillation (SGMD) and (iv) vacuum membrane distillation (VMD).

In this work, the optimization of the process parameters such as feed temperature, vacuum degree, flow rate and initial dye concentration for maximization of permeate flux and percentage removal and minimization of specific energy consumption using the central composite design method is studied. The 3D CFD model has been developed for studying the interfacial temperatures and permeates flux through the membrane which comprises heat and mass transfer effects. Heat and mass transfer coefficients are determined using heat and mass transfer correlations, and the comparison is carried out with another developed model.

## **1.1. Organization of Thesis**

The thesis is divided into the following chapters:

**Chapter 1** deals with the introductory information regarding the problems arising due to the presence of dyes in water and membrane process to remove the dyes from water.

**Chapter 2** is regarding the literature review about the key aspects of vacuum membrane distillation and objective of the thesis.

**Chapter 3** presents the theoretical modeling of the VMD process along with recovery, sensitivity and ANN modeling.

**Chapter 4** is regarding the information about the experimental materials and methods along with an experimental procedure for conducting various experiments.

**Chapter 5** includes a detailed discussion of results obtained through the previous sections.

**Chapter 6** is the concluding chapter which summarizes the thesis.

## CHAPTER 2. LITERATURE REVIEW

---

Treatment of dye-containing wastewater is a major problem for many industries like paint, pigment, textile, pulp and paper industries. A large amount of water is required for the production of textile and discharged as wastewater which contains a high concentration of azo dyes, reactive dyes, other chemical residue and non-biodegradable compounds with high BOD and COD (Dasgupta et al. 2015; Tang & Chen 2002). The discharge of colored wastewater into fresh water sources caused the problem of non-aesthetic, eutrophication, due to their high solubility. The degradation of dye can form toxic and carcinogenic products even at a lower concentration. Azo dyes are characterized by the presence of azo bonds ( $-N=N-$ ) with aromatic rings and auxochromes such as  $-OH$ ,  $-NH_2$ ,  $-COOH$ ,  $-SO_3H$  etc. Due to high solubility in water, the removal of azo dyes from wastewater is very difficult using conventional techniques coagulation, sedimentation, activated sludge process, etc.. Biological methods and physicochemical methods cannot remove dye from wastewater to the desired limit that has a great impact on the environment and human health. These conventional techniques also have various limitations such as high cost, a large amount of sludge production, the complexity of the process, etc. (Maria et al. 2008). Nowadays, dissolved air flotation (DAF) is also used for removal of oil and solids from the water and commercially used for deinking of newspapers. The air is dissolved in the flotation tank and then release at atmospheric pressure. The tiny bubbles are formed with the air, and the suspended solids float to the upper water surface and removed using various skimming devices (Amaral Filho et al. 2016; Xuezhi Zhang et al. 2016). The colloidal particles are coagulated using different coagulant such as ferric chloride/aluminum sulfate and the bigger clusters can form from the coagulated particles using flocculent. Effective removal and easy to use are the major benefits of this process. The major disadvantages of this system include size, percent air, and power usage.

Membrane-based separation processes are considered as promising techniques for treatment of textile effluent wastewater due to its simplicity, higher rejection rate and easy maintenance (Alcaina-Miranda et al. 2009; Aouni et al. 2012; Han et al. 2009; Kyoungjin et al. 2017; Mo et al. 2008; Yatmaz et al. 2017). One of the membrane technique is membrane distillation considered as a prominent technique for known about 55 years. Membrane distillation (MD) process is the hybrid system of thermal distillation and the membrane technology known for about 50 years. In this process, the vapor molecules are transported through the non-wetted porous hydrophobic membrane, the driving force being the vapor

pressure difference across both sides of the membrane. The membrane in MD acts as a physical barrier which does not allow passing liquid molecules through the membrane and forms liquid/vapor interface at the entrance on the pores of the membrane.

The first patent was made in 1963 on MD, and the first paper published 4 years later. The MD processes became more attractive and interesting in the early 1980s when the novel membranes with better membrane characteristics became available. MD became more promising separation technique due to the capability to utilize waste and alternative energy sources for different purposes. Simultaneous heat and mass transfer occur in all the MD configurations such as (i) direct contact membrane distillation (DCMD), (ii) air gap membrane distillation (AGMD), (iii) sweeping gas membrane distillation (SGMD) and (iv) vacuum membrane distillation (VMD), as explained below.

## **2.1. Membrane Distillation Configurations**

The MD processes are classified based on condensation of the vapors on the permeate side while feed solution remains in direct contact with the feed side membrane surface. The various MD configurations are described below:

### **2.1.1. Direct Contact Membrane Distillation**

This is the simplest form of MD configuration shown in Figure 2.1. In this configuration, the feed solution remains in direct contact with one side of the hot membrane surface. Feed solution is evaporated at the surface of the membrane, and due to the hydrophobic nature of the membrane, only vapor molecules pass through the dry pores of the membrane. An aqueous solution which is colder than the feed solution is maintained at the permeate side of the membrane to condense the vapor molecules passing through the membrane. Due to direct contact of cold aqueous solution on the permeate side, this configuration is known as direct contact membrane distillation. There is another variant of DCMD known as DCMD with the liquid gap, in which a stagnant of cold distilled water is kept in direct contact with the permeate side of the membrane (Figure 2.1). The major disadvantage of the DCMD process is the heat loss by conduction inside the membrane module.

### **2.1.2. Air Gap Membrane Distillation**

In this configuration, the stagnant air gap is introduced between the condensing surface and the membrane surface on the permeate side. The vapor passes through the membrane and is condensed on the condensing surface after passing through the air gap in the membrane module shown in Figure 2.1. The main advantage of the stagnant air gap is to reduce heat loss by

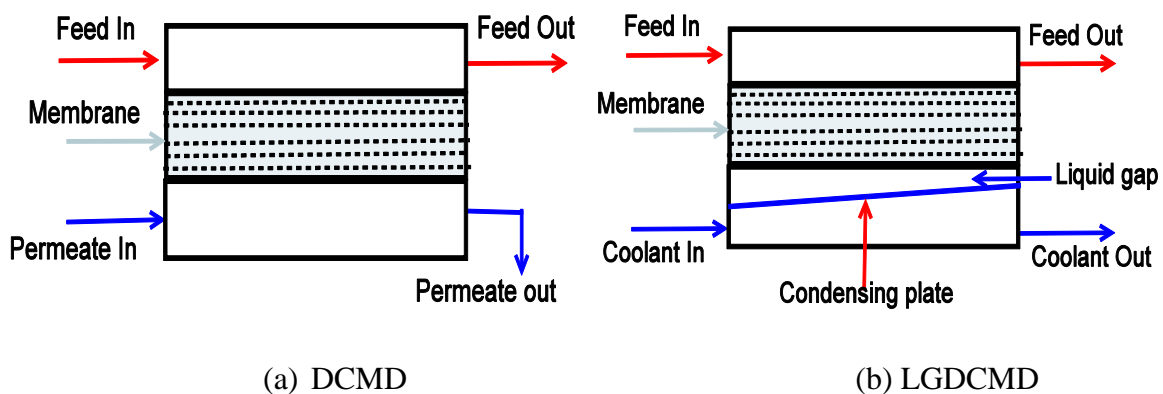
conduction however additional mass transfer resistance is created which is considered a major disadvantage of this process.

### 2.1.3. Sweeping Gas Membrane Distillation

In this configuration, vapor molecules passing through the membrane are carried out outside the membrane module from the permeate side by using cold inert gas shown in Figure 2.1. The condensation takes place outside the membrane module in the external condenser. Due to sweeping of vapor molecules, heat loss by conduction and mass transfer resistances are reduced, but the sweeping gas temperature increases on the permeate side considerably due to heat transferred from feed side to the membrane along the length of the membrane module which results in the reduction in driving force. So, to minimize the temperature of the sweeping gas, a cold wall is used on the permeate side of the membrane; this SGMD variant is known as Thermostatic Sweeping Gas Membrane Distillation (TSGMD). The operational cost of the system is also increased due to external condensation system.

### 2.1.4. Vacuum Membrane Distillation

In this configuration, the vacuum is applied on the permeate side of the porous membrane so that driving force can be maintained as shown in Figure 2.1. The heat loss and the mass transfer resistances are reduced due to the vacuum on the permeate side. The applied permeate pressure should be lower than the equilibrium vapor pressure of the feed. The vapors are taken outside the membrane module and condensed in the external condenser. The major disadvantage of this process is the probability of pore wetting.



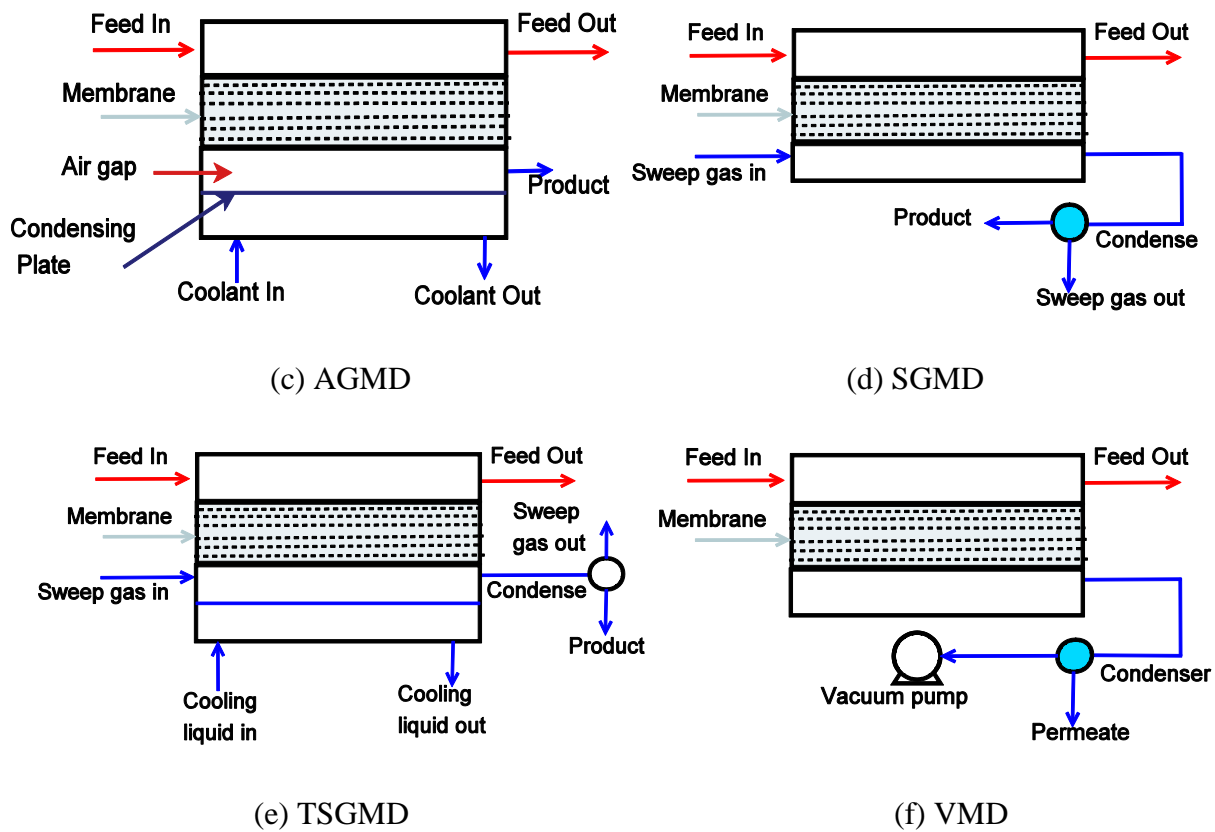


**Figure 2.1 various membrane distillation techniques**

The comparison of different MD configurations is given by Table 2.1.

**Table 2.1: Advantages and disadvantages of different MD configurations**

Configurations	Advantages	Disadvantages
Direct Contact Membrane Distillation	<ol style="list-style-type: none"> <li>1. Permeate flux is high.</li> <li>2. Simple in design and easy to operate.</li> <li>3. Recovery of internal heat is possible</li> </ol>	<ol style="list-style-type: none"> <li>1. Effect of concentration and temperature polarization is high.</li> <li>2. Thermal efficiency is low.</li> <li>3. Higher purity cannot be obtained</li> </ol>
Air Gap Membrane Distillation	<ol style="list-style-type: none"> <li>1. Thermal Efficiency is high.</li> <li>2. Heat recovery is possible.</li> </ol>	<ol style="list-style-type: none"> <li>1. Lower permeate flux due to resistance.</li> <li>2. Large footprint.</li> </ol>
Sweeping Gas Membrane Distillation	<ol style="list-style-type: none"> <li>1. Heat loss by conduction is low.</li> <li>2. Mass transfer rate is higher.</li> </ol>	<ol style="list-style-type: none"> <li>1. External condenser is required.</li> <li>2. Recovery of heat is very difficult.</li> <li>3. Flux reduction due to the high sweeping gas temperature</li> </ol>
Vacuum Membrane Distillation	<ol style="list-style-type: none"> <li>1. Permeate flux is higher.</li> <li>2. Heat loss due to conduction is lower.</li> </ol>	<ol style="list-style-type: none"> <li>1. Pore wetting is possible due to vacuum.</li> <li>2. Heat recovery is difficult.</li> </ol>

Compared to other membrane distillation Techniques, higher permeate flux can be obtained due to higher partial pressure gradients in vacuum membrane distillation. The major drawback of VMD process is higher energy requirement to heat the feed solution to the desired temperature. So, to overcome this problem, the recovery of heat from permeate is necessary, and various internal and external heat recovery techniques are used in MD. A heat pump is also newer technology for the transfer of heat from the low-temperature energy source to a high-temperature energy source like a refrigerator by Zhang et al. (2015). Wang et al. (2009) studied the lithium bromide absorption refrigeration system for desorption in Vacuum membrane distillation system. The PVDF hollow fiber membrane module was used for carried out experiments, and the high rejection ratio of 99.99% was observed for lithium bromide solution.

One of the most important benefits provided by VMD is coupling with possibly available various industrial applications in different fields like osmotic distillation, multi-stage flash evaporation, reverse osmosis and direct contact membrane distillation, etc. and renewable energy sources such as geothermal energy, solar energy, etc. In the food industry, the VMD process coupled with osmotic distillation played a significant role in the recovery of volatile aroma compounds because aroma compounds can't bear higher temperatures. Bagger-Jørgensen et al. (2004) studied the recovery of seven black aroma compounds from current black juice at low temperature ranges from 10 to 45 °C at lab scale. Knudsen diffusion is found as the significant mechanism of vapor transport across the membrane by obtaining the linear relationship between the permeate and vapor pressure difference experimentally. The highest amount of more volatile aroma compounds mainly esters were achieved at 10 °C and 400 l/h. In VMD, 68% to 83% highly volatile and 32% to 38% poorly volatile aroma compounds were extracted from the feed. Due to low operating temperature, VMD is considered a suitable technique for conservation of thermosensitive aroma compounds of various fruit juices in its original qualities as compared to other conventional processes. Hasanoglu et al. (2012) also studied the coupled system of osmotic distillation with vacuum membrane distillation for recovery of four volatile aroma compounds namely ethyl acetate, ethanol, butanol, and acetaldehyde from aqueous fruit juices. 74.5% volatile aroma compounds were recovered from feed on the distillate side due to low feed temperature and high vacuum pressure, which is much higher compared to traditional thermal systems. It was found that recovery was significantly affected by membrane properties such as porosity, the affinity of aroma compounds with the hydrophobic membrane surface as well as operating variables like feed circulation velocity and vacuum pressures.



In desalination plant, Xing et al. (2016) utilized the Polytetrafluoroethylene hollow fiber membranes modules to test the performance of integrated multi-effect vacuum membrane distillation with multi-effect flash evaporation system for production of 2.0 t/d fresh water. The hollow fiber membrane module was used for experiments with specifications as membrane pore size 0.2 $\mu$ m, membrane porosity 50%, membrane thickness 0.4mm, fiber inner diameter 0.8 mm, fiber number 2000 pcs and effective fiber length 0.7m. The exponential increment in the permeate flux by 55% was observed on increasing feed temperature from 75 °C to 90 °C. While 25% increment in water production and 4.5% decrement in gain output ratio (GOR) were observed on improving the vacuum degree from 70 kPa to 82 kPa. The minor effects of feed flow rate and the feed concentration were found on permeate flux.

Carnevale et al. (2016) also studied the treatment of oil mill wastewater (OMWW) using direct contact and vacuum membrane distillation to recover polyphenols and to purify the steam so that it can be disposed of without any environmental problem. The commercially available polypropylene membranes are used in the capillary membrane module to treat the OMWW. The rejection of up to 99.9% was observed at 50 °C with around 6.5 kg/m<sup>2</sup>.h permeate flux in DCMD, but after 20 hours 25% reduction in permeate flux was obtained. VMD is coupled to DCMD to enhance the process efficiency, and the DCMD waste with 2500 ppm was treated at 50 °C. The permeate flux was obtained around 19 kg/m<sup>2</sup>.h with the rejection of 99% and thus the DCMD followed by VMD was found as the promising alternative for treatment of oil mill wastewater in a single unit. Mericq et al. (2010) also studied desalination of seawater brine using vacuum membrane distillation coupled with the reverse osmosis to treat reverse osmosis concentrated brine to increase the global recovery of the system. Three different types of synthetic salt solutions are used as feed solution at various salt concentrations such as 94.2 g/L, 148.6 g/L and 291.1 g/L which only containing mineral part of seawater. Due to coupling, the water production was more than doubled, and the recovery was increased up to 89% which was 40% in the case of only the RO system and the rejected volume reduced by a factor of 5.5. The linear decrement in permeate flux was seen for increasing the permeate pressure from 2000 Pa to 10000 Pa while the exponential increment in permeate flux was seen on increasing feed temperature from 20 °C to 70 °C. For obtaining higher permeate flux ranges 7 l/m<sup>2</sup>h to 17 l/m<sup>2</sup>h using VMD for concentration RO brines from 64 g/l to 300 g/l, the optimized conditions of operating parameters was found 6000 Pa, 50 °C, and 4000 as permeate pressure, feed temperature and Reynolds number respectively. The fouling on the membrane surface was observed due to higher feed concentration using SEM analysis. During the continuous operation,

the decrement in permeate flux and permeability was obtained but after that permeate flux and permeability found constant which emphasizes that the impact of scaling, organic fouling and biofouling was very limited. The fouling was mainly responsible due to the calcium crystals deposition. The deposition of various crystals such as Na, K, Ca, Mg, Br was confirmed using the EDS analysis. This flouling can be easily removed by washing of membrane with water.

## 2.2. Characterization of membrane for VMD

The performance of the vacuum membrane distillation process has a direct relationship with the structural and physiochemical parameters of the membrane. The membranes used in VMD are commercially available in flat sheet and capillary forms(Chernyshov et al. 2003) and the essential membrane properties required for VMD are given by many authors(Khayet & Matsuura 2001; Lawson & Lloyd 1997; Findley 1967; Khayet & Matsuura 2003; Bier & Plantikow 1995; Khayet, Mengual & Zakrzewska-Trznadel 2005; Couffin et al. 1998). A good hydrophobic membrane possesses lower mass and heat transfer resistances, high liquid to entry pressure, good thermal conductivity, and high chemical resistance to the feed solutions. The relationship between flux and membrane parameters is given as follows(Lawson & Lloyd 1997):

$$N \propto \frac{r^a \varepsilon}{\delta_m \tau} \quad (2.1)$$

Where  $N$  is the molar flux,  $r$  is the mean pore size of the membrane,  $a$  factor has value equals to 1 and 2 for Knudsen and viscous flow respectively, &  $\varepsilon$  is the membrane porosity,  $\delta_m$  thickness of the membrane,  $\tau$  is the membrane tortuosity. The effect of the different membrane parameters is discussed in the subsequent sections in detail.

### 2.2.1. Membrane Thickness

The membrane thickness has a significant role in the VMD process. The permeate flux is inversely proportional to the thickness of the membrane because on increasing thickness the mass transfer resistances increases but the heat loss from the membrane is reduced. So, to achieve the permeate flux, membrane should be as thin as possible, while to reduce the heat transfer losses by conduction the membrane should be as thick as possible (Lawson & Lloyd 1997; Schofield et al. 1987; Khayet et al. 2003; Lagana et al. 2000; SAKAI et al. 1986). By using the computer simulation, it was found that the optimum thickness of the membrane should be in the range of 30 to 60  $\mu\text{m}$ (Lagana et al. 2000) but Upadhyaya et al. (2015) used a PTFE membrane of 175 $\mu\text{m}$  thickness with thermal conductivity 0.28 W/m.K in VMD for desalination.

### 2.2.2. Membrane Porosity

Membrane porosity is defined as the ratio of the volume of the pores to the total available volume of the membrane. The permeate flux is directly proportional to the porosity of the membrane because it provides the larger evaporation surface area and also the heat loss by conduction is lower. The porosity ( $\varepsilon$ ) of the membrane can be determined by the Smolder-Franken equation (2.2).

$$\varepsilon = 1 - \frac{\rho_m}{\rho_{pol}} \quad (2.2)$$

Where  $\rho_m$  and  $\rho_{pol}$  are the densities of the membrane and the polymeric material respectively. Generally, membrane porosity varied from 30 to 85%. The higher porous membrane exhibit lower heat loss because the heat transfer coefficient depends on the gases filled in the pores of the membrane which results in the higher flux (Lawson & Lloyd 1997; Schofield et al. 1987; Schofield, Fane, Fell, et al. 1990; Schofield, Fane & Fell 1990; Khayet, Mengual & Matsuura 2005).

### 2.2.3. Membrane Tortuosity

In VMD processes, the vapor molecules which diffuse through the hydrophobic membranes pass through tortuous path. It happens because the pores of the membranes are not straight so pore tortuosity of the membrane is defined as the deviation of the average length of the pores structure compared to the membrane thickness from the cylindrical shape. Tortuosity ( $\tau$ ) is considered as the correction factor as a value of 2 in various VMD processes which is used to predict the flux across the membrane (Lawson & Lloyd 1997; Schofield et al. 1987; Bandini et al. 1997; Phattaranawik et al. 2003a; KHAYET et al. 2004; Khayet et al. 2001) while the highest value of the tortuosity factor was reported as 3.9 (Fernandez-Pineda et al. 2002). The tortuosity ( $\tau$ ) of the membrane is proportional to the thickness of the membrane, and due to this fact, the permeate flux is inversely proportional to the tortuosity factor. The tortuosity of the membrane can be determined using the Macki-Mearns equation (El-Bourawi et al. 2006):

$$\tau = \frac{(2 - \varepsilon)^2}{\varepsilon} \quad (2.3)$$

Upadhyaya et al. 2011 carried out the sensitivity analysis of different parameters such as membrane characteristics, feed inlet temperature, downstream pressure and diameter of pores for vacuum membrane distillation system. They were found that the normalized sensitivity was positive in all cases except downstream pressure which indicates that the permeate flux decreased with increase in downstream pressure.

#### 2.2.4. Liquid Entry Pressure and Wettability

In VMD processes, porous and hydrophobic membranes are used which does not allow to penetrate the liquid molecules through the pores of the membrane until the pressure applied on the membrane does not exceed from the limit of the membrane. This limited pressure is known as the liquid entry pressure of the membrane after this the liquid molecules can penetrate through pores of the membrane(Banat et al. 2007a; Li & Sirkar 2005). LEP is mostly affected by the pore size and the hydrophobicity of the membrane. If the maximum pore size of the membrane increases then there is more chance of the membrane pore wetting(Banat et al. 2007b). The LEP can be estimated using the following equation(Saffarini et al. 2013):

$$\Delta P = P_f - P_p = \frac{-2B_m\gamma_l \cos \theta}{r_{max}} \quad (2.4)$$

Where  $\Delta P$  is defined as the difference in the hydraulic pressure ( $P_f$  &  $P_p$ ) on the feed and the permeate side of the membrane.  $B_m$  is the geometric pore coefficient which is considered as 1 for cylindrical pores.  $\gamma_l$  is the surface tension of the liquid.  $\theta$  is the contact angle of the water on the membrane surface; it should be as high as possible for the strong hydrophobicity of the membrane. The value of contact angle varied from  $107^\circ$  to  $109^\circ$  for PVDF membranes;  $120^\circ$  for PP membranes and  $108^\circ$  to  $115^\circ$  for Teflon surfaces membranes(Zhou et al. 2014). The ceramic membranes have higher contact angle varied from  $177^\circ$  to  $179^\circ$  so these are more hydrophobic as compared to polymeric membranes.  $r_{max}$  is the maximum pore size of the membrane (Dong et al. 2014).

In VMD processes, the wettability of the membrane pores is higher due to the higher pressure drop across the membrane. So, the membrane should have a minimum pore size and the contact angle should high to prevent the pore wetting.

#### 2.2.5. Thermal Conductivity

Thermal conductivity of the membrane depends on the thermal conductivity of the polymeric material and the air. Thermal conductivity of the membrane should be low to reduce the heat transfer losses due to conduction through the membrane. Generally, thermal conductivity of the membrane is defined using the volume average of conductivities of polymeric material and air as follows(Zhang, Dow, et al. 2010):

$$\lambda_m = (1 - \varepsilon)\lambda_p + \varepsilon\lambda_a \quad (2.5)$$

where  $\lambda_m$  is the thermal conductivity of the membrane.  $\lambda_p$  is the thermal conductivity of the polymeric material and  $\lambda_a$  is the thermal conductivity of the air or gas. The heat transfer coefficient through the membrane can be computed as follows:

$$h_m = \frac{\lambda_m}{\delta_m} \quad (2.6)$$

Where  $h_m$  is the coefficient of heat transfer and  $\delta_m$  is the membrane thickness. Phattaranawik, Jiraratananon, and Fane 2003b also proposed the method of calculation of thermal conductivity based on the volume-average of gas (or air) and polymeric material resistances as follows:

$$\lambda_m = \left[ \frac{\varepsilon}{\lambda_a} + \frac{(1-\varepsilon)}{\lambda_p} \right]^{-1} \quad (2.7)$$

### 2.2.6. Membrane pore size and pore size distribution

The pore size of the membranes ranges from 100 nm to 1  $\mu$ m for VMD processes and it was found that the permeate flux of VMD is directly proportional to the membrane pore size. It is due to the fact that the mass transfer through the membrane is controlled by Knudsen diffusion if the pore size of the membrane is small, although, Knudsen-viscous transition diffusion is the controlling mechanism when the pore size of the membrane is large which shows higher permeate flux (Schneider et al. 1988; Cath et al. 2004). But in VMD, the membrane pore wetting is high due to the higher trans-membrane pressure difference so the small pore sizes are desired to prevent the pore wetting.

The pore size distribution is considered in the VMD membranes other than the uniform pore size. It was found that more than one transport mechanism takes place simultaneously in the system depending upon the pore size of the membrane on particular operating conditions. The structural properties and permeation parameters are used to analyze the pore size and pore size distribution for VMD membranes. The effect of the pore size distribution is rarely studied in VMD (KHAYET et al. 2004; Khayet & Matsuura 2004). The various methods for determining the pore size distribution are as follows:

#### 2.2.6.1. Scanning Electron (SE) & Atomic Force (AF) Microscopy

SEM is used to study the geometry of the pores of the membrane by analyzing the top and bottom surfaces. It is used to estimate the surface morphology, pore size, and pore size distribution. In this technique, the electron beam with high energy strike on the atom of the surface of the sample which increases the energy level of the atoms of the surfaces. The atoms with higher energy liberated from the surface of the sample which determines the micrograph. A thin layer of the gold is coated to protect the surface of the sample. M Khayet, Mengual, and Zakrzewska-Trznadel 2005 used the SEM technique to analyze the surface morphology of the

membrane. Franken et al. 1987 are used SEM technique to analyze the thickness of the hydrophobic ceramic membranes also.

AFM is the high resolution newly developed technique which is used to study the three-dimensional topographical surface morphology of the membranes down to the nanometer scale. Firstly, it was developed by Binnig and Gerber 1986, and the main benefit of this technique is that no sample preparation is required as in SEM analysis. Albrecht and Quate 1988 first used this technique to analyze the surface morphology of the polymeric material then this technique is extensively used for studying various types of membranes and materials (Khulbe & Matsuura 2000; Sorenson 1999). Nowadays, it is extensively used for MD membranes (KHAYET et al. 2004; Khayet 2005) for obtaining the information regarding surface morphology, pore density, porosity, pore size, etc..

#### 2.2.6.2. Gas permeation method (Permeability test)

Gas permeation test is one of the famous method originally given by Yasuda and Tsai 1974. It is used to determine mean not only pore size but also the effective porosity of the membrane used in the VMD. In this, the gas (generally nitrogen) is allowed to flow at the different trans-membrane pressures; the rate of flow of gas is controlled by the gas flow meter. Figure 2.2 shows the experimental setup used for the gas permeation test for the flat sheet membranes (Yasuda and Tsai 1974). The total gas flow rate through the dry pores of the membrane can be regulated by the Knudsen-Poiseuille mechanism, and the total flux  $J_{K-P}$  can be given as:

$$J_{K-P} = \frac{N_{K-P}}{\Delta P} = \frac{8 \varepsilon r}{3 \tau} \frac{1}{\sqrt{2\pi RMT}} + \frac{\varepsilon r^2}{\tau \delta} \frac{p_m}{8\eta RT} \quad (2.8)$$

Equation (2.8) can be rearranged as:

$$\frac{N_{K-P}}{\Delta P} = A_0 + B_0 p_m \quad (2.9)$$

Where  $A_0$  and  $B_0$  can be expressed as

$$A_0 = \frac{8 \varepsilon r}{3 \tau} \frac{1}{\sqrt{2\pi RMT}} \quad (2.10)$$

$$B_0 = \frac{\varepsilon r^2}{\tau \delta} \frac{1}{8\eta RT} \quad (2.11)$$

Equation (2.10) and (2.11) are used to calculate the mean pore size and the effective porosity of the membrane.

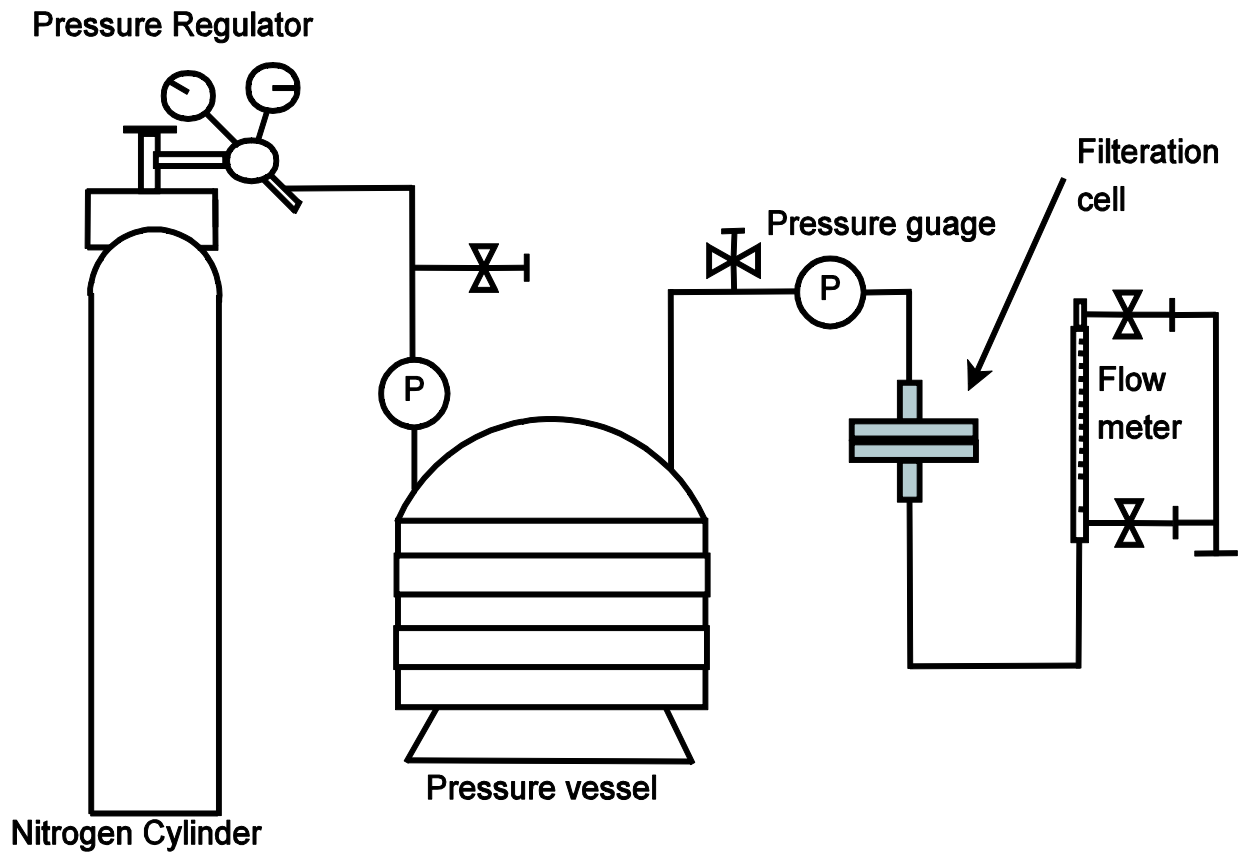


**Figure 2.2: Gas permeation setup**

The commercial porous hydrophobic membranes made of PTFE, PP and PVDF are used in flat sheet, tubular and capillary forms. Initially, these membranes are developed for microfiltration, but due to fulfilling the requirements of the membrane in VMD these are used in VMD processes. The choice of the membrane for the VMD process depends upon the higher permeate flux, low thermal conductivity, high separation factor under the given operating conditions and feed solutions. Generally, these properties of the membrane should be provided by the manufacturers to help customers to select their appropriate membrane. Table 2.2 shows the Commercially available membranes used by some researchers in their work.

**Table 2.2: Commercially available membranes used by some researchers**

Membrane Material	Manufacturer	Membrane Type	Pore size ( $\mu\text{m}$ )	Membrane Thickness ( $\mu\text{m}$ )	Porosity (%)	LEP (bar)	References
PTFE	Gore	Flat sheet	0.20	64	90	3.68	(Khayet & Matsuura 2011)
PVDF	Gore	Flat sheet	0.45	77	89	2.88	(Khayet & Matsuura

							2011)
PTFE/PP	Gore	Flat sheet	0.2	184	44	4.63	(Khayet & Matsuura 2011)
PTFE	Millipore	Flat sheet	0.22	175	40 & 70	4.2	(Meriq et al. 2010; Pangarkar et al. 2011)
PVDF	Millipore	Flat sheet	0.22	60 & 35	70	2.6	(A. Criscuoli et al. 2013)
PVDF	Millipore	Flat sheet	0.45	110	75	1.05	(Banat 1994)
PP Accurel 2E	Millipore	Flat sheet	0.2	163	75	6.7	(Safavi & Mohammadi 2009)
PP	Millipore	Flat sheet	0.45	170	75	2	(Banat 1994)
PE	Millipore	Flat sheet	0.2	91	70	6.7	(Banat 1994)
PP <sup>a</sup>	-	Capillary Membranes	0.2	1500	75	-	(A Criscuoli et al. 2008)
PP Accurel 2E	Membrana	Flat Sheet	0.2	163	75	-	(Mohammadi & Akbarabadi 2005)
PVDF <sup>b</sup>	-	Hollow fiber membranes	0.162	-	60	-	(Wu et al. 2006)
PP <sup>c</sup>	Membrana	Capillary Membranes	0.20	510	75	-	(A Criscuoli et al. 2008)
PVDF	Tianjin Motian membrane Eng & Techco. Ltd.	Hollow fiber membranes	0.16	150	85	-	(Yang et al. 2011)
PP <sup>d</sup>	-	Hollow fiber membranes	0.05-0.3	-	60	-	(Shao et al. 2013)
PP <sup>e</sup> PVDF <sup>e</sup> PTFE <sup>e</sup>	DD water group Co. Ltd. & SOA Tianjin China	Hollow fiber membranes	0.28 0.14 0.26	- - -	50.76 83.82 45.07	1.32 2.97 1.67	(Hou et al. 2015)
PTFE	-	Flat sheet	0.22	230	85	-	(Mohammadi & Kazemi 2014)
PP PP	Membrana (Germany)	Flat sheets	0.2 0.45	91 170	70 75	6.7 2	( a. Criscuoli et al. 2013)



PVDF			0.2	60	70	3.5	
PVDF			0.2	35	70	2.5	
PTFE	GE	Flat sheet	0.2	179	70-75	-	(Naidu et al. 2014)
PP	Membrana	Flat sheet	0.2	91	70	-	( a. Criscuoli et al. 2013)
PP <sup>f</sup>		Capillary	0.2	400	70	-	

<sup>a</sup>Shell and tube module: Effective filtration area, 0.036 m<sup>2</sup>; Inside diameter of the tube, 5.5 mm; Inside diameter of shell , 25 mm; Number of tubes 3.

<sup>b</sup>Hollow fiber membrane module: Total membrane area 0.159 m<sup>2</sup>; Inside diameter of hollow fibers, 0.52 mm; Effective length of the fibers, 0.51 m; Number of hollow fibers 143; Packing density, 2000 m<sup>2</sup>/ m<sup>3</sup>.

<sup>c</sup>Capillary membrane module: effective membrane area 0.0028 m<sup>2</sup>; Inner diameter 1.79 mm; Fibers in the module, 3.

<sup>d</sup>Hollow fiber membrane module: Inner diameter, 0.028 mm; number of fibers, 60; Useful length of the fiber, 12 cm.

<sup>e</sup>Hollow fiber membrane module: Effective membrane area, 50.2, 150.7, 198.4 cm<sup>2</sup>; Inner diameter, 0.20, 0.90, 0.80 mm with contact angle 94.8°, 99.5°, 129.3° for PP, PVDF and PTFE respectively.

<sup>f</sup>Capillary module: Effective membrane area, 0.1 m<sup>2</sup> ; Inner fiber diameter, 1.8 mm ; Fiber length, 47 cm ; fibers in membrane module 40.

## 2.3. Membrane Modules

The various membrane modules used in vacuum membrane distillation are discussed below. The different types of lab scale membrane module designs are shown in Figure 2.3 for flat sheet membranes as well as capillary membranes.

### 2.3.1. Plate and frame module

It is observed throughout the VMD literature(Safavi & Mohammadi 2009; Mohammadi & Safavi 2009; Lawson & Lloyd 1996a) that the laboratory-scale plate and frame modules are designed for the commercial flat sheet membrane (dimensions ranging from 10x10 to 30x300 cm<sup>2</sup> and diameter 13 to 142 mm). In this module, flat sheet membranes can be easily changed, replaced, examined or cleaned but there is a requirement of the support to hold the membrane if the flow of the feed solution is high. The membrane and the support plates with spacers are stacked together that are placed in appropriate place. The support is chosen, should have low heat and mass transfer resistances and enough strength to prevent rupture and deflection of the membrane. The packing density can vary between 100 m<sup>2</sup>/m<sup>3</sup> to 400 m<sup>2</sup>/m<sup>3</sup> depending on the number of membrane sheets. In these configurations feed solution are allowed to flow in the radial direction(Safavi & Mohammadi 2009; Mohammadi & Safavi 2009; Fan & Peng 2012; Bandini et al. 1997; Jun et al. 2006). Lawson and Lloyd 1996a; Lawson and Lloyd 1996b used

the laboratory scale modules with small cross sectional area of 0.63cm\*0.63cm to avoid the problem of support.

### **2.3.2. Tubular module**

Tubular membranes are housed inside the stainless steel glass shell and tube module. The support is not required in this module and the membrane cannot be replaced easily because it is the integrated part of it. Low tendency to fouling and high effective area makes it more attractive. The operating cost of the tubular module is high and the packing density of the module is low. Generally, the diameter of the tubular membranes vary from 1.0 cm to 2.5 cm with the packing density in shell and tube modules around 300 m<sup>2</sup>/m<sup>3</sup> In VMD configurations, tubular ceramic membranes are used to treat the aqueous solution of NaCl and more than 99% rejection of the salt is observed by Cerneaux et al. 2009.

### **2.3.3. Hollow fibre membrane**

In VMD system, thousands of hollow fibre membranes with diameter below 1mm are bundled and fixed in the shell and tube unit(Xu et al. 2006; Hasanouglu et al. 2012). There are two types of the flow arrangements; first outside/in shell and tube arrangements, the feed solution flows outside the shell of fibre and the permeate is collected inside the shell of the fibres(Wu et al. 2006; X. Wang et al. 2009; Z. Wang et al. 2009). Second, inside/out shell and tube arrangements in which the feed solution flows through inside the shell of the fiber and the permeate is collected from the outside of the fibre of the module(Hasanouglu et al. 2012). The hollow fiber membranes are quite cheaper and packing density is higher as compared to other modules. However, hollow fiber membrane modules have several disadvantages such as difficult to clean; low resistance to fouling and replacement of the membrane is difficult.

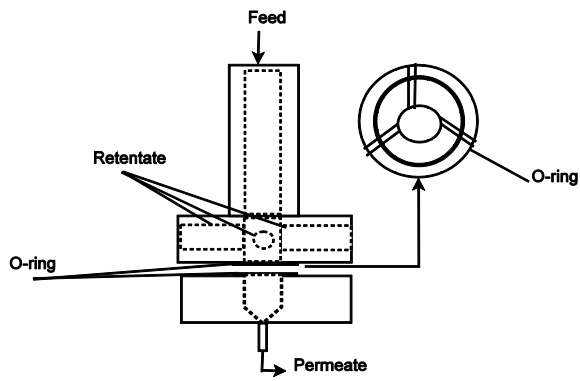
### **2.3.4. Capillary module**

In Capillary module, a large number of capillary tubes with a diameter range between 1 to 3mm are assembled in a single module. There is no need for the support (Self-supporting) for the capillaries, and the free ends of the capillary fibers are potted with different agents such as silicone rubber, epoxy resins, etc. There is also two types of flow arrangements(outside/in & inside/out) as in the hollow fiber membrane modules, and the choice of the flow arrangements depends on the different operating parameters such as pressure drop, membrane available, etc.(Mengual et al. 2004; Wirth & Cabassud 2002). The packing density of the capillary module is about 600 m<sup>2</sup>/m<sup>3</sup> to 1200 m<sup>2</sup>/m<sup>3</sup> as compared to hollow fiber membrane but the capillary

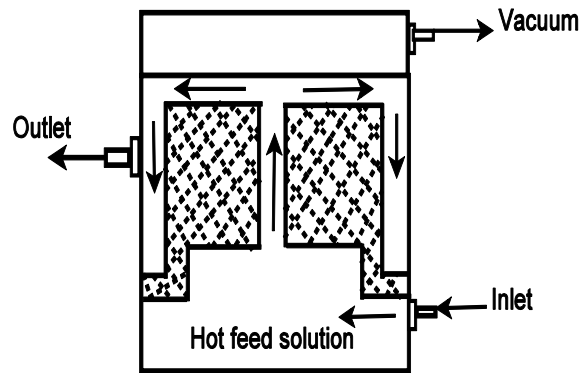
module is easier to clean and liquid channeling is better due to more uniform distribution of the capillaries inside the module as compared to hollow fibre membrane.

#### **2.3.5. Spiral wound module**

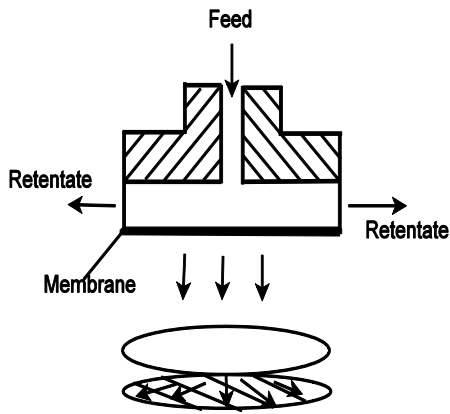
Gore & Associated Co. and Hanbury & Hodgkiess first introduced the use of the spiral wound module in MD processes. To form a spiral wound membrane module, the feed and permeate spacers, the flat sheet membrane and the supports are rolled and enveloped around the perforated central collection tube(Gore 1982; Hanbury & Hodgkiess 1985). The packing density of the spiral wound module is high and depending upon the channel height the packing density ranges from  $300 \text{ m}^2/\text{m}^3$  to  $1000 \text{ m}^2/\text{m}^3$ . It has higher energy consumption and average tendency to the membrane fouling(Hanbury & Hodgkiess 1985).



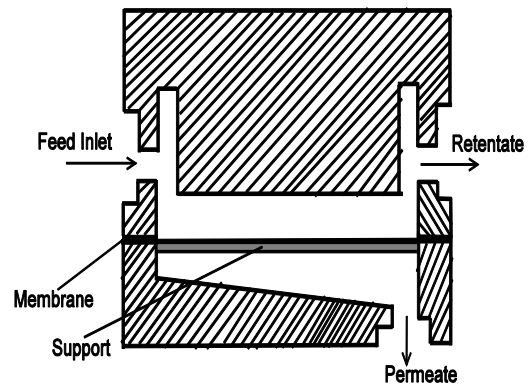
(a) Flat sheet membrane module



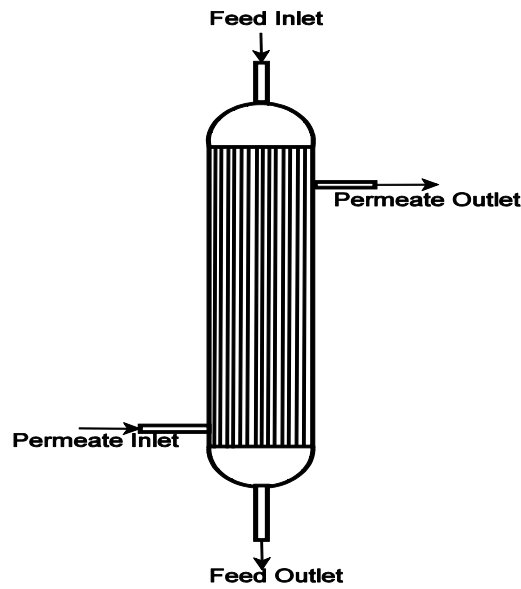
(b) Flat sheet membrane module



(c) Flat sheet membrane module



(d) Flat sheet membrane module



(e) hollow fibre, capillary, and tubular membrane module

**Figure 2.3: Schematic diagram of different laboratory-scale membrane modules**

## 2.4. Transport mechanism in VMD

Simultaneous heat and mass transfer take place through the membrane during the process in VMD. Heat transfer is carried out from liquid to solid and then solid to gas phases, while the mass transfer is carried out from liquid to gas phases.

### 2.4.1. Heat Transfer

Heat transfer is a very important phenomena in VMD configuration because it is considered as the rate controlling step in the processes. The driving force in the VMD is the vapor pressure gradient across the membrane which results due to the temperature difference across the membrane. In VMD, Heat transfer is carried out in three ways: (i) heat transfer from the bulk feed solution to the membrane surface through the thermal boundary layer; (ii) Heat transfer by conduction through the membrane and gas which is filled in membrane pores; (iii) Heat transfer from the membrane surface to the permeate side of the membrane. So, the overall heat transfer coefficient for the VMD process can be obtained from the resistances in series model (Lawson & Lloyd 1997; Khayet et al. 2000b; Termpiyakul et al. 2005):

$$\frac{1}{H} = \frac{1}{h_f} + \frac{1}{h_m + (J\Delta H_v / \Delta T_m)} + \frac{1}{h_p} \quad (2.12)$$

Where  $H$  is the overall heat transfer coefficient;  $h_f$ ,  $h_m$  and  $h_p$  are the individual heat transfer coefficient of bulk feed side, membrane surface and permeate side respectively;  $J$  is the permeate flux;  $\Delta H_v$  is the heat of vaporization and  $\Delta T_m$  is the temperature difference across the both sides of the membrane.

In VMD, heat transfer resistances on the permeate side is negligible due to low pressure or vacuum is applied on the downstream side of the membrane (KHAYET et al. 2004; Izquierdo-Gil & Jonsson 2003; Couffin et al. 1998; Izquierdo-Gil et al. 2004). So equation (2.12) can be rearranged as:

$$\frac{1}{H} = \frac{1}{h_f} + \frac{1}{h_m + (J\Delta H_v / \Delta T_m)} \quad (2.13)$$

#### 2.4.1.1. Heat transfer through feed bulk side boundary layers

Convective heat transfer mechanism occurs during the heat transfer from the bulk feed side to the membrane surface can be computed as follows:

$$Q_f = h_f(T_f - T_{fm}) \quad (2.14)$$

Where  $Q_f$  is the heat transfer flux through the feed side boundary layer,  $T_f$  is the feed bulk temperature,  $T_{fm}$  is the feed side membrane surface temperature,  $h_f$  is the convective heat transfer coefficient.

From equation (2.14), it can be seen that the rate of heat flow is more when the temperature difference across the bulk feed side and the membrane surface is more. The thermal boundary layer formed on the feed side membrane surface poses resistances to heat transfer which results in the lower temperature difference at liquid/membrane interface than that applied at the feed bulk phase. Thus, the driving force for mass transfer is negatively affected and this phenomenon is known as temperature polarization effect described in subsequent section.

The convective heat transfer coefficient  $h_f$  can be calculated using various empirical correlations developed using different dimensionless parameters for different flow regimes (Lawson & Lloyd 1997; Mengual et al. 2004; Serth & Lestina 2014; Khayet, Mengual & Zakrzewska-Trznadel 2005). The simplest form of heat transfer correlations is as follows:

$$Nu = a(Re)^b(Pr)^c \quad (2.15)$$

Where  $Nu$ ,  $Re$  and  $Pr$  are the dimensionless Nusselt number, Reynolds number and the Prandtl number while  $a$ ,  $b$  and  $c$  are the characteristics constants of the module organization and the flow regimes.

The bulk feed side heat transfer coefficient can be obtained from Nusselt number:

$$Nu = \frac{h_f d_h}{k_l} \quad (2.16)$$

Where  $d_h$  is the feed channel hydraulic diameter,  $k_l$  is the thermal conductivity of the feed solution. The Reynolds number and Prandtl number can be defined as:

$$Re = \frac{\rho v d_h}{\mu} \quad (2.17)$$

$$Pr = \frac{C_p \mu}{k_l} \quad (2.18)$$

Where  $\rho$ ,  $v$ ,  $\mu$  and  $C_p$  are density, velocity, viscosity and heat capacity respectively.

The above empirical correlation was fitted using the tool solver in MS Excel, which gives the optimum values of the constant  $a$ ,  $b$ , and  $c$  by minimizing the error between experimental and

calculated values using Newton's method. Various heat transfer correlations developed by various researchers are shown in Table 2.3.

**Table 2.3: Various Heat Transfer Correlations**

Heat Transfer Correlations	Descriptions	VMD Module	References
$Nu = 1.86(\text{Re} \cdot \text{Pr} \cdot d_h / L)^{1/3}$	Laminar flow; Re<2100	Flat-sheet module; hollow fiber module; tubular module; capillary module	(Li & Sirkar 2005; Fan & Peng 2012; Mengual et al. 2004; Al-Asheh et al. 2006)
$Nu = 3.66 + \frac{0.0668(\text{Re} \cdot \text{Pr} \cdot d_h / L)}{1 + 0.045(\text{Re} \cdot \text{Pr} \cdot d_h / L)^{1/3}}$	Laminar flow at constant wall temperature	hollow fiber module	(Sarti et al. 1993)
$Nu = 1.04 \text{Re}^{0.4} \text{Pr}^{0.36} \left( \frac{\text{Pr}}{\text{Pr}_w} \right)^{0.25} F_c$	10<Re<500	hollow fiber module	(Li & Sirkar 2005; Wang et al. 2011)
$Nu = 0.116(\text{Re}^{2/3} - 125) \text{Pr}^{1/3} \left[ 1 + (d_h / L)^{2/3} \right] (\mu_b / \mu_l)^{0.14}$	Transitional flow; 2100<Re<10000	Capillary module; Flat sheet module	(Mengual et al. 2004; Soni et al. 2008)
$Nu = 0.023 \text{Re}^{0.8} \text{Pr}^n$	Turbulent flow with n=0.4 for heating, n=0.3 for cooling Re>10000	Flat sheet module; tubular module	(Al-Asheh et al. 2006; Khayet & Matsuura 2004; Lawson & Lloyd 1996a; KHAYET et al. 2004)
$Nu = 0.04 \text{Re}^{0.75} \text{Pr}^{0.33}$	Turbulent flow; for a rectangular pipe	Flat sheet module	(Izquierdo-Gil & Jonsson 2003)
$Nu = 0.023 \text{Re}^{0.8} \text{Pr}^{1/3} (\mu_b / \mu_l)^{0.14}$	Turbulent flow 2500 < Re < 1.25*10 <sup>5</sup>		(Lawson & Lloyd 1997)
$Nu = 0.023 \text{Re}^{4/5} \text{Pr}^n (\mu_b / \mu_l)^{0.14}$	Turbulent flow with n=0.4 for heating, n=0.3 for cooling Re>10000		(Srisurichan et al. 2006)
$Nu = 0.023 \left( 1 + \frac{6d}{L} \right) \text{Re}^{0.8} \text{Pr}^{1/3}$	Turbulent flow		(Termpiyakul et al. 2005; Phattaranawik et al. 2003a; Phattaranawik et al. 2003b)
$Nu = 1 + 1.44 \left( 1 - \frac{1708}{\text{Re}} \right) + \left[ \left( \frac{\text{Re}}{5830} \right)^{1/3} - 1 \right]$	not mentioned		(Sarti et al. 1985)

$Nu = 0.036 Re^{0.96} Pr^{0.33} \left(\frac{d}{L}\right)^{0.055}$	Turbulent flow in Tube, $10 \leq d/L \leq 400$		(Izquierdo-Gil et al. 2008)
$Nu = 0.036 Re^{0.8} Pr^{0.33} \left(\frac{d}{L}\right)^{0.055}$	Turbulent flow		(Curcio & Drioli 2005)
$Nu = 0.298 Re^{0.646} Pr^{0.316}$	Laminar flow, $150 < Re < 3500$	Plate and frame module	(Gryta et al. 1997)
$Nu = 0.74 Re^{0.2} (Gr Pr)^{0.1} Pr^{0.2}$	Laminar flow	Plate and frame module	(Gryta et al. 1997)
$Nu = 1.86 Re^{0.96} Pr^{1/3} \left(\frac{d}{L}\right)^{1/3}$	Laminar flow		(Izquierdo-Gil et al. 2008)
$Nu = 1.86 Re^{1/3} Pr^{1/3} \left(\frac{d}{L}\right)^{1/3} \left(\frac{\mu_b}{\mu_l}\right)^{1/7}$	Laminar flow		(Tun et al. 2005; Tomaszewska et al. 1994)
$Nu = 0.042 Re^{0.59} Pr^{0.33}$		Shell and tube Capillary membrane	(Mengual et al. 2004)
$Nu = 0.43 Re^{0.837} Pr^{0.33}$	Laminar Flow	Flat sheet membrane Module	(Upadhyaya et al. 2016b)

#### 2.4.1.2. Heat transfer by conduction through the membrane

Heat transfer by conduction through the membrane is the fraction of the heat transferred by conduction through both the membrane matrix and gas filled in the pores. At the membrane surface, hot feed evaporates into vapors and transferred through the membrane due to hydrophobic nature of the membrane at a transfer rate  $Q_v = J \Delta H_v$ , where  $Q_v$  is the latent heat carried through the membrane,  $J$  is the rate of mass transfer and  $\Delta H_v$  is the latent heat of vaporization. Typically 50-80% heat is carried out by water vapors in the form of latent heat and 20-50% heat is lost due to conduction (Lawson & Lloyd 1997; Fane et al. 1987; Lian et al. 2016; Zhong et al. 2016).

In VMD, heat loss through conduction across the membrane and the resistances due to thermal boundary layer on permeate side are negligible due to lower pressure or vacuum, so the heat transported through the membrane can be expressed as follows:

$$h_f(T_f - T_{fm}) = J \Delta H_v \quad (2.19)$$

The value of feed bulk inlet temperature ( $T_f$ ) can be easily measured and sometimes,  $T_f$  is considered as the mean feed bulk inlet temperature as given in equation below:



$$T_f = \left[ \frac{T_{fi} + T_{fo}}{2} \right] \quad (2.20)$$

Where  $T_{fi}$  and  $T_{fo}$  are the feed side inlet temperature and the feed side outlet temperature (retentate feed temperature) respectively. But it is difficult to measure membrane surface temperature ( $T_{fm}$ ) due to presence of thermal boundary layer on the feed side. However, it is calculated by mathematical modeling and simulation using simply enthalpy balance. Upadhyaya et al. (2015) developed a two dimensional model in CFD to predict the membrane surface temperature and used in mathematical model which consist of the effect of various operating parameters. Wang et al. (2014) also developed a two dimensional model using finite element method in hollow fibers for VMD. They considered the effect of various operating parameters and predicted that the cost of water production can be reduced upto 38% through VMD using the optimized conditions. A list of different attempts is provided in Table 2.4:

**Table 2.4: Different aspects of heat and mass transfer in VMD**

Nature of Study	Description	References
Theoretical	Mathematical and CFD modeling of VMD for desalination	(Upadhyaya et al. 2016a)
Theoretical	Development of ballistic transport model to describe mass transfer in VMD	(Kim 2014)
Theoretical and experimental	Use of gas permeability data to predict the membrane performance	(Zhang et al. 2013)
Theoretical and experimental	Development of simultaneous heat and mass transport model to simulate the effect of operating conditions on VMD performance	(Lovineh et al. 2013)
Theoretical	Performance evaluation of multi-VMD process by using a one dimensional model	(Shim et al. 2014)
Theoretical and experimental	Modeling and analysis of vacuum membrane distillation for the recovery of volatile aroma compounds from black current juice	(Soni et al. 2008)
Theoretical	Numerical modeling of the vacuum membrane distillation process	(Lee & Kim 2013)
Experimental	Heat and mass transfer in vacuum membrane distillation	(Mengual et al. 2004)
Theoretical	Analysis of heat and mass transfer in vacuum membrane distillation for water desalination using computational fluid dynamics	(Hayer et al. 2014)

## 2.5. Mass Transfer

In VMD, Mass transport refers to the transport of vapor molecules from aqueous feed side to the permeate side. Mass transport of vapors can be divided into three sections as follows: (i) from bulk feed solution to the membrane surface; (ii) from membrane surface to the pores of the membrane; and (iii) from membrane pores to the permeate side. So, the overall mass transfer coefficient can be represented using the series model (Khayet & Matsuura 2001; Banat & Simandl 1996):

$$\frac{1}{k} = \frac{1}{k_f} + \frac{1}{k_m} + \frac{1}{k_p} \quad (2.21)$$

Where  $k$  is the overall mass transfer coefficient;  $k_f$ ,  $k_m$  and  $k_p$  are the individual liquid feed side, membrane and permeate side mass transfer coefficients respectively. The mass transfer resistances on the permeate side is negligible due to lower pressure so the above equation can be arranged as follows (Khayet & Matsuura 2001; Banat & Simandl 1996; El-Bourawi et al. 2007):

$$\frac{1}{k} = \frac{1}{k_f} + \frac{1}{k_m} \quad (2.22)$$

### 2.5.1. Mass transfer through feed side boundary layer

The rate of mass transfer or mass transfer coefficient through the feed side boundary layer can be computed by mass balance as follows (Mericq et al. 2010; Soni et al. 2008; Sarti et al. 1993; Mulder 1996):

$$N = k_f C \left[ \frac{x_{fm} - x_v}{x_f - x_v} \right] \quad (2.23)$$

Where  $N$  is the rate of mass transfer  $k_f$  is the feed side mass transfer coefficient;  $C$  is the bulk feed side molar concentration;  $x_f$ ,  $x_{fm}$  and  $x_v$  are the feed side, membrane surface and permeate side mole fraction of solute respectively. Feed side mass transfer coefficient  $k_f$  is calculated using the various mass transfer analogies given in Table 2.5, have the simply form of dimensionless numbers as follows:

$$Sh = a Re^b Sc^c \quad (2.24)$$

Where  $Sh$  and  $Sc$  are the dimensionless Sherwood and Schmidt number and  $a$ ,  $b$ , and  $c$  are the characteristics constants of module organization and flow regimes. The Sherwood number is expressed as  $(k_f \cdot d_h)/D$  and Schmidt number can be defined as  $\mu/(\rho_f \cdot D)$ , where  $D$  is the diffusion coefficient in the liquid phase.

**Table 2.5 Various mass transfer correlations**

Mass transfer correlations	Descriptions	VMD module	References
$Sh = 1.86(Re.Sc.d_h / L)^{1/3}$	Laminar flow; Re<2100	Tubular Module, Flat sheet module	(Soni et al. 2008; Diban et al. 2009)
$Sh = 1.62(Re.Sc.d_h / L)^{1/3}$	Laminar flow	Hollow fiber module	(Bandini et al. 1997; Mengual et al. 2004)
$Sh = 3.66 + \frac{0.0668(Re.Sc.d_h / L)}{1 + 0.045(Re.Sc.d_h / L)^{2/3}}$	Laminar flow at constant wall temperature	Hollow fibre module	(Bandini et al. 1992)
$Sh = 0.116(Re^{2/3} - 125) Sc^{1/3}$ $\left[1 + (d_h / L)^{2/3}\right] \left(\frac{\mu_b}{\mu_l}\right)^{0.14}$	Transitional flow; 2100<Re<10000	Flat sheet module	(Soni et al. 2008)
$Sh = 0.023 Re^{0.8} Sc^n$	Turbulent flow with n=0.4 for heating and n=0.3 for cooling Re>10000	Flat sheet module, tubular module, hollow fibre module	(Soni et al. 2008; Khayet & Matsuura 2004; Lawson & Lloyd 1996a; Bandini & Sarti 1999; Urriaga et al. 2000)
$Sh = 0.04 Re^{0.75} Sc^{0.33}$	Turbulent flow for rectangular pipe	Flat sheet module	(Izquierdo-Gil & Jonsson 2003)
$Sh = 0.023 Re^{0.875} Sc^{0.25}$	Turbulent flow		(Gekas & Hallstrom 1987)
$Sh = 2.0 Re^{0.483} Sc^{0.33}$	Not mentioned		(Sudoh et al. 1997)
$Sh = 31.79 Re^{0.46} Sc^{0.33}$	Laminar Flow	Flat sheet module	(Upadhyaya et al. 2016b)

### 2.5.2. Mass transport through the membrane pores

The mass transport across the membrane pores is driven by the applied vapor pressure difference across the both sides of the membrane. The diffusive and convective mass transfer mechanism is depicted by the dusty gas model and the kinetic theory of gases(El-Bourawi et al. 2006; Khayet 2011). The model suggest that the molar flux through the membrane is directly proportional to the vapor pressure gradient across the membrane.

$$N = B.M \left[ P_{fm} - P_{pm} \right] \quad (2.25)$$

Where  $N$  is the molar flux,  $B$  is membrane mass transfer coefficient which depends upon the diffusion mechanism inside the membrane pores,  $P_{fm}$  and  $P_{pm}$  are the feed and permeate side membrane surface partial pressures,  $M$  is the molar mass of water. The feed side water vapor pressure can be obtained using Antoine equation (Al-Obaidani et al. 2008; Gryta et al. 2006; Lei et al. 2005).

$$\log(P_{fm}) = \left( A - \frac{B}{T_{fm} + C} \right) \quad (2.26)$$

According to dusty gas model, the mechanism of mass transfer is governed by three basic mechanism such as Knudsen diffusion (Fan et al. 2013; Khayet & Matsuura 2001; Zhang, Duke, et al. 2010; Khayet & Matsuura 2004), Poiseuille (viscous) flow and molecular diffusion (KHAYET et al. 2004; Lawson & Lloyd 1997; Khayet et al. 2003; Khayet & Matsuura 2004; Lawson & Lloyd 1996b; Phattaranawik et al. 2003a; El-Bourawi et al. 2006; Godino et al. 1997; Martinez et al. 2002; Khayet et al. 2000a; Lawson et al. 1995). In VMD, small amount of air is present in the pores of the membrane so either Knudsen diffusion, viscous flow model or both of them is used to define the mass transfer mechanism. The Knudsen number ( $Kn$ ) is used to identify the governing mass transfer mechanism inside the pores of the membrane and it is defined as the ratio of the mean free path ( $\lambda$ ) of the transported molecules to the pore size of the membrane. The mean free path for any species  $i$  is defined by using following equation (2.27).

$$\lambda_i = \frac{k_B T}{\sqrt{2\pi \bar{p}} \sigma_i^2} \quad (2.27)$$

where  $k_B$  is the Boltzmann constant,  $\bar{p}$  is the average pressure within the pores,  $T$  is the absolute temperature and  $\sigma_i$  is the collision diameter which have different values for different species shown in Table 2.6.

Table 2.6: Collision diameter of various species

Species	Collision diameter
Water vapor	2.64 °A
Ethanol	4.53 °A
Ammonia	2.90 °A
Acetone	4.60 °A
Chloroform	5.39 °A

If the molecule-pore wall collisions are dominant ( $Kn > 10$ ) and ( $\bar{r} < 0.05\lambda_i$ ) as compared to molecule-molecule collisions then Knudsen diffusion model (Khayet & Matsuura 2001; El-Bourawi et al. 2006; Imdakm & Matsuura 2004; Zhang, Duke, et al. 2010) is used to predict the mass transfer mechanism through the pores of the membrane and expressed as follows:

$$B_i^K = \frac{2}{3RT} \frac{\varepsilon \bar{r}}{\tau \delta} \left( \frac{8RT}{\pi M_i} \right)^{1/2} \quad (2.28)$$

where  $\bar{r}$  is the mean pore radius,  $R$  is the gas constant,  $T$  is the absolute temperature,  $M_i$  is the molecular weight of the species  $i$ ,  $\varepsilon$  is the membrane porosity,  $\tau$  is the pore tortuosity factor,  $\delta$  is the thickness of the membrane.

If the molecule-molecule collisions are dominant ( $Kn < 0.01$ ), viscous (Poiseuille) flow model is the mass transfer control mechanism through the membrane and expressed as follows:

$$B_i^P = \frac{1}{RT \delta} \frac{\varepsilon \bar{r}^2}{8 \tau \eta_i} \bar{p} \quad (2.29)$$

Where  $\eta_i$  is the viscosity of specie  $i$ ,  $\bar{r}$  is the average pressure in the membrane pores.

When the Knudsen number lies between 0.001 to 10, both molecule-molecule collisions and molecule-pore wall collisions are considered. It is known as transition region and Knudsen-viscous model is used as the mass transfer control mechanism and described as follows:

$$B_i^{K-P} = \frac{2}{3RT} \frac{\varepsilon \bar{r}}{\tau \delta} \left( \frac{8RT}{\pi M_i} \right)^{1/2} + \frac{1}{RT \delta} \frac{\varepsilon \bar{r}^2}{\tau \delta} \bar{p} \quad (2.30)$$

In VMD, if a membrane is used with pore size distribution, all mechanisms can occur simultaneously so the membrane permeability can be evaluated using the combination of different diffusion mechanism shown in equation (2.31).

$$B_i^m = \frac{N}{\tau \delta} \left( \sum_{j=1}^{m(r=0.05\lambda_i)} G_i^k f_j r_j^3 + \sum_{j=m(r=0.05\lambda_i)}^{p(r=50\lambda_i)} (G_i^k f_j r_j^3 + G_i^v f_j r_j^4 \bar{p}) + \sum_{j=p(r=50\lambda_i)}^{m(r=r_{\max})} G_i^v f_j r_j^4 \bar{p} \right) \quad (2.31)$$

$$G_i^k = \left( \frac{32\pi}{9M_iRT} \right)^{\frac{1}{2}} \quad (2.32)$$

$$G_i^v = \left( \frac{\pi}{8\eta_iRT} \right) \quad (2.33)$$

Where  $f_i$  is the fraction of pores with pore radius  $r_j$ ,  $m$  is the pores in Knudsen region,  $p$  is the pores in transition region,  $N$  is the total no. of pores per unit area.

## 2.6. Temperature and concentration polarization

In VMD, simultaneous heat and mass transfer occurs through the hydrophobic membrane, therefore, the concentration and the temperature at the vapor/liquid interface are different as compared to that for bulk feed conditions. Vaporization of water takes place at the liquid/vapor interface on the feed bulk side of the membrane building the temperature difference at the feed side boundary layer. This phenomenon is known as temperature polarization (causing 50 to 80% reduction in driving force)(Imdakm & Matsuura 2004; Zhang, Duke, et al. 2010). If the salt concentration on the membrane surface became higher than the feed bulk solution, this phenomenon is known as concentration polarization.

### 2.6.1. Temperature polarization coefficient

Temperature polarization coefficient (TPC) is the measure of degree of temperature polarization and it is defined as the fraction of trans-membrane temperature to the bulk temperature difference(Ramon et al. 2009). TPC can be evaluated using one of the following expressions:

$$TPC = \frac{T_{fm}}{T_{fb}} \quad (2.34)$$

$$TPC = \frac{T_{fb} - T_{fm}}{T_{fb} - T_p} \quad (2.35)$$

$$TPC = \frac{T_{fm} - T_p}{T_{fb} - T_p} \quad (2.36)$$

Where  $T_{fb}$  is the feed bulk inlet temperature,  $T_{fm}$  is the feed side membrane surface temperature,  $T_p$  is the equilibrium temperature on permeate side.

Equation (2.34) is used to calculate temperature polarization coefficient during concentration of sucrose solutions and methylene blue dye solutions and also in sea water desalination(Banat et al. 2005; Al-Asheh et al. 2006; Mericq et al. 2011).

According to equation (2.35), as the value of TPC approaches to unity, the process is limited by the heat transfer through the boundary layer, however, if the value of TPC approaches to zero, the process is limited by the mass transfer. The value of TPC increases with feed temperature if the working membrane has low permeability. The TPC has been found as high as 0.7 for the membranes having high permeability by some researchers(Wu et al. 2006; Bandini et al. 1997; Lawson & Lloyd 1996a; Bandini & Sarti 2002).

Following equation (2.36), the process is limited by heat transfer through the boundary layer as the value is TPC approaches to zero and vice versa. With increase in membrane permeability, it is observed that value of TPC decreases from 0.98 to 0.67(Khayet & Matsuura 2004; Lovineh et al. 2013).

## **2.7. Membrane Fouling**

Fouling is the deposition of the unwanted particles, surfactants and organic matters on the surface or inside the pores of the membrane which results in the decrement in the membrane performance. In membrane based systems, fouling is considered as the one of the major problem and it can be divided into three major categories: Inorganic fouling or precipitation fouling, organic fouling, Biofouling(Curcio et al. 2010; Gryta 2007a; Krivorot et al. 2011; Gryta 2012b; Gryta 2007b; He et al. 2008). The classical DLVO theory described the mechanism of formation of fouling due to interaction forces between the particles and the membrane surface(Derjaguin & Landau 1993; Verwey et al. 1999). According to this theory, the fouling on the membrane is due to vanderwaal forces and electrical double layer forces during interaction of the particles and surface. If the membrane surface and the particles have opposite charges, then the fouling on the membrane is more due to attractive interaction. However, if the membrane surface and the particles have like charges, then the fouling on the membrane is minimum due to repulsive interaction.

Fouling has very significant effect in pressure driven membrane technologies such as RO, NF, UF in desalination and other purification processes(El-Bourawi et al. 2006; Gryta et al. 2006; He et al. 2008; Bott 1995; Gryta 2008). However, the fouling in MD processes is different due to difference in membrane pore size, operational parameters and properties of the membrane.

### **2.7.1. Types of Fouling**

In MD, the fouling can be divided into three categories based on the fouling material(Meng et al. 2009; Srisurichan et al. 2005): (a) inorganic fouling due to deposition of the mineral salts such as silicate, calcium phosphate NaCl etc., (b) organic fouling due to deposition of organic matters

such as proteins, polysaccharides etc., (c) biological fouling mainly caused by microorganism such as bacteria, fungi etc.. In most MD processes, a combination of different fouling mechanism occur which make it more complicated.

#### 2.7.1.1. Inorganic fouling

Inorganic fouling occurs due to deposition of the hard minerals and colloidal particles on the membrane surface which is present in the feed solution. Inorganic fouling can be categorized into three categories such as alkaline, non-alkaline and neutral molecule fouling. In MD processes, the super saturation conditions arise due to the change in the feed temperature and the evaporation of the water which results in the nucleation and growth of the foulant on the membrane surface. If the nucleation of the foulant occurs on the membrane surface then it is known as surface (heterogeneous) crystallization. However, if it occurs in bulk then it is considered as homogeneous (bulk) crystallization. There are several scale foulants in MD such as  $\text{CaCO}_3$ ,  $\text{CaSO}_4$ ,  $\text{MgSO}_4$ ,  $\text{SrSO}_4$ ,  $\text{BaSO}_4$ , calcium phosphate, silicate etc.

#### 2.7.1.2. Organic fouling

The deposition or adsorption of the unwanted organic matters such as proteins, humic acid, carboxylic acid etc. at the membrane surface and pores at molecular level and in the form of gel layer. These organic matters alter the membrane morphology and these are not easy to remove by washing of the membrane. The fouling due to the natural organic matter (NOM) was considered as the most common organic fouling in the MD processes because MD processes are frequently used for the desalination of the surface water sources such as ponds, river and ocean which consist the higher amount of natural organic compounds consist of different humic substances. There are three ways of deposition of the NOM on the membrane surface:(a) partial or complete blocking of the pores of the membrane due to adsorption of the NOM into the pores of the membrane; (b)reduction in the flow passage through the pores of the membrane by forming a gel layer at the membrane interface;(c) formation of the low permeable particle/NOM layer by binding particle at the membrane surface(Karakulski & Gryta 2005; Schäfer et al. 2000; Guo et al. 2012).

#### 2.7.1.3. Biological fouling

The decrement in the performance in the VMD processes due to the growth of the biological species on the surface of the membrane is termed as biological fouling or biofouling. The biological fouling in the VMD processes is limited because the feed with higher salinity and higher operating temperature are used in different processes which limited the growth of the



microorganism. The biological fouling in VMD systems are lower as compared to other separation processes such RO, NF, UF etc.

### **2.7.2. Different factors affecting the membrane fouling**

Fouling in membrane distillation is influenced by various operating parameters and conditions such as temperature, water sources, dissolved gases etc.

#### **2.7.2.1. Temperature**

Temperature is considered as the most dominating factor in membrane fouling because the solubility of the salts greatly affect by the temperature. Generally, the solubility of the alkaline salts (such as NaCl) have negative relation with the temperature and the formation of scale depend upon the dissociation of the water in the hydroxyl ions. So at higher temperature, the rate of dissociation of water molecule is higher which results in higher fouling. However, the non-alkaline salts (such as calcium carbonate, calcium sulfate) have positive solubility which also deposited on the membrane surface. The declination in the permeate flux was observed upto 16% and 43% at 50 o C and 70 o C respectively for the feed solution contain Humic acid. Generally, the permeate flux increased at higher temperature but this may also lead to deposition of the organic matter on the interface of the membrane termed as concentration polarization effect(Tijing et al. 2015; Meng et al. 2014; Warsinger et al. 2015). Due to concentration polarization, the temperature of the membrane surface increases so the rate of evaporation is increased towards feed side direction and termed as temperature polarization.

#### **2.7.2.2. Water sources and dissolved gases**

VMD process is used for the desalination of the ground water including ocean, river, lake which also contains some dissolved gases in it. In most of the water sources, the saturation of calcium carbonate is significant as compared to the other salts which have great impact on membrane fouling. The dissolved gases in the water sources escape during the breakdown of the bicarbonates and have no direct impact on membrane fouling but it provides additional resistance to the diffusion of the vapor because it moves along the flow. The water sources containing higher amount of dissolved salts such as ocean, river have great impact on membrane fouling(Zhao et al. 2013; Gryta et al. 2001; Tijing et al. 2015).

### **2.7.3. Effects of fouling**

Fouling have the adverse effects on the different MD processes such as pore wetting, physically and chemically degradation and increase in polarization effects which results in the reduction in performance with purity concern.

#### 2.7.3.1. Membrane pore wetting

In VMD operations, only vapor molecules are allowed to pass through the pores of hydrophobic porous membranes. When the hydro-static pressure on the feed channel exceeds from the liquid entry pressure (LEP) of the membrane then the liquid molecules are allowed to enter into the membrane pores and it is considered as pore wetting. During the fouling, the deposition of the salts on the membrane surface increases which leads to the reduction of hydrophobicity of the membrane. Pore wetting reduces the membrane performance by reducing the evaporation interface which results in the reduction in amount of vapor produced and also reduce the non-wetting characteristics of the membrane(Gryta et al. 2001; Gryta 2002). After the membrane pore wetting, water can easily penetrate into the pores of the membrane and the salt layer was also accumulated at the membrane surface which further enhance the membrane pore wetting. So, it is necessary to minimize the possibility of the pore wetting to get the desired performance of different MD processes.

#### 2.7.3.2. Chemical and physical degradation of membrane

Various studies have reported the Chemical and physical degradation of the membrane properties due to fouling. The chemical and physical degradation was observed in different forms such as deterioration in hydrophobic nature, change in pore size and pore distribution, reduction in the permeate quality, change in strength of the membrane, modification of surface chemistry. Generally, the physical damage of the membrane occurred due to the deposition of the salt layer at the membrane surface of different foulants such as NaCl, CaCO<sub>3</sub>, CaSO<sub>4</sub>, MgSO<sub>4</sub>, SrSO<sub>4</sub>, BaSO<sub>4</sub>, calcium phosphate, silicate etc. which leads to the reduction in the flux due to blockage of the pores of the membrane. The problem of accumulation of insoluble salts on the membrane can be removed by washing the membrane with distilled water or HCl(Gryta 2002; Guillen-Burrieza et al. 2013; Gryta 2012a; Dao et al. 2016; Zuo & Chung 2016; Gryta & Waszak 2016). The properties and the morphological structure of the membrane change due to the chemical degradation of the membrane observed by various researchers. The minor change in the structure of the pores of the PP membranes by observed by M Gryta et al. 2009 due to the presence of hydroxyl and carbonyl groups at the membrane surface during the desalination of the feed solution after 4500h.

#### 2.7.3.3. Polarization Enhancement

Fouling on the membrane surface also enhances the concentration and temperature polarization effects by reducing the flow of feed at the membrane surface. If the residence time of the feed solution on the membrane surface increased, then the salt deposition on the membrane surface

increases, which increases the effect of concentration polarization. Due to concentration gradient at the membrane surface additional mass transfer resistances are created which lead to the increment in the membrane surface temperature and due to this increment an additional thermal boundary layer is created, which results in the reduction of the heat transfer coefficient for evaporation which is termed as temperature polarization effect (Yang et al. 2016; Kujawski et al. 2016; Xinmiao Zhang et al. 2016).

#### 2.7.3.4. Reduction in permeate amount

Various studies carried out show significant deterioration effect of membrane fouling on the permeate flux as well as permeate quality (Karakulski & Gryta 2005). The rate of membrane fouling can be obtained by using the rate of change in flux and can express as following:

$$fouling(\% / h) = \frac{P_i - P_f}{P_f} * \frac{100}{t} \quad (2.37)$$

Where  $P_i$  &  $P_f$  are amount of permeate flux initially and finally and  $t$  is the operating time.

The flux reduction profiles depend on the operating conditions (such as feed temperature, feed concentration, feed flow rate etc.) as well as membrane characteristics (such as porosity, degree of hydrophobicity etc.) (Lawson & Lloyd 1997; Karakulski & Gryta 2005; Van Gassel & Schneider 1986). Flux declination is related to the thickness as well as the porosity of the foulant layer formed at the membrane surface (Gryta 2007a). In various separation processes, it is observed that there is no significant declination in the permeate flux after long operating time (in months) due to the low solubility and lower concentration of the foulant materials (Karakulski & Gryta 2005). However, some operations show the significant reduction in permeate flux within 2-3 days or within some hours due to higher crystals growth at the membrane surface after exceeding the level of super saturation (Tun et al. 2005; He et al. 2011). Less than 15% reduction was observed in permeate flux after a 150 hrs run time due to deposition of salt on the membrane surface and it can be easily removed by water washing.

## 2.8. Operating parameters affecting VMD process

In VMD process, permeate flux is significantly affected by the operating parameters. Each operating parameters are discussed separately in the subsection as:

### 2.8.1. Feed Temperature

In VMD, Various studies have been carried out to estimate the effect of feed bulk temperature. It was observed that the permeate flux increased exponentially with increase in feed bulk

temperature due to increase in water vapor pressure which results in enhancement in driving force. Feed bulk temperature significantly affects the permeate flux and the energy requirement thus it is considered as the very sensitive parameter. F. Banat, Al-Rub, and Bani-Melhem (2003) observed that the feed bulk temperature is highly sensitive to flux at higher permeate pressure by using the sensitivity analysis. Table 2.7 shows the effect of feed temperature on the permeate flux; the feed bulk temperature is kept lower than the boiling point of feed solution while the other parameters remain constant.

**Table 2.7 Effect of feed temperature on permeate flux**

Membrane Type	Solution	Pore size ( $\mu\text{m}$ )	Permeate Pressure	Flow rate	$T_f(^{\circ}\text{C})$	Flux ( $\text{kg}/\text{m}^2.\text{h}$ )	References
PTFE	Salt (30000 mg/lt)	0.22	30 kPa	54 lph	40-60	3.3-11.5	(Pangarkar et al. 2010)
PP	100 g/lt	0.2	30 mbar	30 ml/s	35-55	8.1-12.9	(Mohammadi & Safavi 2009)
PTFE-120	NaCl (30g/lt)	0.75	VP= -0.095 Mpa	40 lph	60-80	~10.9-16.8	(Zhu et al. 2013)
PP hollow fibers	NaCl (80g/lt)	0.05-0.3	58 mmHg	5 lph	40-80	0.2-7.8	(Shao et al. 2013)
PP membrane	NaCl (100g/lt)	0.2	40 mbar	30ml/s	25-55	9-14	(Safavi & Mohammadi 2009)
PP membrane		0.2	4000 Pa	1.8 lps	37-65	3.3-25.3	(Bahmanyar et al. 2012)
PP membrane	Methylene Blue dye (18.5 ppm)		5 mm Hg	14 ml/s	40-70	4.28-6.37	(Banat et al. 2005)
PP Accurel 2E	Ethylene glycol solution (40wt%)	0.2		0.8 lpm	40-60	6.5-12	(Mohammadi & Akbarabadi 2005)
PTFE	multi-ions	0.22	5.5 kPa	2 lpm	45-60	5.5-27.5	(Chaurasia et al. 2013)

### 2.8.2. Feed Concentration

The reduction in the permeate flux was reported by various researchers with increase in concentration of the aqueous feed solution due to reduction of driving force as well as increment in concentration polarization (Safavi & Mohammadi 2009; Martinez 2004; Cath et al. 2004; Martinez & Rodriguez-Maroto 2007). Various researchers observed very high rejection ratio in different processes such as removal of dye, concentration of aqueous solutions, desalination etc. (A Criscuoli et al. 2008; Cerneaux et al. 2009; Khayet et al. 2003; Tang et al. 2010; Xu et al. 2006; Al-Asheh et al. 2006). Lawson and Lloyd 1997 have explained the three reasons for the reduction of permeate flux; 1) Increase in the effect of concentration polarization, 2) decrease in water activity, and 3) reduction in heat transfer coefficient at the boundary layer. From the comparison of RO and VMD (Mericiq et al. 2010; Mohammadi & Safavi 2009; Wirth & Cabassud 2002), it was observed that the reduction in the permeate flux is lower at higher salt concentration in VMD as compared to other membrane processes such as RO. Table 2.8 shows the effect of feed concentration on permeate flux observed by some researchers.

**Table 2.8: Effect of feed concentration on permeate flux**

Membrane Type	Pore size ( $\mu\text{m}$ )	Permeate pressure	Flow rate	$T_f$ ( $^{\circ}\text{C}$ )	Concentration	Flux ( $\text{kg}/\text{m}^2\cdot\text{h}$ )	References
PTFE-220	0.75	-0.095 MPa	40 lph	70	10-100 g/l	17.5-12.7	(Zhu et al. 2013)
PP	0.2	40 mbar	30 ml/s	55	100-300 g/l	13-9.2	(Safavi & Mohammadi 2009)
PP membrane	0.2	5 mm Hg	14 ml/s	50	0.2 to 1 M Salt solution	No significant effect	(Banat et al. 2005)
PP Accurel 2E	0.2		0.8 lpm	60	20 -60 (wt%) Ethylene glycol	13.5-4.6	(Mohammadi & Akbarabadi 2005)
PTFE	0.22	200 mmHg	90 lph	60	10-40 ppm NaF solution	16.98-13.85	(Singh et al. 2013)

### 2.8.3. Vacuum Degree

The permeate flux increases in S-shaped or inverted S-shaped manner with increase in the degree of vacuum applied (should be lower than the saturation vapor pressure of water) on the permeate side of the membrane. In VMD processes, the permeate flux and the trans-membrane pressure difference (driving force) across membrane increase with increase in vacuum level (decrease with the downstream pressure) but the possibility of the pore wetting is high at high vacuum. Generally, the vacuum level should be as high as possible to get the higher flux when the feed solution containing non-volatile solutes. In case of volatile solutes, if the degree of vacuum is kept high then the water flux is lower as compared to the volatile solutes which leads to the higher solute concentration in the permeate side at lower feed temperature. On the other hand, if the degree of vacuum is low (higher downstream pressure) then the solute concentration is lower in the permeate side due to reduction of driving force. Therefore, if higher recovery is required in favor of the volatile solutes from the feed solution then the level of vacuum should be high at lower feed temperature or vice versa(Sarti et al. 1993). It is worth noting that the energy consumption is higher at higher vacuum level or lower downstream pressure and it was observed that by increasing the downstream pressure from 10 to 60 mbar, the energy consumption decreased from 441.2 to 223.9 W and the reduction in permeate flux was observed from 56.2 to 50.5 kg/m<sup>2</sup>.h at operating feed temperature of 59.2 °C and the feed flow rate of 235 l/h(Alessandra Criscuoli et al. 2008). The effect of vacuum pressure on the permeate flux was investigated by various researchers listed in Table 2.9. Compositions of different parameter depending on downstream pressure and other relative considerable aspect, feed solution containing volatile solute in condition of low downstream pressure, much lower saturation V.P. of water corresponding to temperature of feed, the water flux becomes lower than volatile solute flux and concentration of solute in the permeate becomes too low.

**Table 2.9: Effect of vacuum pressure on permeate flux**

Membrane Type	Solution	Pore size (µm)	T <sub>f</sub> (°C)	Flow rate	Vacuum pressure	Flux kg/m <sup>2</sup> .h	References
PTFE-220	NaCl(30g/l)	0.75	70	40lph	0.080-0.095 MPa	7.6-14.8	(Zhu et al. 2013)
PP hollow fibers	NaCl (40g/l)	0.05-0.3		5 lpm	0.02-0.10 MPa	0.1-5.5	(Shao et al. 2013)
PP membrane	NaCl (100 g/l)	0.22	40	30 ml/s	40-120 mbar	11.8-5.8	(Safavi & Mohammadi 2009)

#### 2.8.4. Operating Time

In VMD, the reduction in the permeate flux was observed due to fouling or pore wetting over time. F Banat, Al-Asheh, and Qtaishat 2005 observed the decrement in the permeate flow rate from 18.2 to 10.5 ml/min at feed temperature 50 °C, feed flow rate 14 ml/s and vacuum pressure 5 mmHg in 100 min operating time for methylene blue dye solution for poly propylene membrane with pore size 0.2µm. The reduction in the permeate flux from 28.34 to 24.89 kg/m<sup>2</sup>.h and 16.39 to 13.84 kg/m<sup>2</sup>.h was depicted by Pangarkar et al. 2011 at vacuum pressure of 1.5 and 3 kPa and at feed temperature of 333 K and 313 K respectively. No significant reduction in the permeate flux of 5.5 kg/m<sup>2</sup>.h and the salt rejection of 99.99% was reported by Xu, Zhu, and Xu 2006 over a period of 5 months and at operating conditions of 55 °C feed temperature and the permeate pressure of 93 kPa. Chaurasia, Upadhyaya, and Singh 2013 observed 8% reduction in permeate flux in 180 hours at the feed temperature 333 K, at 6 kPa permeate pressure and the feed flow rate of 120 lph.

From the literature survey, following gray areas have emerged:

- i. Various authors have studied the effect of different operating parameters on permeate flux. However, the optimization of operating parameters is not studied yet for permeates flux along with specific energy consumption and percentage removal.
- ii. The individual effect of operating conditions is studied by several researchers. However, the interaction effects of operating parameters is not considered which have different relation with permeate flux, specific energy consumption and percentage removal
- iii. 2D numerical models have been developed by considering Knudsen and Poiseuille flow for estimation of interfacial membrane surface temperature and then the permeate flux is calculated by using the available model. No complete model for estimation of permeate flux is not developed yet.
- iv. Effect of concentration and the flow rate is not considered during the mathematical modeling which comprising all three mechanism of transport. However, it is expected that it should be considered to obtain the better result.

On the basis of above gaps, following objectives are decided for the present study:

- i) To fabricate a VMD setup and carry out experiments at different process conditions for removal of dyes from aqueous solutions (Methylene Blue, Sudan III, Naphthol Blue Black, Basic Red 9). The selected dyes are azo and disperse in nature which is difficult to remove using conventional techniques(Kanadasan et al. 2010; Baghel, Kalla, et al. 2017; Laminsi et al. 2015; Hu et al. 2006).
- ii) Optimization of process parameters using Design of Experiments (DOE) tool in *MINITAB*.
- iii) To develop 3D CFD Model comprising heat and mass transfer effect for the estimation of permeate flux and its dependency on various operating parameters such as Feed Temperature, Flow rate, Initial Concentration, and Vacuum Degree.
- iv) Validation of 3D CFD model for permeate flux in VMD process in porous media.
- v) To Develop heat and Mass Transfer Correlations.
- vi) To calculate theoretical recovery and its comparison with experimental data.
- vii) To Develop *ANN* Model.



## CHAPTER 3. THEORETICAL AND MATHEMATICAL ASPECTS

### 3.1. Computational fluid dynamic (CFD) simulation for permeate flux

The CFD simulation was carried out using COMSOL Multiphysics software for prediction of permeate flux which comprising heat and mass transfer properties of vacuum membrane distillation process for removal of dyes from aqueous solutions. The effect of different operating conditions such as feed temperature, vacuum degree, flow rate and initial dye concentration on permeate flux was studied and compared with experimental data. The overview of CFD simulation is given in Figure 3.1.

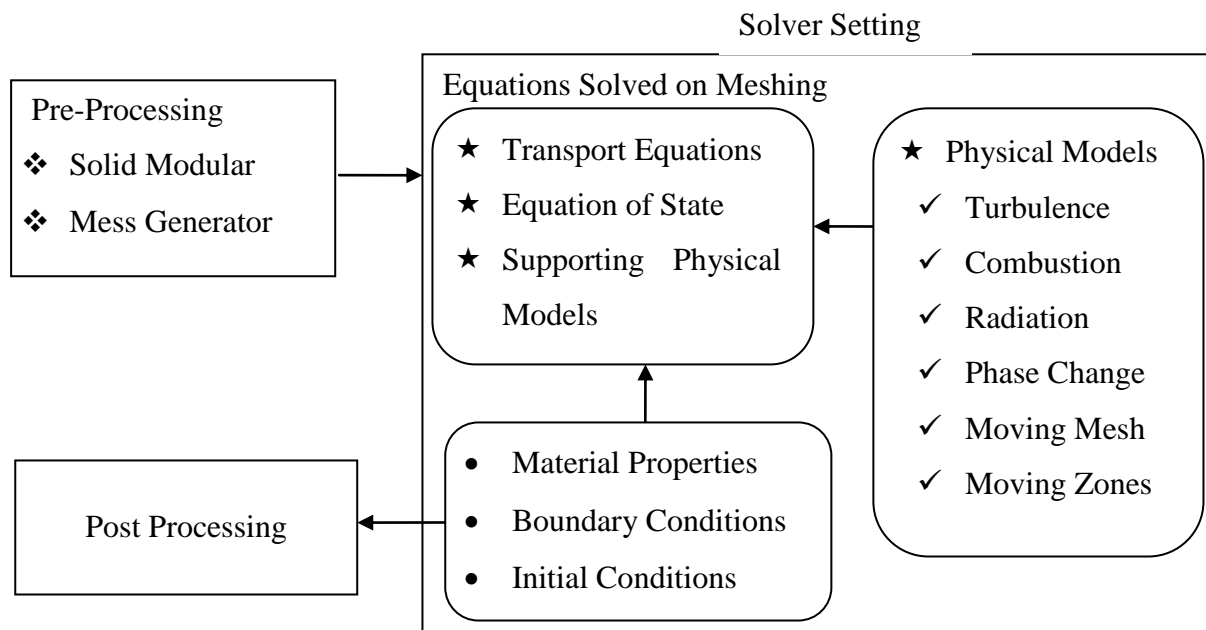


**Figure 3.1 Overview of Computational fluid dynamics simulation**

#### 3.1.1. Geometry development and meshing

The 3D geometry of membrane module was created in COMSOL Multiphysics comprising heat and mass transfer effects. The simulation is carried out for both PTFE and PVDF membrane which is purchased from the Millipore supplier. The pore size of the membrane is  $0.22 \mu\text{m}$  with membrane thickness of  $175 \mu\text{m}$  and the porosity of the membrane is 85%. The thermal conductivity of the both membranes is depend on the thermal conductivity of the membrane material and the air which is filled inside the pores of the membrane. The steel is chosen as the module material during the development of the membrane module which as same as an experimental module. The dimensions of the membrane and its module are given in Table 3.1.

**Table 3.1: Cell dimensions of the membrane and its module**

Parameter	Value
Feed inlet diameter	10mm
Feed section outer diameter	60mm
Length of the Feed section	120mm
Retentate diameter	10 mm
Permeate outlet diameter	10mm
Permeate outer section diameter	60mm
Effective membrane diameter	52mm

The meshing of the generated geometry is done by considering the physics controlled mechanism. During meshing, different meshing criteria available in COMSOL Multiphysics which depends upon the size of the element are chosen. To minimize the error between the experimental and the predicted flux, the element size should be as fine as possible. So, fine meshing is considered during the generation of meshing of the geometry. The grid independence test is also performed to check the error in between experimental and model flux. The fine meshing consist of 26717 elements. The geometry and their meshing is given in Figure 3.2 and Figure 3.3 respectively.

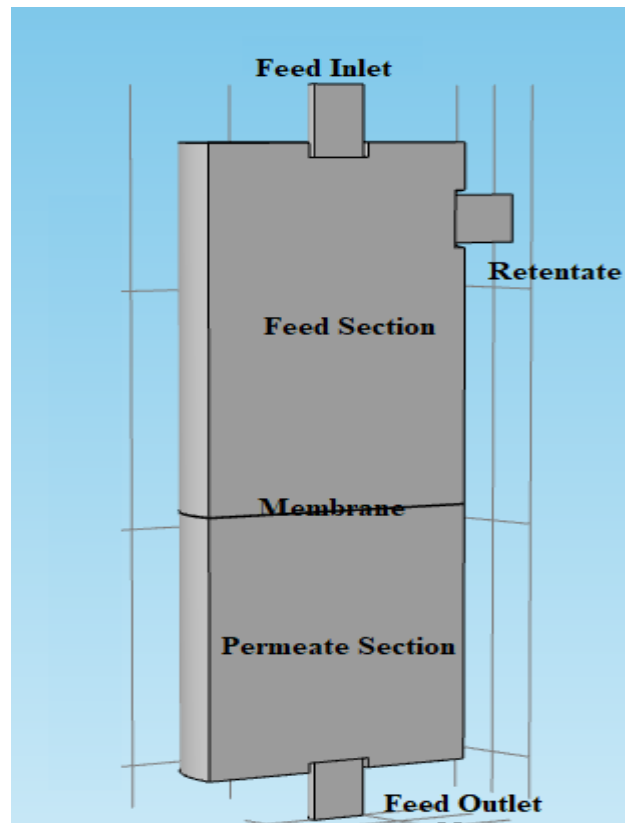


**Figure 3.2: Membrane module with membrane test cell**

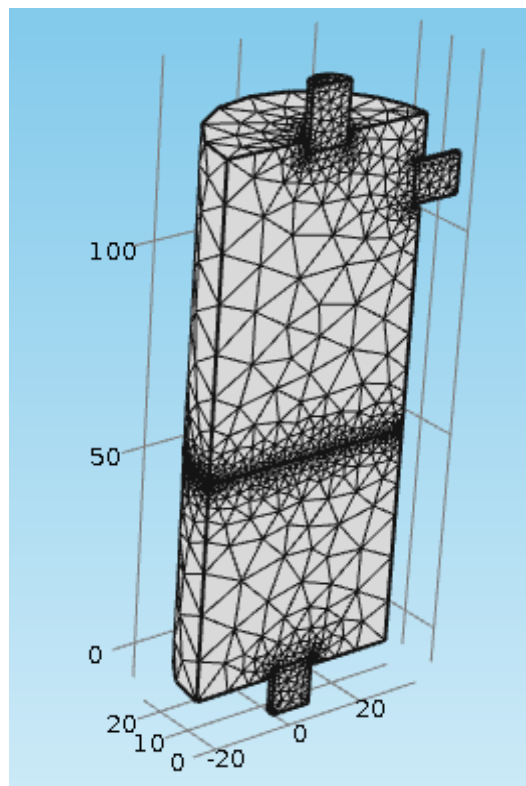


**Figure 3.3: Meshing of the test cell**

### 3.1.2. Equations involved in CFD study in COMSOL Multiphysics

The permeate flux through the membrane is given by equation (3.1), where  $D_{eff}$  is the effective diffusivity of the vapor molecules. The diffusion of water vapor through the membrane is governed by the combination of Knudsen diffusion and Poiseuille flow. So, the effective diffusivity of the membrane can be obtained by the equation (3.2)(Khayet & Matsuura 2011).

$$N = D_{eff} * \Delta C \quad (3.1)$$

$$D_{eff} = \left( \frac{1}{D_p} + \frac{1}{D_k} \right)^{-1} \quad (3.2)$$

Where  $D_p$  and  $D_k$  are the diffusion coefficient of Knudsen and Poiseuille flow.

The thermal conductivity of the membrane is given by the equation (3.3) (Baghel, Upadhyaya, et al. 2017; El-Bourawi et al. 2006):

$$k_m = \varepsilon k_g + (1 - \varepsilon) k_p \quad (3.3)$$

Where,  $k_m$  is the thermal conductivity of the membrane,  $\varepsilon$  is membrane porosity,  $k_g$  is the thermal conductivity of the gas filled into the pores of the membrane,  $k_p$  is the thermal conductivity of the polymeric material used for the membrane.

#### *Feed Section*

The flow of the incompressible fluid is calculated using the coupled form of continuity equation and Navier-stokes equation.

$$\nabla \cdot u = 0 \quad (3.4)$$

$$\frac{\partial \rho u}{\partial t} + \nabla \cdot \rho u u = -\nabla p + \nabla \cdot \mu (\nabla u + \nabla^T u) \quad (3.5)$$

Where,  $p$  is the pressure in Pa,  $\rho$  is the density of the fluid in  $\text{kg/m}^3$ ,  $\mu$  is the viscosity of the flowing fluid, and  $u$  is the velocity of flowing fluid. The properties of the flowing fluid and the velocity of the fluid is specified for the feed section at the starting of the 3D modeling.

As the hot fluid is flowing into the feed channel, so there is heat transfer due to conduction as well as convection for feed flow which is given by equation (3.6):

$$\rho C_{ph} u_h \nabla T_h = \nabla \cdot (k_h \nabla T_h) \quad (3.6)$$

Where  $k_h$  is the thermal conductivity of the hot fluid,  $T_h$  is the hot feed temperature in the feed section. The boundary conditions of the feed section are given in Table 3.2:

### Membrane Section

Conductive heat transfer is considered significant for the transfer of heat through the membrane solid and pores of the membrane:

$$k_m \left[ \frac{\partial^2 \Delta T_m}{\partial x^2} + \frac{\partial^2 \Delta T_m}{\partial y^2} + \frac{\partial^2 \Delta T_m}{\partial z^2} \right] = 0 \quad (3.7)$$

Where,  $k_m$  is the membrane thermal conductivity,  $\Delta T_m$  is temperature inside the membrane matrix which is the difference of feed side membrane surface temperature ( $T_{fm}$ ) and permeate side membrane surface temperature ( $T_{pm}$ ).

During the transport of species through porous media, it is considered that only vapor molecules are passing through the membrane, dye and water molecules are retained at the feed side membrane surface. The boundary conditions considered for the membrane is shown in Table 3.2.

### Permeate Section

In the permeate section, the vacuum is applied which removed the air filled into the pores of membrane and maintained the driving force across the membrane. The flow rate through the permeate side of the membrane is very low because only vapor molecules are passing, so laminar flow is considered in the permeate section, and it will be same as the feed section. The boundary conditions for the permeate section is shown in Table 3.2.

**Table 3.2: Boundary Conditions**

Position	Y=entry of feed	Y=end of the feed section	Y=feed side membrane surface	Y= permeate side membrane surface	Y= permeate section at start	Y=end of permeate section
Momentum in Feed side	$V = V_{in}$	$P = P_{atm}$	No slip condition	-	-	-
Heat transfer in Feed side	$T = T_{in}$	Convective flux	$T = T_{fm}$	-	-	-
Heat transfer in membrane	-	-	$T = T_{fm}$	$T = T_{pm}$	-	-
Mass transfer in Membrane	-	-	$C = C_{feed}$	$C = 0$	-	-
Heat transfer in permeate	-	-	-	-	$T = T_{pm}$	$T = T_v$

side						
Momentum in permeate side	-	-	-	-	$V=V_{\text{permeate}}$	$P=P_{\text{vacuum}}$
$V_{\text{in}}$ – Velocity of feed enter at the feed section $P_{\text{atm}}$ – Pressure at the feed side on the membrane surface $T_{\text{in}}$ – Temperature of the entering feed $T_{\text{fm}}$ – Feed side membrane surface temperature $C_{\text{feed}}$ – Concentration of the feed $T_{\text{pm}}$ – Permeate side membrane surface temperature $T_{\text{v}}$ – Temperature on the permeate side $V_{\text{permeate}}$ – velocity of the permeate coming through the membrane $P_{\text{vacuum}}$ – Vacuum degree on the permeate side						

### 3.1.3. Solution of governing equations

The equations derived for feed, membrane and permeate section with its boundary conditions are solved using CFD module available in commercial COMSOL Multiphysics software package. The time-dependent equations of momentum, energy, and mass are solved using PARDISO solver. For meshing of a geometry, physics controlled meshing scheme is selected, and fine meshing is used to create meshing of the module. The grid independence test is also performed to check the independency of permeate flux from meshing. For solving this numerical model, a system with specification as i5 Intel core processor, 4GB RAM, 64 bit with window 8 operating system is used. The procedure for estimation of interfacial temperatures and permeate flux through the CFD modeling is given in Figure 3.4.

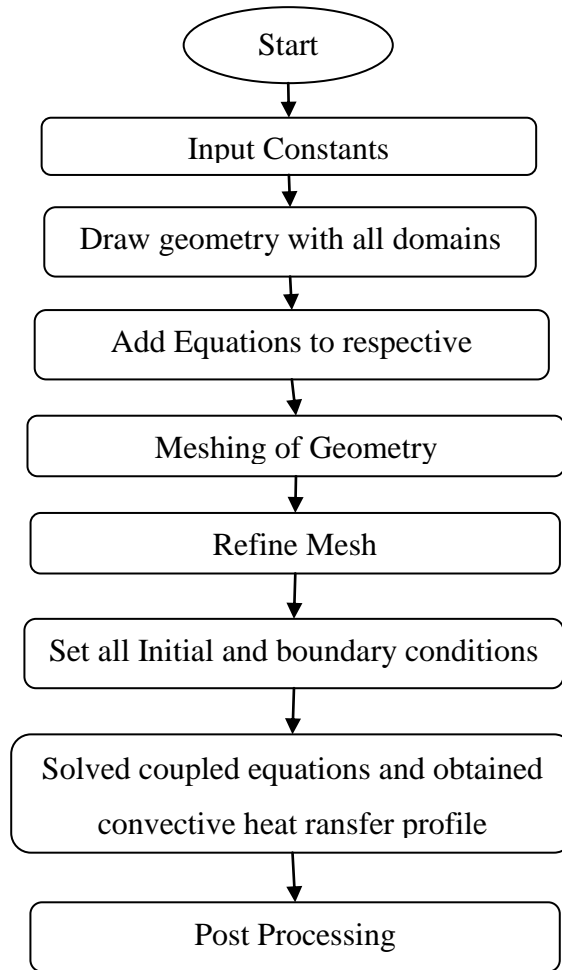


**Figure 3.4: Flow chart for the numerical simulation of VMD process**

### 3.2. Recovery

It can be expressed as fractional amount of water recovered from the feed solution in VMD process through membrane. It varies from 0 to 1 or can be expressed in terms of percentage ranging from 0 to 100%. Recovery is considered as important parameter from the economic point of view. So, the value of recovery should be high for the wide acceptability of the process. Figure 3.5 represents the block diagram for the water recovery through VMD process.

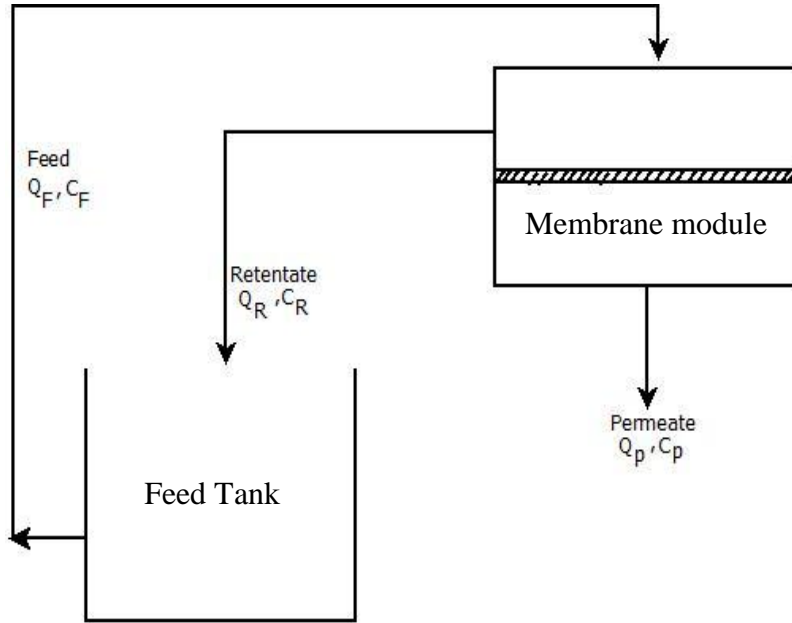


**Figure 3.5 Block diagram for recovery analysis through VMD**

For recovery analysis, a mathematical model was developed by writing the material balance for VMD process. The feed solution contains only water and dye in it so the density of the feed solution is assumed to be constant. The total and component material balance through the membrane module is as follows:

$$Q_f = Q_R + Q_p \quad (3.8)$$

$$\frac{d(C_R V_m)}{dt} = Q_F C_F - Q_R C_R - Q_P C_P \quad (3.9)$$

In VMD process, only vapor molecules are passing through the membrane, so  $C_p = 0$ .

$$\frac{d(C_R V_m)}{dt} = Q_F C_F - Q_R C_R \quad (3.10)$$

$$\frac{d(C_R)}{dt} = \frac{Q_F C_F - Q_R C_R}{V_m} \quad (3.11)$$

Overall and component material balance for feed tank

$$\frac{dV}{dt} = Q_R - Q_F \quad (3.12)$$

$$\frac{d(C_F V)}{dt} = Q_R C_R - Q_F C_F \quad (3.13)$$

From equation (3.12) and (3.13), we get



$$\frac{dC_F}{dt} = \frac{(C_R - C_F)Q_R}{V} \quad (3.14)$$

Where,  $Q_F$ ,  $Q_P$  and  $Q_R$  is the flow rate of feed, permeate and retentate respectively.  $C_F$ ,  $C_P$  and  $C_R$  is the concentration of dye in feed, permeate and retentate respectively.  $V$  is the volume of the tank and  $V_m$  is the minimum volume requirement in the tank for continuous operation. The equations (3.11), (3.12) and (3.14) are further solved in MATLAB using ODE15s solver for calculating the theoretical recovery through VMD process.

### 3.3. Sensitivity analysis

It is carried out to predict the behavior of the system which is affected by various operating conditions like feed temperature, vacuum degree, initial dye concentration, and flow rate, etc. The performance of the system changes sharply with a small change in operating conditions in the sensitive region. The normalized sensitivity factor of different operating parameters is derived using the mathematical model by considering the Knudsen diffusion. The generalized normal sensitivity factor is defined as follows:

$$S(R, P_i) = \frac{\partial \ln R}{\partial \ln P_i} = \frac{P_i}{R} \frac{\partial R}{\partial P_i} = \frac{P_i}{R} S(R, P_i) \quad (3.15)$$

The normalized sensitivity factor is calculated for feed temperature, and vacuum degree because these two parameters are considered as the most significant parameters as compared to flow rate and initial dye concentration.

The normalized sensitivity factor of permeate flux to feed temperature is given by

$$S(N, T_f) = \frac{\partial \ln N}{\partial \ln T_f} = \frac{T_f}{N} \frac{\partial N}{\partial T_f} \quad (3.16)$$

Where  $N$  is permeated flux and  $T_f$  is feed temperature.

After solving this normalized sensitivity factor for permeate flux following expression is obtained.

$$S(N, T_f) = \frac{R_1}{(1 + R_1)R_2} \quad (3.17)$$

Where

$$R_1 = \frac{\lambda^2 M^{3/2} P_i K_m}{RT_f^2 h} \quad (3.18)$$

$$R_2 = \frac{T_f}{T_f - T_{fm}} \quad (3.19)$$

The normalized sensitivity factor for permeate flux to vacuum degree is given as follows:

$$S(N, P_p) = \frac{\partial \ln N}{\partial \ln P_p} = \frac{P_p}{N} \frac{\partial N}{\partial P_p} \quad (3.20)$$

After solving this normalized sensitivity factor for permeate flux following expression is obtained.

$$S(N, P_p) = \left( \frac{-1}{1 + R_1} \right) * \frac{1}{R_3} \quad (3.21)$$

Where

$$R_3 = \frac{P_f - P_p}{P_p} \quad (3.22)$$

The detailed set of equations is given in Appendix I for sensitivity analysis of permeate flux to feed temperature and vacuum degree.

The normalized sensitivity factor for permeate flux to flow rate is given as follows:

$$S(N, Q) = \frac{\partial \ln N}{\partial \ln Q} = \frac{Q}{N} \frac{\partial N}{\partial Q} \quad (3.23)$$

$$S(N, Q) = \frac{Q}{N} \frac{\partial N}{\partial T_{fm}} \frac{\partial T_{fm}}{\partial Q} \quad (3.24)$$

$$S(N, Q) = \frac{Q}{N} \frac{\partial T_{fm}}{\partial Q} \frac{\partial N}{\partial T_{fm}} = \frac{Q}{N} \frac{\partial T_{fm}}{\partial Q} S(N, T_{fm}) \quad (3.25)$$

$$S(N, Q) = \frac{Q}{N} \frac{\partial T_{fm}}{\partial Q} \frac{\partial \ln T_f}{\partial \ln T_{fm}} S(N, T_f) \quad (3.26)$$

The normalized sensitivity factor for permeate flux to membrane characteristics is given as follows:

$$S\left(N, \frac{\varepsilon}{\tau \delta}\right) = \frac{\partial \ln N}{\partial \ln \frac{\varepsilon}{\tau \delta}} = 1 \quad (3.27)$$

### 3.4. Artificial Neural Network (ANN)

Neural network tool is very useful for analyzing the engineering properties which are dependent on many input variables. ANN has turned out to be exceptionally viable in taking care of issues where the connection between physical aspects and their parameters are perplexing and exceedingly nonlinear and with an extensive level of vulnerability. ANN can gain from existing information and receive to delineate arrangement of information parameters into an arrangement of yield parameters, without knowing the complex relationship among them. There are a few ANN models and structures that have been utilized in engineering applications to display or rough properties.

#### 3.4.1. Back-propagation Algorithm

This algorithm is very effective method for training of neural network which consist of multilayer parameters for solving various engineering problems. In this algorithm, an input signal is provided to each input which broadcasted to the hidden layers. The hidden layers analysed the broadcast signal and send the computed signal to output layer. Then the response of the network is analyzed and the input pattern is recognized.

The gradient descent is the basic optimization technique considered in backpropagation. In gradient descent technique, the error is considered as the function, and the weights of the hidden layer in the network are considered as variables which provide the direction to move function indefinite path to minimize error (negative gradient provide the way where function decreased rapidly). In backpropagation algorithm, there are several steps considered such as initialization, data's normalization, criteria for stopping the algorithm, and structure of the network.

#### 3.4.2. Models

Artificial neural networks (ANNs) are nothing but neural network models in artificial intelligence; these are basic mathematical models defining a function.

All type of ANN models are related to *class* of such functions.

$Y = f(X)$  where

- X is input from set of numerical values
- Y is output from set of numerical values
- f is an function relating the input and the output which is unknown

The function should be predicted by the ANN approximately so that appropriate of results could be calculated for every set of inputs.

*Activation Function*

Activation function is kind of a squashing function, as the neural network having the output of neuron are in a range of certain values (which lie between either 0 and 1, or -1 and 1). Activation functions have generally three types denoted by  $\Phi$ . Out of which first is the Threshold Function in which if the sum of all input is less than the threshold value ( $v$ ) then it takes a value of 0, and if the sum ends up to threshold value or greater than that then the value 1 is taken.

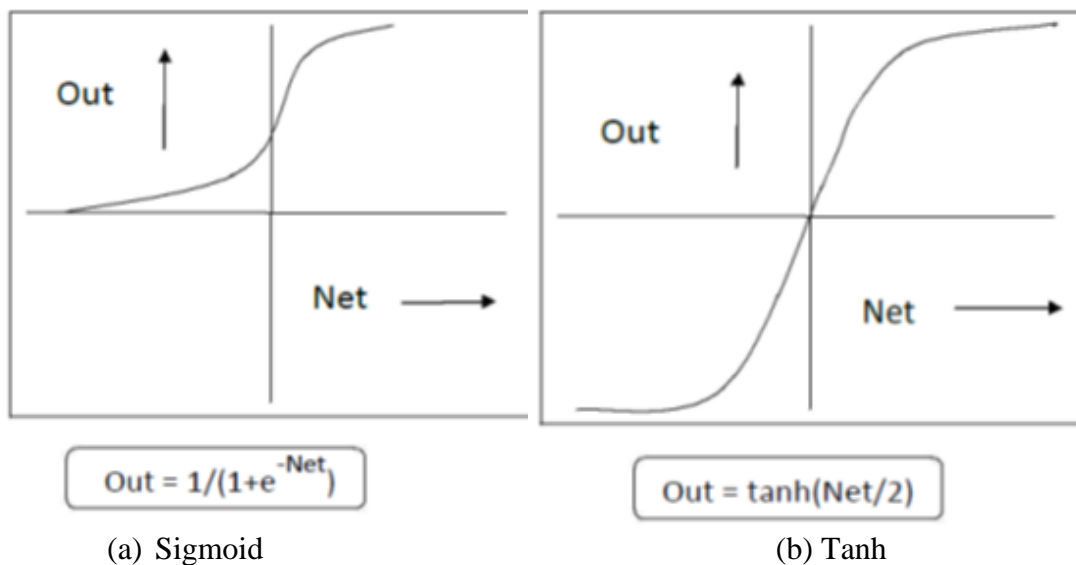
$$f(x) = \begin{cases} 1, & v \geq 0 \\ 0, & v < 0 \end{cases} \quad (3.28)$$

Piecewise-Linear function is another type which can again take value either 0 or 1. The difference between this function and threshold function is it can consider a value between 0 and 1 if the amplification factor lies in a certain region of the linear operation.

Third type of function is sigmoid function. In this function the range lies in the range of 0 and 1, but it can also use a value lying between -1 to 1. Hyperbolic tangent function is the example of the sigmoid function.

$$\phi(v) = \tanh \frac{v}{2} = \frac{1 - e^{-v}}{1 + e^v} \quad (3.29)$$

A collection of parallel processing units that are joined altogether by decision weights can be called as an artificial neural network. All artificial neural networks may be constructed by basic building block but the fundamentals might vary. A period of trial and error must be there during the design decisions before a satisfactory design can be achieved. The system developers generally face few concerns related to design issues of neural networks are complex.



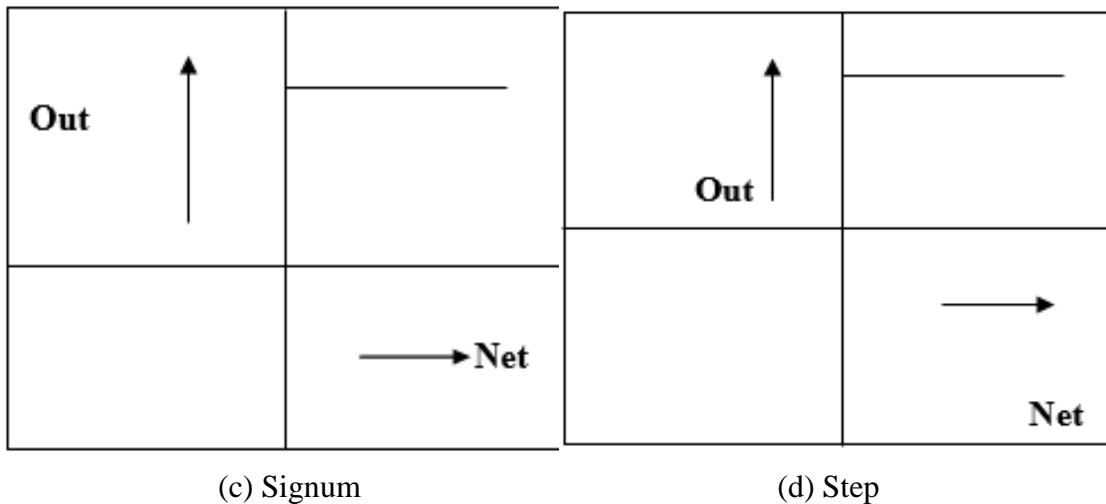


**Figure 3.6: Non-linear Transfer Functions used for Synaptic Inhibition**

Neural network designing steps are as follows:

- Arrangement of neurons in different layers.
- Analysing the connecting patterns between neurons.
- Input and output way for neurons.
- Apply network learning to identify the connection strength and provide appropriate weight to training data set.

Naturally, neural systems are built in a three dimensional manner from minute parts. These neurons appear to be able to do about unhindered interconnections. This isn't valid in any man-made system. Counterfeit neural systems are the basic grouping of the crude fake neurons. Figure 3.6 shows the clustering of layers which shows the connection with each other. Fundamentally, all counterfeit neural systems have a comparable structure of topology. A portion of the neurons interface this present reality to get its sources of info and different neurons give this present reality the system's yield. The remainder of the neurons are avoided see.

The layers with grouped neurons are shown in Figure 3.7 considering one hidden layer. The info layer comprise of neurons get from the outside condition. The yield layer comprises of neurons that impart the yield of the framework to the client or outside condition. There are normally various shrouded layers between these two layers. At the point when the information layer gets the information its neurons produce yield, which progresses toward becoming contribution to different layers of the framework. The procedure proceeds until a specific condition is fulfilled or until the yield layer is summoned and fires their yield to the outside condition.

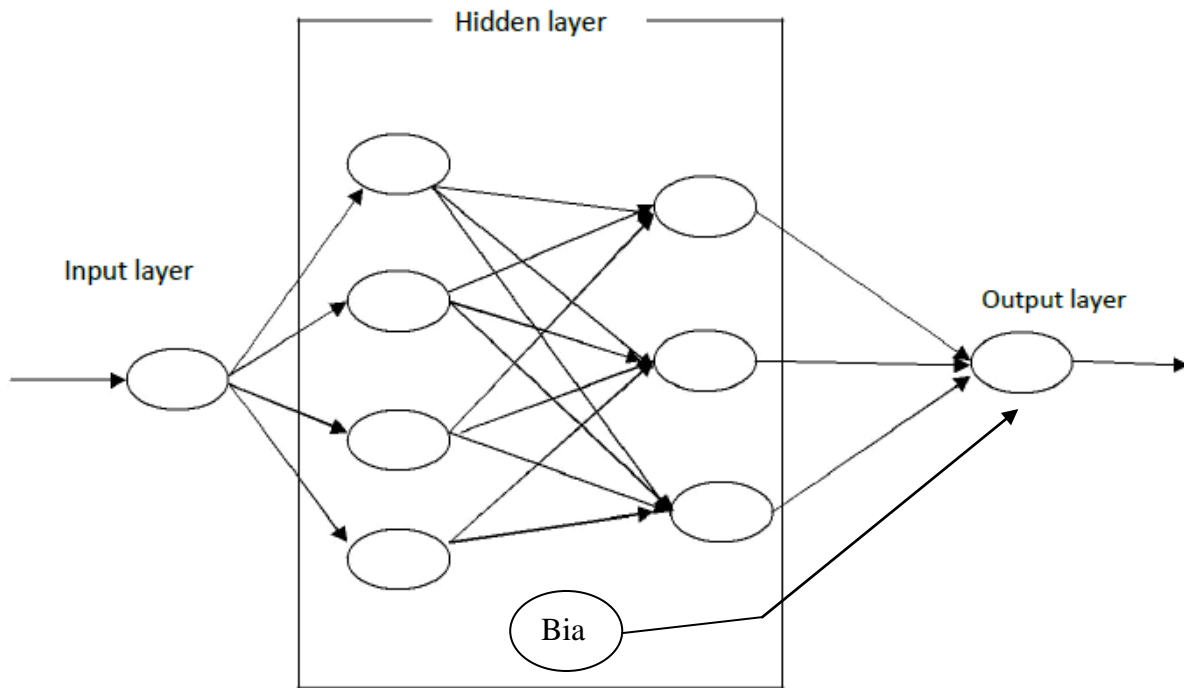


**Figure 3.7: Structure of neural network with single hidden layer**

The network should be performing its best so that the number of hidden neurons can be determined. An over fit could be created if hidden number of neurons increased too much. The network will be useless on new data if training set data are memorized(Shetty and Chellam, 2003).

### 3.4.3. Neural Network toolbox (NNtool)

Inbuilt Neural network toolbox is used for recognition of pattern between 4 input and 1 output variable using a commercial package of MATLAB R2014b. Generally, NN toolbox is consisting of two graphical user interfaces (GUI). One GUI is neural network/data manager who work as a communication bridge between the NNtool and MATLAB, along with creation, the addition of a neural network as shown in Figure 3.8. The main GUI of the neural network is divided into two sections as network and data like inputs, outputs, Networks, errors, etc. The data into the nntool can be exported from the MATLAB console or from the data file.

NNtool was mostly utilized in this investigation to get more precise outcomes from a pre developed neural net utilizing the content composed for the programmed age of ANN models. The NNtool is extremely easy to use GUI that can be utilized in making of modest number of models in particular issue areas.

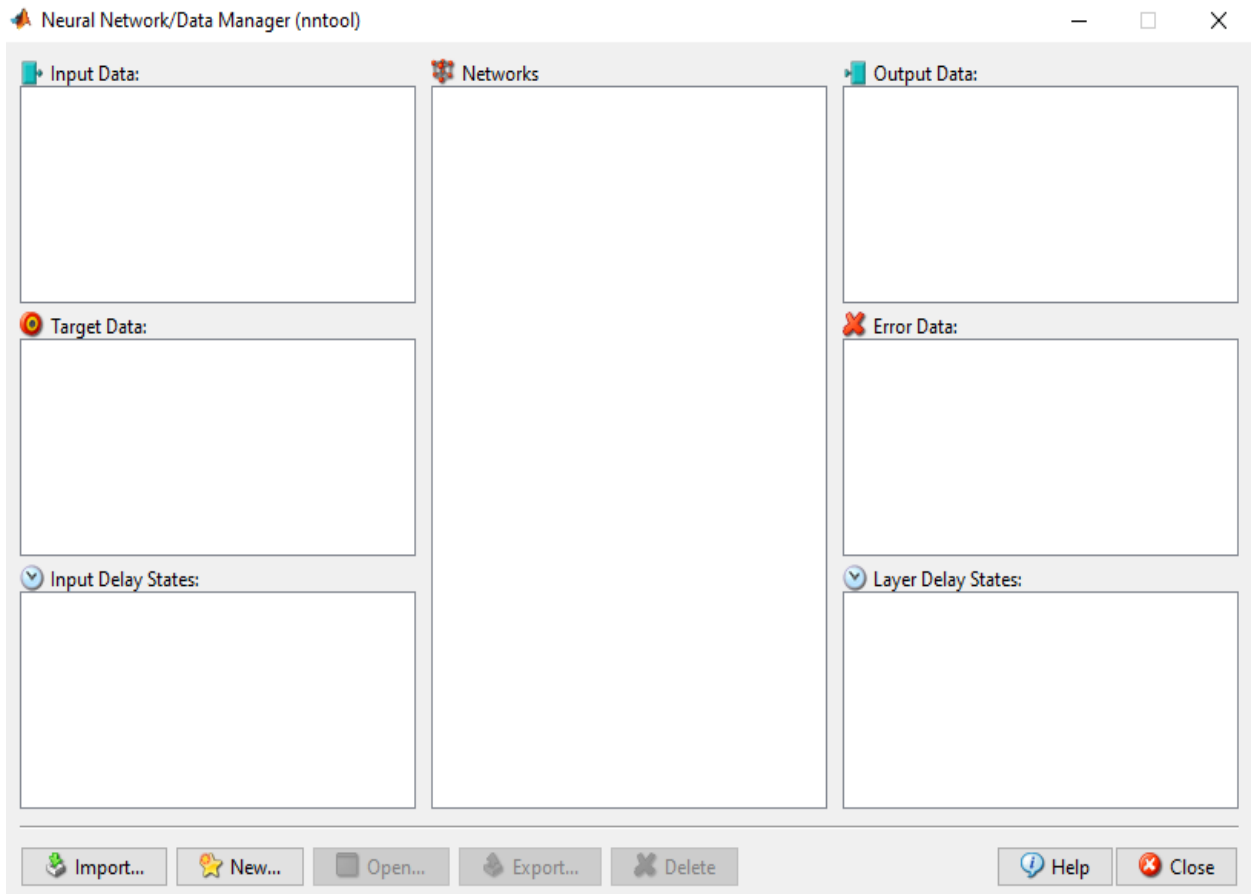


**Figure 3.8: Data manager graphical user interface**

## CHAPTER 4. EXPERIMENTAL MATERIALS AND METHODS

A detailed property of various materials and methods used in presented work is described in this chapter.

### 4.1. Materials used:

#### 4.1.1. Distilled water

Distilled water is used for preparation of different feed solutions in present experimental work. The distilled water is produced in the lab from stainless steel distillation unit. The purity of the distilled water is analyzed by measuring the electrical conductivity of the produced water. The properties of the distilled water are given in Table 4.1.

**Table 4.1: Properties of distilled water**

Molecular formula	H <sub>2</sub> O
Appearance & odour	Colorless & odourless
Molar mass	18.02 kg/kmol
Density at 25 °C	1000 kg/m <sup>3</sup>
Boiling point	99.98 °C
Melting point	0 °C
Viscosity 25 °C	1.0*10 <sup>-3</sup> Pa
Thermal conductivity	0.58 W/m.K

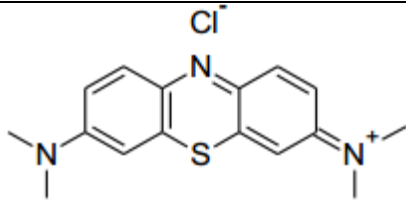
#### 4.1.2. Methylene Blue

Methylene blue is also referred to as methylthioninium chloride which is used in the treatment of methemoglobinemia. It is also used for the coloring of clothing in different textiles industries. It has various side effects such as vomiting, breath shortage, high blood pressure, headache, etc. This dye is directly purchased from Fisher Scientific(India) and used as such for preparing different feed solutions. The properties of methylene blue are provided in Table 4.2.

**Table 4.2: Properties of methylene blue**

Characteristics	Methylene Blue
Molecular formula	C <sub>16</sub> H <sub>18</sub> N <sub>3</sub> SCl
$\lambda_{\max}$	663 nm
Molecular weight	319.85 kg/kmol

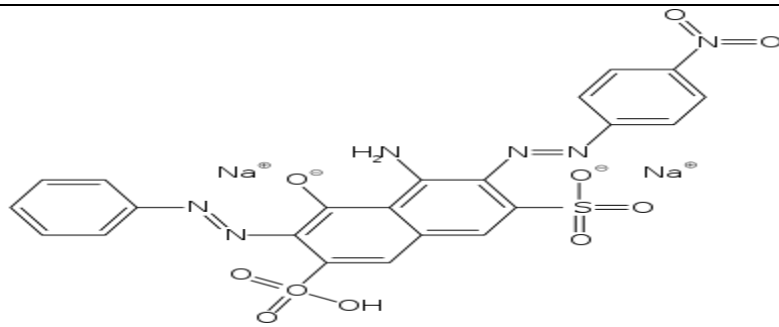


Color Index	52015
CAS number	61-73-4
Solubility in water	40 g/L at 20 °C
Molecular Structure	

#### 4.1.3. Naphthol Blue Black Dye

Naphthol Blue black is an amino corrosive recoloring azo color utilized in biochemical research to recolor for aggregate protein on exchanged layer smears, for example, the western blotch. It is additionally utilized in criminal examinations to recognize blood present with inactive fingerprints. It recolors the proteins in blood a blue-dark shading. Amido Black can be either methanol or water based as it promptly breaks down in both. With picric corrosive, in a van Gieson methodology, it very well may be utilized to recolor collagen and reticulin. This dye is directly purchased from Sigma Aldrich (India) and used as such for preparing different feed solutions. The properties of naphthol blue-black dye are given in Table 4.3.

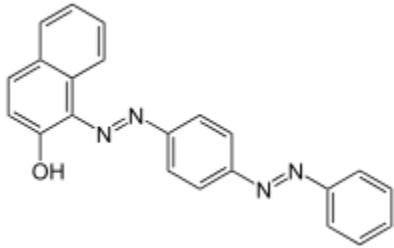
**Table 4.3: Properties of Naphthol Blue Black Dye**

Characteristics	Naphthol Blue Black
Molecular formula	$C_{22}H_{14}N_6Na_2O_9S_2$
$\lambda_{max}$	618 nm
Molecular weight	616.49 kg/kmol
Color Index	86230
CAS number	1064-48-8
Solubility in water	30 g/L at 20 °C
Molecular Structure	

#### 4.1.4. Sudan III Dye

It is utilized to shading nonpolar substances, for example, oils, fats, waxes, oils, different hydrocarbon items, and acrylic emulsions. Its principle utilize is as a fuel color in the United States of America ordered by the IRS to separate low-exhausted warming oil from car diesel fuel, and by the EPA to stamp fills with higher sulfur content; it is a supplanting for Solvent Red 26 with better dissolvability in hydrocarbons. The fixation required by IRS is a ghostly likeness 3.9 pounds for every 1000 barrels, or 11.13 mg/l, of Solvent Red 26 in strong shape; the focuses required by EPA are approximately 5 times lower. This dye is directly purchased from Fisher Scientific(India) and used as such for preparing different feed solutions. The properties of Sudan III dye is given in Table 4.4.

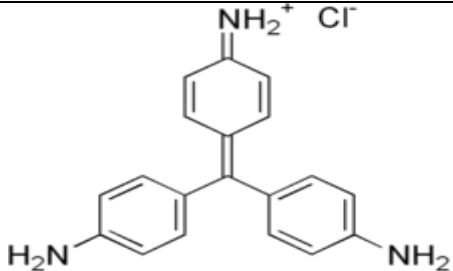
**Table 4.4: Properties of Sudan III Dye**

Characteristics	Sudan III Dye
Molecular formula	C <sub>22</sub> H <sub>16</sub> N <sub>4</sub> O
$\lambda_{\max}$	510 nm
Molecular weight	352.40 kg/kmol
Color Index	83535
CAS number	85-86-9
Solubility in water	5 g/L at 20 °C
Molecular Structure	 <p>The chemical structure of Sudan III Dye is shown. It consists of a naphthalene ring system with a hydroxyl group (-OH) at the 1-position. At the 4-position of the naphthalene ring, there is a diazo group (-N=N-) connected to a para-substituted benzene ring. This benzene ring is further connected via another diazo group (-N=N-) to a third benzene ring.</p>
Dye type	Diazo dye

#### 4.1.5. Basic Red 9 dye

Basic Red 9 is an organic compound with magenta color and solid crystalline structure. It is generally used for the coloring of fibers made of polyacrylonitrile. This dye is purchased from Sigma Eldrich and used as such for experimentation. The properties of basic red 9 dye are given in Table 4.5.

**Table 4.5: Properties of Basic Red 9 Dye**

Characteristics	Basic Red 9
Molecular formula	$C_{19}H_{17}N_3$
$\lambda_{max}$	730 nm
Molecular weight	323.830 kg/kmol
Color Index	87663
CAS number	569-61-9
Solubility in water	Slightly solubility
Appearance	Green Crystalline solid
Molecular Structure	 <chem>Nc1ccc(cc1)C(=N2C=CC=C2[NH2+])c3ccc(N)cc3.[Cl-]</chem>
Dye type	Basic Dye

## 4.2. Experimental Setup

In the present work, a setup of a vacuum membrane distillation unit on a laboratory scale is fabricated, and the schematic and pictorial diagram is shown in Figure 4.1 & Figure 4.2 respectively. For conducting various experiments, hydrophobic porous membranes of PTFE and PVDF material is used with a diameter of 90 mm. The properties of both types of membranes are given in Table 4.6. The heating of the feed is carried out in feed tank by heating element at varying temperature ranging from 25 to 85 °C. The temperature of the feed tank is measured using the thermocouple attached in it, and the controlling was done using a PID controller. The feed solution is circulated throughout the membrane module using a centrifugal pump, and the desired flow rate of feed is maintained by using the rotameter, the excess amount of feed solution is bypassed into the feed tank. In the membrane module, the membrane is placed with support and the effective membrane area which is utilized for the transfer of vapor through the pores of the membrane is 52 mm. A vacuum pump is used for maintaining the vacuum degree at the permeate side of the membrane by which the vapor pressure difference through the membrane is maintained. The helically coiled stainless steel condenser is attached on the permeate side of the membrane which condensed the vapors coming on the permeate side due to vapor pressure difference and collected in the receiver. The energy consumed by the heating element, feed pump, cooling pump, and the vacuum pump is measured by the electrical meters. Table 4.7 represents the properties of various instruments attached in an experimental setup.

**Table 4.6: Properties of the used membranes**

Properties	Specifications
Membrane material	PTFE & PVDF
Surface property	Hydrophobic
Diameter, mm	90
Effective membrane diameter, mm	52
Pore size, $\mu\text{m}$	0.22
Thickness, $\mu\text{m}$	175
Porosity %	85
Effective membrane area, $\text{m}^2$	0.00212
Maximum operating temperature, °C	130 & 110
Supplier	Millipore

**Table 4.7: Specifications of different instruments attached in experimental setup**

Instrument	Specification	Make
Thermocouple	0-125 °C with least count of 1 °C.	PT 100
Rotameter	Range 0-10 lpm, with least count 0.2 lpm, Accuracy 99.16%	Star Flow India
Vacuum Pump	Oil based	Parag Engg.
Vacuum Gauge	0 to -760 mmHg with least count of 20 mm Hg	Monometer
Centrifugal Pump	½ hp	Crompton

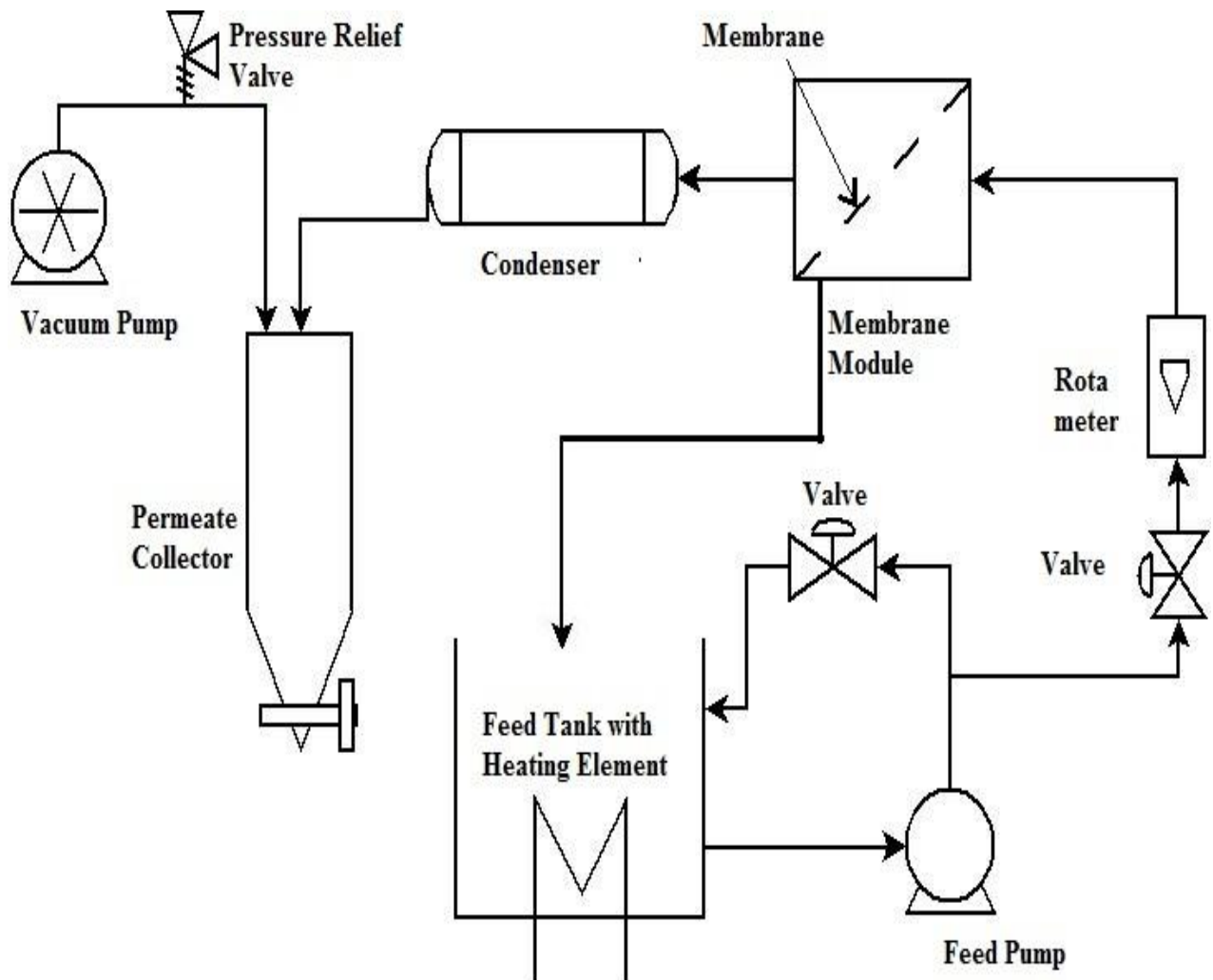


**Figure 4.1: Schematic Diagram of Vacuum membrane Distillation unit**



**Figure 4.2: Pictorial diagram of lab scale vacuum membrane distillation unit**

### 4.3. Experimental Procedure

The experimental procedure for performing the experiments on lab setup is as follows:

1. The experiments were carried out at different initial dye concentrations in vacuum membrane distillation setup.
2. The feed solution was fed to feed tank and heated up to the desired temperature.
3. The centrifugal feed pump was used to pump the heated feed solution to the flat sheet membrane module in which a porous hydrophobic membrane was placed.
4. On the permeate side, a vacuum is applied to maintain the driving. Force.
5. The vapors passed through the dry pores of the membrane are condensed in the external condenser and collected in permeate collector.
6. UV-vis spectrophotometer was used for testing the quality of permeate.

### 4.4. UV-Vis spectrophotometer

The concentration of dye molecules in feed and the permeate samples was analyzed using the double beam UV-spectrophotometer. This analytical device generally operates at Beer-Lambert Law and measured the absorbance of dye molecules present in sample. The calibrations curve for different dye solutions was prepared by measuring the absorbance of the known concentrations which follow the linear plot. The technical specifications of UV-vis spectrophotometer is given in Table 4.8.

**Table 4.8: Properties of UV-vis spectrophotometer**

Manufacturer	Shimadzu corporation analytical instruments, Japan
Light source	Tungsten halogen and Deuterium lamp
Model	UV-1800
Operating temperature of the lamp	30-50 °C
Optics arrangement	Double beam
Frequency	50Hz
Range of wavelength	1100-190 nm

#### **4.5. Microscopic methods for characterization**

Scanning electron microscopy (SEM) with EDS is used for the study of the surface morphology of fresh and used membrane as shown in Figure 4.3 & Figure 4.4 in *Material and Research Center, MNIT Jaipur*. The images of the sample in SEM are produced by scanning of the sample with the help of electron beam at different magnifications. The electrons produced by electron beam are a strike on the surface of the sample and produced the signals that the system detects signals and the surface morphology of the surface is determined. The analysis of the sample is carried out the complete vacuum with the fine resolution lower than 1 nanometer at the operating voltage of 5kV. Generally, for amplifying the signals coming after the strike with the surface, electron amplifier is used which displayed the vibrations on the computer monitor. The distance between the sample and the electron beam is very narrow. So, the images produced by the SEM are depended upon the angle and between the electron beam and the surface beam. The steps involved in the characterization of porous hydrophobic PTFE and PVDF membranes morphology is as follows:

- I. Gold Coating is done for keeping away the sample from heating.
- II. Placing the samples into the holder of the SEM instrument.
- III. The analysis of the coated sample is done at different magnification for the study of morphology.
- IV. The elemental composition of the sample is identified using the EDS analysis of the sample.





**Figure 4.3: Scanning Electron Microscope**

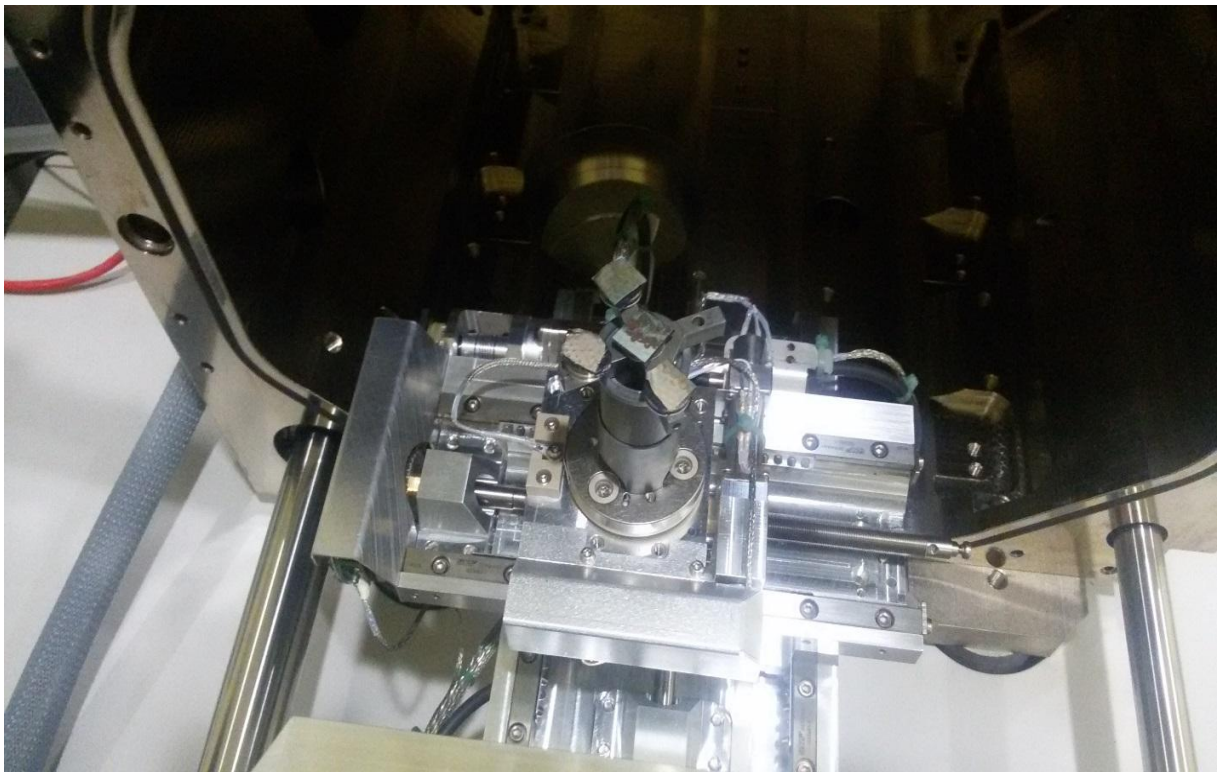


**Figure 4.4: SEM Opened Sample Chamber**

#### 4.6. Permeate flux, Specific energy consumption and percentage removal calculation

The experimental permeate flux is calculated using equation (3.14):

$$N = \frac{V_{col} \cdot \rho}{A_{eff} \cdot t} \quad (4.1)$$

Where  $V_{col}$  is the volume of permeate collected (lt),  $\rho$  is the density of permeate water,  $A_{eff}$  is the effective membrane area available and  $t$  is the experiment run time to collect permeate.

The specific energy consumption (kWh/m<sup>3</sup>) is calculated using equation (4.2):

$$\text{Specific Energy Consumption} = \frac{TEC}{V_{col}} \quad (4.2)$$

Where  $TEC$  is the total energy consumption calculated using energy meters (kWh) and  $V_{col}$  is the volume of permeate collected (lt).

The concentration of dye in feed sample and the permeate water was calculated using UV-Vis spectrophotometer. The percentage removal of dye from wastewater was calculated using equation (4.3).

$$\text{Percentage Removal} = \frac{C_f - C_p}{C_f} * 100 \quad (4.3)$$

Where  $C_f$  and  $C_p$  is the concentration of dye in feed and permeate respectively.

## CHAPTER 5. RESULTS AND DISCUSSIONS

A detailed description of results obtained from experimental investigations and its validation with existing mathematical models and subsequent discussion/ interpretation along with membrane characterization, Central Composite Design Optimization, and recovery calculation have been carried out and effects of various parameters on permeate flux, specific energy consumption and percentage removal were also discussed in this section.

### 5.1. Statistical analysis of Experiments

Before performing design of experiments, the standard deviation (SD) and coefficient of variance(COV) were computed as shown in Table 5.1. It was observed that the coefficient of variance is far less than one for all responses. It implies that the data are well suited for performing central composite design of experiment in order to determine the optimum condition.

**Table 5.1: Statistical analysis of experimental runs**

Variable	Mean	SE Mean	Standard Deviation	Minimum	Maximum	Median	Coefficient of Variation
Permeate flux	20.33	2.13	11.88	1.13	52.23	17.90	0.584358
Specific Energy Consumption	7.876	0.377	2.097	4.228	12.630	7.77	0.266252
Percentage Removal	99.188	0.0861	0.479	98.125	99.784	99.452	0.004829

### 5.2. Central Composite Design for PTFE and PVDF membranes

The optimization of process variables of a system is considered as important stage for enhancing the system efficiency with minimum number of experiments. Traditionally, one-factor-at-a-time technique (only one factor kept varying while other factors remain constant) is used for optimization of process variables which is time-consuming and also does not predict the interaction effects of process variables. Moreover, in this technique, the experimentation work is very large which leads to higher consumption of chemicals and materials and become very costly and time-consuming.

To remove this problem, Response surface methodology (RSM), a multivariate statistical analysis technique, was used for designing of minimum experimental conditions set to optimize the process variables. RSM is a combined technique of empirical statistical and mathematical analysis for the quantitative analysis of experimental problems which fit the polynomial model

for the experimental analysis. In RSM, a series of experimental conditions was conducted by varying the input conditions and the influenced in response variable is determined. The main aim of RSM technique is to optimize the response variables which are highly affected by the input operating conditions (Khataee 2010; Aslan 2008; Shafeeyan et al. 2012; Mook et al. 2016; Cho & Zoh 2007; Quist-Jensen et al. 2015).

The steps considered during the optimization of responses using response surface methodology are as follows: (1) define the input operating conditions which affect the responses; (2) Choose proper experimental design and perform the runs according to design matrix; (3) perform mathematical-statistical analysis and fit the polynomial equation for the experimental conditions; (4) check the fitness of developed model with experimental responses; (5) define the necessary conditions for the optimization of process responses; (6) Obtained optimum value and perform confirmation test.

In this study, central composite design (CCD), one of the best technique of RSM, was chosen for the optimization of process variables within the minimum number of experiments and fitting second-order non-linear model. For studying the effect of operating variables on permeate flux, specific energy consumption, and percentage removal, four significant factors were considered as feed temperature ( $^{\circ}\text{C}$ ), flow rate (lpm), Initial dye concentration (ppm) and vacuum degree (mmHg). The sum of factorial runs ( $2^n$ ), axial runs ( $2n$ ) and center runs ( $n_c$ ) are provide set of the number of experiments to be performed, where  $n$  represents the number of operating variables. After deciding the range of operating variables, the variables are coded so that they can lie at  $\pm 1$  (lower and higher) for factorial points, 0 for center points and  $\pm\beta$  (lowest and highest) for axial points. Coded value of each operating variable is calculated from the actual values using the relationship is given in Table 5.2. where  $a_{min}$  and  $a_{max}$  are the actual minimum and maximum values of that operating variable and  $\alpha = 2^{n/4}$ . The experimental ranges of each operating variables for both PTFE and PVDF membrane are given in Table 5.3.

**Table 5.2: Relationship between coded and actual values**

Coded variable	Actual values of the variable
Lowest axial point ( $-\beta$ )	$a_{\min}$
Lower cube point ( $-1$ )	$[(a_{\max} + a_{\min}) / 2] - [(a_{\max} - a_{\min}) / 2\alpha]$
Center ( $0$ )	$(a_{\max} + a_{\min}) / 2$
Higher cube point ( $+1$ )	$[(a_{\max} + a_{\min}) / 2] + [(a_{\max} - a_{\min}) / 2\alpha]$
Highest axial point ( $+\beta$ )	$a_{\max}$

**Table 5.3: Experimental levels of independent variables for PTFE and PVDF membrane**

Variables	Symbol	Coded Variable Level				
		$-\beta$	$-1$	$0$	$+1$	$+\beta$
Feed Temperature ( $^{\circ}\text{C}$ )	A	25	40	55	70	85
Flow rate (lpm)	B	2	4	6	8	10
Initial dye concentration (ppm)	C	10	40	70	100	130
Vacuum Degree (mmHg)	D	670	690	710	730	750

### 5.2.1. CCD model analysis for PTFE and PVDF membrane

Total 31 numbers of experimental run sets were obtained using central composite design for each membrane. The four factorial central composite designs is shown in Table 5.4 regarding actual and coded values. Thirty-one experimental run was performed on VMD experimental setup, and various responses are shown in Table 5.5 for each membrane. After applying the CCD using MINITAB, the predicted values of the different responses such as permeate flux, specific energy consumption, and percentage removal are given in Table 5.5.

**Table 5.4: Four-factorial central composite design regarding coded and actual values**

Run	Feed Temp. (A)		Flow rate (B)		Initial Dye Concentration (C)		Downstream Pressure (D)		
	Coded	Actual	Coded	Actual	Coded	Actual	Coded	Actual	
1.	-1	40	-1	4	-1	40	-1	690	Factorial Design
2.	1	70	-1	4	-1	40	-1	690	
3.	-1	40	1	8	-1	40	-1	690	
4.	1	70	1	8	-1	40	-1	690	
5.	-1	40	-1	4	1	100	-1	690	

6.	1	70	-1	4	1	100	-1	690		
7.	-1	40	1	8	1	100	-1	690		
8.	1	70	1	8	1	100	-1	690		
9.	-1	40	-1	4	-1	40	1	730		
10.	1	70	-1	4	-1	40	1	730		
11.	-1	40	1	8	-1	40	1	730		
12.	1	70	1	8	-1	40	1	730		
13.	-1	40	-1	4	1	100	1	730		
14.	1	70	-1	4	1	100	1	730		
15.	-1	40	1	8	1	100	1	730		
16.	1	70	1	8	1	100	1	730		
17.	$-\beta$	25	0	6	0	70	0	710		Axial Points
18.	$+\beta$	85	0	6	0	70	0	710		
19.	0	55	$-\beta$	2	0	70	0	710		
20.	0	55	$+\beta$	10	0	70	0	710		
21.	0	55	0	6	$-\beta$	10	0	710		
22.	0	55	0	6	$+\beta$	130	0	710		
23.	0	55	0	6	0	70	$-\beta$	750		
24.	0	55	0	6	0	70	$+\beta$	750		
25.	0	55	0	6	0	70	0	710	Central Points	
26.	0	55	0	6	0	70	0	710		
27.	0	55	0	6	0	70	0	710		
28.	0	55	0	6	0	70	0	710		
29.	0	55	0	6	0	70	0	710		
30.	0	55	0	6	0	70	0	710		
31.	0	55	0	6	0	70	0	710		

To study the adequacy of the CCD models, the residual (difference between actual and predicted values of responses) plots were evaluated. Residual is used to explain the variation of the predicted model according to the normal distribution which is a graphical method used for studying the normality of the residual. Generally, the normal probability of the residual should follow the straight line, but due to large number of experimental results, the slight difference from the normality line does not affect the response results seriously. Figure 5.1 shows the residual plots for permeate flux, specific energy consumption, and percentage removal for PTFE membrane. From this Figure 5.1, it can be seen that the maximum number of experimental results lie on the normality line, so the response values are normally distributed for all responses. From the residual versus fitted values, it can be observed that the residuals are randomly scattered about zero. Histogram and residual versus observation order show that the values fluctuate in a random manner around the central line for three responses. It can be seen that the

error between experimental and predicted permeate flux is within the range of -2 to +1.5 in the residual plot, which is acceptable. For specific energy consumption, the developed model is more accurate, and the error is within the range of -0.8 to +0.6. For percentage removal, the error is very less, and it is within the range of -0.10 to +0.15. By error analysis between experimental and predicted values of all responses, the developed model is acceptable.

Similarly, Figure 5.2 represents the residual analysis for PVDF membrane of 0.22 micron pore size. It can be stated that the error lies within the range of  $\pm 1.5$  for permeate flux, -0.8 to +0.6 for specific energy consumption and  $\pm 0.12$  in case of percentage removal. From this residual analysis, it was seen that the error between the experimental and predicted values lies within the acceptable range of error. So, present model is acceptable for PVDF membrane.

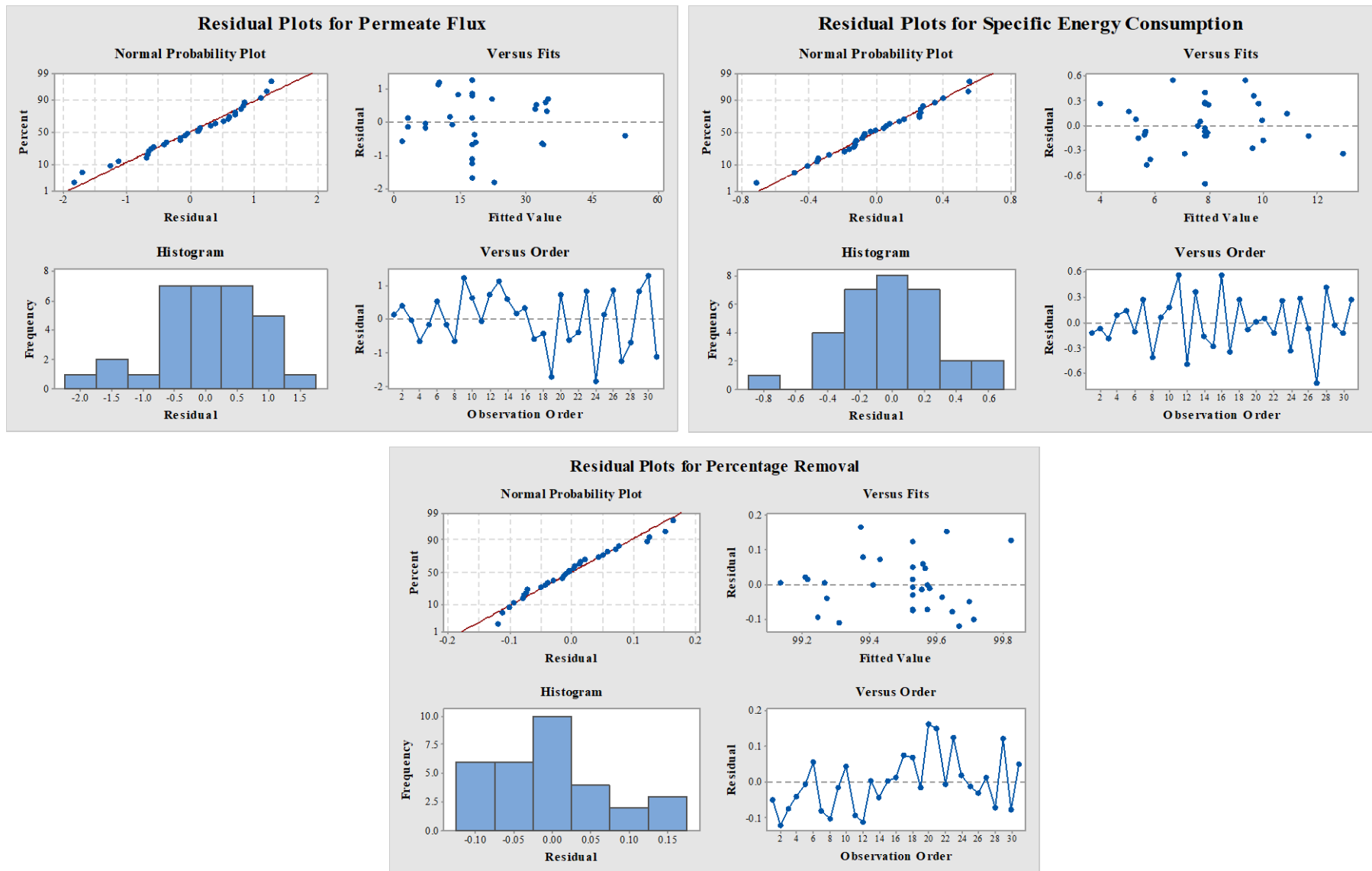


**Figure 5.1: Residual Plots for PTFE Membrane**



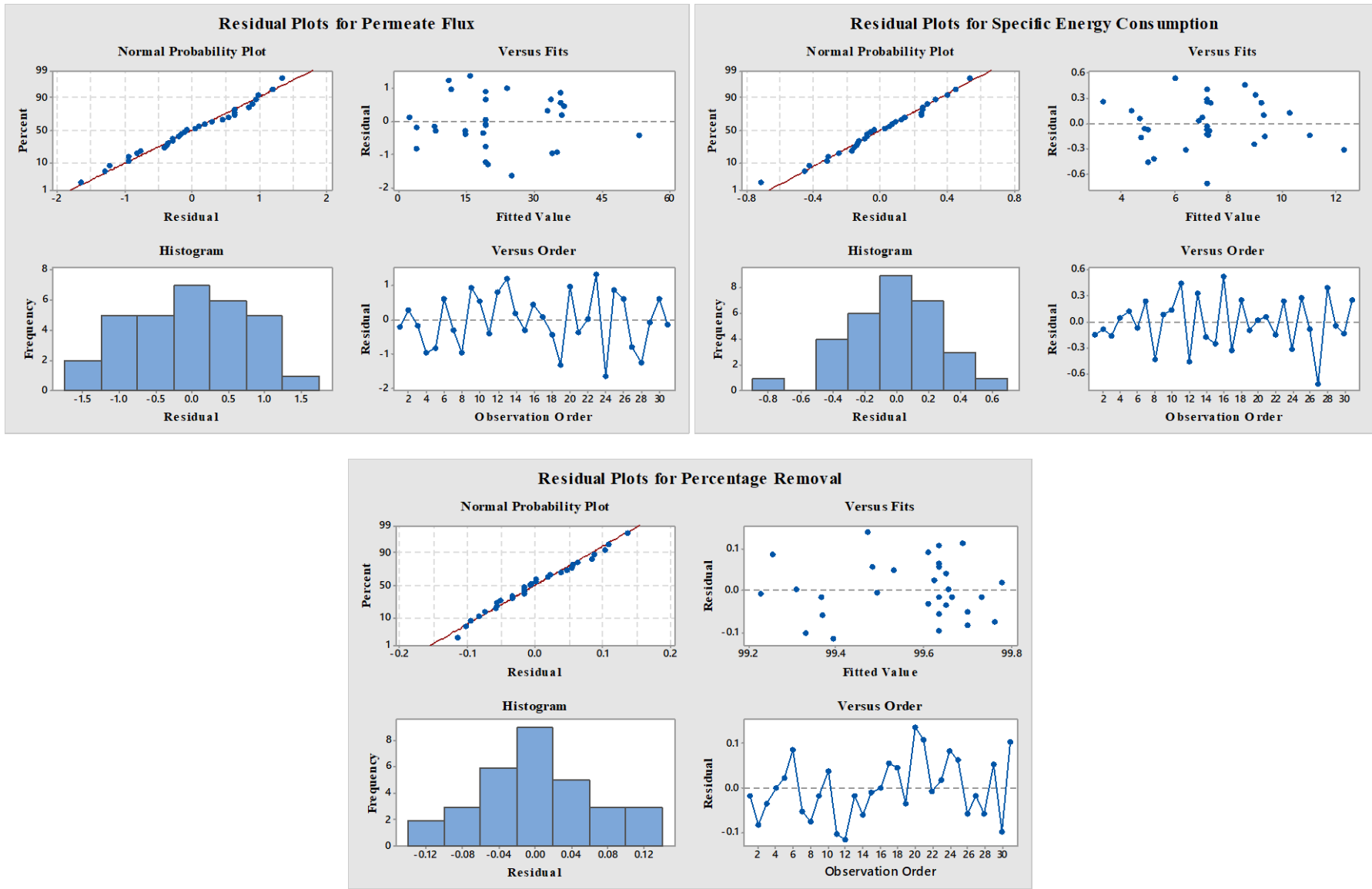


Figure 5.2: Residual Plots for PVDF Membrane

**Table 5.5. Observed and predicted outputs of various experimental runs**

Run	PTFE Membrane of 0.22 $\mu\text{m}$						PVDF Membrane of 0.22 $\mu\text{m}$					
	Permeate Flux		Specific Energy Consumption		Percentage Removal		Permeate Flux		Specific Energy Consumption		Percentage Removal	
	E*	P*	E*	P*	E*	P*	E*	P*	E*	P*	E*	P*
1.	3.15	3.03	11.56	11.68	99.65	99.70	3.82	4.01	10.92	11.06	99.72	99.74
2.	32.55	32.16	5.57	5.64	99.55	99.51	33.45	33.14	4.93	5.01	99.62	99.70
3.	7.15	7.20	9.85	10.03	99.50	99.52	7.84	8.01	9.21	9.37	99.58	99.61
4.	33.15	33.82	5.37	5.29	99.58	99.62	33.1	34.04	4.73	4.67	99.66	99.66
5.	2.96	3.11	11.05	10.91	99.57	99.57	3.14	3.95	10.41	10.28	99.65	99.63
6.	32.86	32.33	5.47	5.59	99.62	99.64	34.54	33.90	4.83	4.89	99.7	99.61
7.	6.90	7.06	10.12	9.85	99.57	99.58	7.95	8.24	9.48	9.24	99.65	99.70
8.	33.13	33.78	5.42	5.83	99.61	99.64	34.15	35.08	4.78	5.20	99.69	99.76
9.	11.52	10.32	10.06	9.99	99.57	99.58	12.65	11.69	9.42	9.33	99.65	99.67
10.	35.15	34.54	5.17	5.00	99.61	99.57	36.45	35.89	4.53	4.38	99.69	99.65
11.	13.25	13.33	9.93	9.38	99.15	99.18	14.52	14.89	9.05	8.60	99.23	99.33
12.	35.76	35.05	5.20	5.69	99.20	99.31	36.84	36.00	4.56	5.02	99.28	99.39
13.	11.15	10.03	10.00	9.65	99.27	99.27	12.45	11.24	9.36	9.03	99.35	99.37
14.	34.95	34.35	5.21	5.37	99.23	99.27	36.45	36.25	4.57	4.74	99.31	99.37
15.	12.99	12.82	9.34	9.62	99.14	99.14	14.45	14.73	8.7	8.95	99.22	99.23
16.	34.96	34.63	7.20	6.65	99.23	99.22	37.1	36.64	6.56	6.03	99.31	99.31
17.	1.13	1.70	12.63	12.98	99.46	99.49	2.45	2.34	11.99	12.31	99.54	99.48
18.	52.23	52.64	4.23	3.96	99.50	99.47	52.98	53.39	3.59	3.33	99.58	99.53
19.	16.15	17.85	7.86	7.95	99.54	99.56	18.45	19.74	7.22	7.31	99.62	99.65
20.	23.01	22.30	7.57	7.57	99.54	99.49	25.12	24.13	6.93	6.90	99.61	99.47
21.	18.12	18.61	7.73	7.69	99.78	99.75	18.45	18.80	7.09	7.02	99.8	99.69
22.	17.90	18.28	7.75	7.88	99.41	99.41	19.45	19.40	7.11	7.25	99.49	99.50
23.	15.46	14.63	8.23	7.97	99.95	99.89	17.25	15.91	7.59	7.34	99.8	99.78
24.	20.95	22.78	6.76	7.10	99.23	99.21	23.51	25.15	6.12	6.43	99.34	99.26
25.	17.85	17.71	8.13	7.84	99.52	99.53	20.11	19.21	7.49	7.20	99.7	99.64
26.	18.57	17.71	7.77	7.84	99.50	99.53	19.85	19.21	7.13	7.20	99.58	99.64
27.	16.46	17.71	7.13	7.84	99.54	99.53	18.45	19.21	6.49	7.20	99.62	99.64
28.	17.02	17.71	8.25	7.84	99.46	99.53	17.99	19.21	7.61	7.20	99.58	99.64

29.	18.51	17.71	7.81	7.84	99.65	99.53	19.14	19.21	7.17	7.20	99.69	99.64
30.	19.05	17.71	7.72	7.84	99.45	99.53	19.85	19.21	7.08	7.20	99.54	99.64
31.	16.58	17.71	8.10	7.84	99.58	99.53	19.1	19.21	7.46	7.20	99.74	99.64

\*E=Experimental flux, \*P=Predicted flux

### 5.2.2. Second-Order Model and Analysis of Variance

The generalized second-order nonlinear model was developed considering the effect of main operating factors and the interaction between them as given by equation(2.1).

$$y = \beta_0 + \beta_1 * A + \beta_2 * B + \beta_3 * C + \beta_4 * D + \beta_{11} * A^2 + \beta_{22} * B^2 + \beta_{33} * C^2 + \beta_{44} * D^2 + \beta_{12} * AB + \beta_{13} * AC + \beta_{14} * AD + \beta_{23} * BC + \beta_{24} * BD + \beta_{34} * CD \quad (5.1)$$

The operating variables such as feed temperature, flow rate, initial dye concentration and permeate pressure is represented by  $A$ ,  $B$ ,  $C$  and  $D$  respectively. The coefficient  $\beta_i$  represents the main effect of individual operating parameters,  $\beta_{ii}$  represents the square effects, and  $\beta_{ij}$  represents the interaction effect of any two parameters. The values of these model coefficients are estimated from the experimental results summarized in Table 5.5 for individual responses. The regression equations for PTFE membrane for different responses are given by equations (5.2) to (5.4). For PVDF membrane, the regression equation is given by equations (5.5)-(5.7).

Regression equations for PTFE membrane

$$\text{Permeate Flux} = 17.712 + 25.459A + 2.227B - 0.168C + 4.074D + 9.461A^2 + 2.365B^2 + 0.733C^2 + 0.991D^2 - 2.50AB + 0.09AC - 4.90AD - 0.22BC - 1.16BD - 0.37CD \quad (5.2)$$

$$\text{Specific Energy Consumption} = 7.842 - 4.508A - 0.189B + 0.095C - 0.436D + 0.630A^2 - 0.086B^2 - 0.061C^2 - 0.307D^2 + 1.30AB + 0.717AC + 1.053AD + 0.590BC + 1.034BD + 0.422CD \quad (5.3)$$

$$\text{Percentage Removal} = 99.5294 + 0.0064A - 0.0228B - 0.0275C - 0.0769D - 0.00773A^2 - 0.00391B^2 - 0.00041C^2 - 0.00086D^2 + 0.00468AB + 0.00105AC + 0.00114AD + 0.01262BC - 0.01293BD - 0.01171CD \quad (5.4)$$

Regression equations for PVDF membrane

$$\text{Permeate Flux} = 140 + 2.834A + 3.37B + 0.094C - 0.785D + 0.009613A^2 + 0.1701B^2 - 0.0000C^2 + 0.000823D^2 - 0.02583AB + 0.00045AC - 0.004108AD + 0.00119BC - 0.00497BD - 0.000165CD \quad (5.5)$$

$$\begin{aligned} \text{Specific Energy Consumption} = & 3.6 - 0.975A - 5.10B - 0.174C + 0.169D + 0.000686A^2 \\ & - 0.0061B^2 - 0.000020C^2 - 0.000199D^2 + 0.01133AB + 0.000367AC + 0.000925AD \\ & + 0.00271BC + 0.00606BD + 0.0002CD \end{aligned} \quad (5.6)$$

$$\begin{aligned} \text{Percentage Removal} = & 160 + 0.0116A + 0.461B + 0.0175C - 0.1756D - 0.000062A^2 \\ & - 0.001B^2 + 0.000011C^2 + 0.000127D^2 + 0.000292AB + 0.00003AC - 0.000008AD \\ & - 0.000167BC - 0.000656BD - 0.000027CD \end{aligned} \quad (5.7)$$

Analysis of variance is carried out to check the consistency of the model and to identify the significance of individual and interaction parameters. The model is considered as significant if the  $p$ -value is less than 0.05 (using 95% level of significance). The significant interaction terms were considered to analyze the better-combined effect on the responses in regression correlations. The analysis of variance for different responses (permeate flux, specific energy consumption, and percentage removal) is carried out to observe the significance of operating parameters. The acceptability of ANOVA table depends upon the lack of fit test, if the  $p$ -value of lack of fit is lower than 0.05 then the ANOVA model is not acceptable. From Table 5.6 and Table 5.7, it can be seen that the  $p$ -value of lack of fit test is higher than 0.05. So, the lack of fit is insignificant, and the model is acceptable.

For PTFE membrane, from the  $p$ -value shown in Table 5.6, it can be observed that linear contribution of three parameters (A, B and D), the quadratic contribution of two parameters ( $A^2$  and  $B^2$ ) and cross product contribution of parameters ( $A*B$ ,  $A*D$ , and  $B*D$ ) were significant for higher permeate flux. For minimum specific energy consumption, it can be concluded that linear contribution of A and D, the quadratic contribution of  $A^2$  and  $D^2$  and cross product of  $A*B$ ,  $A*D$ , and  $B*D$  were significant by  $p$ -values shown in Table 5.6. Moreover, the linear contribution of B, C, and D and cross product contribution of three combinations ( $B*C$ ,  $B*D$ , and  $C*D$ ) are found significant for maximum percentage removal.

For PVDF membrane, from the  $p$ -value shown in Table 5.7, it can be seen that the linear contribution of three variables as A, B, and D, the quadratic contribution of two as  $A^2$  and  $B^2$  and cross product contribution of  $A*B$ ,  $A*D$  and  $B*D$  were significant parameters for higher permeate flux. In the case of minimum specific energy consumption, the linear contribution of A and D, the square contribution of  $A^2$  and the cross product of  $A*B$ ,  $A*D$  and  $B*D$  were found significant. Moreover, the linear contribution of B, C, and D, as well as the cross product of  $B*C$ ,  $B*D$  and  $C*D$ , are found significant for maximum percentage removal. The level of significance of each factor is based on 95% of confidence level.

**Table 5.6: Analysis of Variance for PTFE Membrane**

Sources	Permeate Flux					Specific Energy Consumption					Percentage Removal				
	DF	Adj SS	Adj MS	F-value	p-value	DF	Adj SS	Adj MS	F-value	p-value	DF	Adj SS	Adj MS	F-value	p-value
Linear Model															
A	1	3891.98	3891.98	3076.40	<0.0001	1	121.924	121.924	724.80	<0.001	1	0.00392	0.003922	0.36	0.559
B	1	29.76	29.76	23.52	<0.0001	1	0.214	0.214	1.27	0.276	1	0.04973	0.049727	4.51	0.049
C	1	0.17	0.17	0.13	0.719	1	0.054	0.054	0.32	0.580	1	0.07240	0.072401	6.57	0.021
D	1	99.59	99.59	78.72	<0.0001	1	1.139	1.139	6.77	0.019	1	0.56756	0.567556	51.49	<0.0001
Square Model															
A*A	1	159.98	159.98	126.46	<0.0001	1	0.708	0.708	4.21	0.057	1	0.02737	0.027369	2.48	0.135
B*B	1	9.99	9.99	7.90	0.013	1	0.013	0.013	0.08	0.784	1	0.00698	0.006981	0.63	0.438
C*C	1	0.96	0.96	0.76	0.396	1	0.007	0.007	0.04	0.845	1	0.00008	0.000076	0.01	0.935
D*D	1	1.76	1.76	1.39	0.256	1	0.168	0.168	1.0	0.332	1	0.00034	0.000338	0.03	0.863
2-way Interaction Model															
A*B	1	6.27	6.27	4.95	0.0041	1	1.690	1.690	10.05	0.006	1	0.00560	0.005604	0.51	0.486
A*C	1	0.01	0.01	0.01	0.935	1	0.515	0.515	3.06	0.099	1	0.00028	0.000282	0.03	0.875
A*D	1	24.06	24.06	19.02	<0.0001	1	1.110	1.110	6.60	0.021	1	0.00033	0.000331	0.03	0.865
B*C	1	0.05	0.05	0.04	0.845	1	0.348	0.348	2.07	0.170	1	0.04075	0.040746	3.70	0.049
B*D	1	1.34	1.34	1.06	0.0318	1	1.070	1.070	6.36	0.023	1	0.04279	0.042790	3.88	0.038
C*D	1	0.14	0.14	0.11	0.747	1	0.178	0.178	1.06	0.319	1	0.03509	0.035090	3.18	0.021
Error	16	20.24	1.27			16	2.691	0.168			16	0.17635	0.011022		
Lack-of-fit	10	13.89	1.39	1.31	0.385	10	1.844	0.184	1.30	0.387	10	0.14653	0.014653	2.95	0.10215
Pure error	6	6.36	1.06			6	0.848	0.141			6	0.02981	0.004969		
Total	30	4237.24				30	131.931				30	1.02682			

**Table 5.7: Analysis of Variance for PVDF Membrane**

Sources	Permeate Flux					Specific Energy Consumption					Percentage Removal				
	DF	Adj SS	Adj MS	F-value	p-value	DF	Adj SS	Adj MS	F-value	p-value	DF	Adj SS	Adj MS	F-value	p-value
Linear Model															
A	1	3909.66	3909.66	3456.01	<0.0001	1	120.871	120.871	790.84	<0.0001	1	0.00350	0.00350	0.42	0.524
B	1	28.91	28.91	25.55	<0.0001	1	0.256	0.256	1.68	0.214	1	0.04950	0.049504	5.98	0.026
C	1	0.53	0.53	0.47	0.504	1	0.079	0.079	0.52	0.482	1	0.05703	0.057037	6.89	0.018
D	1	128.07	128.07	113.21	<0.0001	1	1.251	1.251	8.19	0.011	1	0.41343	0.41343	49.96	<0.0001
Square Model															
A*A	1	133.77	133.77	118.24	<0.0001	1	0.681	0.681	4.46	0.049	1	0.02919	0.029190	3.53	0.079
B*B	1	13.24	13.24	11.70	0.004	1	0.017	0.017	0.11	0.743	1	0.00947	0.009471	1.14	0.301
C*C	1	0.02	0.02	0.02	0.888	1	0.009	0.009	0.06	0.807	1	0.00327	0.003274	0.40	0.538
D*D	1	3.10	3.10	2.74	0.118	1	0.180	0.180	1.18	0.294	1	0.02480	0.02480	3.0	0.103
2-way Interaction Model															
A*B	1	9.61	9.61	8.49	0.010	1	1.85	1.85	12.10	0.003	1	0.00600	0.00600	0.73	0.407
A*C	1	0.66	0.66	0.58	0.457	1	0.436	0.436	2.85	0.111	1	0.00030	0.000306	0.04	0.850
A*D	1	24.30	24.30	21.48	<0.0001	1	1.232	1.232	8.06	0.012	1	0.00030	0.000306	0.04	0.850
B*C	1	0.08	0.08	0.07	0.792	1	0.422	0.422	2.76	0.116	1	0.03900	0.039006	4.71	0.045
B*D	1	7.63	7.63	5.56	0.0466	1	0.941	0.941	6.16	0.025	1	0.04515	0.045156	5.46	0.033
C*D	1	0.16	0.16	0.14	0.715	1	0.230	0.230	1.51	0.237	1	0.03705	0.037056	4.48	0.050
Error	16	18.10	1.13			16	2.445	0.153			16	0.13239	0.008275		
Lack-of-fit	10	14.39	1.44	2.33	0.157	10	1.601	0.160	1.14	0.457	10	0.09882	0.009882	1.77	0.251
Pure error	6	3.71	0.62			6	0.844	0.141			6	0.03357	0.033571		
Total	30	4263.19				30	131.005				30	0.83735			

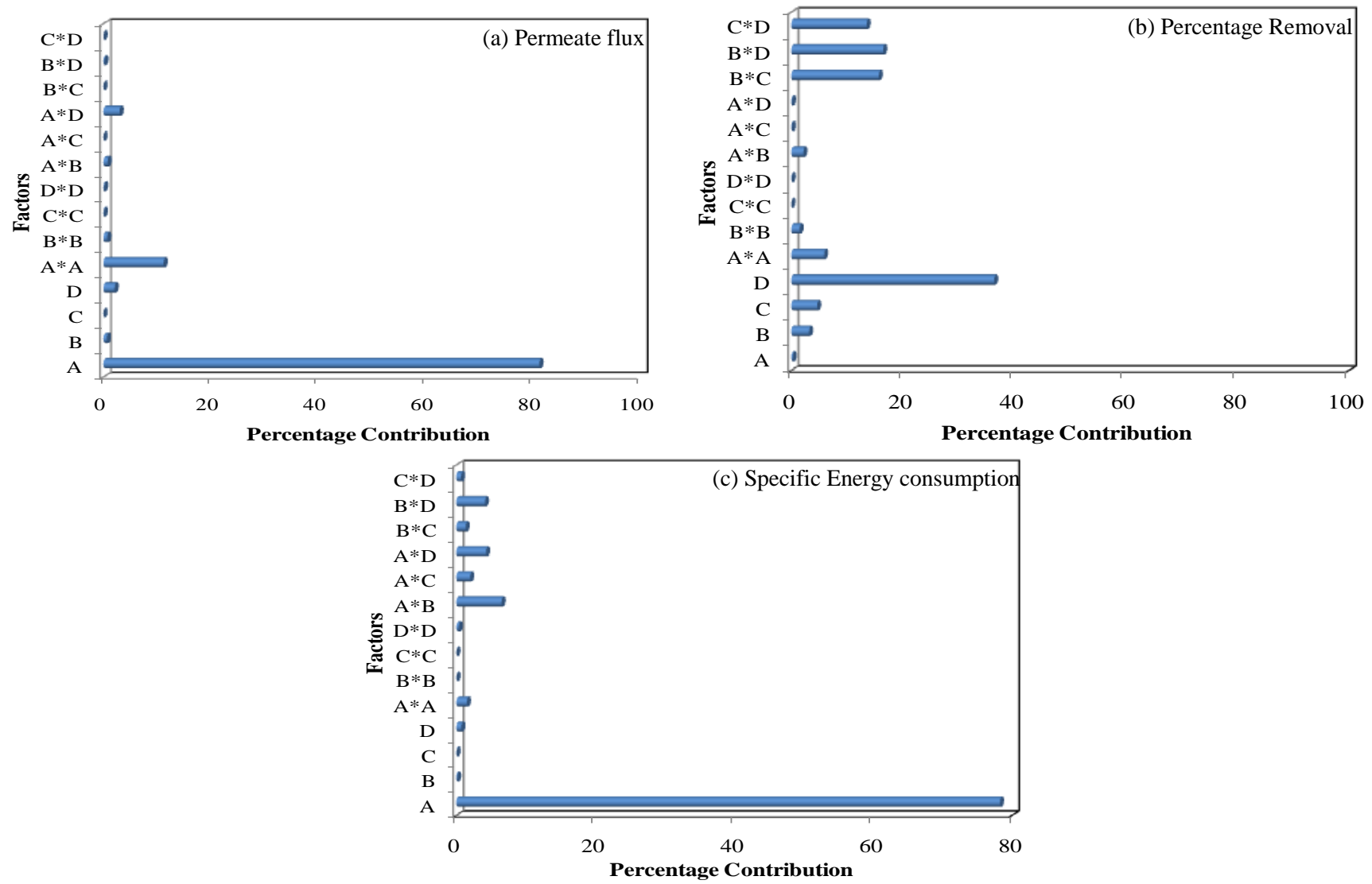


Figure 5.3: Pareto graphic analysis of Percentage contributions of each factor for PTFE membrane

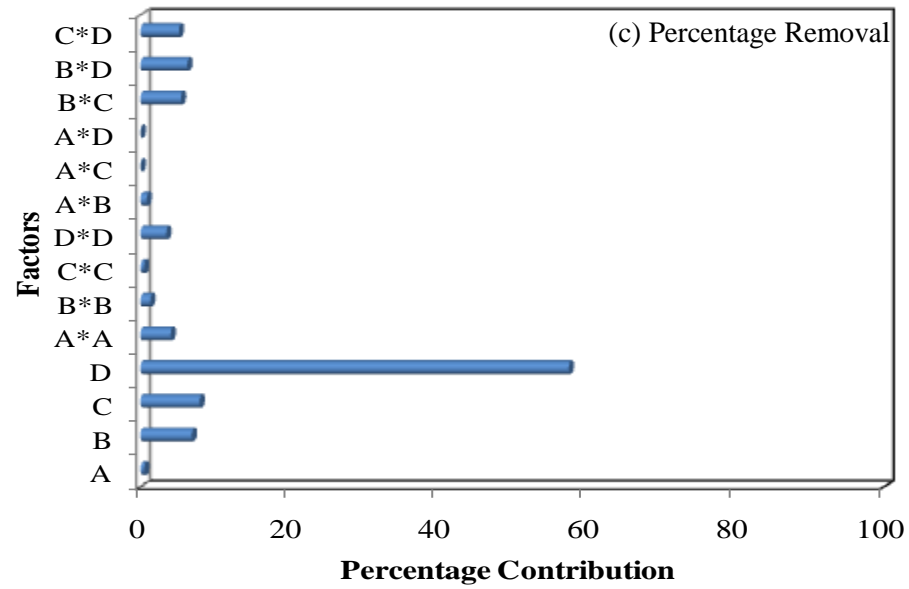
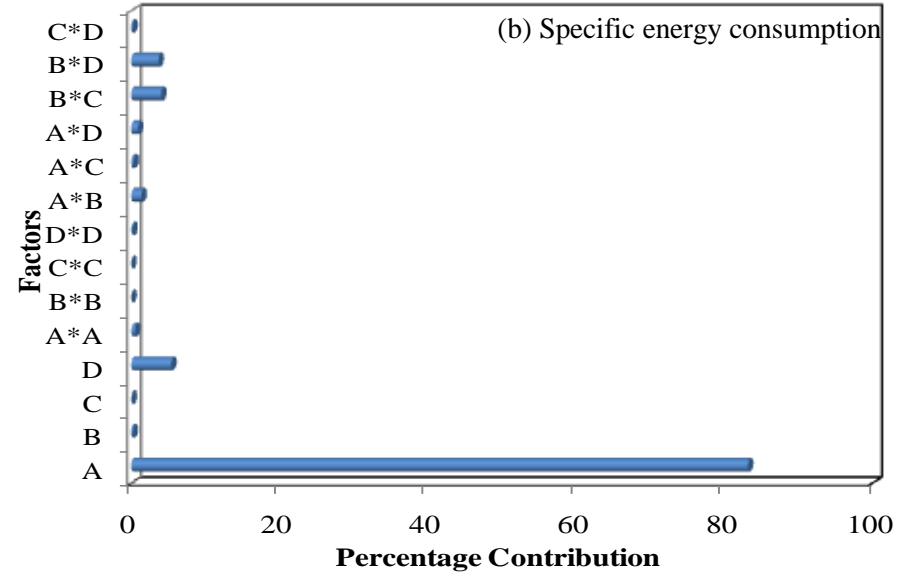
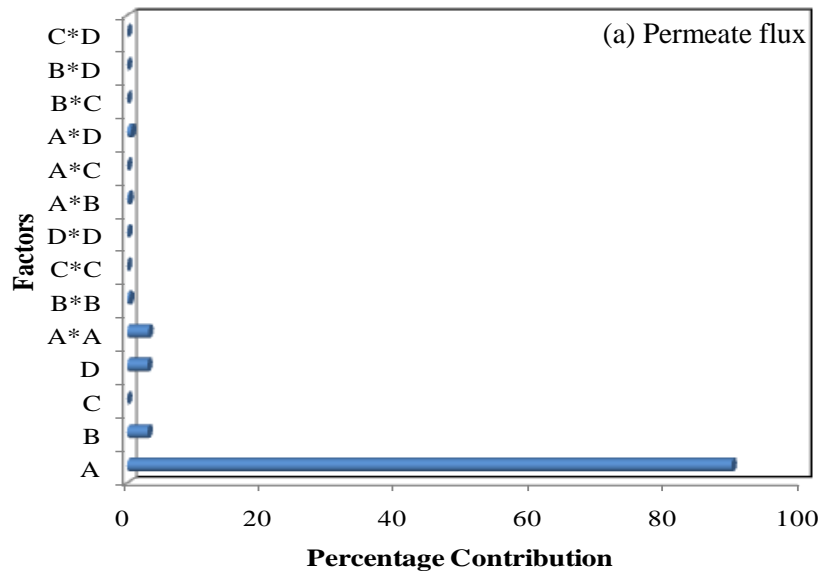


Figure 5.4: Pareto graphic analysis of Percentage contributions of each factor for PVDF membrane



### 5.2.3. Optimization and percentage contribution of process variables

#### 5.2.3.1. Percentage contribution of process variables

The percentage contribution of individual and interaction parameters on permeate flux, specific energy consumption and percentage removal for PTFE and PVDF membrane is shown in Figure 5.3 and Figure 5.4 respectively using Pareto graphs. From Figure 5.3, it can be seen that the percentage contribution of feed temperature is 81.21 % for permeate flux and specific energy consumption is 78.25 for the PTFE membrane which is higher as compared to other operating parameter. However, the flow rate, initial dye concentration and vacuum degree have significant contribution as 3.187%, 4.63% and 36.366% respectively in percentage removal as compared to feed temperature. For PVDF membrane, the percentage contribution of feed temperature is more than 89.5% and 83.2% for permeate flux and specific energy consumption respectively. The contribution effect of vacuum degree and interaction parameter flow rate\*vacuum degree is significant for specific energy consumption. Moreover, the individual factors such as flow rate, vacuum degree and initial dye concentration have a significant effect on percentage removal. The interaction effects such as flow rate\*initial dye concentration (B\*C), flow rate\*vacuum degree (B\*D) and initial dye concentration\*vacuum degree (C\*D) has significant effect on percentage removal as compared to other interactive factors as shown in Figure 5.4 for PVDF membrane.

#### 5.2.3.2. Optimization for PTFE and PVDF membrane

To determine the best-operating conditions, response optimizer toolbox available in central composite design was used to identify the optimum combination of various operating process variables that jointly optimize the permeate flux, specific energy consumption and percentage removal for both PTFE and PVDF membrane. For maximization of permeate flux, percentage removal and minimization of specific energy consumption, the optimized condition were found to be 85 °C, 5 lpm, 30 ppm and 750 mmHg for feed temperature, flow rate, initial dye concentration and vacuum degree respectively for both PTFE and PVDF membrane as shown in Figure 5.5. For these optimized conditions, the composite desirability is 0.9577 and 0.9877 for PTFE and PVDF membrane respectively which makes the optimum values acceptable. The individual desirability of permeate flux and specific energy consumption is one which indicate that these optimum conditions are highly acceptable for PTFE and PVDF membrane. However, the individual desirability of percentage removal is 0.878 and 0.963 which indicate lower acceptability of these optimum conditions for maximization of percentage removal. But from all experiments, it was seen that the percentage removal was more than 99% for all sets of conditions which is acceptable. So, on the basis of experimental results, the individual and composite desirability is

acceptable for each response variables. The optimum conditions of each operating variables are shown in Table 5.8 and the comparison of predicted values with experimental data was carried out. The predicted values are found to be in good agreement with experimental data. Therefore, these set of optimum conditions can be considered as acceptable for PTFE and PVDF membrane.

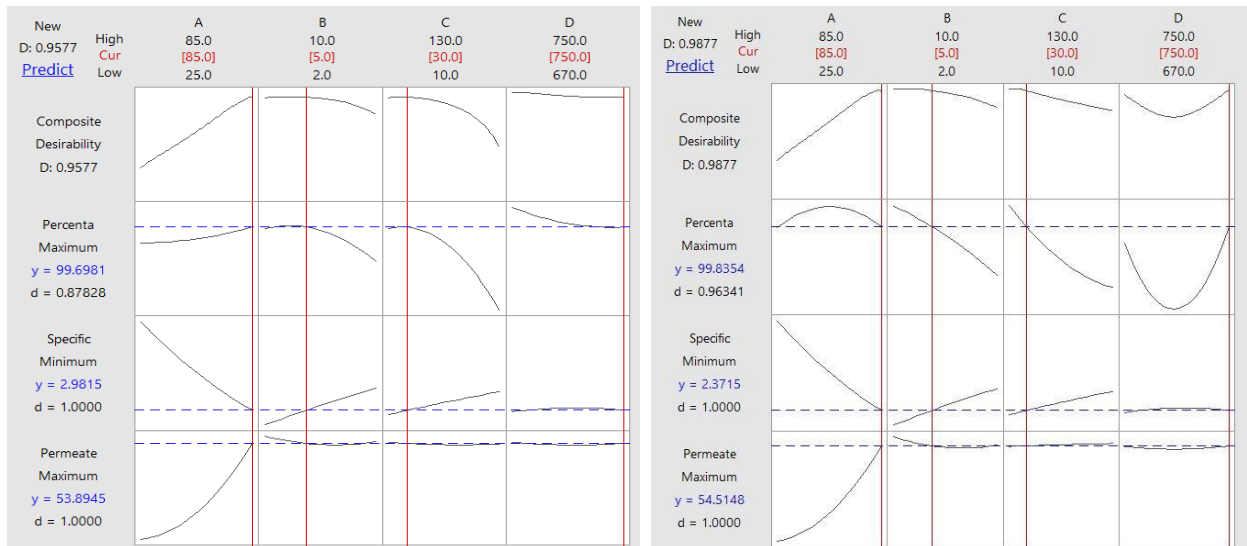


**Figure 5.5: Optimization of process variables for PTFE and PVDF membrane**

**Table 5.8: Confirmation test for PTFE and PVDF membrane**

Operating Conditions		Permeate Flux(kg/m <sup>2</sup> h)		Specific Energy Consumption (kWh/kg)		Percentage Removal	
Parameters	Optimum	Predicted	Observed	Predicted	Observed	Predicted	Observed
Feed Temperature	85 °C	PTFE MEMBRANE					
Feed Flow Rate	5 lpm	53.89	53.51	2.98	3.1	99.698	99.9
Feed Concentration	30 ppm	PVDF MEMBRANE					
Vacuum Degree	750 mmHg	54.51	54.12	2.23	2.6	99.851	99.9

### 5.3. Estimation of Permeate flux and membrane surface temperatures using CFD

CFD is employed during a large choice of disciplines and industries, together with region, automotive, power generation, chemical producing, chemical compound process, fossil fuel exploration, medical analysis, etc. In process industry, the use of CFD technique results in a reduction in time and energy consumption due to process optimization and development. It additionally minimizes the demand for experimentation, enhances style reliableness. CFD has a colossal potential impact on industries as a result of the resolution of the equations of motion provides a purposeful result.

In this study, computational fluid dynamics is applied for estimation of permeate flux and membrane surface temperatures (which is very difficult to measure experimentally). The detailed description of CFD modeling is given in Chapter 3. 3D geometry is developed in comsol multiphysics comprising three different sections named as feed, permeate and membrane section. The equations derived for feed, membrane and permeate section with its boundary conditions are solved using CFD module available in commercial COMSOL Multiphysics software package. The time-dependent equations of momentum, energy, and mass are solved using PARDISO solver. For meshing of geometry, physics controlled meshing scheme is selected, and fine meshing is used to create meshing of the module. The grid independence test is also performed to check the dependability of permeate flux from meshing. The grid independence test is performed at the optimum conditions of the operating variables such as feed temperature of 85 °C, vacuum degree of 750mmHg, flow rate of 5lpm and initial dye concentration of 30 ppm as shown in Table 5.9. It can be stated from Table 5.9 that the percentage error between CFD model flux and experimental flux is lower in fine meshing of the geometry. So, fine meshing mechanism is considered for the grid generation of the defined geometry.

**Table 5.9: Grid Independence test**

Meshing	Cells	CFD Flux	Experimental Flux	Percentage Error
Extremely Coarse	982	Not Determined	53.51	
Extra coarse	1657	57.61	53.51	7.662119
Coarser	2728	56.985	53.51	6.494113
Coarse	4601	56.544	53.51	5.669968
Normal	9851	54.98	53.51	2.74715
Fine	26717	54.41	53.51	1.681929

The contours for the temperature and the convective heat flux through the membrane is generated at the varying conditions of operating parameters such as feed temperature from 25 to 85 °C, vacuum degree of 670 to 750 mmHg, flow rate of 2 to 10 lpm and initial concentration of 10 to 130 ppm. The temperature contour at 55 °C and 85 °C feed temperature is shown in Figure 5.6 & Figure 5.7. By comparing these two figures, it can be observed that the temperature difference across the membrane at 55 °C is lower as compared to 85 °C. The possible reason for this temperature profile may be the driving force of the process. As the driving force of vacuum membrane distillation is trans-membrane vapor pressure difference which increased exponentially on increasing feed temperature. So, the transport of vapors from the feed section to permeate section through the membrane is increased which results in rapid reduction the temperature at the feed side membrane surface. The temperature contour at different operating conditions is given in Appendix II. The temperature decreases from feed side to membrane side. The mean temperature of the feed side membrane surface temperature was found by taking average of the temperature at several locations. The permeate flux is estimated from the convective heat flux profile. As only vapor molecules are transported through the membrane so the heat taken by the vapor molecules can be given by convective heat flux. So, the permeate flux can be obtained by dividing the convective heat flux by latent heat of vaporization of feed solution. The convective heat flux at the optimum conditions is shown in Figure 5.8.

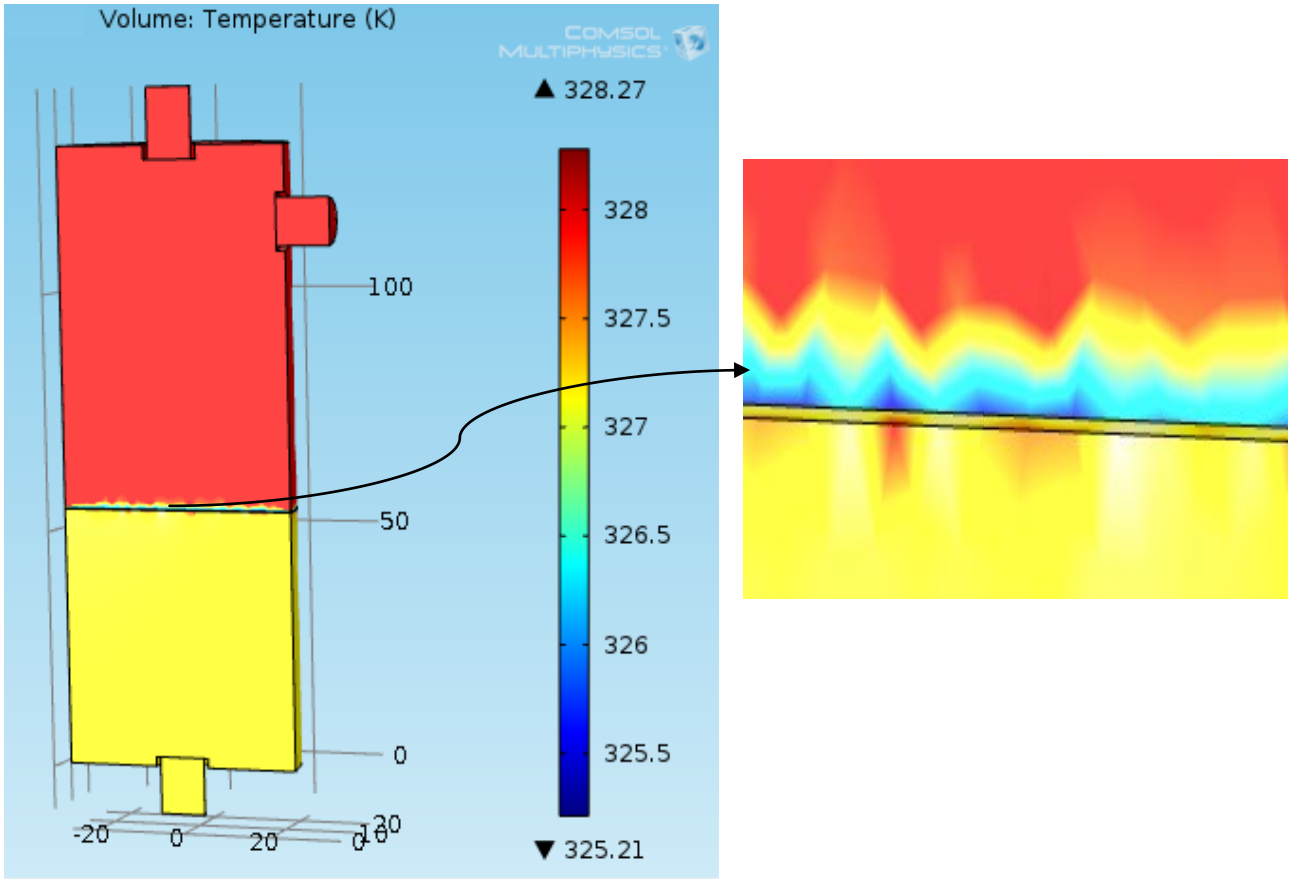


**Figure 5.6: Temperature contour at 328 °K/55 °C feed temperature  
[Flow rate=5 lpm, Vacuum degree=750mmHg, Initial dye concentration=30ppm]**

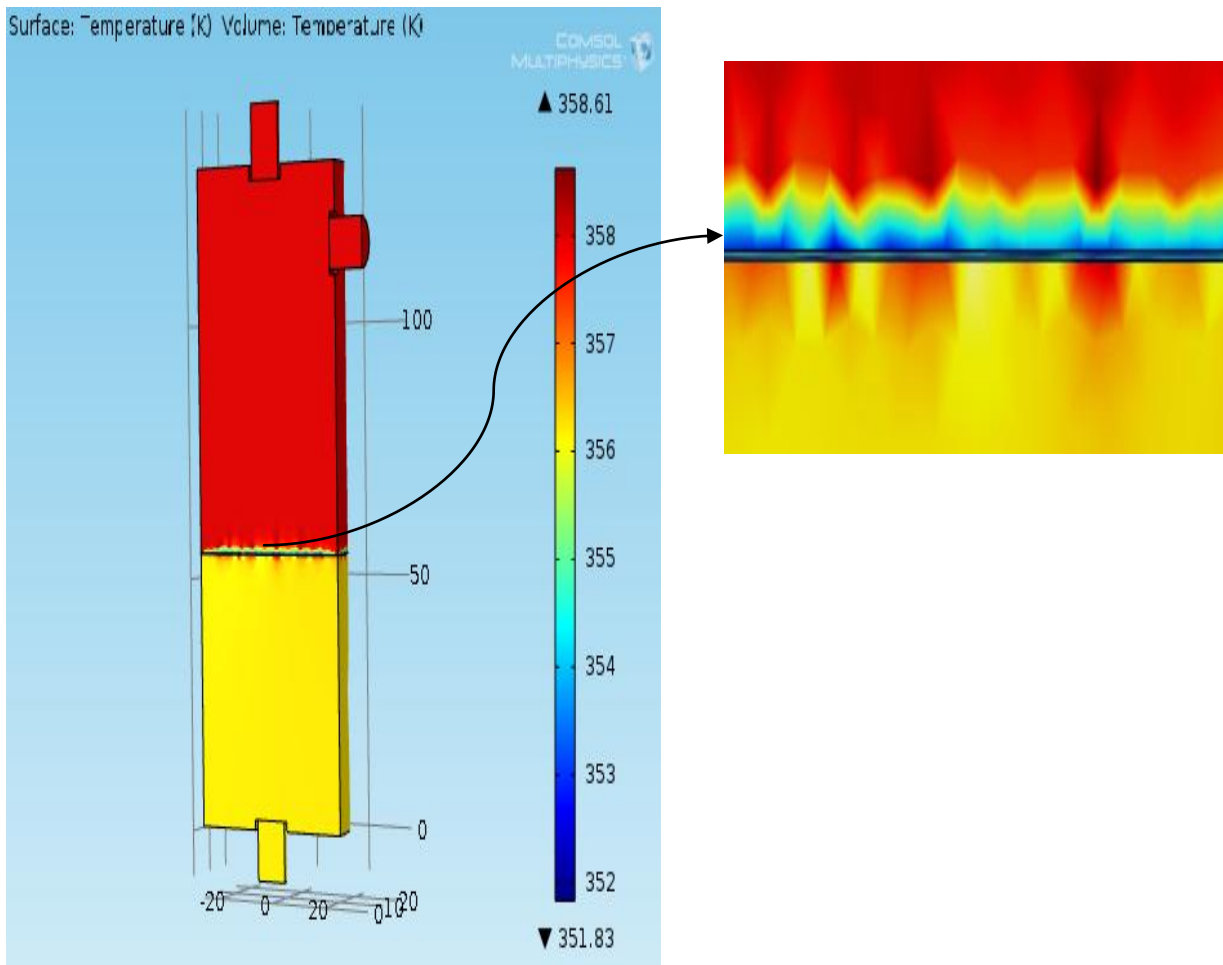


**Figure 5.7: Temperature contour inside membrane module at 358 °K/85 °C feed temperature [flow rate=5 lpm, vacuum degree=750mmHg, initial concentration=30ppm]**

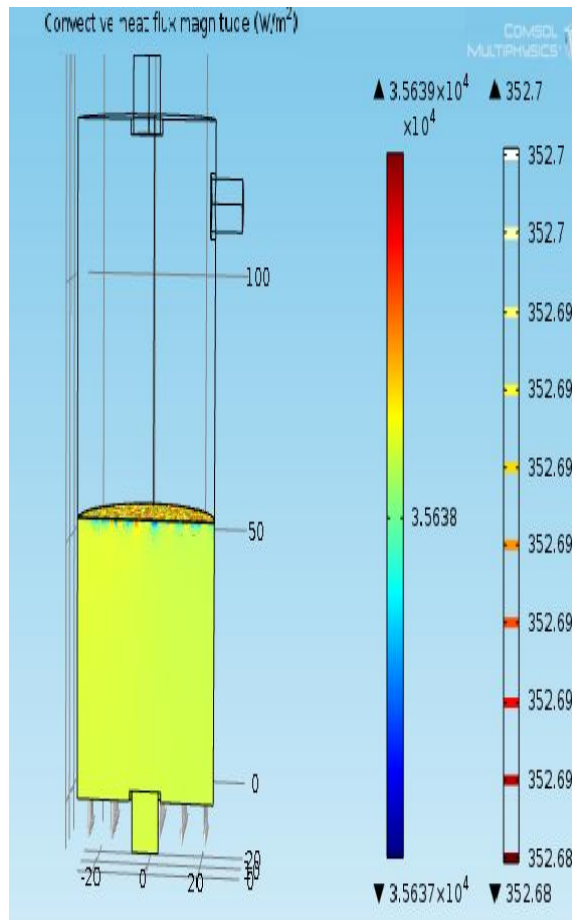


**Figure 5.8: Contour for convective heat flux**  
**[Feed temperature =358 °K/85 °C, flow rate=5 lpm, vacuum degree=750mmHg, initial dye concentration=30ppm]**

#### 5.4. Effect of process variables on various responses in PTFE and PVDF membrane

To estimate the effect of process variables on different responses, several experiments have been conducted at varying operating conditions for feed temperature from 25 to 85 °C, the flow rate from 2 to 10 lpm, vacuum degree of 670 to 750 mmHg and initial dye concentration from 10 to 130 ppm for both PTFE and PVDF membrane. The individual and interaction effects of different process variables have been described in the following sections:

##### 5.4.1. Effect of feed temperature

The effects of feed temperature on permeate flux and specific energy consumption are shown in Figure 5.10 for both PTFE and PVDF membrane. From Figure 5.10(a), it can be seen that the permeate flux increased exponentially from 1.95 to 53.51 kg/m<sup>2</sup>.h on increasing feed temperature from 25 to 85 °C for PTFE membrane at a flow rate of 5 lpm, vacuum degree of 750 mmHg and the initial dye concentration of 30 ppm. This may be possible due to increase in vapor pressure on the feed side of the membrane (according to Antoine equation) which results in higher trans-

membrane vapor pressure difference (driving force) and ultimately enhanced the mass transfer across the membrane. It can also be stated from Figure 5.10(a) that CCD and CFD models are in good agreement with experimental data observed with  $R^2$  and MAPE as 0.989, 10.16 and 0.995, 7.63 respectively given in Table 5.10. So, both CCD and CFD models are acceptable but CFD model is more accurate as compared to CCD model. Moreover, the specific energy consumption is decreased rapidly from 7.12 to 0.96 kWh/kg with increasing temperature from 25 to 85 °C for PTFE membrane at optimized operating conditions. The probable reason is the exponential increment in permeate volume with an increase in feed temperature. The specific energy consumption is inversely proportional to collected permeate volume. So, the sharp reduction in specific energy consumption was observed on increasing feed temperature.

Similarly, from Figure 5.10(b), it can be stated that exponential increment in permeate flux from 2.85 to 55.12 kg/m<sup>2</sup>.h with increased in feed temperature from 25 to 85 °C for PVDF membrane at a vacuum degree of 750 mmHg, the flow rate of 5 lpm and the initial dye concentration of 30 ppm. The reasons in an exponential increment in permeate flux for PVDF membrane is the same as in PTFE membrane. Theoretical flux was obtained from CCD and CFD model with  $R^2$  and MAPE as 0.985, 9.61 and 0.991, 5.81 respectively given in Table 5.10. Both models were found in good agreement with experimental data.

From Figure 5.10(a) & (b), it can be also observed that the magnitude of permeate flux is higher for PVDF membrane as compared to PTFE membrane at same operating conditions which is also confirmed by Table 5.10. The thermal conductivity of the PTFE membrane (0.26 W/m.K) is higher as compared to PVDF membrane (0.18 W/m.K). So, the heat loss through the membrane solid matrix is higher in case of PTFE membrane which is inversely proportional to permeate flux. Moreover, the hydrophobicity of PTFE membrane is higher in comparison of PVDF membrane because hydrophobicity is inversely proportional to coefficient of friction. The PTFE membrane has lower coefficient of friction as compared to PVDF membrane. So, the permeate flux in PTFE membrane is lower than PVDF membrane at same operating conditions.

The effect of feed temperature on temperature polarization coefficient is shown in Figure 5.11 for both PTFE and PVDF membrane. Temperature polarization coefficient (TPC) is defined as the ratio of difference in interface temperatures to the difference in bulk temperatures on feed and permeates side as given in equation (5.8). The decreasing trend with constant rate was observed in TPC value with feed temperature which represents that the difference between the interface temperature on feed and permeate side is increased which results in decrement of thermal



boundary layer thickness. Due to this the transport of vapors through the pores of the membrane is increased which results in higher permeate flux.

$$TPC = \frac{T_{fm} - T_{pm}}{T_f - T_p} \quad (5.8)$$

The fractional contribution of Poiseuille flow has also been evaluated as shown in Figure 5.9. It can be clearly seen that the fractional contribution is increased with increase in feed temperature. This happens due to the higher rate of vaporization at the membrane surface.

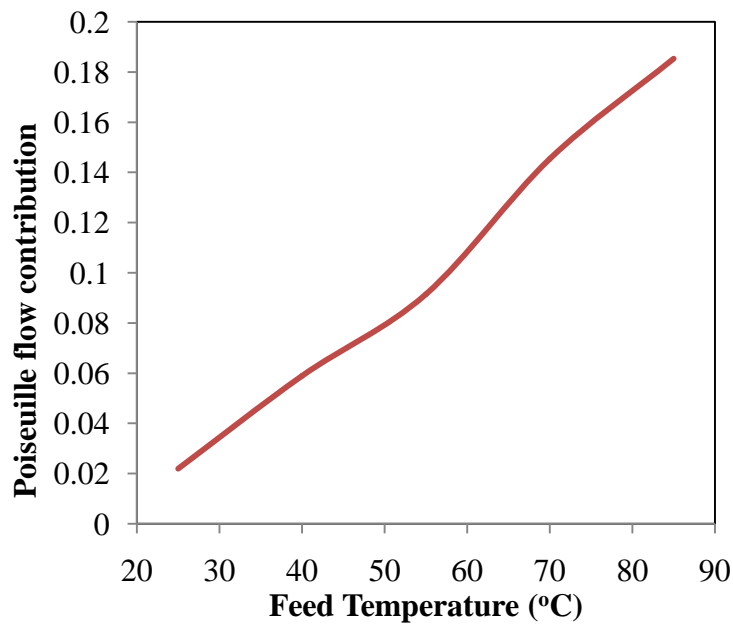
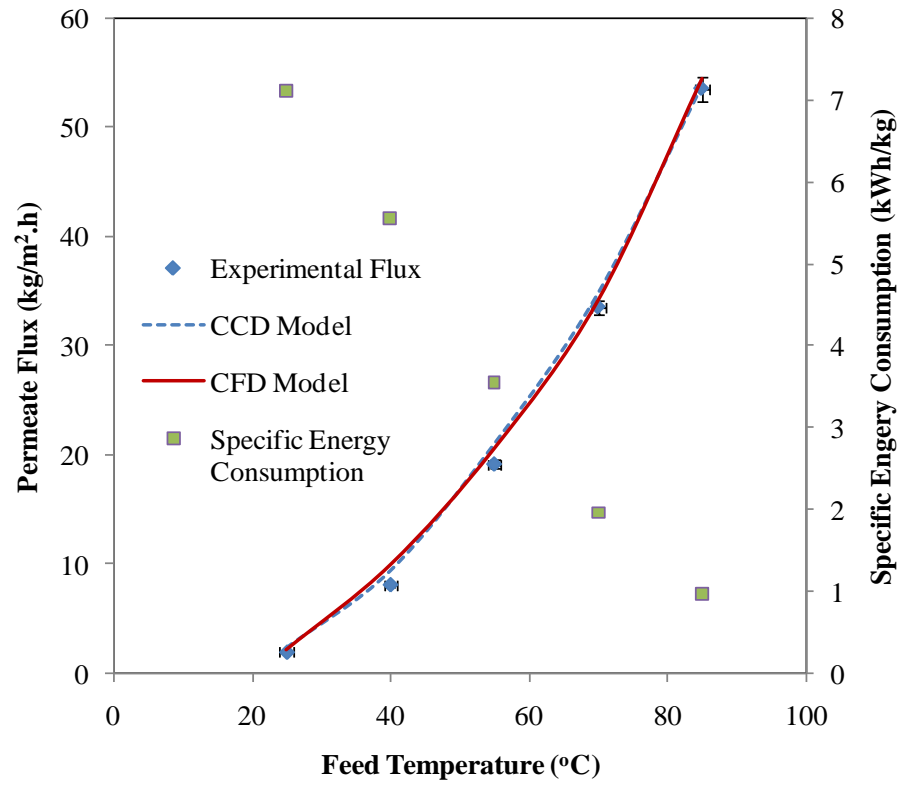
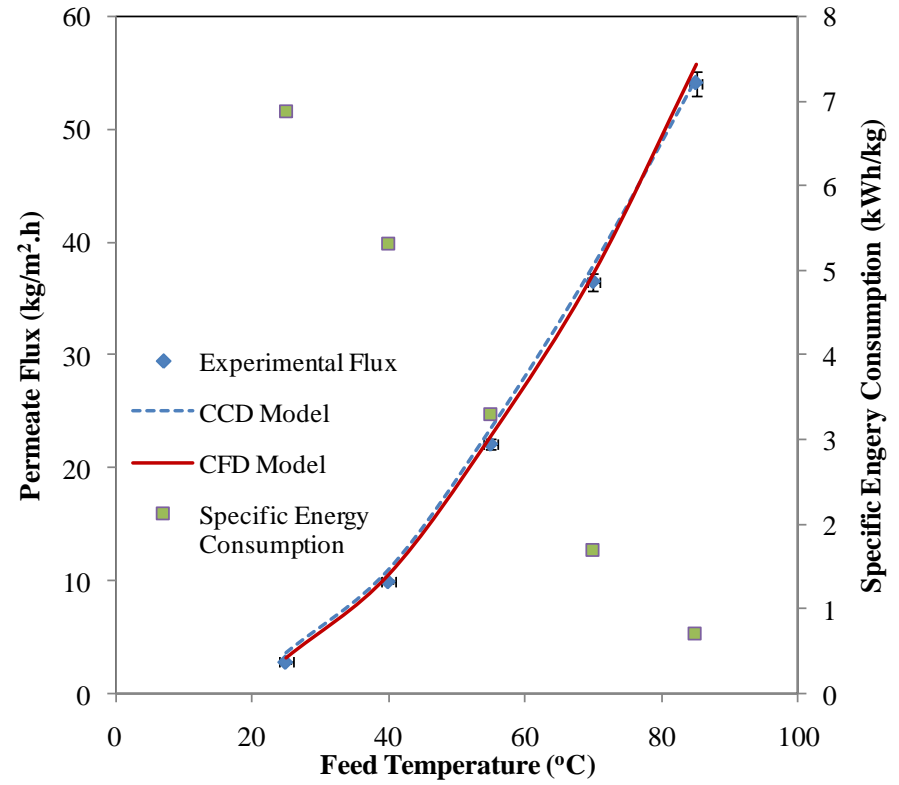


**Figure 5.9: Effect of feed temperature on fractional contribution of Poiseuille flow**



(a)

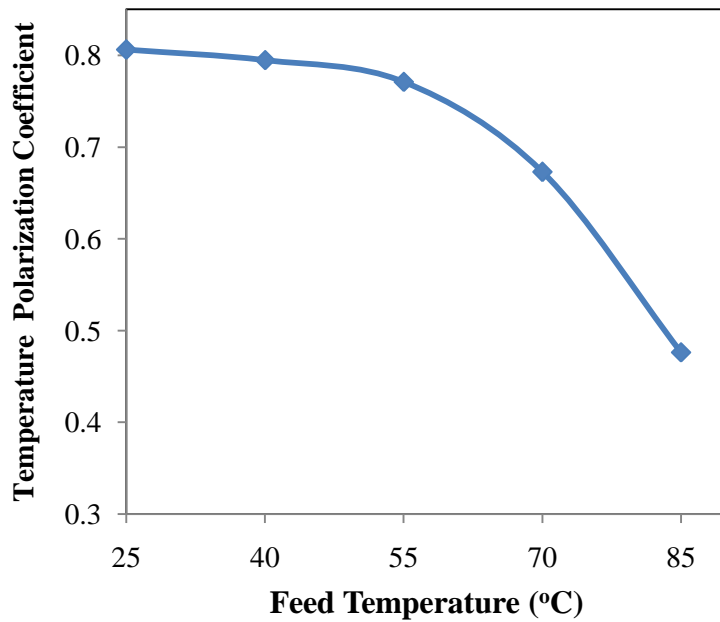


(b)

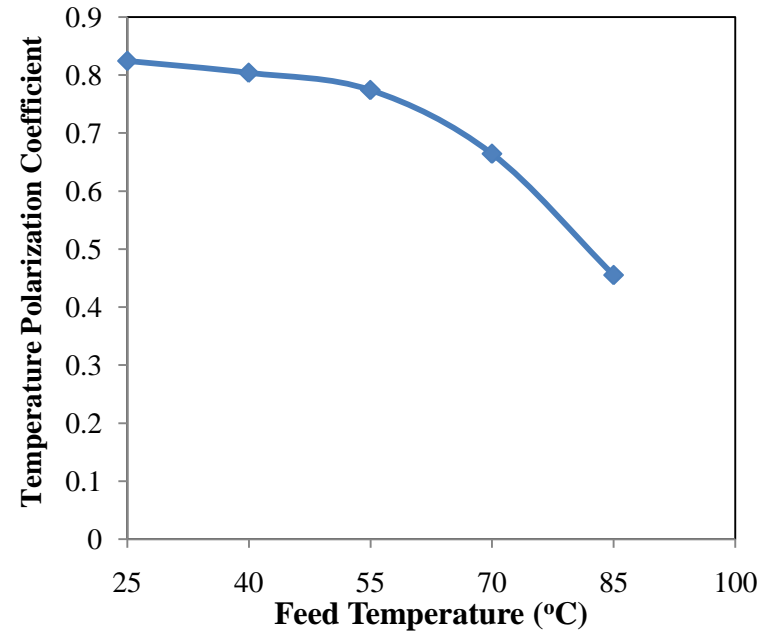
Figure 5.10: Effect of feed temperature of permeate flux and specific energy consumption (a) PTFE and (b) PVDF membrane

**Table 5.10: Comparative analysis of feed temperature on permeate flux for PTFE and PVDF membrane**

Temperature	PTFE Membrane					PVDF Membrane				
	Exp. Flux	CCD Model (1)	CFD Model (2)	R <sup>2</sup> & MAPE (1)	R <sup>2</sup> & MAPE (2)	Exp. Flux	CCD Model	CFD Model	R <sup>2</sup> & MAPE (1)	R <sup>2</sup> & MAPE (2)
25	1.95	2.35	2.09	0.989 & 10.16	0.995 & 7.63	2.85	3.61	3.26	0.985 & 9.61	0.991 & 5.81
40	8.13	9.41	9.86			9.98	10.98	10.63		
55	19.16	21.03	20.51			22.15	23.54	22.95		
70	33.55	34.85	34.09			36.54	37.99	37.35		
85	53.51	53.89	54.41			55.12	54.51	55.85		

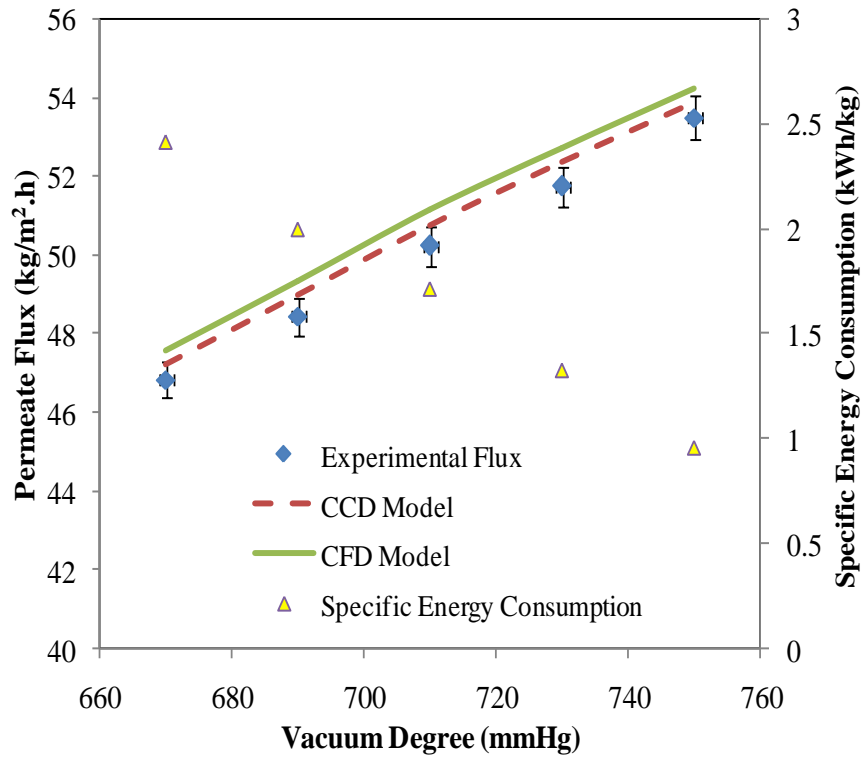


**(a) PTFE Membrane**

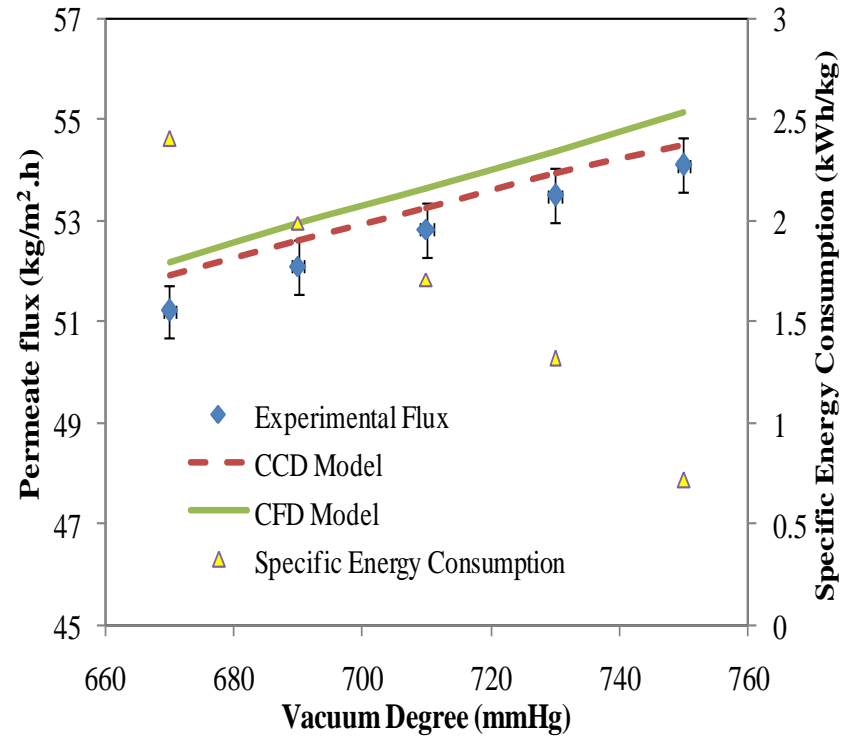


**(b) PVDF Membrane**

**Figure 5.11: Effect of feed temperature on temperature polarization coefficient (a) PTFE membrane, (b) PVDF membrane**



(a) PTFE Membrane



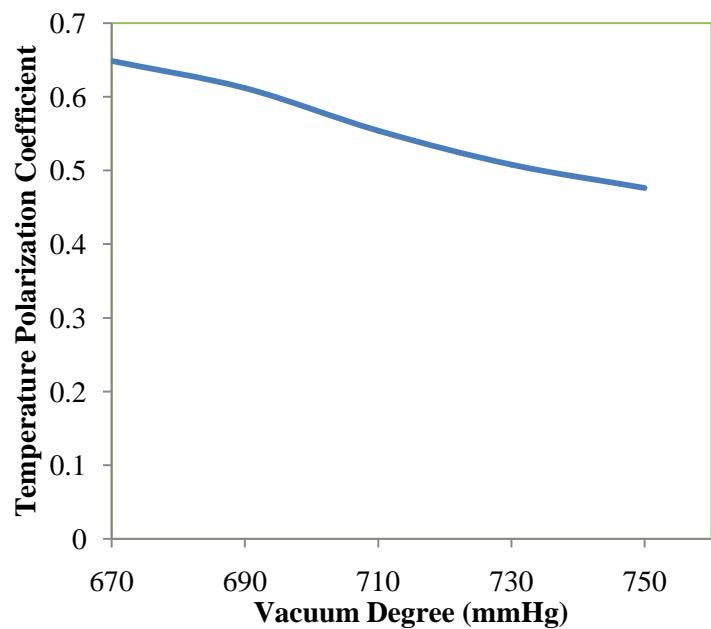
(b) PVDF Membrane

Figure 5.12 Effect of vacuum degree on permeate flux for different membranes

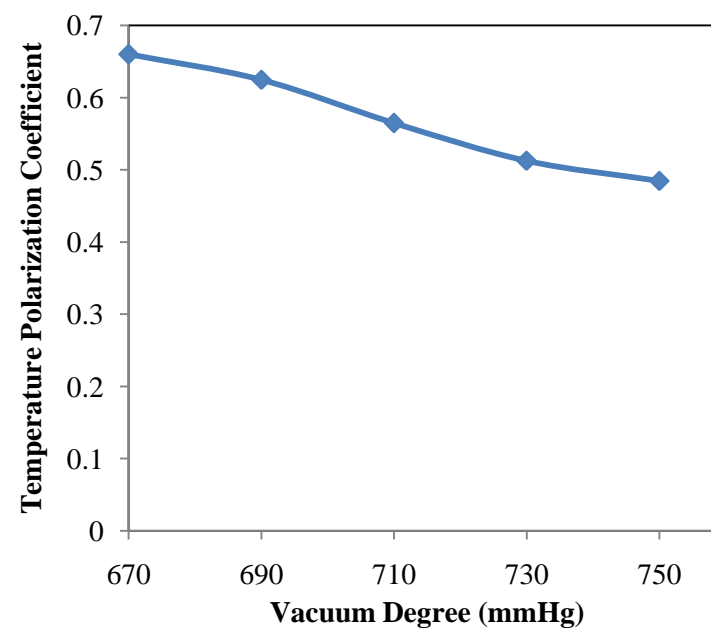
Table 5.11: Comparative analysis of vacuum degree on permeate flux for PTFE and PVDF membrane

Vacuum Degree (mmHg)	PTFE Membrane					PVDF Membrane				
	Exp. Flux	CCD Model (1)	CFD Model (2)	R <sup>2</sup> & MAPE (1)	R <sup>2</sup> & MAPE (2)	Exp. Flux	CCD Model	CFD Model	R <sup>2</sup> & MAPE (1)	R <sup>2</sup> & MAPE (2)
670	46.85	47.25	47.59	0.989	0.995	46.85	47.25	47.59	0.985	0.991
690	48.45	48.99	49.35	&	&	48.45	48.99	49.35	&	&

710	50.24	50.79	51.15	0.95	1.8	50.24	50.79	51.15	0.93	1.57
730	51.75	52.36	52.75			51.75	52.36	52.75		
750	53.51	53.89	54.26			53.51	53.89	54.26		

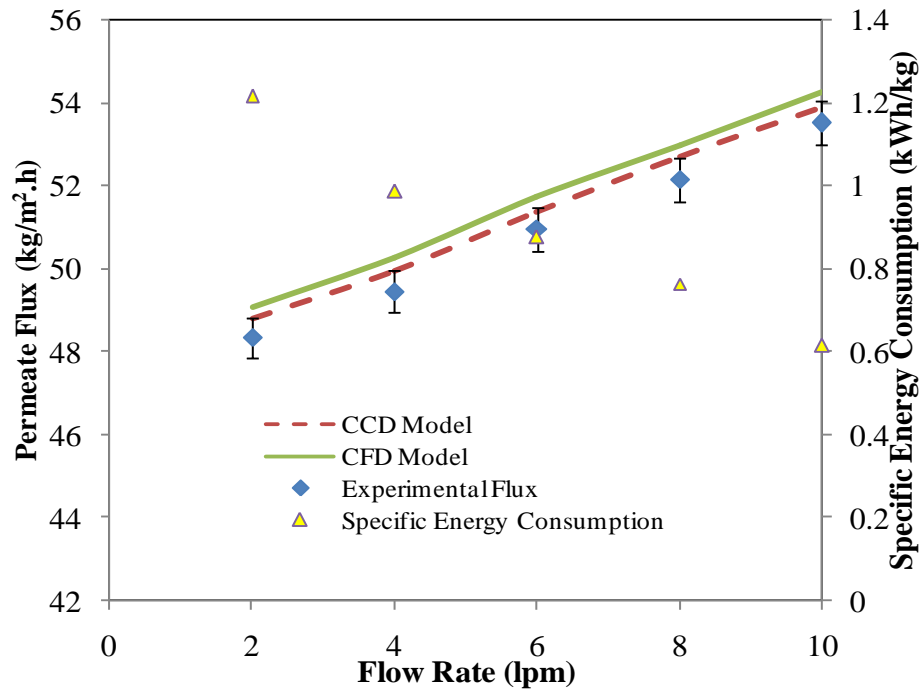


(a) PTFE membrane

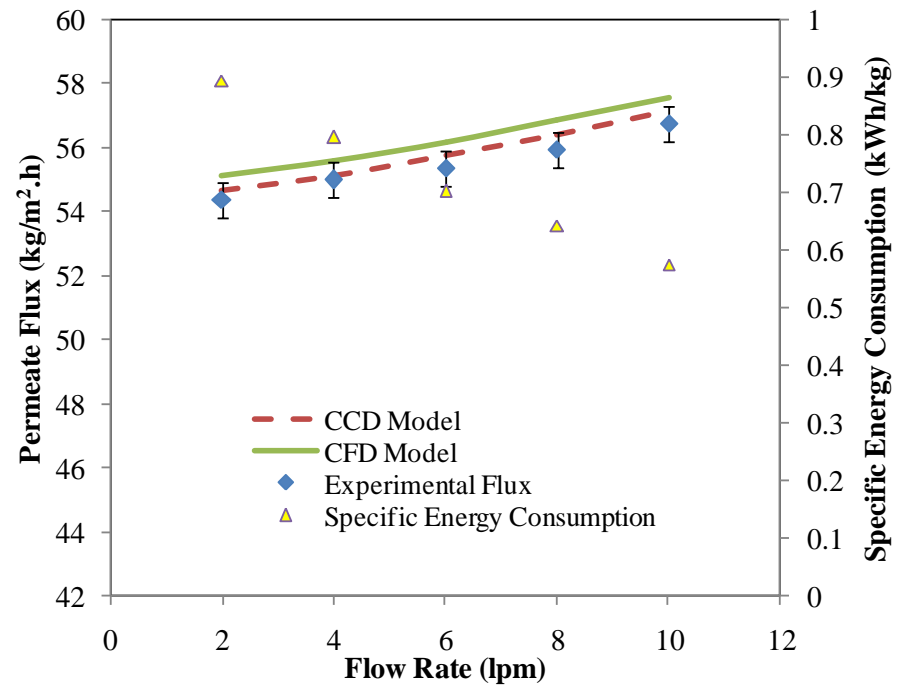


(b) PVDF membrane

Figure 5.13: Effect of vacuum degree on temperature polarization coefficient



(a) PTFE Membrane



(b) PVDF Membrane

Figure 5.14: Effect of flow rate on permeate flux and specific energy consumption

Table 5.12: Comparative analysis of flow rate on permeate flux for PTFE and PVDF membrane

Flow rate (lpm)	PTFE Membrane					PVDF Membrane				
	Exp. Flux	CCD Model (1)	CFD Model (2)	R <sup>2</sup> & MAPE (1)	R <sup>2</sup> & MAPE (2)	Exp. Flux	CCD Model	CFD Model	R <sup>2</sup> & MAPE (1)	R <sup>2</sup> & MAPE (2)
2	48.33	48.79	49.06	0.989 & 0.908	0.995 & 1.39	54.37	54.68	55.13	0.985 & 0.61	0.991 & 1.24
4	49.45	49.95	50.28			54.99	55.13	55.58		
6	50.95	51.35	51.71			55.36	55.75	56.15		
8	52.14	52.71	52.98			55.95	56.43	56.85		
10	53.51	53.89	54.26			56.75	57.14	57.55		

#### 5.4.2. Effect of vacuum degree

Vacuum degree is the level of vacuum applied on the permeate side of the membrane. The absolute pressure at the downstream side will be the difference between the atmospheric pressure and vacuum applied. Figure 5.12 depict the effect of vacuum degree on permeate flux at the optimized conditions of other operating variables like feed temperature as 85 °C, flow rate of 5 lpm and initial dye concentration of 30 ppm for both PTFE and PVDF membranes. It can be seen from Figure 5.12 that permeate flux is linearly increased from 46.85 to 53.51 kg/m<sup>2</sup>.h and 54.37 to 56.75 kg/m<sup>2</sup>.h with increasing vacuum degree from 670 to 750 mmHg for PTFE and PVDF membrane respectively. On increasing the vacuum degree, the mass transfer resistances arising due to presence of air inside the pores of the membrane is removed which results in higher rate of vapor transfer through the pores of the membrane which results in higher permeate flux. This may also be supported by the statement that the driving force (trans-membrane vapor pressure difference) is increased due reduction in vapor pressure on the permeate side of the membrane which results in higher permeate flux. The comparison with developed CCD and CFD model is carried out with experimental data. The R<sup>2</sup> and MAPE was found to 0.989 & 0.995 and 0.95 and 1.8 of CCD and CFD model for PTFE model and 0.985 & 0.991 and 0.93 & 1.57 for PVDF membrane as shown in Table 5.11.

On increasing vacuum degree, the permeate volume is increased linearly. So, the specific energy consumption is reduced from 2.53 to 0.95 kWh/kg and 2.47 to 0.85 kWh/kg for PTFE and PVDF membrane. The temperature polarization coefficient is also reduced linearly with increase in vacuum degree as shown in Figure 5.13. This may be due to the temperature of the permeate section ( $T_p$ ) is reduced which increased the denominator according to equation (5.8). So, the temperature polarization coefficient is reduced and Hence, the permeate flux is increased.

#### 5.4.3. Effect of flow rate

The linear increment in permeate flux was observed on increasing flow rate from 2 lpm to 10 lpm for both PTFE and PVDF membrane as shown in Figure 5.14. This increment in permeate flux may be due to decrease in thermal and concentration boundary layer thickness at the surface of the membrane. The permeate flux increased from 48.33 to 53.51 kg/m<sup>2</sup>.h and 54.37 to 56.75 kg/m<sup>2</sup>.h on increasing flow rate from 2 to 10 lpm at constant feed temperature of 85 °C, vacuum degree of 750 mmHg, and initial dye concentration of 30 ppm. The specific energy consumption is decreased linearly from 1.21 to 0.61 and 0.89 to 0.575 kWh/kg with increase in flow rate from 2 to 10 lpm. The permeate volume is increased with flow rate due to turbulence created on the membrane surface which results in reduction in specific energy consumption. The comparison of

CCD and CFD model is carried out with experimental data. The both models are found best fitted with  $R^2$  values as 0.989 & 0.995 and MAPE values as 0.908 & 1.39 of CCD and CFD model for PTFE membrane. For PVDF membrane, the  $R^2$  value as 0.985 & 0.991 and MAPE value as 0.61 and 1.24 of CCD and CFD model is found to be best fitted.

## **5.5. Interaction effects of process variables**

The 2D contour plots of the dependent responses (permeate flux, specific energy consumption and percentage removal) as the function of any two independent operating variables (feed temperature, vacuum degree, flow rate and initial dye concentration), keeping other variables constant at optimum conditions can be helpful for understanding the interaction behavior and relationship of these two operating parameters with responses. These interaction plots for the dependent responses were developed using the quadratic model developed using CCD design for both membranes.

### **5.5.1. Interaction effects for permeate flux**

For permeate flux, three interactions (A\*B, A\*D, B\*D) were found significant according to the analysis of variance as shown in Table 5.6 and the contour plots are shown in Figure 5.15 for PTFE membrane. Figure 5.15(a) represents the interaction effect of feed temperature and flow rate on permeate flux at constant initial dye concentration (30ppm) and vacuum degree (750mmHg). Within the range of experimental design, the permeate flux increases with both feed temperature and flow rate. From this contour, it can be clearly seen that the effect of feed temperature is higher as compared to feed flow rate on permeate flux. This is because, temperature has the exponential relationship with vapor pressure by Antoine equation. So, the driving force increased exponentially on increasing feed temperature. However, the concentration boundary layer thickness is reduced by increasing flow rate from 2 to 10 lpm due to turbulence at the membrane surface which allows more vapor to pass through the pores of the membrane. Thus the permeate flux is also increased with flow rate but not as high with feed temperature.

Another significant interaction effect of feed temperature and vacuum degree at constant flow rate of 5 lpm and the initial dye concentration of 30ppm is shown in Figure 5.15(b). It is clear that the interaction effect of permeate pressure and feed temperature is higher as compared to interaction effect of flow rate and feed temperature. This happens because permeate pressure increased the transmembrane membrane vapor pressure difference (driving force) by applying vacuum on the permeate side which directly influenced the permeate flux.



The significant combined effect of flow rate and vacuum degree on permeate flux is shown in Figure 5.15(c). It can be noted that permeate flux increases on increasing flow rate and vacuum degree from 2 lpm to 10 lpm and 670 mmHg to 750 mmHg respectively at constant feed temperature 85 °C and the initial dye concentration of 30ppm. From Figure 5.15, it can also be observed that the effect of flow rate on permeate flux is lesser as compared to vacuum degree. This may be due to fact that vacuum degree directly increased the driving force by lowering the vapor pressure on permeate side while flow rate only reduced the polarization effect at membrane surface which indirectly increased the transport of more vapor through membrane but it is not such effective. So, the vacuum degree has a significant effect as compared to feed flow rate on permeate flux. Similarly, the significant interaction effects of permeate flux for PVDF membrane is given in Figure 5.16. In case of PVDF membrane, A\*D, B\*D and B\*D is found as significant interaction parameter as in case of PTFE membrane. Similar effects was obtained in case of PVDF membrane as in PTFE membrane.

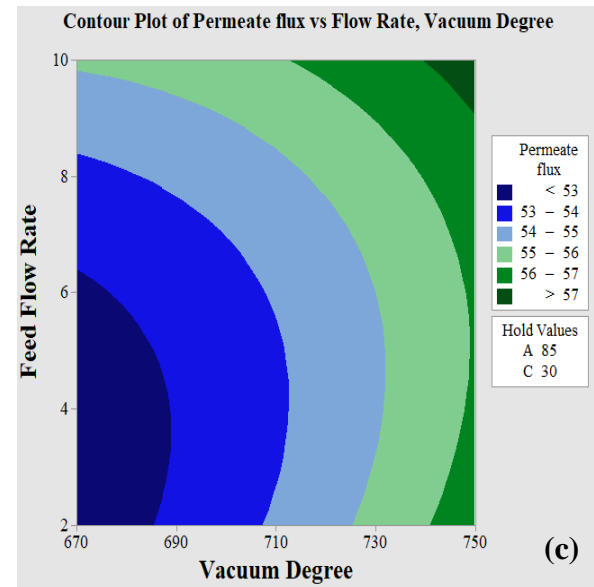
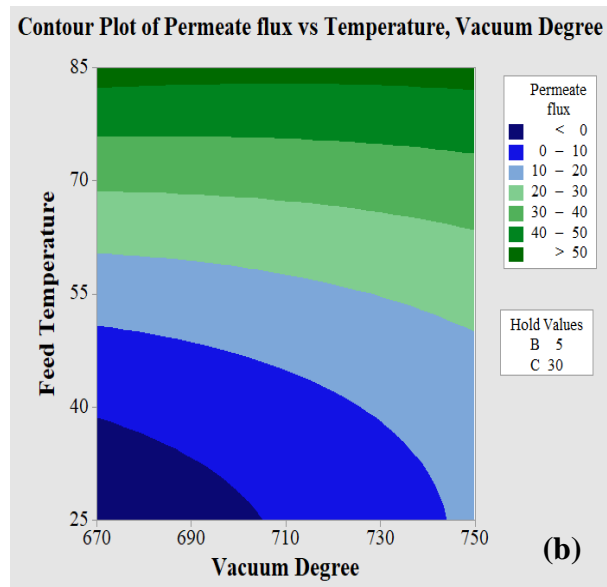
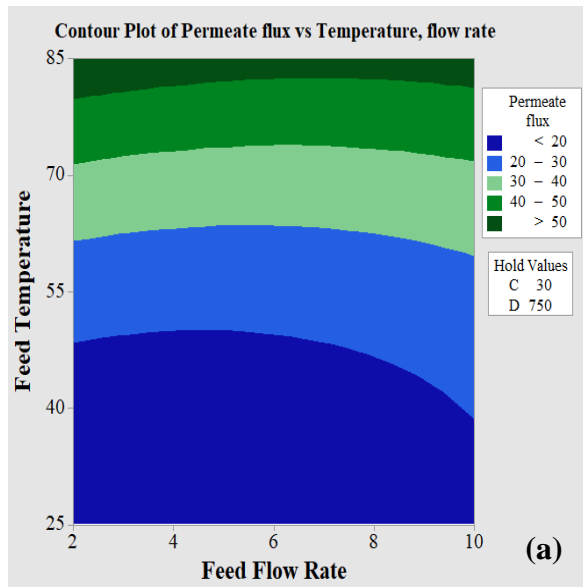


**Figure 5.15: Interaction plots of permeate flux for PTFE membrane**

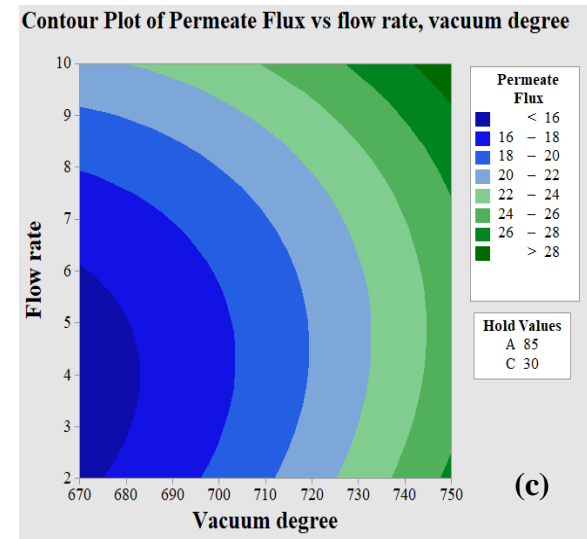
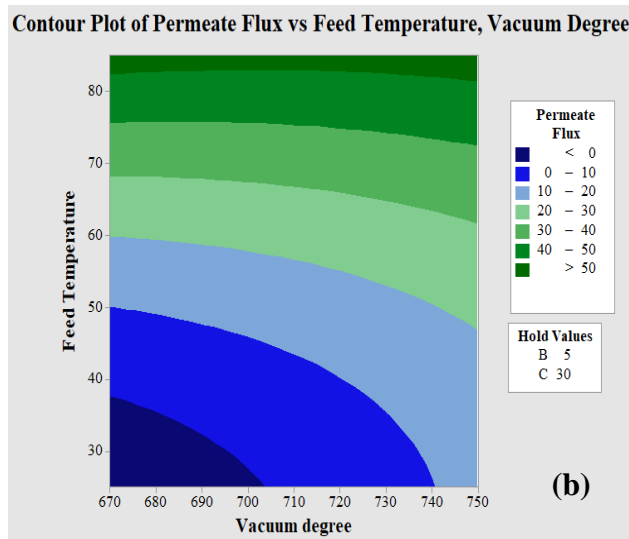
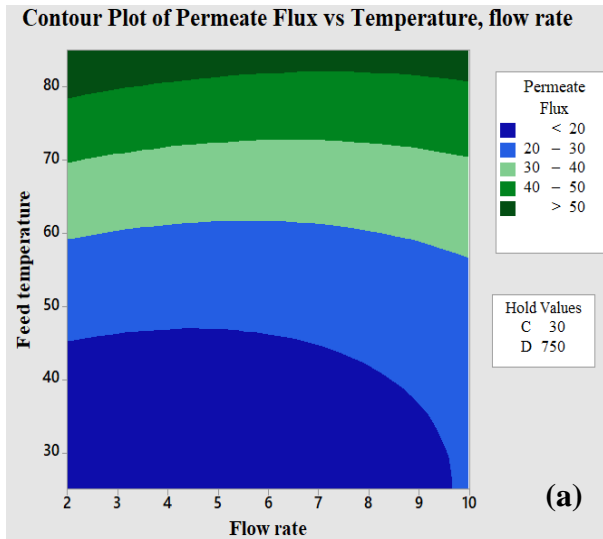


**Figure 5.16: Interaction plots of permeate flux for PVDF membrane**

### 5.5.2. Interaction effects for specific energy consumption

Three significant interaction plots (A\*B, A\*D & B\*D) for specific energy consumption is shown in Figure 5.17 & Figure 5.18 for PTFE and PVDF membrane respectively. It can be seen from the Figure 5.17(a) & Figure 5.18(a), that specific energy consumption is rapidly reduced on increasing feed temperature and flow rate from 25 to 85 °C and 2 to 10 lpm respectively. From equation(4.2), it can be seen that specific energy consumption is inversely proportional to the volume of permeate collected and an exponential increment in permeate volume was seen on increasing feed temperature. So, the specific energy consumption is reduced significantly from 12.96 to 3.1 kWh/kg and 11.85 to 2.5 on increasing feed temperature from 25 to 85 °C at 30 ppm feed concentration, and 750 mmHg vacuum degree for PTFE and PVDF membrane respectively. Moreover, the volume of permeate collected was also increased on increasing feed flow rate from 2 to 10 lpm due to a reduction in concentration polarization effect but this increment in volume of permeate collected is not much higher as compared to feed temperature as shown in Figure 5.17(a) & Figure 5.18(a). So, the specific energy consumption is reduced significantly on increasing feed temperature as compared to flow rate.

Figure 5.17(b) & Figure 5.18(b) shows the significant interaction effect of feed temperature and vacuum degree on specific energy consumption at constant flow rate of 5 lpm and the initial dye concentration of 30 ppm for PTFE and PVDF membrane. From these figures, it can be seen that on increasing feed temperature from 25 °C to 85 °C, the specific energy consumption reduced from 15 to less than 5 kWh at 670 mmHg permeate pressure. However, on increasing vacuum degree from 670 to 750 mmHg, the less reduction in specific energy consumption was observed from 15 to 10 kWh at 50 °C feed temperature. So, it can be concluded that the feed temperature is highly significant as compared to permeate pressure for less specific energy consumption. However, from the interaction effect of feed temperature and vacuum degree, it can be seen that at higher feed temperature and permeate pressure as 85 °C and 750mmHg respectively, the specific energy consumption will be lower than 3 kWh/kg.

For lower specific energy consumption, the third significant interaction of vacuum degree and feed flow rate is shown in Figure 5.17(c) & Figure 5.18(c) at a constant feed temperature of 85 °C and the initial dye concentration of 30ppm for PTFE and PVDF membrane. From these figures, it can be observed that the interactive effect of vacuum degree is higher as compared to flow rate. This may be due to the fact that the vacuum degree increased transmembrane vapor pressure difference (driving force) which allows more vapors to pass through the pores of the membrane and results in higher permeate flux and thus the specific energy consumption is lower. However, at higher permeate pressure of 750 mmHg and 10 lpm, the specific energy consumption was found lowest as less than 3 kWh at 30 ppm initial dye concentration and 85 °C. But at flow rate of 10 lpm, the chance of pore wetting is very high which can reduce the life of the

membrane. So, vacuum degree of 750mmHg and flow rate of 5 lpm was found the optimized condition to run the experiments without compromising with the life of the membrane.

### 5.5.3. Interaction effects for percentage removal

For higher percentage removal, three interaction effects (B\*C, B\*D, and C\*D) were found significant, and interaction plots are shown in Figure 5.19 & Figure 5.20 for both PTFE and PVDF membranes. From these interaction plots, it can be seen that the percentage removal decreased slightly from 99.8 to 99.12 on increasing feed flow rate from 2 to 10 lpm, the initial dye concentration of 10 to 130 ppm at a constant vacuum degree of 750 mmHg and Feed temperature of 85 °C. In all the experimental runs, it was found that the lowest percentage removal is 99.14% and at the optimum conditions as 85°C of feed temperature, 5 lpm of feed flow rate, 30 ppm of initial dye concentration and 750 mmHg of vacuum degree, the percentage removal is 99.7%. So, optimum conditions can be chosen as best conditions for maximum percentage removal. However, from the contour plots of Figure 5.19 & Figure 5.20, it can be clearly seen that the percentage removal decreased significantly on increasing the vacuum degree as compared to feed flow rate and initial dye concentration. Because the chances of pore wetting is higher at higher vacuum degree. Moreover, there is no significant reduction was observed by increasing the feed temperature.

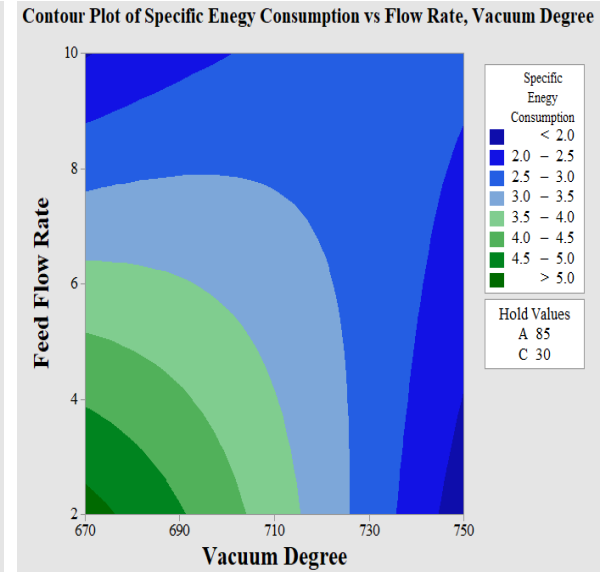
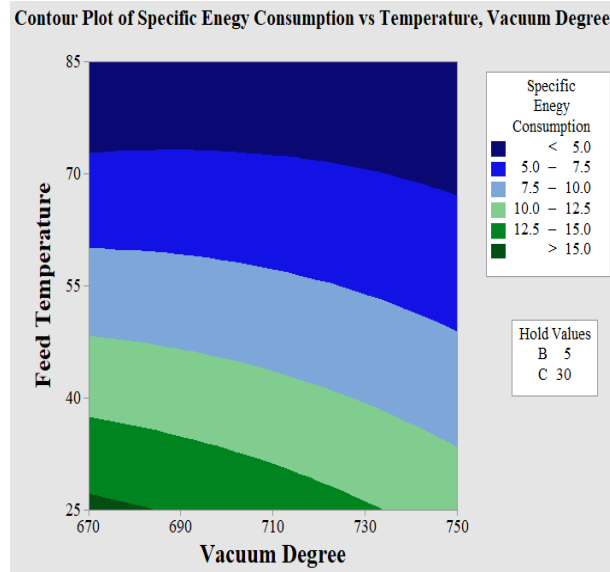
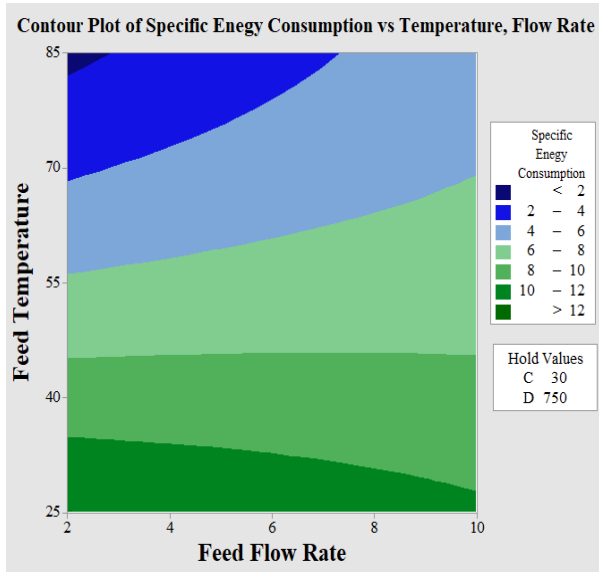


Figure 5.17 Interaction plots of specific energy consumption for PTFE membrane

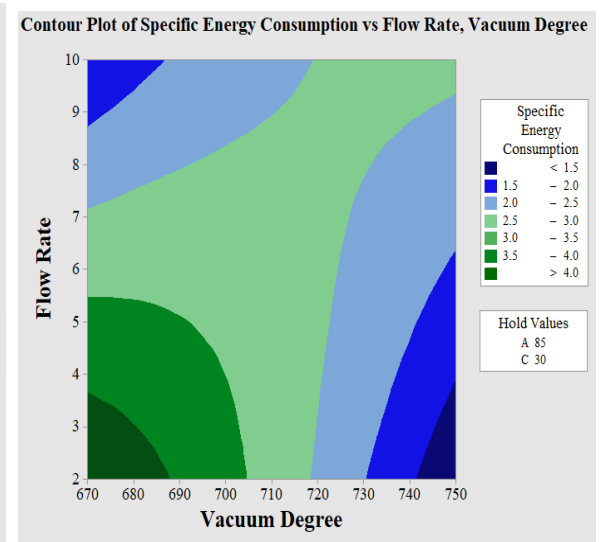
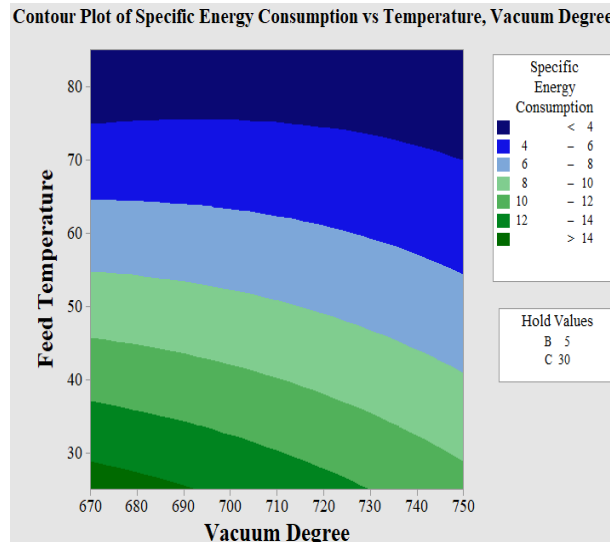
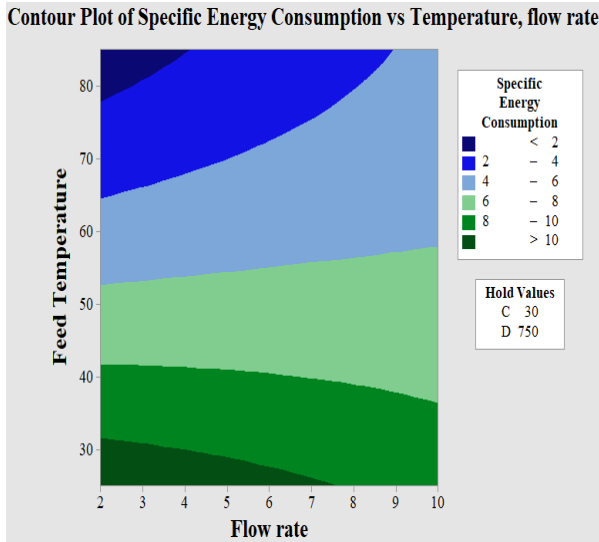


Figure 5.18: Interaction plots of specific energy consumption for PVDF membrane

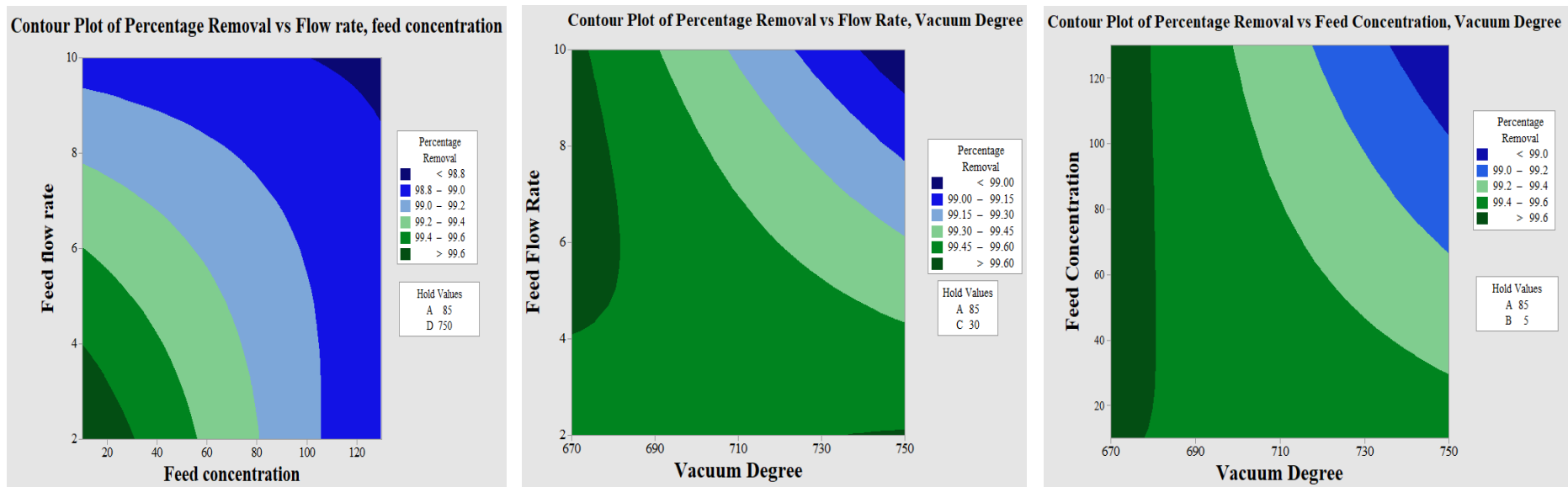


Figure 5.19: Interaction plots of percentage removal for PTFE membrane

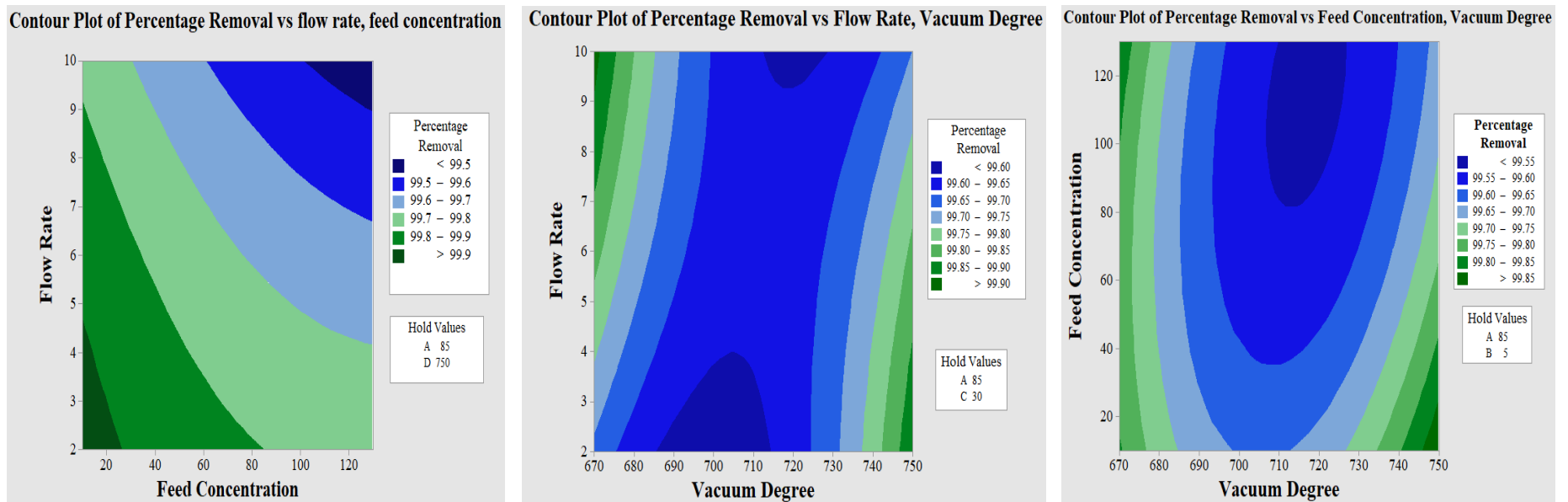


Figure 5.20: Interaction plots of percentage removal for PVDF membrane

## 5.6. Development of Heat and Mass Transfer Correlation

### 5.6.1. Heat Transfer Correlation

Heat transfer correlations are used for calculating the heat transfer coefficient across the boundary layers which is extensively used for rigid heat exchangers. However, the heat transfer mechanism is quite different in membrane processes due to its porous nature. Moreover, in VMD process, the heat transfer is associated with mass transfer so the correlation coefficients are different from rigid heat exchangers. In the present work, heat transfer phenomena for VMD were studied using the lab scale test module which consists of flat sheet hydrophobic porous PTFE membrane. Various sets of experimental conditions was considered for flow rates of ranging from 2 to 10 lpm, feed temperature from 25 to 85 °C at two different vacuum degree as 730 and 750 mmHg and initial dye concentration of 30ppm and the results are shown in Table 5.13. For given experimental conditions, the heat transfer correlation is developed using the dimensionless numbers such Prandtl number, Nusselt number and Reynolds number.

**Table 5.13: Experimental and model data for heat transfer correlation at 30 ppm initial dye concentration**

S.No.	Flow Rate (lpm)	Feed Temp. (°C)	Vacuum Degree (mmHg)	Flux (kg/m <sup>2</sup> .h)	Re	Pr	Model Nu	Exp. Nu	Exp h <sub>f</sub>
1.	2	25	750	1.79	887.8	6.32	894.16	647.40	768.48
2.	4	25	750	1.87	1753.9	6.52	1643.23	1287.49	1528.27
3.	6	25	750	2.04	2650.2	6.23	2326.28	1922.23	2281.72
4.	8	25	750	2.09	3542.3	6.28	3009.75	1937.15	2299.44
5.	10	25	750	2.14	4417.0	6.37	3669.59	2445.19	2902.48
6.	2	40	750	5.99	982.3	5.59	938.25	858.51	1019.07
7.	4	40	750	6.69	1953.9	5.55	1713.12	1706.40	2025.53
8.	6	40	750	7.06	2922.8	5.60	2447.03	2646.14	3141.01
9.	8	40	750	7.38	3907.7	5.59	3155.76	3381.89	4014.37
10.	10	40	750	7.96	4858.2	5.64	3833.40	3820.78	4535.33
11.	2	55	750	18.54	1230.1	4.32	1050.31	1171.59	1390.71
12.	4	55	750	18.82	2435.0	4.39	1923.56	1761.20	2090.58
13.	6	55	750	19.24	3665.0	4.34	2743.84	2253.94	2675.47
14.	8	55	750	19.64	4903.4	4.32	3538.99	3247.68	3855.06
15.	10	55	750	20.18	6108.3	4.36	4305.74	4562.69	5416.00
16.	2	70	750	34.18	1685.7	3.06	1236.58	1394.66	1655.48
17.	4	70	750	34.59	3339.7	3.11	2265.70	2159.46	2563.32

18.	6	70	750	35.06	5033.2	3.09	3241.10	2961.28	3515.09
19.	8	70	750	35.64	6774.9	3.04	4186.06	4853.48	5761.18
20.	10	70	750	35.86	8428.5	3.07	5088.52	5775.50	6855.63
21.	2	85	750	52.56	1999.6	2.52	1347.28	1692.11	2008.56
22.	4	85	750	53.42	3954.5	2.57	2468.61	5004.23	5940.11
23.	6	85	750	53.78	5866.1	2.59	3497.21	6008.21	7131.86
24.	8	85	750	54.21	7998.6	2.51	4549.01	6972.47	8276.45
25.	10	85	750	54.74	9886.3	2.55	5507.13	8340.83	9900.72
26.	2	25	730	0.97	887.8	6.32	894.16	517.19	613.91
27.	4	25	730	1.04	1753.9	6.52	1643.23	1157.27	1373.71
28.	6	25	730	1.22	2650.2	6.23	2326.28	1792.01	2127.16
29.	8	25	730	1.26	3542.3	6.28	3009.75	1806.94	2144.88
30.	10	25	730	1.31	4417.0	6.37	3669.59	2314.97	2747.92
31.	2	40	730	5.17	982.3	5.59	938.25	728.30	864.50
32.	4	40	730	5.86	1953.9	5.55	1713.12	1576.19	1870.96
33.	6	40	730	6.24	2922.8	5.60	2447.03	2515.92	2986.45
34.	8	40	730	6.55	3907.7	5.59	3155.76	3251.68	3859.81
35.	10	40	730	7.13	4858.2	5.64	3833.40	3690.56	4380.77
36.	2	55	730	17.72	1230.1	4.32	1050.31	1041.38	1236.14
37.	4	55	730	17.99	2435.0	4.39	1923.56	1630.99	1936.01
38.	6	55	730	18.41	3665.0	4.34	2743.84	2123.73	2520.90
39.	8	55	730	18.82	4903.4	4.32	3538.99	3117.47	3700.49
40.	10	55	730	19.35	6108.3	4.36	4305.74	4432.47	5261.43
41.	2	70	730	33.35	1685.7	3.06	1236.58	1264.44	1500.92
42.	4	70	730	33.77	3339.7	3.11	2265.70	2029.25	2408.76
43.	6	70	730	34.24	5033.2	3.09	3241.10	2831.07	3360.53
44.	8	70	730	34.82	6774.9	3.04	4186.06	4723.27	5606.61
45.	10	70	730	35.04	8428.5	3.07	5088.52	5645.29	6701.07
46.	2	85	730	51.74	1999.6	2.52	1347.28	1561.90	1854.00
47.	4	85	730	52.59	3954.5	2.57	2468.61	4874.01	5785.55
48.	6	85	730	52.95	5866.1	2.59	3497.21	5878.00	6977.30
49.	8	85	730	53.38	7998.6	2.51	4549.01	6842.26	8121.89
50.	10	85	730	53.92	9886.3	2.55	5507.13	8210.61	9746.16



The amount of heat required to vaporize the water on feed side of the membrane is provided by heat transfer coefficient. The heat flux can be given as:

$$q_f = h_f(t_f - t_{fm}) \quad (5.9)$$

The transfer of heat through the membrane can be assumed by contribution of conduction in membrane material and evaporation into the pores of membrane. So, the heat flux through membrane can be given as

$$q_m = N\Delta H + h_m(t_{fm} - t_{pm}) \quad (5.10)$$

By solving equation (5.9) and (5.10) simultaneously, the heat transfer coefficient can be obtained for experimental data. The empirical correlation for heat transfer as given in equation (5.11) is fitted in MS-excel solver by optimizing the constant parameter values of a, b, and c using Newton solver method.

$$Nu = a Re^b Pr^c \quad (5.11)$$

After fitting, the correlation is found to be as follows:

$$Nu = 1.25 Re^{0.87} Pr^{0.33} \quad (5.12)$$

Figure 5.21 shows the plot of experimental and theoretical values of  $\log(Nu / Pr^{0.33})$  versus  $\log(Re)$ . It was that the theoretical model is best fitted with experimental results with  $R^2$  as 0.989.

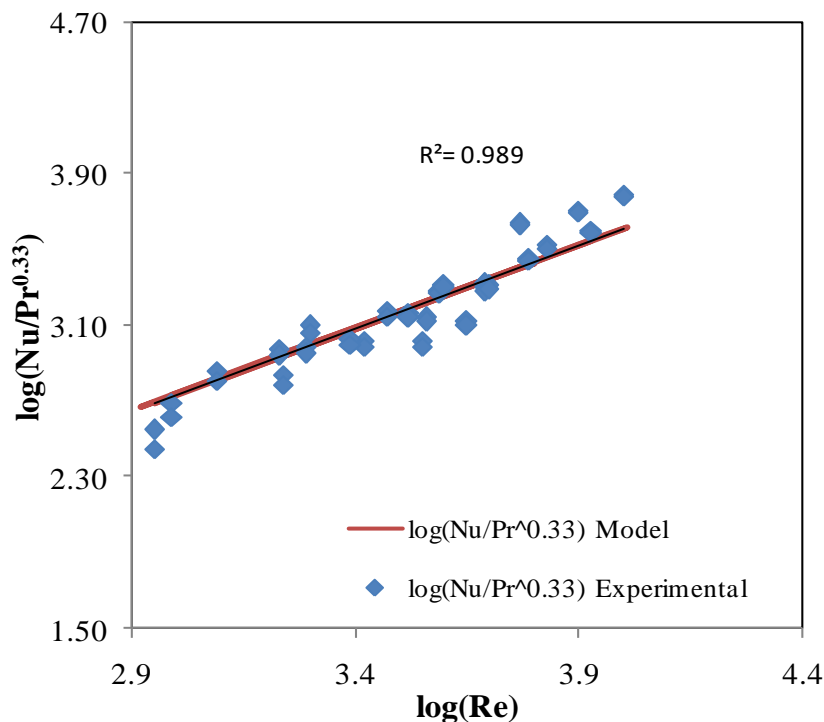


**Figure 5.21: Fitting of heat transfer correlation at 30 ppm initial dye concentration**

The effect of feed temperature on heat transfer coefficient is shown in Figure 5.22 at 8 and 10 lpm of flow rate. It can be observed that the value of heat transfer coefficient is increased significantly on increasing the feed temperature as well as flow rate at constant vacuum degree of 750 mmHg. This may due to

reduction in the effect of temperature polarization coefficient which signifies that the feed side bulk temperature and membrane surface temperature becomes identical and the difference between feed side and permeate side membrane surface temperature is become maximum which results in higher driving force. The relationship between heat transfer coefficient and feed temperature is given by equation (5.13), and (5.14).

At 10 lpm flow rate and 750 mmHg vacuum degree

$$h_f = 0.058T_f^3 - 8.531T_f^2 + 474.3T_f - 4530 \quad (5.13)$$

At 8 lpm flow rate and 750 mmHg vacuum degree

$$h_f = 0.053T_f^3 - 7.599T_f^2 + 402.7T_f - 3785 \quad (5.14)$$

The value of  $R^2$  is found to be 0.99 and 0.984 at 10 and 8 lpm flow rate respectively.

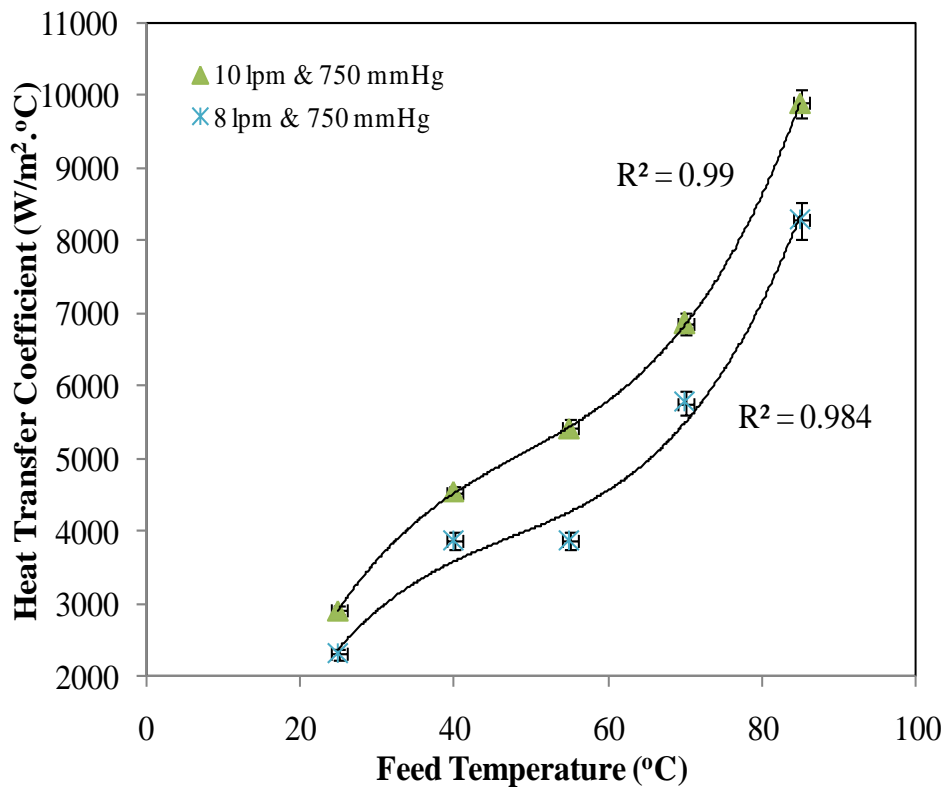


**Figure 5.22: Effect of feed temperature on heat transfer coefficient**

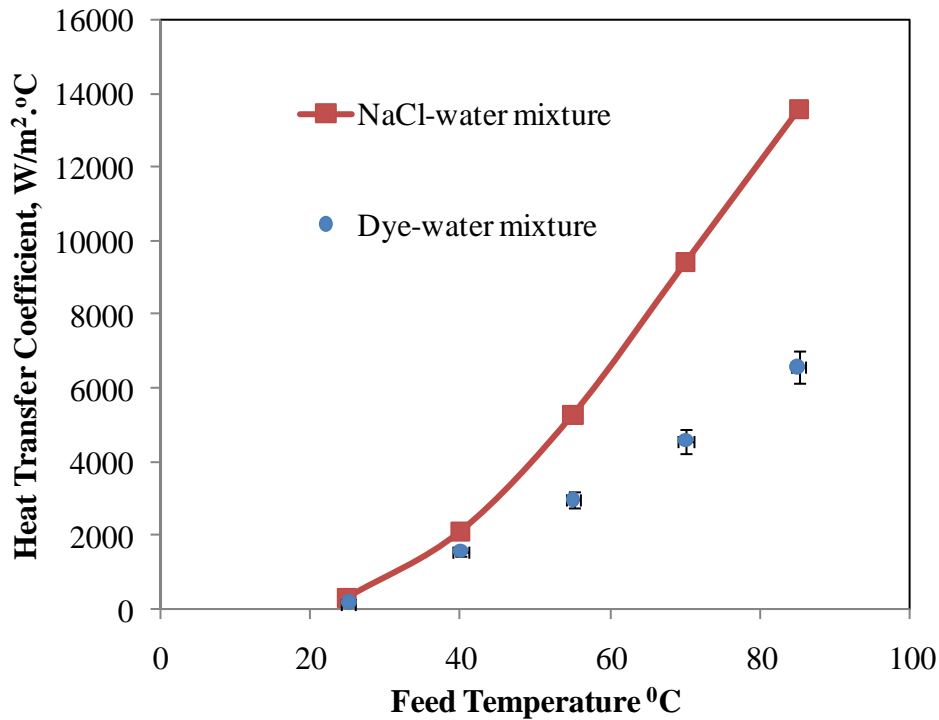


**Figure 5.23: Comparison of heat transfer coefficient of Dye-water and NaCl-water mixture**

In literature various heat transfer correlations are reported by various researchers which are differentiated on the basis of hydrodynamic conditions as well as module geometry. The comparison of heat transfer coefficient for different feed systems was carried out by considering the same module geometry and hydrodynamic conditions. The heat transfer coefficient for NaCl-water mixture is reported by (Upadhyaya et al. 2016c) as the function of feed temperature used for comparison. After comparing the heat transfer coefficients of Dye-water mixture and NaCl-water mixture, it can be seen that the heat transfer coefficient is higher for NaCl-water as compared to Dye-water mixture. This is because the viscosity of NaCl-water is lower as compared to Dye-water mixture which results in lower heat transfer as heat transfer coefficient is the function of  $\mu^{-0.5}$ . Moreover, the molecular weight of the dye larger as compared to NaCl so it takes larger time to stay at membrane surface and blocks the pores of the membrane. Due to blockage of pores, the transfer of vapor molecules is reduced simultaneously the heat transfer coefficient is reduced.

### 5.6.2. Mass Transfer Correlation

In VMD process, vapor molecules are transported through the pores of the hydrophobic membrane. So, it is essential to determine the mass transfer coefficient for the process. In VMD process mass transfer coefficient is the function of feed temperature, vacuum degree and flow rate so the correlation should be developed in the form of dimensionless numbers to estimate the mass transfer coefficient. The dimensionless mass transfer correlation can be expressed in terms of Sherwood number, Schmidt number, and Reynolds number as follows:

$$Sh = a Re^b Sc^c \quad (5.15)$$

Where,  $Sh = \frac{k_f d}{D_{AB}}$  and  $Sc = \frac{\mu}{\rho D_{AB}}$ . The experiments was carried out at different feed temperature ranging from 25 to 85 °C, flow rate of 2 to 10 lpm and vacuum degree of 730 and 750 mmHg at constant dye concentration of 30 ppm. The experimental mass transfer coefficient is calculated by solving the different equations (5.16), (5.17), and (5.18) in MS excel.

$$N = k_f \Delta C \quad (5.16)$$

$$C = \frac{PM}{RT_{avg}} \quad (5.17)$$

$$N = k_f \frac{M \Delta P}{RT_{avg}} \quad (5.18)$$

The experimental data at different operating conditions is given in Table 5.14. From experimental analysis, it was found that the mass transfer is increased with increase in feed temperature, flow rate and vacuum degree. This increment in mass transfer is due to reduction in concentration polarization coefficient at the membrane surface. The theoretical mass transfer correlation was developed using the Ms-Excel Newton solver which is freely available by minimizing the error between the experimental and model values given as follows.

$$Sh = 45.58 Re^{0.13} Sc^{0.33} \quad (5.19)$$

The plot of theoretical and experimental values of  $\log(Sh/Sc^{0.33})$  versus  $\log(Re)$  is shown in Figure 5.24. It was observed that the theoretical model is in good agreement with the experimental data. The  $R^2$  value was found to be 0.953.

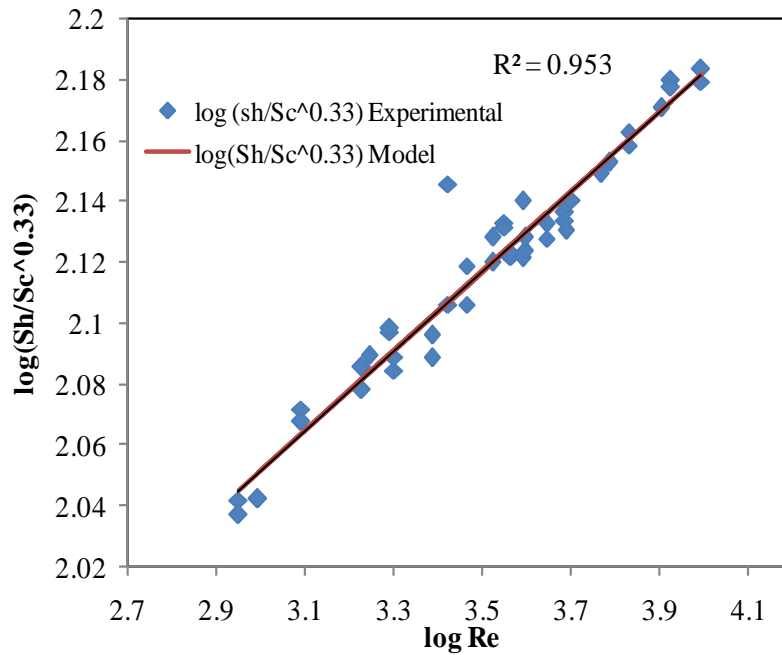


**Figure 5.24: Fitting of mass transfer correlation at 30 ppm initial dye concentration**

**Table 5.14: Experimental and model data for mass transfer correlation at 30 ppm initial dye concentration**

S.No.	Flow Rate (lpm)	Feed Temp. (°C)	Vacuum Degree (mmHg)	Flux (kg/m <sup>2</sup> .h)	Re	Sc	Model Sh	Exp. Sh	Exp. Kf
1	2	25	750	1.79	887.8	0.038	37.788	37.533	0.0173
2	4	25	750	1.87	1753.9	0.039	41.479	42.016	0.0194
3	6	25	750	2.04	2650.2	0.039	43.676	43.593	0.0201
4	8	25	750	2.09	3542.3	0.038	45.330	46.359	0.0214
5	10	25	750	2.14	4417.0	0.039	46.697	46.332	0.0214
6	2	40	750	5.99	982.3	0.035	37.035	36.309	0.0168
7	4	40	750	6.69	1953.9	0.035	40.597	41.292	0.0191
8	6	40	750	7.06	2922.8	0.035	42.833	43.460	0.0201
9	8	40	750	7.38	3907.7	0.035	44.453	43.686	0.0202
10	10	40	750	7.96	4858.2	0.035	45.820	45.014	0.0208
11	2	55	750	18.54	1230.1	0.028	35.413	36.113	0.0167
12	4	55	750	18.82	2435.0	0.028	38.856	37.650	0.0174
13	6	55	750	19.24	3665.0	0.028	40.946	40.612	0.0187
14	8	55	750	19.64	4903.4	0.028	42.489	41.365	0.0191

15	10	55	750	20.18	6108.3	0.028	43.778	43.637	0.0201
16	2	70	750	34.18	1685.7	0.020	33.259	33.599	0.0155
17	4	70	750	34.59	3339.7	0.020	36.487	37.182	0.0172
18	6	70	750	35.06	5033.2	0.020	38.440	38.187	0.0176
19	8	70	750	35.64	6774.9	0.020	39.840	40.068	0.0185
20	10	70	750	35.86	8428.5	0.020	41.060	41.751	0.0193
21	2	85	750	52.56	1999.6	0.017	32.148	31.658	0.0146
22	4	85	750	53.42	3954.5	0.017	35.280	34.801	0.0161
23	6	85	750	53.78	5866.1	0.017	37.286	37.074	0.0171
24	8	85	750	54.21	7998.6	0.017	38.545	38.636	0.0178
25	10	85	750	54.74	9886.3	0.017	39.776	39.551	0.0183
26	2	25	730	0.97	887.8	0.038	37.788	37.112	0.0171
27	4	25	730	1.04	1753.9	0.039	41.479	42.059	0.0194
28	6	25	730	1.22	2650.2	0.039	43.676	47.750	0.0220
29	8	25	730	1.26	3542.3	0.038	45.330	46.180	0.0213
30	10	25	730	1.31	4417.0	0.039	46.697	45.812	0.0211
31	2	40	730	5.17	982.3	0.035	37.035	36.312	0.0168
32	4	40	730	5.86	1953.9	0.035	40.597	41.392	0.0191
33	6	40	730	6.24	2922.8	0.035	42.833	42.218	0.0195
34	8	40	730	6.55	3907.7	0.035	44.453	45.606	0.0210
35	10	40	730	7.13	4858.2	0.035	45.820	45.297	0.0209
36	2	55	730	17.72	1230.1	0.028	35.413	35.754	0.0165
37	4	55	730	17.99	2435.0	0.028	38.856	38.300	0.0177
38	6	55	730	18.41	3665.0	0.028	40.946	40.732	0.0188
39	8	55	730	18.82	4903.4	0.028	42.489	42.190	0.0195
40	10	55	730	19.35	6108.3	0.028	43.778	43.637	0.0201
41	2	70	730	33.35	1685.7	0.020	33.259	33.016	0.0152
42	4	70	730	33.77	3339.7	0.020	36.487	36.482	0.0168
43	6	70	730	34.24	5033.2	0.020	38.440	38.187	0.0176
44	8	70	730	34.82	6774.9	0.020	39.840	39.670	0.0183
45	10	70	730	35.04	8428.5	0.020	41.060	41.534	0.0192
46	2	85	730	51.74	1999.6	0.017	32.148	31.995	0.0148

47	4	85	730	52.59	3954.5	0.017	35.280	35.146	0.0162
48	6	85	730	52.95	5866.1	0.017	37.286	37.040	0.0171
49	8	85	730	53.38	7998.6	0.017	38.545	38.637	0.0178
50	10	85	730	53.92	9886.3	0.017	39.776	39.948	0.0184

The effect of feed temperature on mass transfer coefficient is given in Figure 5.25 at 2 and 10 lpm flow rate respectively. From this Figure 5.25, it can be stated that the mass transfer coefficient is slightly increased/nearly constant over the entire range of feed temperature. This may be due to reduction in thermal boundary layer at the membrane surface. The comparison between the mass transfer coefficient of Dye-water mixture and NaCl-water solutions is carried out and shown in Figure 5.26. From this figure, it can be seen that the mass transfer coefficient of NaCl-water mixture is around 10 times higher than the dye-water mixture. This may be due to the retention time of dye molecules on the surface of the membrane. The dye molecules take more retention time on the surface of the membrane due to higher molecular weight as compared to salt. Another possible reason may be the affinity of dye molecules to the fibre surface which formed vander-waal forces. So, the mass transfer coefficient of dye-water mixture is lower as compared to NaCl-water mixture.

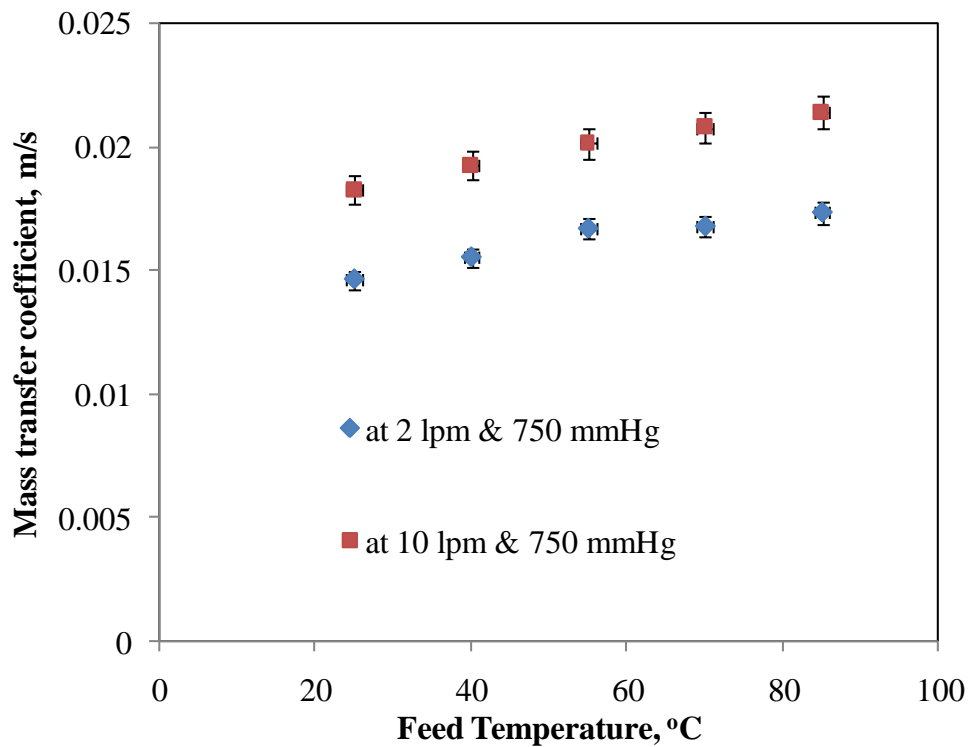


**Figure 5.25: Effect of Feed Temperature on mass transfer coefficient**

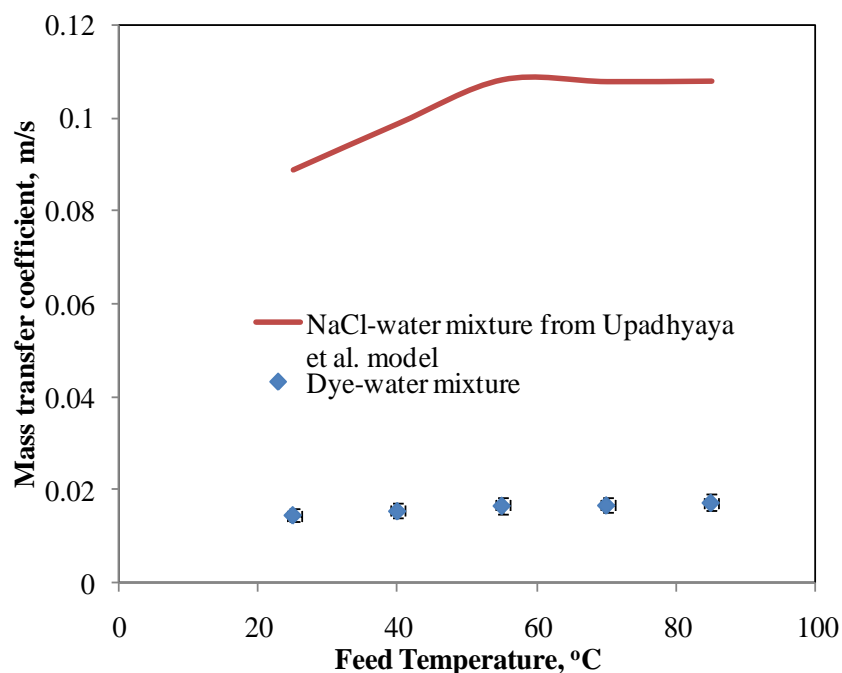
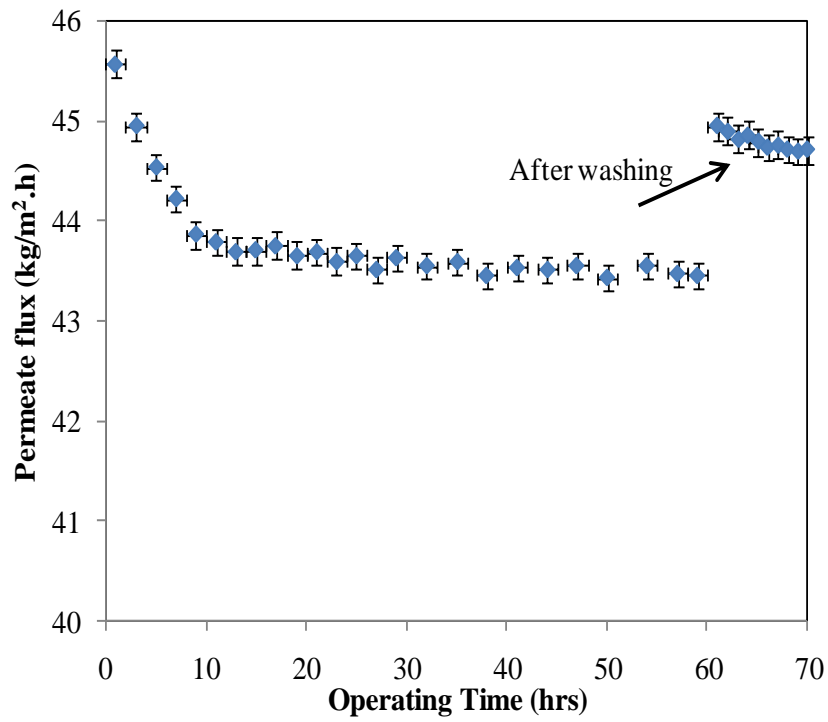


**Figure 5.26: Comparison of mass transfer coefficient of Dye-water and NaCl-water mixture**

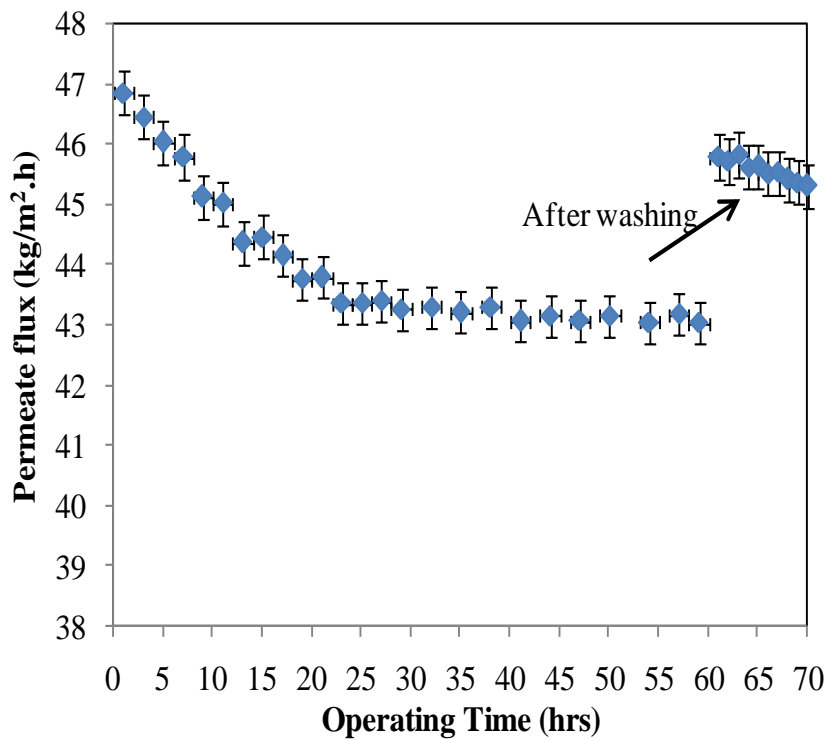
### 5.7. Membrane Characterization and fouling study

In the continuous run, the initial dye concentration of 30 ppm was fed to feed tank and operated in VMD setup. The permeate flux was collected over a period of 60 hrs for both PVDF and PTFE membrane. The effect of operating time on permeate flux for PTFE and PVDF membrane is shown in Figure 5.27. It can be seen that the permeate flux is decreased continuously from 45.51 to 43.45 kg/m<sup>2</sup>.h and 46.85 to 43.03 kg/m<sup>2</sup>.h in 60 hrs for PTFE and PVDF membrane respectively. Nearly 4.5% and 8.08% reduction in permeate flux was observed in PTFE and PVDF membrane respectively at 85 °C of feed temperature, vacuum degree of 750 mmHg, flow rate of 5 lpm and initial dye concentration of 30ppm. This reduction may be due to deposition of dye molecules at the surface of the membrane. It was also found that the percentage reduction in permeate flux is lower in case of PTFE membrane as compared to PVDF membrane because the hydrophobicity of the PTFE membrane is higher. After 60 hrs of continuous operation, the washing of the membranes are carried out using water. After washing, the performance of the membranes are further checked that the permeate flux is regained to about 44.94 and 45.78 kg/m<sup>2</sup>.h in case of PTFE and PVDF membrane at the same operating conditions with removal of dyes upto 99.9%. Moreover, it can be seen that the permeate flux is not regained as original (in case of fresh membrane) which may due to entrapment of dye molecules inside the pores of the membrane which results in permanent blockage of membrane pores.





(a) PTFE

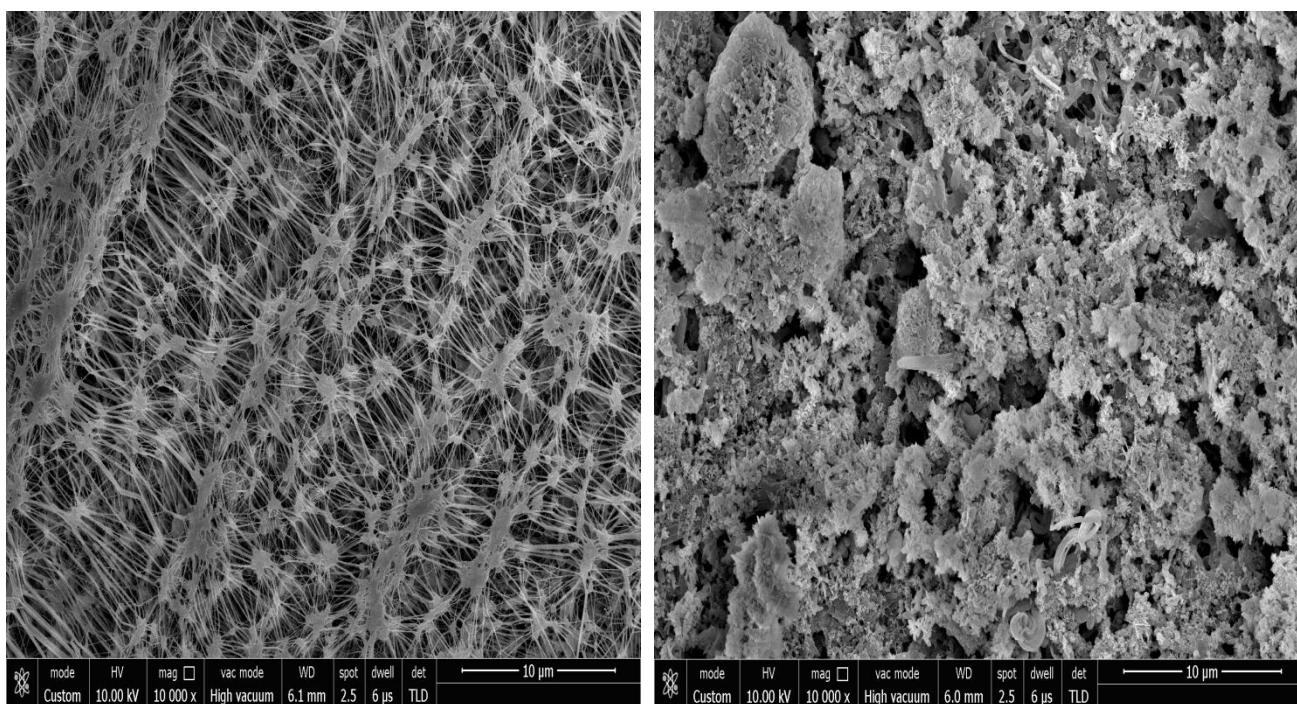


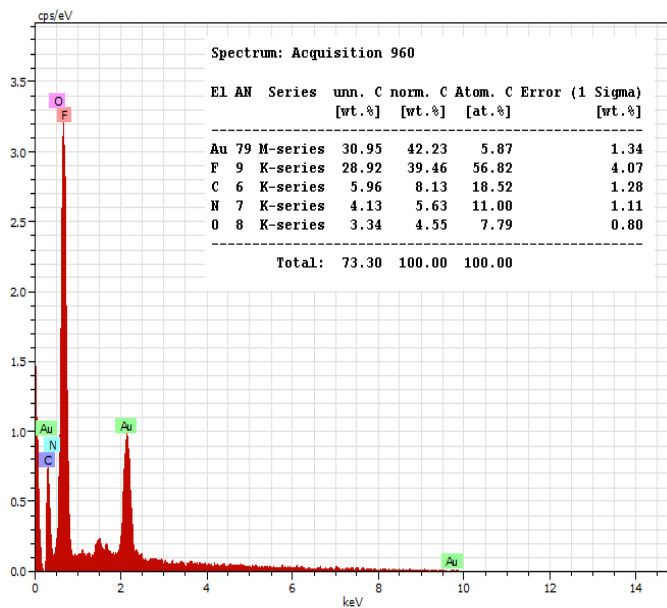
(b) PVDF

**Figure 5.27: Effect of operating time on permeate flux**

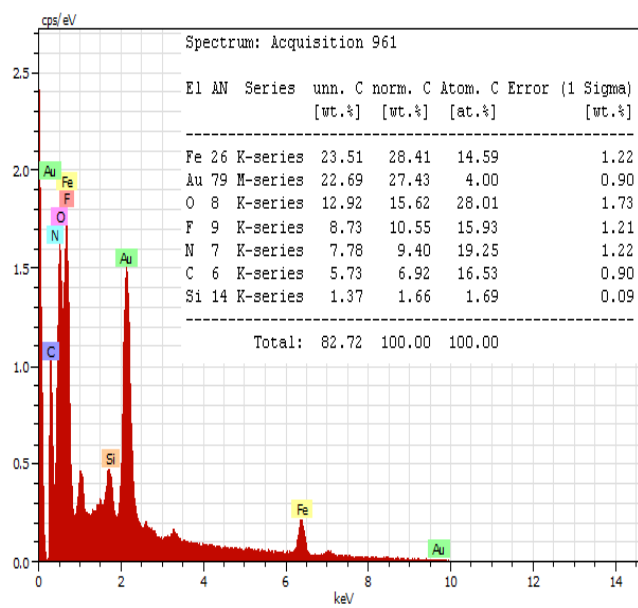
The characterization of membrane surface was carried out before and after use of membrane using scanning electron microscopy and EDS. The SEM images with EDS of the fresh and used membranes

(after 60 hrs operation run) is shown in Figure 5.28 and Figure 5.29 for PTFE and PVDF membranes respectively. By comparing the SEM images of fresh and used membranes, fouling of dye molecules at the membrane surface can be easily detected. Pore size distribution graph for PTFE and PVDF membrane is generated using the SEM images of fresh and used membrane with the help of *ImageJ* Software. From the PSD graph shown in Figure 5.30, it can be seen that the average pore size of fresh PTFE and PVDF membrane is around 0.22  $\mu\text{m}$  which is same as provided by the manufacturer (Millipore). It can be also stated that the average pore size of both PTFE and PVDF membrane is reduced for used membrane which is confirmed the blockage of pores of the membrane which results in lower permeate flux. The SEM images of PTFE and PVDF membrane after washing is shown in Figure 5.31. It can be seen from Figure 5.31 that fouling is effectively removed after the washing of the membrane and due to this the flux is recovered.



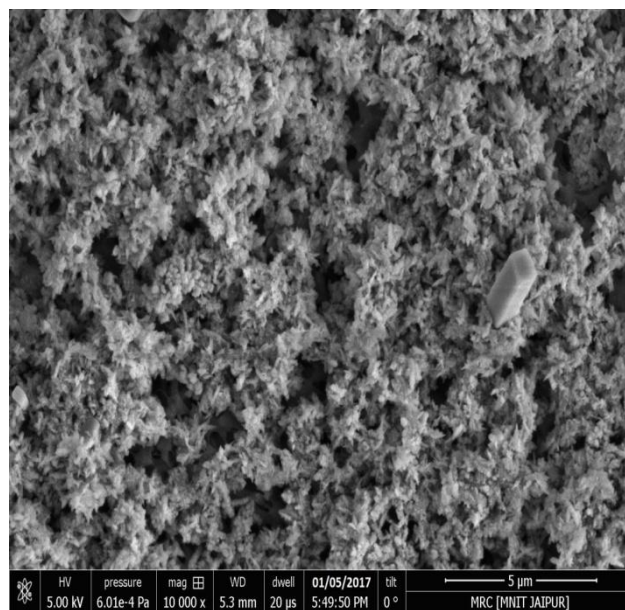
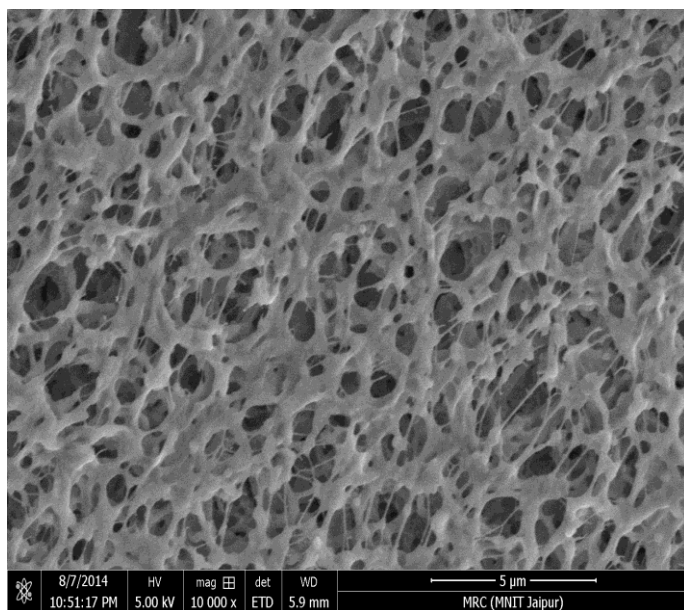


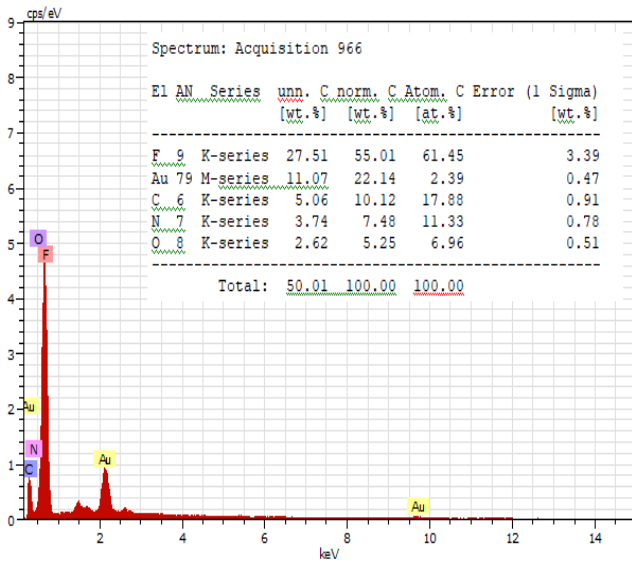
(a)



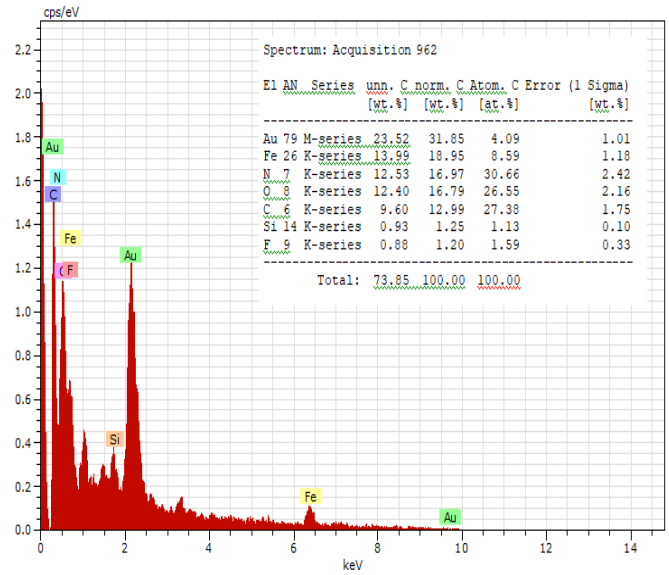
(b)

**Figure 5.28: Surface morphology analysis of PTFE membrane (a) fresh, and (b) used membrane after 60hrs using SEM and EDS analysis**



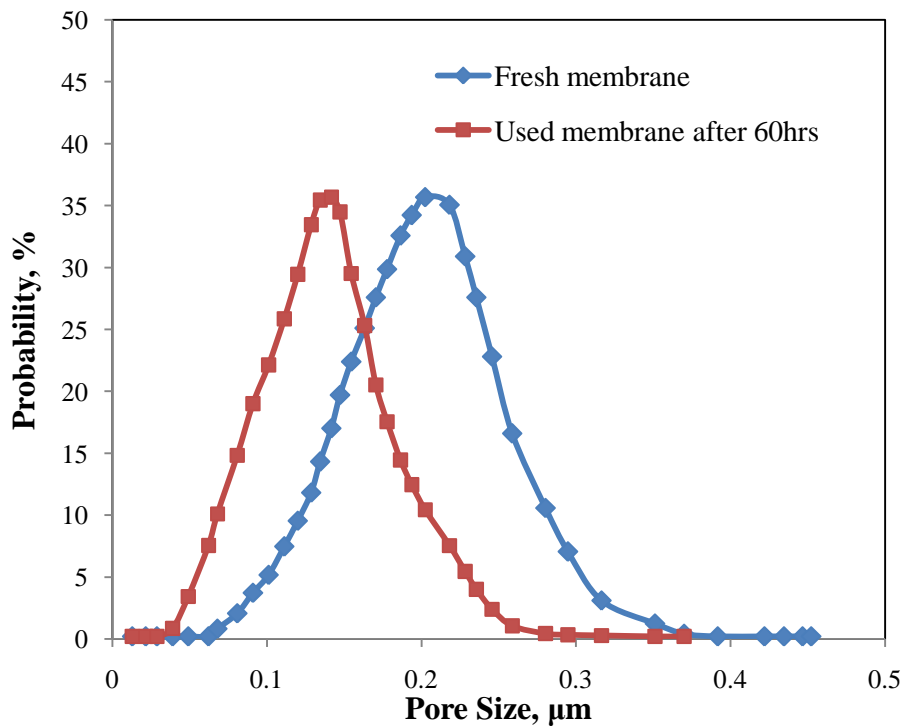


(a)

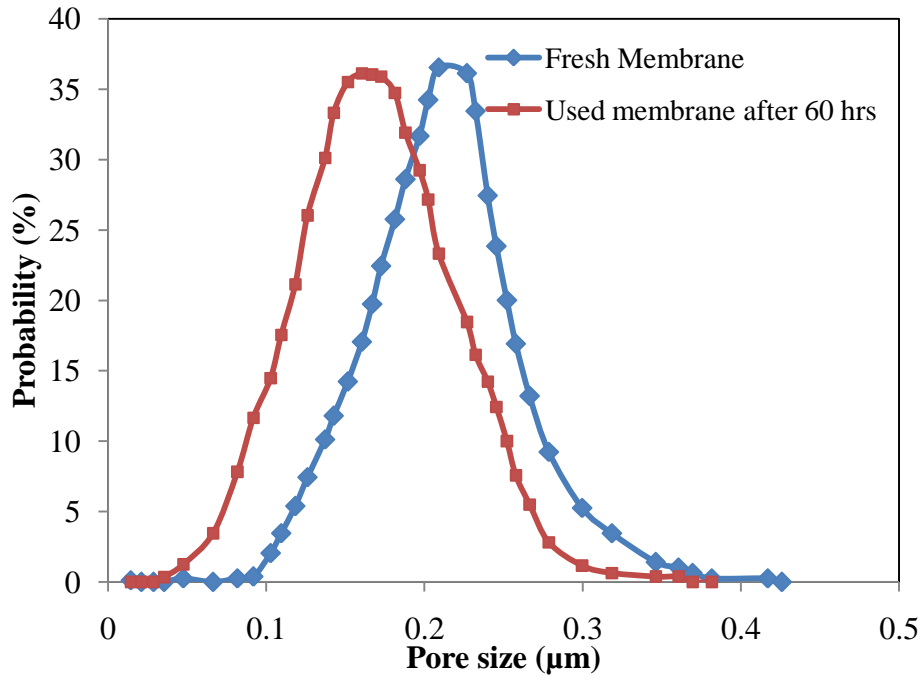


(b)

**Figure 5.29: Surface morphology analysis of PVDF membrane (a) fresh, and (b) used membrane after 60hrs using SEM and EDS analysis**

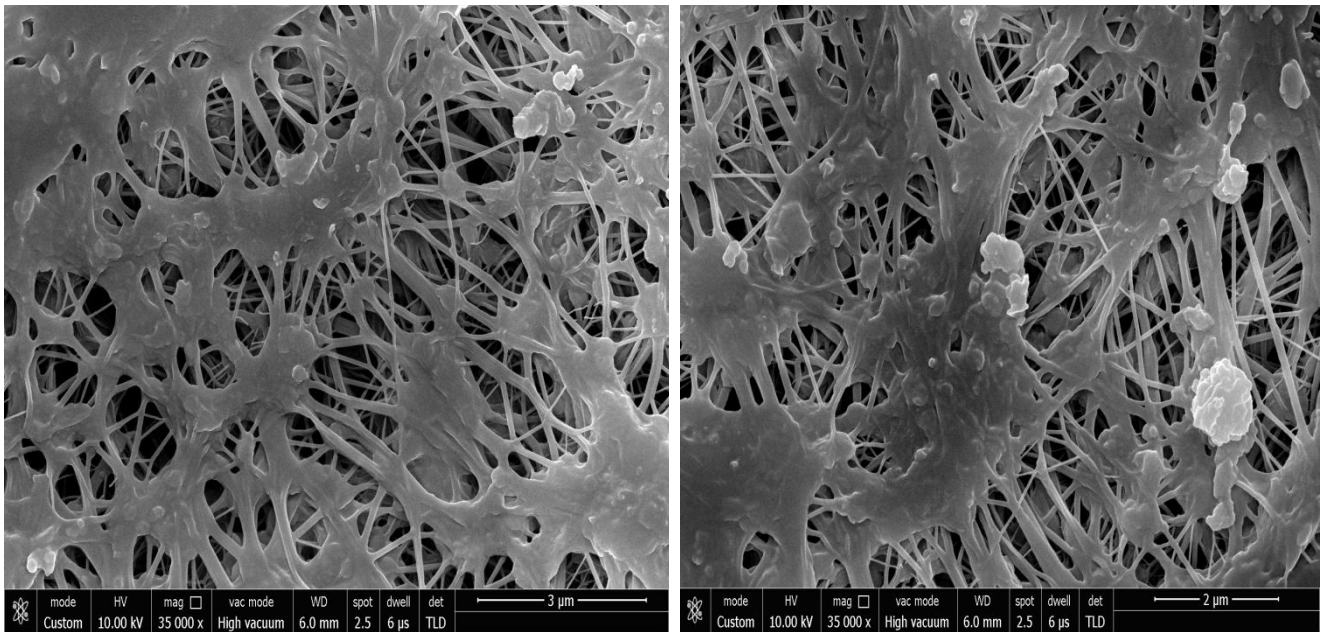


(a) PTFE Membrane



(b) PVDF Membrane

Figure 5.30: Pore size distribution of Fresh and used membranes for PTFE and PVDF membrane



(a) PTFE Membrane

(b) PVDF Membrane

Figure 5.31: SEM images of PTFE and PVDF membrane after washing

## 5.8. Recovery Model

The recovery of water through VMD process was evaluated by solving the model equations provided in Chapter 3. For recovery analysis, the lab scale VMD setup was operated for 60 hrs and the flux was obtained to be 0.12 kg/hr which is considered as constant over the period of operating time through the membrane area of 0.00212 m<sup>2</sup>. Feed solution of 10 litres with initial dye concentration of 30 ppm is fed to the feed tank and operated at 85 °C of feed temperature, 5 lpm of flow rate and 750 mmHg of vacuum degree for 60 hrs continuous run. From experiments, it was found that the concentration of the dye in the feed tank is increased gradually from 30 to 70 ppm over the run time as shown in Figure 5.32 and theoretical transition dye concentration is also estimated by solving model equations in MATLAB which was best fitted. Moreover, the volume of the tank decreased from 10 lt to 2.8 lt in 60 hrs. So, to conduct further experiment, the feed tank should be refilled with fresh feed solution because the minimum volume requirement is 2.5 lt for continuous operation. The percentage recovery of water on permeate side is increased with time and become around 70% in 60 hrs. In lab scale setup, the effective surface area of membrane is 0.00212 m<sup>2</sup> which is very low that's why the time of water recovery is very high. If this membrane area is replaced by 1 m<sup>2</sup> area then the same recovery can be obtained in less than 15 min. It can also be seen that the theoretical recovery is in good agreement with experimental data as shown in Figure 5.33.

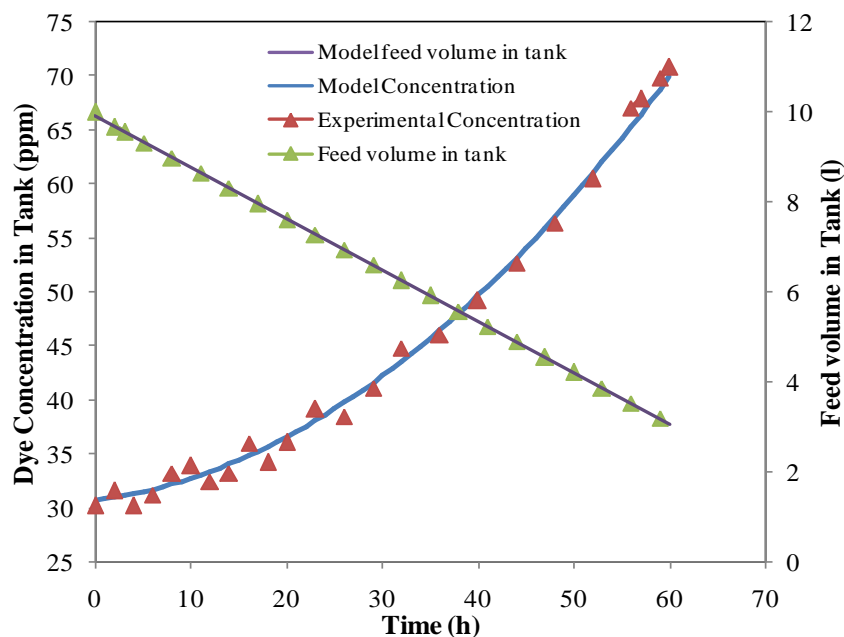


**Figure 5.32: Variation of Dye concentration and volume of feed in tank with operating time**

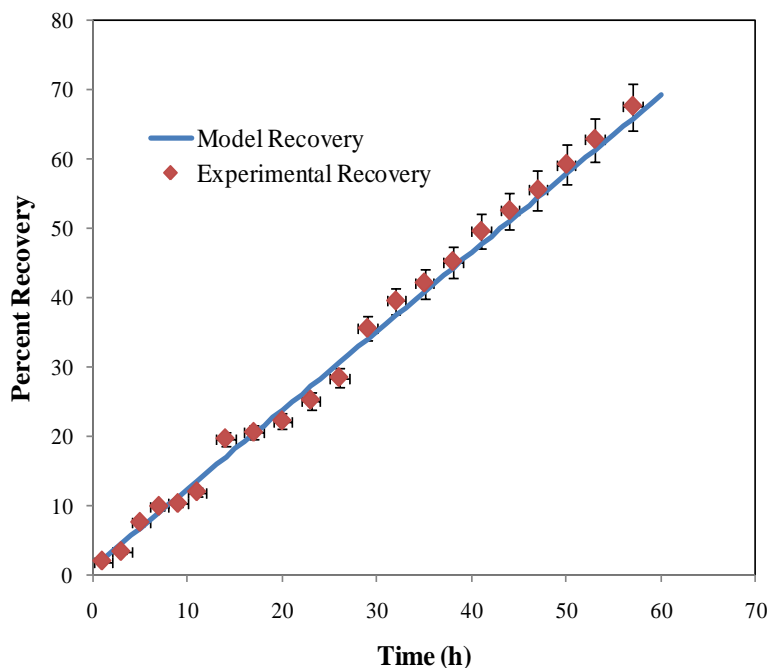


**Figure 5.33: Comparison of experimental and model recovery**

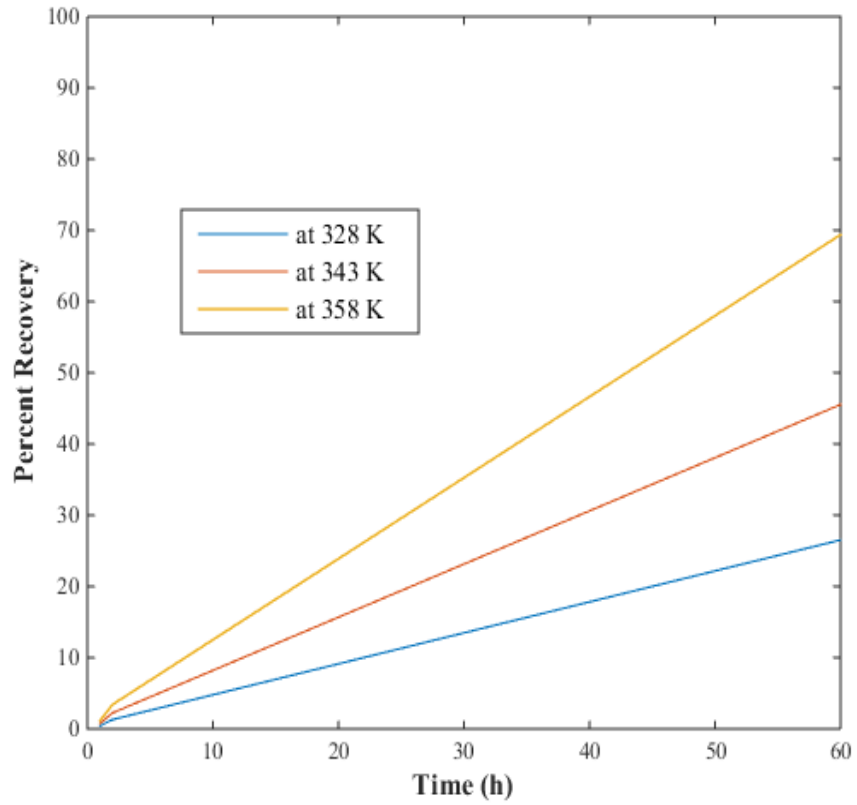
#### 5.8.1. Effect of operating parameters on recovery

The effect of the different operating parameters such as feed temperature, vacuum degree, flow rate and initial dye concentration is studied in a continuous operation for 60 hrs. From Figure 5.34(a), it can be seen that the percentage recovery is increased from 43.48% to 69.38% on increasing the feed temperature from 55 to 85 °C in 60 hrs. The possible reason for this increment is that the permeate flux increased exponentially with increasing feed temperature due increased in trans-membrane vapor pressure difference. The percentage recovery is also increased from 63.94% to 69.38% with increasing vacuum degree from 670 to 750mmHg as shown in Figure 5.34(b) in 60hrs. This may be possible due to reduction in mass transfer resistances on the permeate side of the membrane which increased the permeate flux and results in higher recovery.

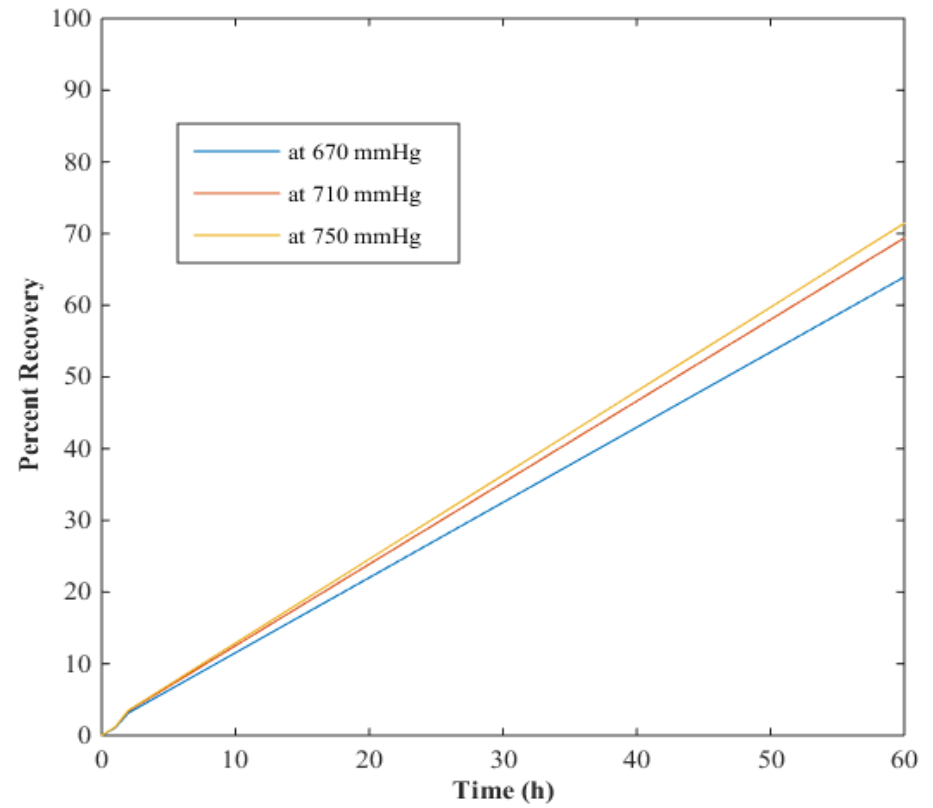
Figure 5.35(a) shows the variation in percentage recovery with increased in flow rate from 2 lpm to 10 lpm at constant feed temperature of 85 °C, vacuum degree of 750 mmHg, and initial dye concentration of 30 ppm in 60hrs continuous operation. From this Figure 5.35(a), it can be seen that the effect of flow rate is not very significant on recovery because feed flow rate is not directly increasing the driving force for vapor transfer through the membrane. As a result, little increment in permeate flux was obtained on increasing flow rate from 2 to 10 lpm as discussed in section 5.4.3. From Figure 5.35(b), it can be seen that no remarkable changes observed in percentage recovery till 20 hours, whereas after 20 hours the variation in percentage recovery is observed on increasing feed dye concentration from 10 to 130 ppm at constant optimized conditions of other operating variables for 60 hrs. This may be due to the fact that the

deposition of dye particles on membrane surface might get increased after 20 hours with increasing the dye concentration because the solubility of dye molecules is small in water so the deposition rate is high at higher concentration. Therefore, the pores of membrane are blocked which create additional resistances for vapor molecules to pass through the membrane. Hence, the percentage recovery is decreased with increasing dye concentration in feed.



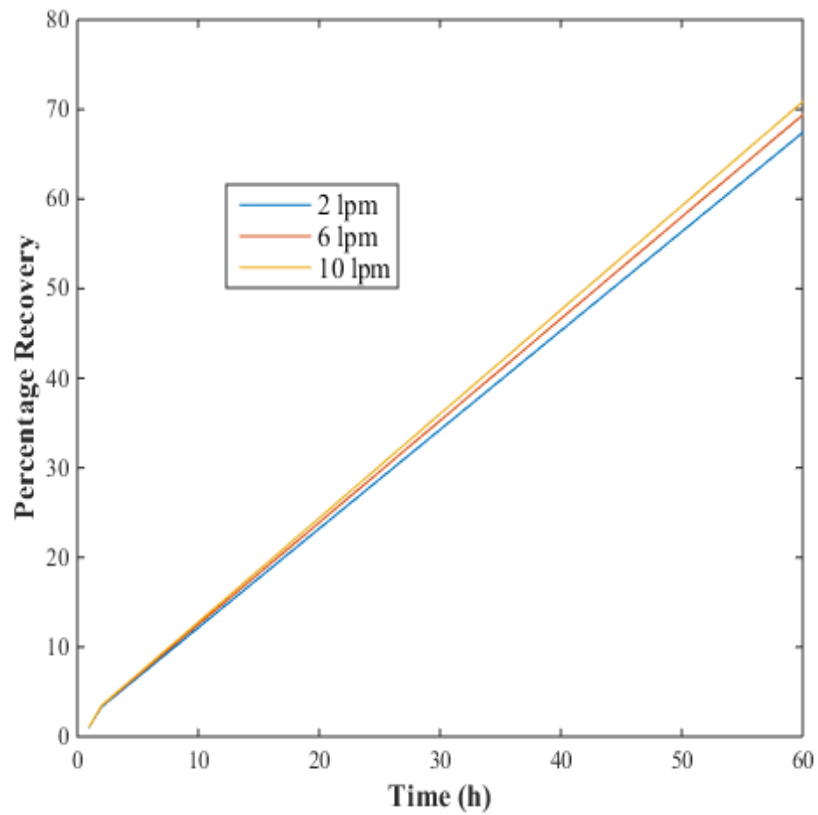


(a)

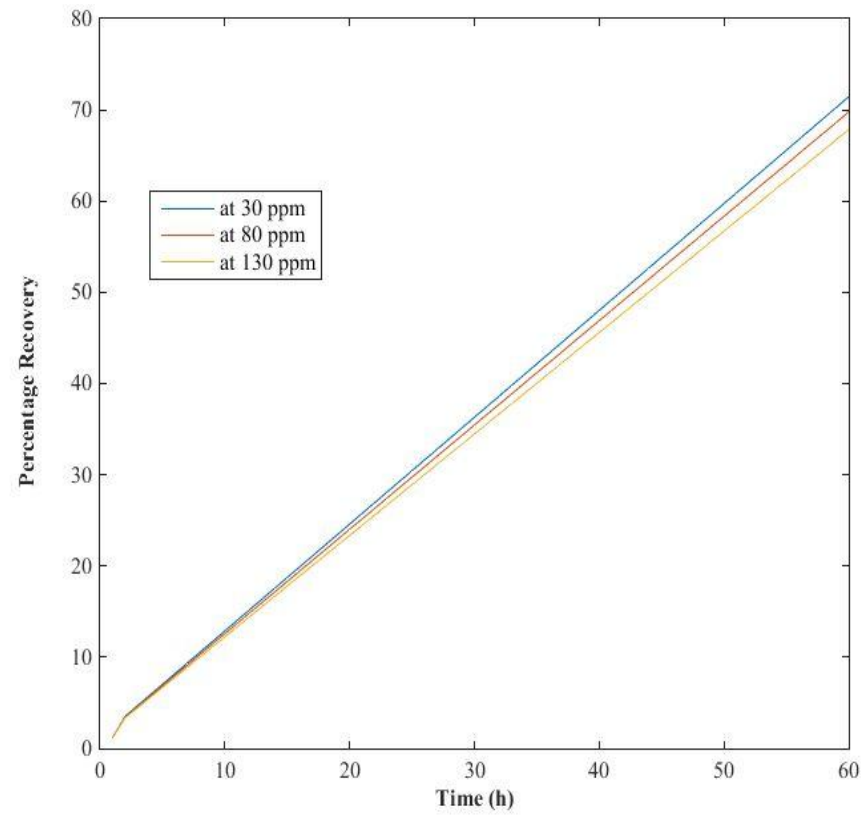


(b)

**Figure 5.34: Effect of (a) feed temperature and (b) vacuum degree on percentage recovery with time**



(a)



(b)

Figure 5.35: Effect of (a) Feed flow rate and (b) Feed concentration on percentage recovery with time

## 5.9. Sensitivity analysis

Process sensitivity analysis is considered an important parameter for analyzing the performance of the process and to improve it for all variables. For enhancing the permeate flux through the VMD process is necessary by analyzing the operating parameters. From the optimization of process variables using CCD, it was found that the feed temperature and vacuum degree was considered as significant operating parameters. So, the sensitivity analysis of these operating parameters with mass flux was evaluated using the equation 3.15 to 3.22.

### 5.9.1. Sensitivity of permeate flux to feed temperature

The sensitivity of permeate flux to feed temperature is shown in Figure 5.36 by normalized sensitivity factor. The permeate flux sensitivity factor with feed temperature is determined by solving the equations 3.17 and 3.18 simultaneously. It can be seen from Figure 5.36 that the sensitivity factor is decreased significantly with increase in feed temperature. This is due to the fact that the little variation in feed temperature is result in significant increment in permeate flux. It can be seen that the sensitivity factor decreased from 148 to 18 with increasing feed temperature from 25 to 85 °C at optimum conditions of flow rate of 5 lpm, vacuum degree of 750mmHg, and initial dye concentration of 30 ppm, which indicate that the permeate flux is higher at higher feed temperature (highly sensitive parameter to permeate flux). So, for the better performance of VMD, the feed temperature of the system should be high.

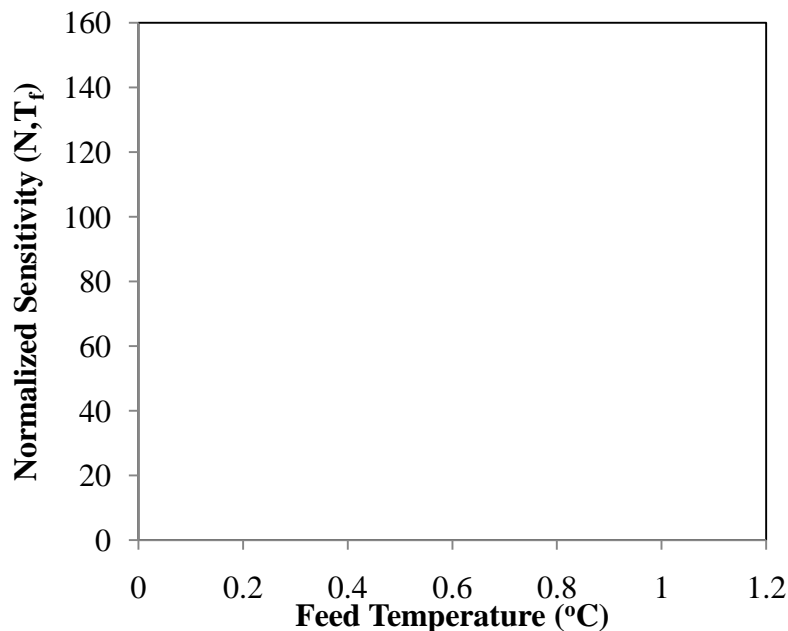


**Figure 5.36: Sensitivity of permeate flux to feed temperature**

[vacuum degree = 750mmHg; feed flow rate = 5lpm; initial dye concentration = 30ppm]

### 5.9.2. Sensitivity of permeate flux to vacuum degree

Figure 5.37 shows the normalized sensitivity factor of permeate flux with vacuum degree at the optimum condition for feed temperature of 85 °C, flow rate of 5 lpm and initial dye concentration of 30 ppm. It can be seen that the at lower vacuum the value of sensitivity factor is -1.3 which reduced to -0.085 on increasing vacuum degree upto 750mmHg. This is because the permeate flux is increased on increasing vacuum degree which is already described in section 5.4.2. It is found that the sensitivity of VMD process is lower at lower vacuum degree; therefore, it is analysed that system should be operated at higher vacuum degree to obtained higher permeate flux.

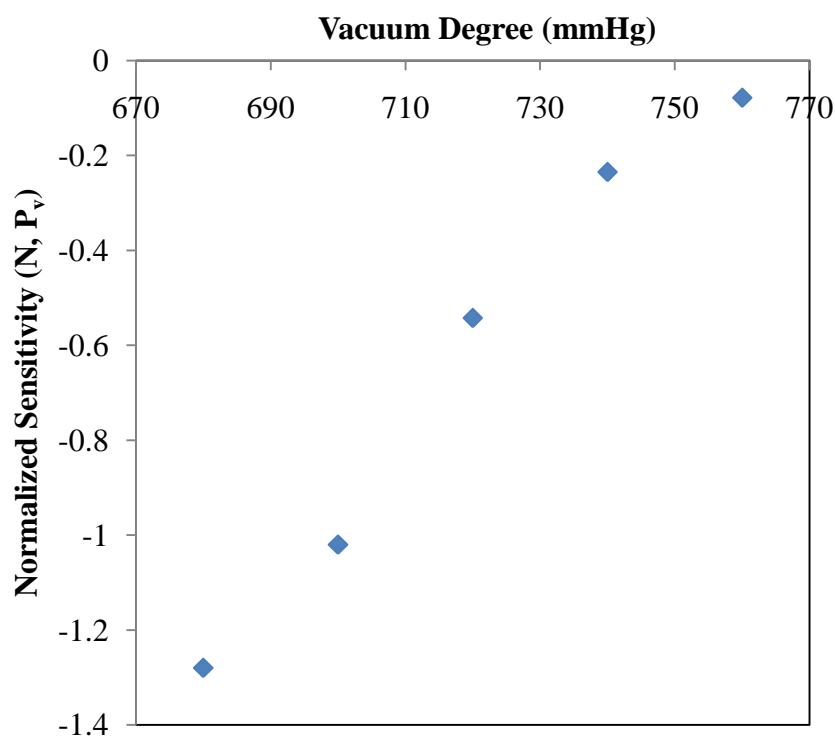


**Figure 5.37: Sensitivity of permeate flux to vacuum degree**

[Feed temperature = 85 °C; feed flow rate = 5lpm; initial dye concentration = 30ppm]

### 5.9.3. Sensitivity of permeate flux to flow rate

The effect of flow rate on sensitivity is shown in Figure 5.38 at feed temperature of 85 °C, flow rate of 5 lpm and initial dye concentration of 30ppm.. It is observed that the value of sensitivity factor is increased with increase in flow rate from 2 lpm to 5 lpm and then decreased. The VMD performance is maximum at 5 lpm since this sensitivity is very high at this point and this fact was also observed from the optimization results.

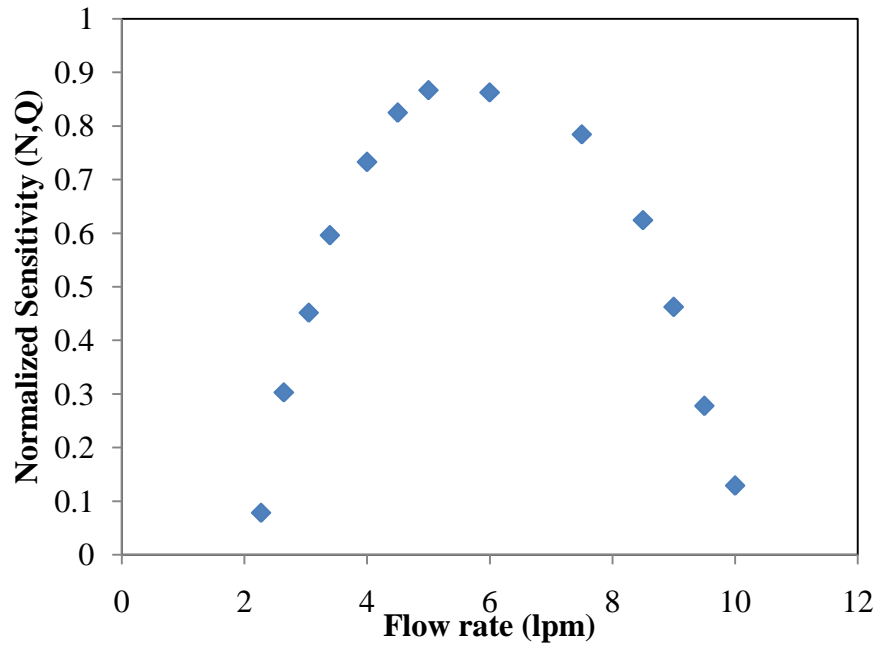


**Figure 5.38: Sensitivity of permeate flux to flow rate**

#### 5.9.4. Sensitivity of permeate flux to membrane characteristics

The effect of membrane characteristics  $\varepsilon/ \tau\delta$  on sensitivity is shown in Figure 5.39. The sensitivity remains constant at 1 on varying the membrane characteristics from 2000 to 10000 because of the linear change in mass flux, which is also evident from Equation 3.27.

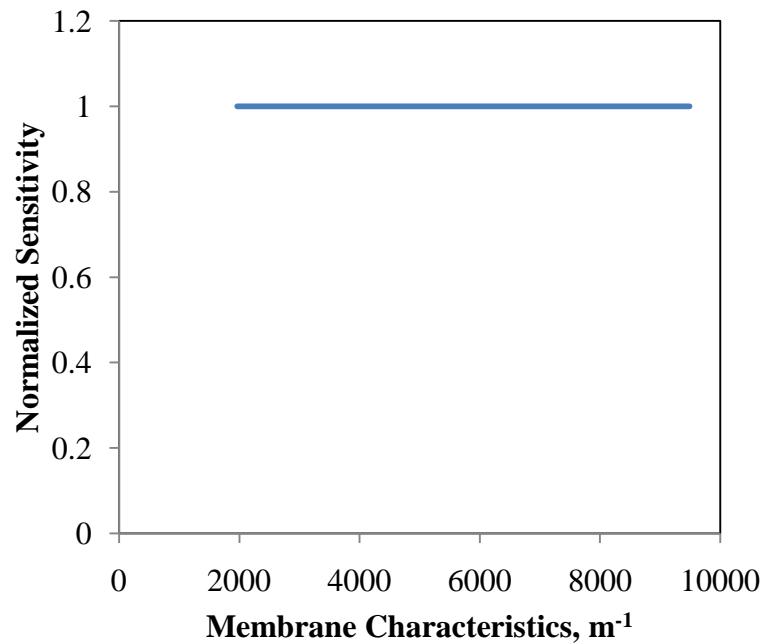


**Figure 5.39: Sensitivity of permeate flux to membrane characteristics**

### 5.10. ANN modeling for permeate flux

Artificial neural networks (ANN) unit is widely used in many engineering analysis comes and not simply restricted to chemical industries. Neural networks offer a straightforward thanks to relating 2 systems of knowledge sets, wherever the primary one is taken into account to be associate degree input vector and is assumed to possess a relationship with the second set, i.e., the output knowledge vector. A man-made neural network contains an assortment of parallel process units connected with every different by call weights. Even although all artificial neural networks unit are made from this basic building block, the basics could vary. Method of coming up with a neural network is an associate degree repetitive process. A general ANN model was created and simulated victimization MATLAB package. These are used for modeling the VMD and determinant the impact of various parameters however they affect the VMD performance.

Artificial neural network with 4 input conditions with 1 target value was created with varying number of neurons from 2-10 using TRAINLM as function of learning. Moreover, the performace function for algorithm learning and transfer functions were assumed to be LEARNINGDM and TANSIG respectively. The neurons are corresponding to input conditions as feed temperature (25 – 85 °C), flow rate (2-10 lpm), vacuum degree (670-750mmHg) and initial dye concentration (10-130 ppm). The training of the network is done with 31 data, 15 data are used for the testing of the network and then 15 data are used for the validation of the results. It was seen that the ANN model is best fitted with the given conditions with  $R^2$  as 0.988, 0.992, and 0.998 for training, testing and validation respectively. So, for the prediction of permeate flux, ANN model can be used. The weights used for the development of this neural network are given in Table 5.15 for the input layer, output layer, input hidden layer and the output hidden layer. The comparison of the developed ANN model with experimental flux is carried out along with CCD model developed so far and the comparison is given in Table 5.16. From this table, it can be observed that the  $R^2$  and MAPE values are found to be 0.998 & 0.995 and 2.06 and 7.88 for ANN and CCD modeling respectively. So, the developed ANN model is well fitted with experimental conditions as compared to CCD model.

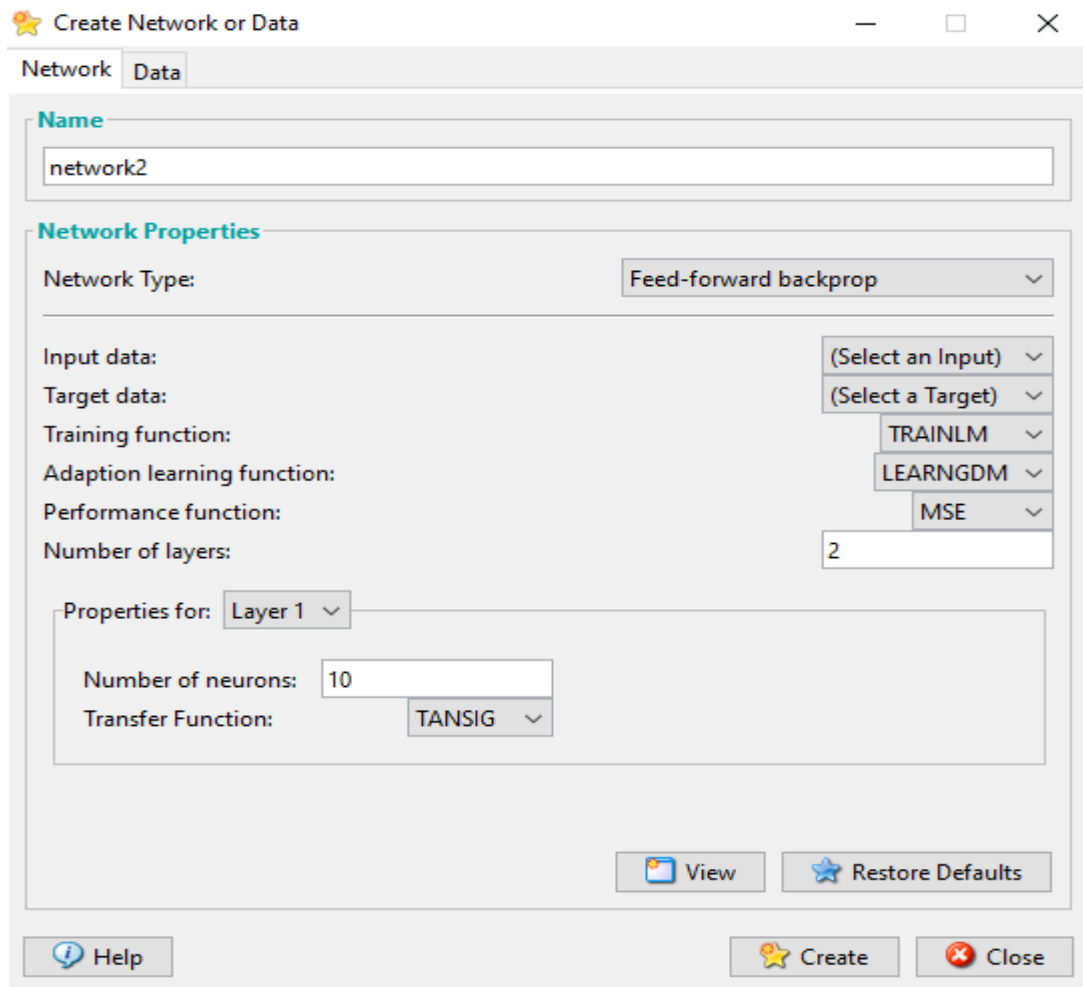


**Figure 5.40: Create network for Training and Adapting learning function**

**Table 5.15: Weights for Artificial Neural Network**

**(a) Weights to different input hidden layers**

Weight to layer 1 from input1	Weight to layer 1 from input 2	Weight to layer 1 from input 3	Weight to layer 1 from input 4
-0.79838	0.12472	0.10292	-0.29514
-0.31011	-0.092513	2.0264	-0.71069
0.50778	-1.7882	-0.82776	-0.67493
-0.65313	-0.33023	0.090036	-1.5539
-1.2049	-1.0016	-1.0313	0.22776
-1.121	2.031	-0.80241	0.13475
-0.33971	1.8433	0.9464	-0.97467
-2.1169	0.74724	-0.15086	1.5093

-1.6667	-1.0228	1.3098	-1.6199
2.0131	-1.5255	-0.01981	0.69974

**(b) Weights to output layer**

-	-	-	0.41319	-	0.3317	-	0.073521	-	0.36711
2.9613	0.028643	0.26135		0.63406		0.33471		0.40411	

**(c) Bias to hidden input layer**

1.2657	2.3002	2.2255	0.91946	0.18893	-1.7756	0.12879	-1.0601	-1.5785	2.31
--------	--------	--------	---------	---------	---------	---------	---------	---------	------

**(d) Bias to hidden output layer**

[1.9291]

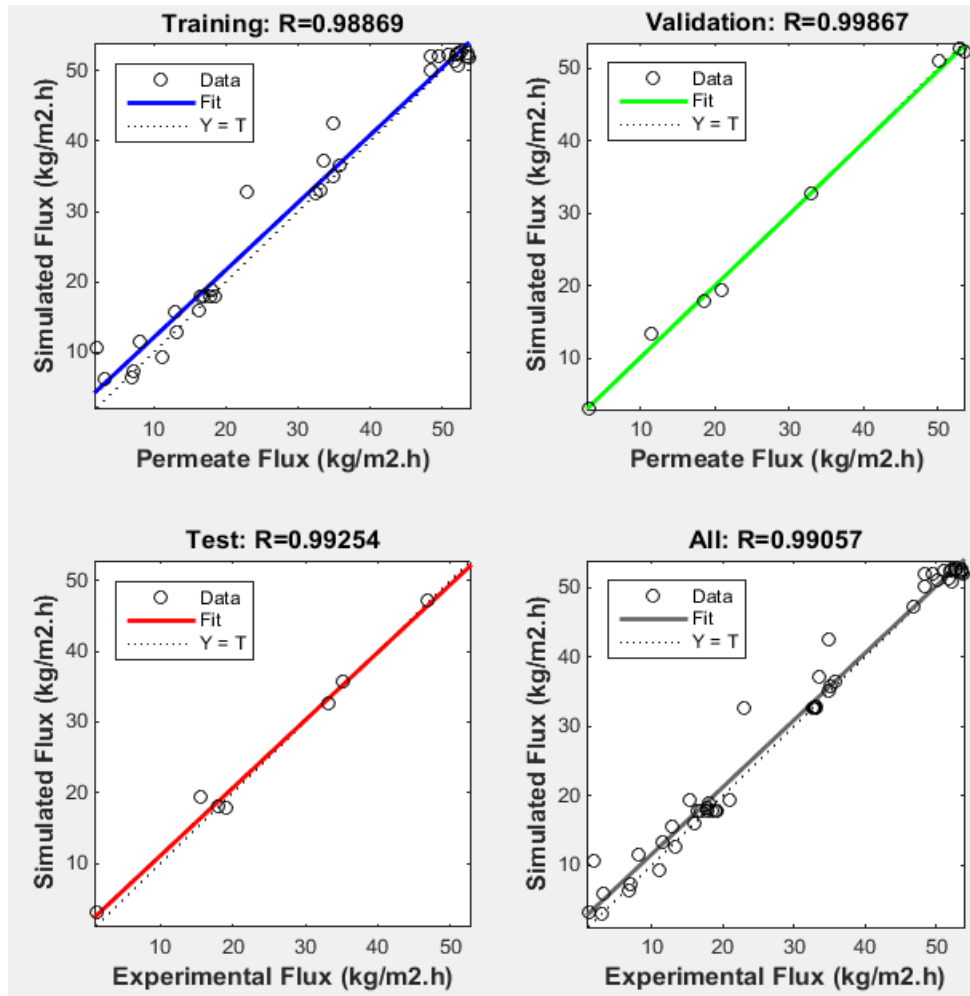


**Figure 5.41: Fitting of artificial neural network with experimental data**



**Table 5.16: Comparison of ANN and CCD model with Experimental Flux**

S.No.	Experimental Flux	Model Flux		R <sup>2</sup> ANN	R <sup>2</sup> CCD	MAPE ANN	MAPE CCD
		ANN	CCD				
1.	3.15	3.06	3.03	0.998	0.995	2.06	7.88
2.	32.55	32.61	32.16				
3.	7.15	7.32	7.2				
4.	33.15	33.42	33.82				
5.	2.96	3.11	3.11				
6.	32.86	32.75	32.33				
7.	6.9	6.86	7.06				
8.	33.13	33.13	33.78				
9.	11.52	11.31	10.32				
10.	35.15	35.35	34.54				
11.	13.25	12.96	13.33				
12.	35.76	35.52	35.05				
13.	11.15	11.26	10.03				
14.	34.95	35.16	34.35				
15.	12.99	12.69	12.82				
16.	34.96	35.09	34.63				
17.	1.13	1.19	1.7				
18.	52.23	52.42	52.64				
19.	16.15	16.03	17.85				
20.	23.01	22.92	22.3				
21.	18.12	18.39	18.61				
22.	17.9	18.09	18.28				
23.	15.46	15.48	14.63				
24.	20.95	19.48	22.78				
25.	17.85	17.92	17.71				
26.	18.57	17.92	17.71				
27.	16.46	16.52	17.71				
28.	17.02	17.92	17.71				
29.	18.51	17.92	17.71				
30.	19.05	17.92	17.71				
31.	16.58	17.92	17.71				

## CHAPTER 6. CONCLUSIONS & FUTURE RECOMMENDATIONS

The following important conclusions can be concluded from this present study.

1. Central composite design is successfully applied to determine the number of experiments and for the optimization of process variables such as feed temperature varies from 25 to 85 °C, vacuum degree varies from 670 to 750 mmHg, flow rate varies from 2 to 10 lpm and initial dye concentration varies from 10 to 130 ppm.
2. From the analysis of variance and percentage contribution, it was found that feed temperature and vacuum degree is highly significant operating parameters and different significant interaction parameters are also identified for all responses.
3. The optimum conditions for both membranes (PTFE and PVDF) were found be as follows: feed temperature of 85 °C, vacuum degree of 750 mmHg, flow rate of 5 lpm and initial dye concentration of 30 ppm for the maximization of permeate flux and percentage removal and minimization of specific energy consumption. The permeate flux, specific energy consumption and percentage removal is as follows:

S.No.	Membrane Type	Permeate flux (kg/m <sup>2</sup> .h)	Specific Energy Consumption (kWh/kg)	Percentage Removal
1.	PTFE	53.89	2.98	99.698
2.	PVDF	54.51	2.23	99.85

4. CFD model is also developed which comprises heat and mass transfer effects to calculate interfacial temperatures and permeate flux through the membrane.
5. The exponential increment in permeate flux was observed from 1.95 to 53.51 kg/m<sup>2</sup>.h and 2.85 to 54.12 kg/m<sup>2</sup>.h on increasing feed temperature from 25 to 85 °C for PTFE and PVDF membrane respectively. This is due to exponential increment in trans-membrane vapor pressure difference across the membrane.
6. The Poiseuille flow contribution is found to be increased from 2 to 19% for permeate flux on increasing feed temperature from 25 to 85 °C. The Knudsen diffusion is dominate over the Poiseuille flow due to smaller pore size of the membrane.
7. The linear increment in permeate flux was observed from 46.85 to 54.12 kg/m<sup>2</sup>.h and 51.23 to 54.12 kg/m<sup>2</sup>.h on increasing vacuum degree from 670 to 750 mmHg for PTFE and PVDF membrane respectively. This may be due to reduction in mass transfer resistances caused by the gas molecules filled in the pores of the membranes.

8. The effect of feed temperature and vacuum degree on temperature polarization is also analyzed. The exponential and linear reduction in temperature polarization coefficient is observed on increasing feed temperature and vacuum degree respectively.
9. Feed temperature\*flow rate, feed temperature\*vacuum degree and flow rate\*vacuum degree are considered as three significant interaction parameters for maximization of permeate flux and minimization of specific energy consumption.
10. Heat transfer correlation was obtained as  $Nu = 1.25Re^{0.87} Pr^{0.33}$  using Newton's solver available in *MS Excel*. The comparison of the available NaCl-water mixture is carried out with the present model and it is found that the heat transfer coefficient is higher for NaCl system because this is directly proportional to  $\mu^{-0.5}$ . Due to this the permeate flux is higher in NaCl-water mixture (reported by (Upadhyaya et al. 2016c)) as compared to present work.
11. Similarly mass transfer correlation was also obtained as  $Sh = 45.58 Re^{0.13} Sc^{0.33}$  and the comparison is carried out with available mass transfer coefficient of NaCl-water mixture. From this comparison, it is found that the mass transfer coefficient of NaCl-water mixture is larger as compared to present system. This is due to the adherence properties of dye molecules with fibre.
12. The performance of the PTFE and PVDF membrane was checked for the continuous operation of 60hrs. It was found that the permeate flux is decreased upto 4.5% and 8.08% in case of PTFE and PVDF membrane respectively. This is due to deposition of dye molecules at the surface of the membrane which is confirmed by SEM and PSD analysis. The original flux is almost regained after washing the used membrane with water.
13. Water recovery was found to be 76 % at 60 hours of operation. The effect of different operating parameters on recovery is also obtained and it was found that feed temperature is highly significant factor for the higher recovery.
14. The sensitivity analysis of permeate flux to feed temperature and vacuum degree is studied. From this analysis, it was found that the performance of the VMD process is maximized at 85 °C of feed temperature and 750 mmHg of vacuum degree. It can be observed that the performance of the VMD process increased with flow rate and maximized at 5 lpm which also verified the optimum conditions obtained from the CCD. The sensitivity of membrane characteristics remain 1 which predict that the permeate flux will enhanced with properties.

15. The experimental data was also trained and validated by ANN successfully. Both CCD model and ANN predicted the data in agreement with experimental data however, the MAPE values for ANN are slightly better.

### **Contribution to Knowledge**

1. The optimization of operating parameters such as feed temperature, flow rate, vacuum degree and initial dye concentration was done for various responses in present study.
2. The individual effect and interaction effect of various operating parameters for various responses for VMD is studied.
3. 3D CFD model was developed which comprises heat and mass transfer effects to estimate the interphase temperatures and permeate flux through membrane in present study.
4. Heat and mass transfer correlations were developed and the comparison was carried out with the existing correlations for treatment of dye-water mixtures.

### **Future Recommendations**

1. More research is needed to develop new membranes with improved hydrophobicity and liquid entry pressure for higher permeate flux.
2. Fabrication of composite membrane for VMD needs more attention.
3. More focused should be done on heat recovery from the vapors during the integration of process to minimize energy consumption.
4. The optimization of the membrane properties such as porosity, tortuosity, liquid entry pressure, hydrophobicity, thermal conductivity and pore size is needed.
5. Economic analysis of the process should be carried out and compared with other processes.
6. Integration of VMD plants with non-conventional energy resources like solar energy, geothermal energy etc. for large scale production is needed to minimize energy consumption.

## REFERENCES

- Ahmadi, M. et al., 2005. Application of the central composite design and response surface methodology to the advanced treatment of olive oil processing wastewater using Fenton ' s peroxidation. , 123, pp.187–195.
- Al-Asheh, S. et al., 2006. Concentration of sucrose solutions via vacuum membrane distillation. *Desalination*, 195(1–3), pp.60–68.
- Al-Obaidani, S. et al., 2008. Potential of membrane distillation in seawater desalination: thermal efficiency, sensitivity study and cost estimation. *Journal of Membrane Science*, 323(1), pp.85–98.
- Albrecht, T.R. & Quate, C.F., 1988. Atomic resolution with the atomic force microscope on conductors and nonconductors. *Journal of Vacuum Science & Technology A*, 6(2), pp.271–274.
- Alcaina-Miranda, M.I. et al., 2009. Nanofiltration as a final step towards textile wastewater reclamation. *Desalination*, 240(1–3), pp.290–297.
- Amaral Filho, J. et al., 2016. Removal of sulfate ions by dissolved air flotation (DAF) following precipitation and flocculation. *International Journal of Mineral Processing*, 149, pp.1–8.
- Aouni, A. et al., 2012. Reactive dyes rejection and textile effluent treatment study using ultrafiltration and nanofiltration processes. *Desalination*, 297, pp.87–96.
- Aslan, N., 2008. Application of response surface methodology and central composite rotatable design for modeling and optimization of a multi-gravity separator for chromite concentration. , 185, pp.80–86.
- Baghel, R., Upadhyaya, S., et al., 2017. A review on membrane applications and transport mechanisms in vacuum membrane distillation. *Reviews in Chemical Engineering*, 34(1), pp.73–106.
- Baghel, R., Kalla, S., et al., 2017. Treatment of Sudan III Dye from wastewater using Vacuum Membrane Distillation. *Journal of Basic and Applied Engineering Research*, 4(3), pp.237–241.
- Bahmanyar, A., Asghari, M. & Khoobi, N., 2012. Numerical simulation and theoretical study on simultaneously effects of operating parameters in direct contact membrane distillation. *Chemical Engineering and Processing: Process Intensification*, 61, pp.42–50.
- Banat, F. et al., 2007a. Desalination by a “compact SMADES” autonomous solarpowered membrane distillation unit. *Desalination*, 217(1), pp.29–37.
- Banat, F. et al., 2007b. Performance evaluation of the “large SMADES” autonomous desalination solar-driven membrane distillation plant in Aqaba, Jordan. *Desalination*, 217(1), pp.17–28.

- Banat, F. a. & Simandl, J., 1996. Removal of benzene traces from contaminated water by vacuum membrane distillation. *Chemical Engineering Science*, 51(8), pp.1257–1265.
- Banat, F., Al-Asheh, S. & Qtaishat, M., 2005. Treatment of waters colored with methylene blue dye by vacuum membrane distillation. *Desalination*, 174(1), pp.87–96.
- Banat, F., Al-Rub, F.A. & Bani-Melhem, K., 2003. Desalination by vacuum membrane distillation: sensitivity analysis. *Separation and Purification Technology*, 33(1), pp.75–87.
- Banat, F.A., 1994. Membrane Distillation For Desalination And RemovalOf Volatile Organic Compounds From Water.
- Bandini, S., Gostoli, C. & Sarti, G.C., 1992. Separation efficiency in vacuum membrane distillation. *Journal of Membrane Science*, 73(2–3), pp.217–229.
- Bandini, S., Saavedra, A. & Sarti, G.C., 1997. Vacuum membrane distillation: Experiments and modeling. *AIChE Journal*, 43(2), pp.398–408.
- Bandini, S. & Sarti, G.C., 2002. Concentration of must through vacuum membrane distillation. *Desalination*, 149(1), pp.253–259.
- Bandini, S. & Sarti, G.C., 1999. Heat and mass transport resistances in vacuum membrane distillation per drop. *AIChE journal*, 45(7), pp.1422–1433.
- Bier, C. & Plantikow, U., 1995. Solar powered desalination by membrane distillation. In *IDA World congress on desalination and water science, Abu Dhabi*. pp. 397–410.
- Binnig, G., Quate, C.F. & Gerber, C., 1986. Atomic force microscope. *Physical review letters*, 56(9), p.930.
- Bott, T.R., 1995. *Fouling of heat exchangers*, Elsevier.
- Cath, T.Y., Adams, V.D. & Childress, A.E., 2004. Experimental study of desalination using direct contact membrane distillation: a new approach to flux enhancement. *Journal of Membrane Science*, 228(1), pp.5–16.
- Cerneaux, S. et al., 2009. Comparison of various membrane distillation methods for desalination using hydrophobic ceramic membranes. *Journal of membrane science*, 337(1), pp.55–60.
- Chaurasia, S.P.P., Upadhyaya, S. & Singh, K., 2013. Water Desalination by Vacuum Membrane Distillation. In *AIChE Annual Meeting, San Francisco, CA*. pp. 21–40.
- Chernyshov, M.N., Meindersma, G.W. & de Haan, A.B., 2003. Modelling temperature and salt concentration distribution in membrane distillation feed channel. *Desalination*, 157(1), pp.315–324.
- Cho, I. & Zoh, K., 2007. Photocatalytic degradation of azo dye ( Reactive Red 120 ) in TiO<sub>2</sub> / UV system : Optimization and modeling using a response surface methodology ( RSM ) based on the central composite design. , 75.

- Chu, H.C. & Chen, K.M., 2002. Reuse of activated sludge biomass: II. The rate processes for the adsorption of basic dyes on biomass. *Process Biochemistry*, 37(10), pp.1129–1134.
- Couffin, N., Cabassud, C. & Lahoussine-Turcaud, V., 1998. A new process to remove halogenated VOCs for drinking water production: vacuum membrane distillation. *Desalination*, 117(1), pp.233–245.
- Crini, G., 2006. Non-conventional low-cost adsorbents for dye removal: A review. *Bioresource Technology*, 97(9), pp.1061–1085.
- Criscuoli, a., Carnevale, M.C. & Drioli, E., 2013. Modeling the performance of flat and capillary membrane modules in vacuum membrane distillation. *Journal of Membrane Science*, 447, pp.369–375.
- Criscuoli, A. et al., 2008. Treatment of dye solutions by vacuum membrane distillation. *Water Research*, 42(20), pp.5031–5037.
- Criscuoli, A., Bafaro, P. & Drioli, E., 2013. Vacuum membrane distillation for purifying waters containing arsenic. *Desalination*, 323, pp.17–21.
- Criscuoli, A., Carnevale, M.C. & Drioli, E., 2008. Evaluation of energy requirements in membrane distillation. *Chemical Engineering and Processing: Process Intensification*, 47(7), pp.1098–1105.
- Curcio, E. et al., 2010. Membrane distillation operated at high seawater concentration factors: role of the membrane on CaCO<sub>3</sub> scaling in presence of humic acid. *Journal of Membrane Science*, 346(2), pp.263–269.
- Curcio, E. & Drioli, E., 2005. Membrane distillation and related operations- a review. *Separation and Purification Reviews*, 34(1), pp.35–86.
- Dao, T.D., Laborie, S. & Cabassud, C., 2016. Direct As(III) removal from brackish groundwater by vacuum membrane distillation: Effect of organic matter and salts on membrane fouling. *Separation and Purification Technology*, 157, pp.35–44.
- Dasgupta, J. et al., 2015. Remediation of textile effluents by membrane based treatment techniques: A state of the art review. *Journal of Environmental Management*, 147, pp.55–72.
- Derjaguin, B. & Landau, L., 1993. Theory of the stability of strongly charged lyophobic sols and of the adhesion of strongly charged particles in solutions of electrolytes. *Progress in Surface Science*, 43(1), pp.30–59.
- Diban, N. et al., 2009. Vacuum membrane distillation of the main pear aroma compound: Experimental study and mass transfer modeling. *Journal of Membrane Science*, 326(1), pp.64–75.
- Dong, Z.-Q. et al., 2014. Superhydrophobic PVDF–PTFE electrospun nanofibrous membranes

for desalination by vacuum membrane distillation. *Desalination*, 347, pp.175–183.

El-Bourawi, M.S. et al., 2006. A framework for better understanding membrane distillation separation process. *Journal of Membrane Science*, 285(1), pp.4–29.

El-Bourawi, M.S.S. et al., 2007. Application of vacuum membrane distillation for ammonia removal. *Journal of Membrane Science*, 301(1–2), pp.200–209.

Fan, H. et al., 2013. Preparation and characterization of hydrophobic PVDF membranes by vapor-induced phase separation and application in vacuum membrane distillation. *Journal of Polymer Research*, 20(6), pp.1–15.

Fan, H. & Peng, Y., 2012. Application of PVDF membranes in desalination and comparison of the VMD and DCMD processes. *Chemical Engineering Science*, 79, pp.94–102.

Fane, A.G., Schofield, R.W. & Fell, C.J.D., 1987. The efficient use of energy in membrane distillation. *Desalination*, 64, pp.231–243.

Fernandez-Pineda, C., Izquierdo-Gil, M.A. & Garcia-Payo, M.C., 2002. Gas permeation and direct contact membrane distillation experiments and their analysis using different models. *Journal of Membrane Science*, 198(1), pp.33–49.

Findley, M.E., 1967. Vaporization through porous membranes. *Industrial & Engineering Chemistry Process Design and Development*, 6(2), pp.226–230.

Franken, A.C.M. et al., 1987. Wetting criteria for the applicability of membrane distillation. *Journal of Membrane Science*, 33(3), pp.315–328.

Van Gassel, T.J. & Schneider, K., 1986. An energy-efficient membrane distillation process. In *Membranes and Membrane processes*. Springer, pp. 343–348.

Gekas, V. & Hallstrom, B., 1987. Mass transfer in the membrane concentration polarization layer under turbulent cross flow: I. Critical literature review and adaptation of existing sherwood correlations to membrane operations. *Journal of Membrane Science*, 30(2), pp.153–170.

Godino, M.P. et al., 1997. Water production from brines by membrane distillation. *Desalination*, 108(1), pp.91–97.

Gore, D.W., 1982. Gore-Tex membrane distillation. *Proc. 10th Ann. Con. Water*, pp.25–29.

Gryta, M., 2007a. Effect of iron oxides scaling on the MD process performance. *Desalination*, 216(1), pp.88–102.

Gryta, M., 2012a. Effectiveness of water desalination by membrane distillation process. *Membranes*, 2(3), pp.415–429.

Gryta, M., 2008. Fouling in direct contact membrane distillation process. *Journal of membrane science*, 325(1), pp.383–394.

Gryta, M., 2007b. Influence of polypropylene membrane surface porosity on the performance of



- membrane distillation process. *Journal of Membrane Science*, 287(1), pp.67–78.
- Gryta, M. et al., 2001. Membrane distillation of NaCl solution containing natural organic matter. *Journal of Membrane Science*, 181(2), pp.279–287.
- Gryta, M., 2012b. Polyphosphates used for membrane scaling inhibition during water desalination by membrane distillation. *Desalination*, 285, pp.170–176.
- Gryta, M., 2002. The assessment of microorganism growth in the membrane distillation system. *Desalination*, 142(1), pp.79–88.
- Gryta, M. et al., 2009. The influence of polypropylene degradation on the membrane wettability during membrane distillation. *Journal of Membrane Science*, 326(2), pp.493–502.
- Gryta, M., Tomaszewska, M. & Karakulski, K., 2006. Wastewater treatment by membrane distillation. *Desalination*, 198(1), pp.67–73.
- Gryta, M., Tomaszewska, M. & Morawski, A.W., 1997. Membrane distillation with laminar flow. *Separation and Purification Technology*, 11(2), pp.93–101.
- Gryta, M. & Waszak, M., 2016. Application of vacuum membrane distillation for concentration of organic solutions. *Chemical Papers*, 70(4), pp.i–x.
- Guillen-Burrieza, E. et al., 2013. Effect of dry-out on the fouling of PVDF and PTFE membranes under conditions simulating intermittent seawater membrane distillation (SWMD). *Journal of Membrane Science*, 438, pp.126–139.
- Guo, W., Ngo, H.-H. & Li, J., 2012. A mini-review on membrane fouling. *Bioresour. technology*, 122, pp.27–34.
- Hameed, B.H. & Ahmad, A.A., 2009. Batch adsorption of methylene blue from aqueous solution by garlic peel, an agricultural waste biomass. *Journal of Hazardous Materials*, 164(2–3), pp.870–875.
- Hameed, B.H., Ahmad, A.L. & Latiff, K.N.A., 2007. Adsorption of basic dye (methylene blue) onto activated carbon prepared from rattan sawdust. *Dyes and Pigments*, 75(1), pp.143–149.
- Han, R. et al., 2009. Treating sulfur black dye wastewater with quaternized poly (phthalazinone ether sulfone ketone) nanofiltration membranes. *Separation and Purification Technology*, 67(1), pp.26–30.
- Hanbury, W.T. & Hodgkiess, T., 1985. Membrane distillation-an assessment. *Desalination*, 56, pp.287–297.
- Hasanouglu, A. et al., 2012. Effect of the operating variables on the extraction and recovery of aroma compounds in an osmotic distillation process coupled to a vacuum membrane distillation system. *Journal of Food Engineering*, 111(4), pp.632–641.
- Hayer, H., Bakhtiari, O. & Mohammadi, T., 2014. Analysis of heat and mass transfer in vacuum

membrane distillation for water desalination using computational fluid dynamics (CFD). *Desalination and Water Treatment*, (ahead-of-print), pp.1–14.

He, F. et al., 2008. Potential for scaling by sparingly soluble salts in crossflow DCMD. *Journal of Membrane science*, 311(1), pp.68–80.

He, K. et al., 2011. Production of drinking water from saline water by direct contact membrane distillation (DCMD). *Journal of Industrial and Engineering Chemistry*, 17(1), pp.41–48.

Hou, D. et al., 2015. An ultrasonic assisted direct contact membrane distillation hybrid process for desalination. *Journal of Membrane Science*, 476, pp.59–67.

Hu, Q.H. et al., 2006. Adsorption study for removal of basic red dye using bentonite. *Industrial & Engineering Chemistry Research*, 45(2), pp.733–738.

Imdakm, A.O. & Matsuura, T., 2004. A Monte Carlo simulation model for membrane distillation processes: direct contact (MD). *Journal of membrane science*, 237(1), pp.51–59.

Izquierdo-Gil, M.A., Abildskov, J. & Jonsson, G., 2004. The use of VMD data/model to test different thermodynamic models for vapour–liquid equilibrium. *Journal of membrane science*, 239(2), pp.227–241.

Izquierdo-Gil, M.A., Fernandez-Pineda, C. & Lorenz, M.G., 2008. Flow rate influence on direct contact membrane distillation experiments: different empirical correlations for Nusselt number. *Journal of Membrane Science*, 321(2), pp.356–363.

Izquierdo-Gil, M.A. & Jonsson, G., 2003. Factors affecting flux and ethanol separation performance in vacuum membrane distillation (VMD). *Journal of Membrane Science*, 214(1), pp.113–130.

Jun, D.U. et al., 2006. A method for experimental determination of mass transfer resistance across membrane in VMD. *Desalination*, 200(1), pp.606–608.

Kanadasan, G., Mashitah, M.D. & Vadivelu, V.M., 2010. Fixed Bed Adsorption Of Methylene Blue By Using Palm Oil Mill Effluent Waste Activated Sludge. *3rd IWA Asia Pacific Young Water Professional Conference 2010*, pp.1–8.

Karakulski, K. & Gryta, M., 2005. Water demineralisation by NF/MD integrated processes. *Desalination*, 177(1), pp.109–119.

Khataee, A.R., 2010. Optimization of UV-promoted peroxydisulphate oxidation of C.I. basic blue 3 using response surface methodology. *Environmental Technology*, 31(1), pp.73–86.

Khattari, S.D. & Singh, M.K., 2000. Colour removal from synthetic dye wastewater using a bioadsorbent. *Adsorption Journal Of The International Adsorption Society*, pp.283–294.

Khayet, M., 2005. Characterization of membrane distillation membranes by tapping mode atomic force microscopy. *Recent Advances in Multidisciplinary Applied Physics. Amsterdam:*

*Elsevier Ltd*, pp.141–148.

Khayet, M., 2011. Membranes and theoretical modeling of membrane distillation: A review. *Advances in colloid and interface science*, 164(1), pp.56–88.

Khayet, M., Godino, M.P. & Mengual, J.I., 2001. Modelling transport mechanism through a porous partition. *Journal of Non-Equilibrium Thermodynamics*, 26(1), pp.1–14.

Khayet, M., Godino, M.P. & Mengual, J.I., 2003. Possibility of nuclear desalination through various membrane distillation configurations: a comparative study. *International journal of nuclear desalination*, 1(1), pp.30–46.

Khayet, M., Godino, P. & Mengual, J.I., 2000a. Nature of flow on sweeping gas membrane distillation. *Journal of membrane science*, 170(2), pp.243–255.

Khayet, M., Godino, P. & Mengual, J.I., 2000b. Theory and experiments on sweeping gas membrane distillation. *Journal of membrane Science*, 165(2), pp.261–272.

KHAYET, M., KHULBE, K.C. & Matsuura, T., 2004. Characterization of membranes for membrane distillation by atomic force microscopy and estimation of their water vapor transfer coefficients in vacuum membrane distillation process. *Journal of membrane science*, 238(1), pp.199–211.

Khayet, M. & Matsuura, T., 2003. Application of surface modifying macromolecules for the preparation of membranes for membrane distillation. *Desalination*, 158(1), pp.51–56.

Khayet, M. & Matsuura, T., 2011. *Membrane distillation: principles and applications*, Elsevier.

Khayet, M. & Matsuura, T., 2004. Pervaporation and vacuum membrane distillation processes: modeling and experiments. *AIChE Journal*, 50(8), pp.1697–1712.

Khayet, M. & Matsuura, T., 2001. Preparation and characterization of polyvinylidene fluoride membranes for membrane distillation. *Industrial & engineering chemistry research*, 40(24), pp.5710–5718.

Khayet, M., Mengual, J.I. & Matsuura, T., 2005. Porous hydrophobic/hydrophilic composite membranes: application in desalination using direct contact membrane distillation. *Journal of Membrane Science*, 252(1), pp.101–113.

Khayet, M., Mengual, J.I. & Zakrzewska-Trznadel, G., 2005. Direct contact membrane distillation for nuclear desalination. Part I: Review of membranes used in membrane distillation and methods for their characterisation. *International journal of nuclear desalination*, 1(4), pp.435–449.

Khulbe, K.C. & Matsuura, T., 2000. Characterization of synthetic membranes by Raman spectroscopy, electron spin resonance, and atomic force microscopy; a review. *Polymer*, 41(5), pp.1917–1935.

- Kim, A.S., 2014. Cylindrical cell model for direct contact membrane distillation (DCMD) of densely packed hollow fibers. *Journal of Membrane Science*, 455, pp.168–186.
- Kiran, I. et al., 2006. Biosorption kinetics and isotherm studies of Acid Red 57 by dried *Cephalosporium aphidicola* cells from aqueous solutions. *Biochemical Engineering Journal*, 31(3), pp.197–203.
- Krivorot, M. et al., 2011. Factors affecting biofilm formation and biofouling in membrane distillation of seawater. *Journal of Membrane Science*, 376(1), pp.15–24.
- Kujawski, W. et al., 2016. Influence of hydrophobization conditions and ceramic membranes pore size on their properties in vacuum membrane distillation of water-organic solvent mixtures. *Journal of Membrane Science*, 499, pp.442–451.
- Kyoungjin, A. et al., 2017. PDMS / PVDF hybrid electrospun membrane with superhydrophobic property and drop impact dynamics for dyeing wastewater treatment using membrane distillation. *Journal of Membrane Science*, 525(August 2016), pp.57–67.
- Lagana, F., Barbieri, G. & Drioli, E., 2000. Direct contact membrane distillation: modelling and concentration experiments. *Journal of Membrane Science*, 166(1), pp.1–11.
- Laminski, S. et al., 2015. Sonochemical removal of naphthol blue black azo dye : influence of parameters and effect of mineral ions. , pp.35–44.
- Lawson, K.W., Hall, M.S. & Lloyd, D.R., 1995. Compaction of microporous membranes used in membrane distillation. I. Effect on gas permeability. *Journal of membrane science*, 101(1), pp.99–108.
- Lawson, K.W. & Lloyd, D.R., 1996a. Membrane distillation. I. Module design and performance evaluation using vacuum membrane distillation. *Journal of membrane science*, 120(1), pp.111–121.
- Lawson, K.W. & Lloyd, D.R., 1996b. Membrane distillation. II. Direct contact MD. *Journal of Membrane Science*, 120(1), pp.123–133.
- Lawson, K.W. & Lloyd, D.R., 1997. Membrane distillation. *Journal of membrane Science*, 124(1), pp.1–25.
- Lee, J.-G. & Kim, W.-S., 2013. Numerical modeling of the vacuum membrane distillation process. *Desalination*, 331, pp.46–55.
- Lei, Z., Chen, B. & Ding, Z., 2005. *Special distillation processes*, Elsevier.
- Li, B. & Sirkar, K.K., 2005. Novel membrane and device for vacuum membrane distillation-based desalination process. *Journal of Membrane Science*, 257(1), pp.60–75.
- Li, Y. & Tian, K., 2009. Application of Vacuum Membrane Distillation in Water Treatment. *Journal of sustainable Development*, 2(3), pp.183–186.

- Lian, B. et al., 2016. A numerical approach to module design for crossflow vacuum membrane distillation systems. *Journal of Membrane Science*, 510, pp.489–496.
- Lovineh, S.G., Asghari, M. & Rajaei, B., 2013. Numerical simulation and theoretical study on simultaneous effects of operating parameters in vacuum membrane distillation. *Desalination*, 314, pp.59–66.
- Maria, F. et al., 2008. Azo Dyes and Their Metabolites : Does the Discharge of the Azo Dye into Water Bodies Represent Human and Ecological Risks ? *Advances in Treating Textile effluent*, 42(2), pp.584–589.
- Martinez, L. et al., 2002. Characterisation of three hydrophobic porous membranes used in membrane distillation: modelling and evaluation of their water vapour permeabilities. *Journal of membrane science*, 203(1), pp.15–27.
- Martinez, L., 2004. Comparison of membrane distillation performance using different feeds. *Desalination*, 168, pp.359–365.
- Martinez, L. & Rodriguez-Maroto, J.M., 2007. On transport resistances in direct contact membrane distillation. *Journal of membrane science*, 295(1), pp.28–39.
- Meng, F. et al., 2009. Recent advances in membrane bioreactors (MBRs): membrane fouling and membrane material. *Water research*, 43(6), pp.1489–1512.
- Meng, S. et al., 2014. Fouling and crystallisation behaviour of superhydrophobic nano-composite PVDF membranes in direct contact membrane distillation. *Journal of Membrane Science*, 463, pp.102–112.
- Mengual, J.I.I., Khayet, M. & Godino, M.P.P., 2004. Heat and mass transfer in vacuum membrane distillation. *International Journal of Heat and Mass Transfer*, 47(4), pp.865–875.
- Mericq, J.-P., Laborie, S.S. & Cabassud, C., 2011. Evaluation of systems coupling vacuum membrane distillation and solar energy for seawater desalination. *Chemical Engineering Journal*, 166(2), pp.596–606.
- Mericq, J.-P.P., Laborie, S.S. & Cabassud, C., 2010. Vacuum membrane distillation of seawater reverse osmosis brines. *Water Research*, 44(18), pp.5260–5273.
- Mo, J.H. et al., 2008. Treatment of dye aqueous solutions using nanofiltration polyamide composite membranes for the dye wastewater reuse. *Dyes and Pigments*, 76(2), pp.429–434.
- Mohammadi, T. & Akbarabadi, M., 2005. Separation of ethylene glycol solution by vacuum membrane distillation (VMD). *Desalination*, 181(1–3), pp.35–41.
- Mohammadi, T. & Kazemi, P., 2014. Taguchi optimization approach for phenolic wastewater treatment by vacuum membrane distillation. *Desalination and Water Treatment*, 52(7–9), pp.1341–1349.

- Mohammadi, T. & Safavi, M.A., 2009. Application of Taguchi method in optimization of desalination by vacuum membrane distillation. *Desalination*, 249(1), pp.83–89.
- Mook, W.T. et al., 2016. Uncorrected Proof Uncorrected Proof. *Ultrasonics - Sonochemistry*, (i), pp.1–11.
- Mulder, M., 1996. *Basic principles of membrane technology*, Springer Science & Business Media.
- Naidu, G. et al., 2014. Experiments and modeling of a vacuum membrane distillation for high saline water. *Journal of Industrial and Engineering Chemistry*, 20(4), pp.2174–2183.
- Navarro, A.E. et al., 2009. Comparative study of the removal of phenolic compounds by biological and non-biological adsorbents. *Journal of Hazardous Materials*, 164(2–3), pp.1439–1446.
- Pangarkar, B.L. et al., 2010. The Heat and Mass Transfer Phenomena in Vacuum Membrane Distillation for Desalination. *International Journal of Chemical and Biological Engineering*, 3(1), pp.33–38.
- Pangarkar, B.L. et al., 2011. Vacuum Membrane Distillation for Desalination of Ground Water by using Flat Sheet Membrane. *International Journal of Chemical and Biological Engineering*, 4, pp.13–18.
- Phattaranawik, J., Jiraratananon, R. & Fane, A.G., 2003a. Effect of pore size distribution and air flux on mass transport in direct contact membrane distillation. *Journal of Membrane Science*, 215(1), pp.75–85.
- Phattaranawik, J., Jiraratananon, R. & Fane, A.G., 2003b. Heat transport and membrane distillation coefficients in direct contact membrane distillation. *Journal of Membrane Science*, 212(1), pp.177–193.
- Quist-Jensen, C.A., Macedonio, F. & Drioli, E., 2015. Membrane technology for water production in agriculture: Desalination and wastewater reuse. *Desalination*, 364, pp.17–32.
- Ramon, G., Agnon, Y. & Dosoretz, C., 2009. Heat transfer in vacuum membrane distillation: Effect of velocity slip. *Journal of Membrane Science*, 331(1–2), pp.117–125.
- Safavi, M. & Mohammadi, T., 2009. High-salinity water desalination using VMD. *Chemical Engineering Journal*, 149(1), pp.191–195.
- Saffarini, R.B. et al., 2013. Effect of temperature-dependent microstructure evolution on pore wetting in PTFE membranes under membrane distillation conditions. *Journal of Membrane Science*, 429, pp.282–294.
- SAKAI, K. et al., 1986. Extraction of solute-free water from blood by membrane distillation. *ASAIO Journal*, 32(1), pp.397–400.

- Sarti, G.C., Gostoli, C. & Bandini, S., 1993. Extraction of organic components from aqueous streams by vacuum membrane distillation. *Journal of membrane science*, 80(1), pp.21–33.
- Sarti, G.C., Gostoli, C. & Matulli, S., 1985. Low energy cost desalination processes using hydrophobic membranes. *Desalination*, 56, pp.277–286.
- Schäfer, A.I. et al., 2000. Microfiltration of colloids and natural organic matter. *Journal of Membrane Science*, 171(2), pp.151–172.
- Schneider, K. et al., 1988. Membranes and modules for transmembrane distillation. *Journal of membrane science*, 39(1), pp.25–42.
- Schofield, R.W., Fane, A.G., Fell, C.J.D., et al., 1990. Factors affecting flux in membrane distillation. *Desalination*, 77, pp.279–294.
- Schofield, R.W., Fane, A.G. & Fell, C.J.D., 1990. Gas and vapour transport through microporous membranes. I. Knudsen-Poiseuille transition. *Journal of Membrane Science*, 53(1), pp.159–171.
- Schofield, R.W., Fane, A.G. & Fell, C.J.D., 1987. Heat and mass transfer in membrane distillation. *Journal of membrane Science*, 33(3), pp.299–313.
- Serth, R.W. & Lestina, T., 2014. *Process heat transfer: Principles, applications and rules of thumb*, Academic Press.
- Shafeeyan, M.S. et al., 2012. The application of response surface methodology to optimize the amination of activated carbon for the preparation of carbon dioxide adsorbents. *Fuel*, 94, pp.465–472.
- Shao, F. et al., 2013. Study on vacuum membrane distillation of PP hollow fiber membranes used in concentrated seawater from low-pressure reverse osmosis. *Desalination and Water Treatment*, 51(19–21), pp.3925–3929.
- Shim, S.M., Lee, J.G. & Kim, W.S., 2014. Performance simulation of a multi-VMD desalination process including the recycle flow. *Desalination*, 338, pp.39–48.
- Singh, J.K., Upadhyaya, S. & Chaurasia, S.P., 2013. Application of Vacuum Membrane Distillation for Fluoride Removal. *International Journal of Chemistry and Chemical Engineering*, 3, pp.209–214.
- Singh, K.P. et al., 2011. Optimizing adsorption of crystal violet dye from water by magnetic nanocomposite using response surface modeling approach. *Journal of Hazardous Materials*, 186(2–3), pp.1462–1473.
- Soni, V. et al., 2008. Modeling and analysis of vacuum membrane distillation for the recovery of volatile aroma compounds from black currant juice. *Journal of Membrane Science*, 320(1–2), pp.442–455.

- Sorenson, T.S., 1999. *Surface Chemistry and Electrochemistry of membranes*, CRC Press.
- Srisurichan, S., Jiratananon, R. & Fane, A.G., 2005. Humic acid fouling in the membrane distillation process. *Desalination*, 174(1), pp.63–72.
- Srisurichan, S., Jiratananon, R. & Fane, A.G., 2006. Mass transfer mechanisms and transport resistances in direct contact membrane distillation process. *Journal of Membrane Science*, 277(1), pp.186–194.
- Sudoh, M. et al., 1997. Effects of thermal and concentration boundary layers on vapor permeation in membrane distillation of aqueous lithium bromide solution. *Journal of membrane science*, 131(1), pp.1–7.
- Tan, I.A.W., Ahmad, A.L. & Hameed, B.H., 2008. Adsorption of basic dye using activated carbon prepared from oil palm shell: batch and fixed bed studies. *Desalination*, 225(1–3), pp.13–28.
- Tang, C. & Chen, V., 2002. Nanofiltration of textile wastewater for water reuse. *Desalination*, 143(1), pp.11–20.
- Tang, N. et al., 2010. Preparation and morphological characterization of narrow pore size distributed polypropylene hydrophobic membranes for vacuum membrane distillation via thermally induced phase separation. *Desalination*, 256(1), pp.27–36.
- Termpiyakul, P., Jiratananon, R. & Srisurichan, S., 2005. Heat and mass transfer characteristics of a direct contact membrane distillation process for desalination. *Desalination*, 177(1), pp.133–141.
- Thomas, H.C., 1944. Heterogeneous ion exchange in a flowing system. *Journal of the American Chemical Society*, 66(2), pp.1664–1666.
- Tijing, L.D. et al., 2015. Fouling and its control in membrane distillation: a review. *Journal of Membrane Science*, 475, pp.215–244.
- Tomaszewska, M., Gryta, M. & Morawski, A.W., 1994. A study of separation by the direct-contact membrane distillation process. *Separations Technology*, 4(4), pp.244–248.
- Tun, C.M. et al., 2005. Membrane distillation crystallization of concentrated salts-flux and crystal formation. *Journal of Membrane Science*, 257(1), pp.144–155.
- Upadhyaya, S. et al., 2015. Mathematical and CFD modeling of vacuum membrane distillation for desalination. *Desalination and Water Treatment*, 3994(October), pp.1–16.
- Upadhyaya, S. et al., 2016a. Mathematical and CFD modeling of vacuum membrane distillation for desalination. *Desalination and Water Treatment*, 57(26), pp.11956–11971.
- Upadhyaya, S. et al., 2011. Parametric Sensitivity Analysis of Vacuum Membrane Distillation for Desalination Process. *International Conference on Chemical, Ecology and Environmental*



*Sciences (ICCEES'2011)*, pp.447–451.

Upadhyaya, S. et al., 2016b. Recovery and development of correlations for heat and mass transfer in vacuum membrane distillation for desalination. *Desalination and Water Treatment*, 3994(July), pp.1–13.

Upadhyaya, S. et al., 2016c. Recovery and development of correlations for heat and mass transfer in vacuum membrane distillation for desalination. *Desalination and Water Treatment*, 57(55), pp.26886–26898.

Urtiaga, A.M., Ruiz, G. & Ortiz, I., 2000. Kinetic analysis of the vacuum membrane distillation of chloroform from aqueous solutions. *Journal of Membrane Science*, 165(1), pp.99–110.

Verwey, E.J.W., Overbeek, J.T.G. & Overbeek, J.T.G., 1999. *Theory of the stability of lyophobic colloids*, Courier Corporation.

Wang, H. et al., 2011. Permeate flux curve characteristics analysis of cross-flow vacuum membrane distillation. *Industrial & Engineering Chemistry Research*, 51(1), pp.487–494.

Wang, L. et al., 2014. Novel design of liquid distributors for VMD performance improvement based on cross-flow membrane module. *Desalination*, 336, pp.80–86.

Wang, X. et al., 2009. Feasibility research of potable water production via solar-heated hollow fiber membrane distillation system. *Desalination*, 247(1), pp.403–411.

Wang, Z. et al., 2009. Application of vacuum membrane distillation to lithium bromide absorption refrigeration system. *international journal of refrigeration*, 32(7), pp.1587–1596.

Warsinger, D.M. et al., 2015. Scaling and fouling in membrane distillation for desalination applications: a review. *Desalination*, 356, pp.294–313.

Wirth, D. & Cabassud, C., 2002. Water desalination using membrane distillation: comparison between inside/out and outside/in permeation. *Desalination*, 147(1), pp.139–145.

Wu, B. et al., 2006. Removal of 1, 1, 1-trichloroethane from water using a polyvinylidene fluoride hollow fiber membrane module: Vacuum membrane distillation operation. *Separation and purification technology*, 52(2), pp.301–309.

Xu, Y., Zhu, B.-K. & Xu, Y., 2006. Pilot test of vacuum membrane distillation for seawater desalination on a ship. *Desalination*, 189(1), pp.165–169.

Yang, X. et al., 2011. Performance improvement of PVDF hollow fiber-based membrane distillation process. *Journal of membrane science*, 369(1), pp.437–447.

Yang, Y. et al., 2016. The heat and mass transfer of vacuum membrane distillation: Effect of active layer morphology with and without support material. *Separation and Purification Technology*, 164, pp.56–62.

Yasuda, H. & Tsai, J.T., 1974. Pore Size of Microporous Polymer Membranes. *Journal of*

*Applied Polymer Science*, 18(3), pp.805–819.

Yatmaz, H.C., Dizge, N. & Kurt, M.S., 2017. Combination of Photocatalytic and Membrane Distillation Hybrid Processes for Reactive Dyes Treatment. , 3330(January).

Zhang, J., Dow, N., et al., 2010. Identification of material and physical features of membrane distillation membranes for high performance desalination. *Journal of Membrane Science*, 349(1), pp.295–303.

Zhang, J. et al., 2013. Modelling of vacuum membrane distillation. *Journal of Membrane Science*, 434, pp.1–9.

Zhang, J., Duke, M., et al., 2010. Performance of asymmetric hollow fibre membranes in membrane distillation under various configurations and vacuum enhancement. *Journal of Membrane Science*, 362(1), pp.517–528.

Zhang, X. et al., 2016. Exploration and optimization of two-stage vacuum membrane distillation process for the treatment of saline wastewater produced by natural gas exploitation. *Desalination*, 385, pp.117–125.

Zhang, X. et al., 2016. Harvesting microalgal biomass using magnesium coagulation-dissolved air flotation. *Biomass and Bioenergy*, 93, pp.43–49.

Zhao, K. et al., 2013. Experimental study of the memsys vacuum-multi-effect-membrane-distillation (V-MEMD) module. *Desalination*, 323, pp.150–160.

Zhong, W. et al., 2016. Evaluation of silica fouling for coal seam gas produced water in a submerged vacuum membrane distillation system. *Desalination*, 393, pp.52–64.

Zhong, Y.-H. et al., 2010. Adsorption of methylene blue onto vanadium-doped magnetite., 31(6), pp.1568–1574.

Zhou, T. et al., 2014. Formation and characterization of polytetrafluoroethylene nanofiber membranes for vacuum membrane distillation. *Journal of Membrane Science*, 453, pp.402–408.

Zhu, H. et al., 2013. Preparation and properties of PTFE hollow fiber membranes for desalination through vacuum membrane distillation. *Journal of Membrane Science*, 446, pp.145–153.

Zuo, J. & Chung, T.S., 2016. In-situ cross-linked PVDF membranes with enhanced mechanical durability for vacuum membrane distillation. *AIChE Journal*, 62(11), pp.4013–4022.

## APPENDIX-I

### 1. Normalized Sensitivity analysis of permeate flux to feed temperature

$$S(N, T_f) = \frac{\partial \ln N}{\partial \ln T_f} = \frac{T_f}{N} \left( \frac{\partial N}{\partial T_f} \right) \dots\dots\dots(1)$$

We also know that

$$N = \frac{h}{\lambda} (T_f - T_p) \dots\dots\dots(2)$$

$$N = k_m \sqrt{m} (P_f - P_p) \dots\dots\dots(3)$$

From equation (2), we get

$$\frac{dN}{dT_f} = \frac{h}{\lambda} - \frac{h}{\lambda} \frac{dT_p}{dT_f} \dots\dots\dots(4)$$

Now to calculate  $\frac{dT_f}{dT_p}$  equating equation (2) and (3).

$$(T_f - T_p) = \frac{\lambda k_m \sqrt{m}}{h} (P_f - P_p)$$

$$T_f = \frac{\lambda k_m \sqrt{m}}{h} (P_f - P_p) + T_p$$

$$dT_f = \frac{\lambda k_m \sqrt{m}}{h} dP_f + dT_p$$

$$\frac{dT_f}{dT_p} = \frac{\lambda k_m \sqrt{m}}{h} \frac{dP_f}{dT_p} + 1 \dots\dots\dots(5)$$

From clausius claperyon equation

$$\frac{dP_f}{dT_p} = \frac{\lambda M P_f}{RT_p^2} \dots\dots\dots(6)$$

From equation (5) and (6)

$$\frac{dT_f}{dT_p} = \frac{\lambda k_m \sqrt{m}}{h} \left( \frac{\lambda M P_f}{RT_p^2} \right) + 1$$

$$\frac{dT_f}{dT_p} = \frac{\lambda^2 M^{3/2} P_f k_m}{h R T_p^2} + 1$$

$$\frac{dT_f}{dT_p} = R_1 + 1$$

Where,  $R_1 = \frac{\lambda^2 M^{3/2} P_f k_m}{hRT_p^2}$

$$\frac{dT_p}{dT_f} = \frac{1}{R_1 + 1}$$

So,

$$\frac{dN}{dT_f} = \frac{h}{\lambda} \left( 1 - \frac{1}{R_1 + 1} \right) = \frac{h}{\lambda} \left( \frac{R_1}{R_1 + 1} \right)$$

$$S(N, T_f) = \frac{h}{\lambda} \left( \frac{R_1}{R_1 + 1} \right) * \frac{T_f}{N}$$

Now from equation (2)

$$\frac{N}{T_f} = \frac{h}{\lambda} \left( \frac{T_f - T_p}{T_f} \right)$$

$$\frac{T_f}{N} = \frac{\lambda}{h} \left( \frac{T_f}{T_f - T_p} \right)$$

So,

$$S(N, T_f) = \frac{h}{\lambda} \left( \frac{R_1}{R_1 + 1} \right) * \frac{\lambda}{h} \left( \frac{T_f}{T_f - T_p} \right)$$

$$S(N, T_f) = \left( \frac{R_1}{R_1 + 1} \right) * \frac{1}{R_2}$$

Where,  $R_2 = \left( \frac{T_f}{T_f - T_p} \right)$

So, normalized sensitivity factor of permeate flux to the feed temperature is

$$S(N, T_f) = \left( \frac{R_1}{R_1 + 1} \right) * \frac{1}{R_2}.$$

## 2. Normalized Sensitivity analysis of permeate flux to vacuum degree

$$S(N, P_p) = \frac{\partial \ln N}{\partial \ln P_p} = \frac{P_p}{N} \left( \frac{\partial N}{\partial P_p} \right) \dots\dots\dots(1)$$

We also know that

$$N = \frac{h}{\lambda} (T_f - T_p) \dots\dots\dots(2)$$

$$N = k_m \sqrt{m} (P_f - P_p) \dots\dots\dots(3)$$

From equation (3), we get

$$dN = k_m \sqrt{m} (dP_f - dP_p)$$

$$\frac{dN}{dP_p} = k_m \sqrt{m} \left( \frac{dP_f}{dP_p} - 1 \right) \dots\dots\dots(4)$$

Now  $\frac{dP_f}{dP_p}$  is required so equate equation (2) and (3).

$$P_f - P_p = \frac{h}{\lambda k_m \sqrt{M}} (T_f - T_p)$$

$$P_p = \left( P_f - \frac{h}{\lambda k_m \sqrt{M}} (T_f - T_p) \right)$$

$$dP_p = dP_f + \frac{h}{\lambda k_m \sqrt{M}} dT_p$$

$$\frac{dP_p}{dP_f} = 1 + \frac{h}{\lambda k_m \sqrt{M}} \left( \frac{dT_p}{dP_f} \right) \dots\dots\dots(5)$$

From clausius claperyon equation

$$\frac{dP_f}{dT_p} = \frac{\lambda M P_f}{R T_p^2} \dots\dots\dots(6)$$

From equation (5) and (6)

$$\frac{dP_p}{dP_f} = 1 + \frac{h}{\lambda k_m \sqrt{M}} \frac{R T_p^2}{\lambda M P_f}$$

$$\frac{dP_p}{dP_f} = 1 + \frac{h}{\lambda^2 k_m} \frac{R T_p^2}{M^{3/2} P_f}$$

$$\frac{dP_p}{dP_f} = 1 + \frac{1}{R_1}$$

Where,  $R_1 = \frac{\lambda^2 M^{3/2} P_f k_m}{hRT_p^2}$

$$\frac{dP_p}{dP_f} = \frac{R_1 + 1}{R_1}$$

$$\frac{dP_f}{dP_p} = \frac{R_1}{1 + R_1}$$

So,

$$\frac{dN}{dP_p} = k_m \sqrt{M} \left( \frac{R_1}{1 + R_1} - 1 \right)$$

$$\frac{dN}{dP_p} = k_m \sqrt{M} \left( \frac{-1}{1 + R_1} \right)$$

So,

$$S(N, P_p) = k_m \sqrt{M} \left( \frac{-1}{1 + R_1} \right) \frac{P_p}{N}$$

Now from equation (2),

$$\frac{N}{P_p} = k_m \sqrt{M} \frac{(P_f - P_p)}{P_p}$$

$$\frac{P_p}{N} = \frac{P_p}{k_m \sqrt{M} (P_f - P_p)}$$

So,

$$S(N, P_p) = k_m \sqrt{M} \left( \frac{-1}{1 + R_1} \right) \left[ \frac{P_p}{k_m \sqrt{M} (P_f - P_p)} \right]$$

$$S(N, P_p) = \left( \frac{-1}{1 + R_1} \right) \frac{1}{R_3}$$

Where,

$$R_3 = \frac{P_f - P_p}{P_p}$$

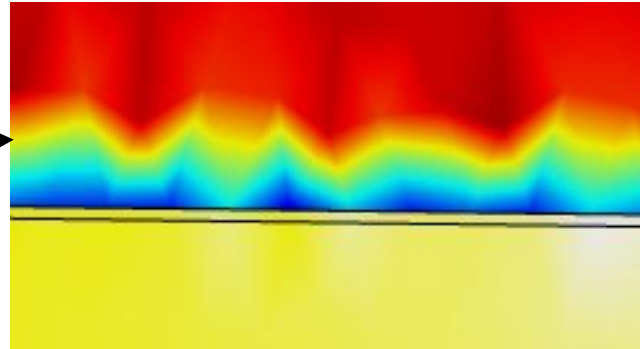
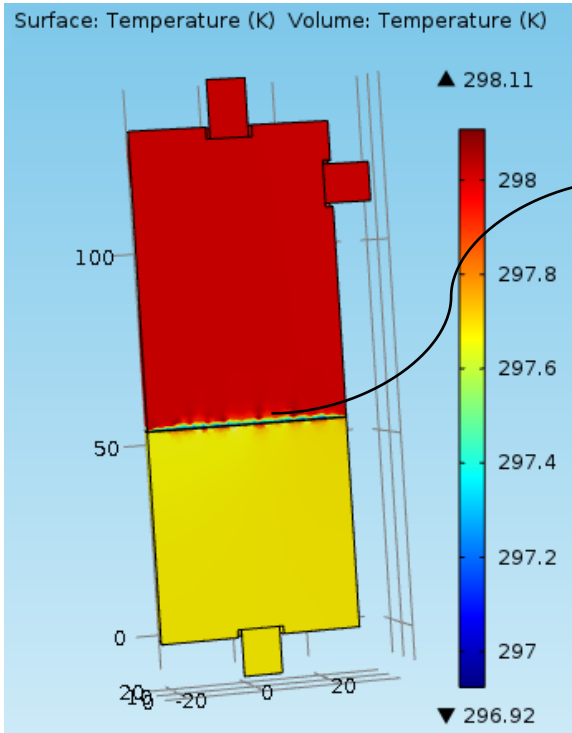
So, normalized sensitivity factor of permeate flux to the feed temperature is

$$S(N, P_p) = \left( \frac{-1}{1 + R_1} \right) \frac{1}{R_3}$$

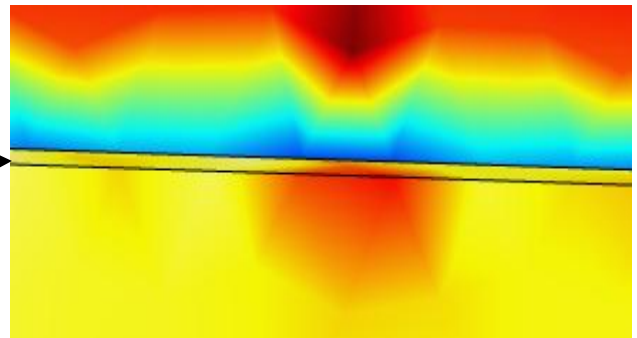
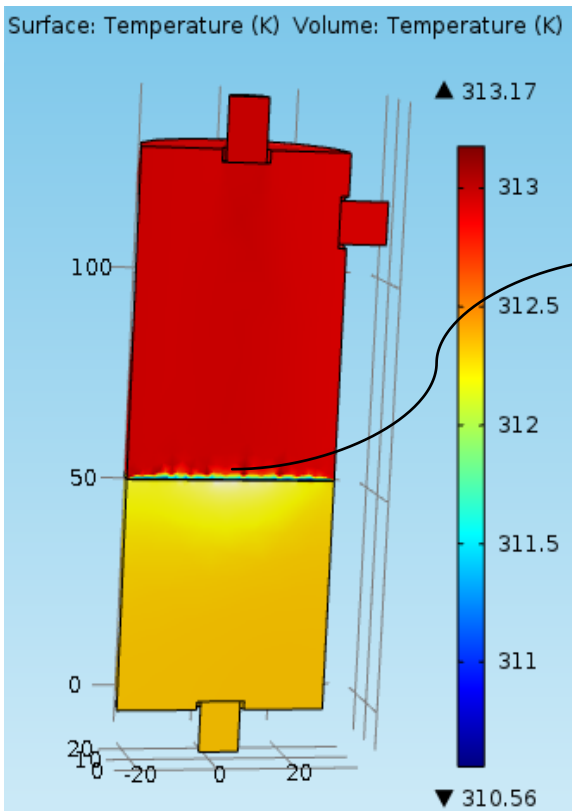
## APPENDIX-II

### 1. CFD Temperature Contour at different feed temperature

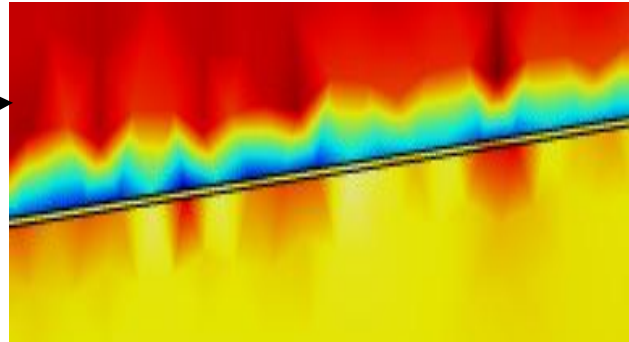
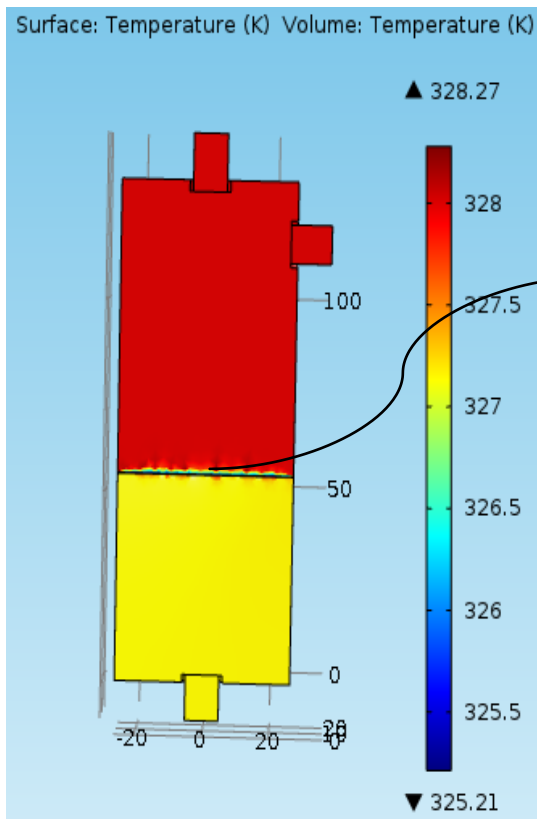
- (i) Feed Temperature = 25 °C, vacuum degree = 750mmHg, flow rate = 5 lpm, initial dye concentration = 30 ppm



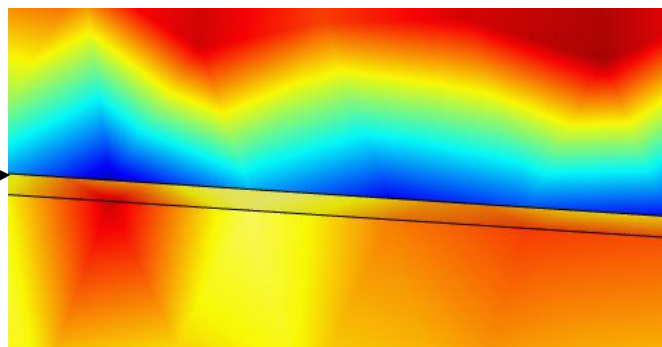
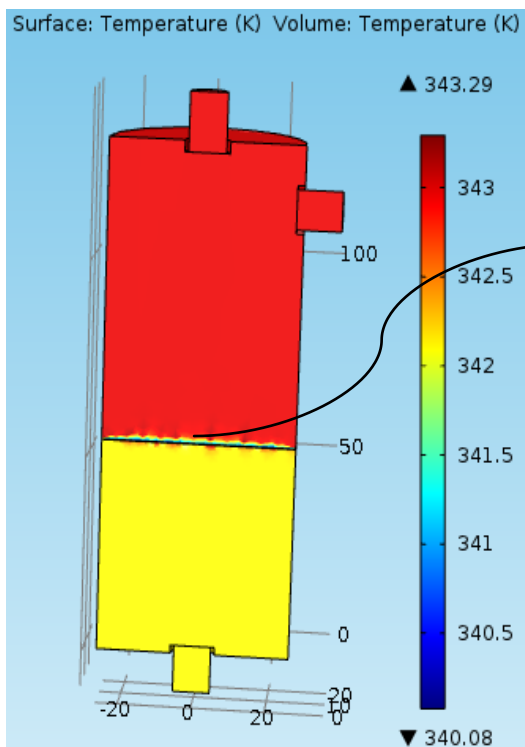
- (ii) Feed Temperature = 40 °C, vacuum degree = 750mmHg, flow rate = 5 lpm, initial dye concentration = 30 ppm



- (iii) Feed Temperature = 55 °C, vacuum degree = 750mmHg, flow rate = 5 lpm, initial dye concentration = 30 ppm



- (iv) Feed Temperature = 70 °C, vacuum degree = 750mmHg, flow rate = 5 lpm, initial dye concentration = 30 ppm





## **BIO-DATA**

Name Rakesh Baghel

Father's Name : Mr. Gya Prasad Baghel

Mother's Name : Late Mrs. Sheela Devi

Date of Birth : 25/09/1990

Marital Status : Single

Education Qualification : M.Tech. Chemical Engineering (2014)  
Malaviya National Institute of Technology Jaipur  
Rajasthan, India  
B.Tech. Chemical Engineering (2012)  
Hindustan College of Science and Technology Farah  
Mathura U.P.

Scientific Membership : Indian Institute of Chemical Engineers (IChE), Life  
Associate Member LAM-52070  
Indian Desalination Association (InDA), Life Member  
LM-400

Publications : International Journals (03) (out of 2 SCI)  
International Conferences (03)  
Allied International Journals (03)  
Allied International Conferences (05)

Short-term Courses : 05  
attended